Springer Series in Materials Science 323

Mpitloane Joseph Hato
Suprakas Sinha Ray *Editors*

Functional Polymer Nanocomposites for Wastewater Treatment

Springer

Springer Series in Materials Science

Volume 323

The Springer Series in Materials Science covers the complete spectrum of materials research and technology, including fundamental principles, physical properties, materials theory and design. Recognizing the increasing importance of materials science in future device technologies, the book titles in this series reflect the state-of-the-art in understanding and controlling the structure and properties of all important classes of materials.

More information about this series at https://link.springer.com/bookseries/856

Mpitloane Joseph Hato · Suprakas Sinha Ray
Editors

Functional Polymer Nanocomposites for Wastewater Treatment

Springer

Editors
Mpitloane Joseph Hato
Nanotechnology Research Group
Department of Chemistry
University of Limpopo (Turfloop)
Polokwane, Sovenga, South Africa

Suprakas Sinha Ray
Centre for Nanostuctures and Advanced Materials
DSI-CSIR Nanotechnology Innovation Centre, Council for Scientific and Industrial Research
Brummeria, Pretoria, South Africa

Department of Chemical Sciences
University of Johannesburg
Johannesburg, South Africa

ISSN 0933-033X ISSN 2196-2812 (electronic)
Springer Series in Materials Science
ISBN 978-3-030-94994-5 ISBN 978-3-030-94995-2 (eBook)
https://doi.org/10.1007/978-3-030-94995-2

This Springer imprint is published by the registered company Springer Nature Switzerland AG
The registered company address is: Gewerbestrasse 11, 6330 Cham, Switzerland

Preface

The deterioration of water quality and unavailability of drinkable water are pressing challenges worldwide. Removal of toxic organic and inorganic pollutants from water is indispensable for a clean environment, as a response to water scarcity, and for human society. This book is dedicated to recent development in Environmental Control techniques owing to polymer nanocomposites, which integrate the benefits of both nanomaterials and composites and offer the expansion of novel and cost-effective technologies for pollution control. Polymer nanocomposites present outstanding mechanical properties and compatibility performance due to their composite nature; the unique physical and chemical properties emanated from their large surface area to volume ratios and high interfacial interactions of the nanomaterials. Based on their morphology and compositions, nanocomposites can provide powerful tools for Environmental Remediation. Furthermore, with the leverage to functionalize the nanomaterials with different functional groups can also enhance their affinity toward target pollutants, which is desired for selective adsorption of contaminants in complex environmental matrices. This book summarizes the recent progress of polymer nanocomposites, fabrication and processing methods, and their applications for pollutant sensing and detection at the experimental scale. The book has been divided into several parts, including the description of different synthesis methods for nanocomposites, metal–organic frameworks-based nanocomposites, hydrogel nanocomposites, nanocomposite membranes, photocatalysts, and bio-nanocomposites for pollution abatement.

The following are key features of this book:

- Fundamental issues that persist concerning polymer nanocomposites;
- An overview of the latest advances in these fields, offering insight into the chemistry and activity of the latest generation activities of nanocomposites (photocatalytic degradation, adsorption, and membranes) applications in wastewater treatment;
- Cuts water science, materials science, and nanotechnology;

- An ideal book for water scientists, material scientists, researchers, engineers (chemical and civil) including under- and postgraduate students who are interested in this exciting field of research; and
- Finally, this book will also help industrial researchers and R&D managers who want to bring advanced nanostructured and nanocomposites into the market.

Polokwane, Sovenga, South Africa — Mpitloane Joseph Hato
Brummeria, Pretoria, South Africa — Suprakas Sinha Ray

Contents

Editors and Contributors

About the Editors

Prof. Mpitloane Joseph Hato received a Ph.D. degree in Chemistry at the University of Free State in 2010 and he is currently the Nanotechnology Research Group Leader in the Department of Chemistry at University of Limpopo, South Africa, since 2014. He has spent a half and year at Inha University (South Korea) and the Council for Scientific and Industrial Research (South Africa) as a Postdoctoral Research Fellow focusing on various properties of different materials for packaging and rheological applications. His multidisciplinary research interest cuts across electrochemistry, water research, materials science, and nanotechnology. It successfully highlights the applicability of conducting polymer nanocomposites for electrochemical hydrogen generation and water treatment.

He is the author of 8 book chapters on aspects of metal–organic frameworks-based composites and conducting polymers and their applications, and author and co-author of 31 articles in high-impact international journals. His honors include the Best Researcher in the School of Physical and Mineral Sciences awarded by the Vice-Chancellor at the Research Excellence Awards 2019 and currently rated C3 as an Established Researcher by the National Research Foundation of South Africa. He has been appointed as the External Research Professor in the Department of Enviromental Sciences at the University of South Africa since 2017 to date.

Prof. Suprakas Sinha Ray is a chief researcher in nanostructured materials at the Centre for Nanostructures and Advanced Materials, Council for Scientific and Industrial Research (CSIR) with a Ph.D. in physical chemistry from the University of Calcutta in 2001 and director of the DSI-CSIR Nanotechnology Innovation Centre. Ray's current research focuses on advanced nanostructured materials and their applications. He is one of the most active and highly cited authors in the field of polymer nanocomposite materials, and he has recently been rated by Thomson Reuters as being one of the Top 1% most impactful and influential scientists and Top 50 high-impact chemists (out of 2 mil Chemists worldwide).

He is the author of 5 books, co-author of 3 edited books, 32 book chapters on various aspects of polymer-based nanostructured materials and their applications, and author and co-author of 450 articles in high-impact international journals, 30 articles in national and international conference proceedings. He also has six patents and seven new demonstrated technologies shared with colleagues, collaborators, and industrial partners. So far, his team commercialized 19 different products. His honors and awards include South Africa's most Prestigious 2016 National Science and Technology Award (NSTF); Prestigious 2014 CSIR-wide Leadership award; Prestigious 2014 CSIR Human Capital development award; Prestigious 2013 Morand Lambla Awardee (top award in the field of polymer processing worldwide), International Polymer Processing Society, USA. He is also appointed as the Extraordinary Professor, University of Pretoria, and Distinguished Professor of Chemistry, University of Johannesburg.

Contributors

Dalia Allouss Laboratory of Materials, Catalysis & Valorization of Natural Resources, FSTM, Hassan II University, Casablanca, Morocco

Abhijit Bandyopadhyay Department of Polymer Science and Technology, University of Calcutta, Kolkata, India

Subhadeep Chakraborty Department of Polymer Science and Technology, University of Calcutta, Kolkata, India

Ch. G. Chandaluri Faculty of Chemistry, Humanities and Sciences Division, Indian Institute of Petroleum and Energy, Visakhapatnam, Andhra Pradesh, India

Mpitloane J. Hato Nanotechnology Research Lab, Department of Chemistry, School of Physical and Mineral Sciences, University of Limpopo(Turfloop), Polokwane, South Africa

Sathish Kumar Kamaraj Instituto Tecnológico El Llano Aguascalientes (ITEL), Tecnológico Nacional de México (TecNM), El Llano, México

Edwin Makhado Nanotechnology Research Lab, Department of Chemistry, School of Physical and Mineral Sciences, University of Limpopo(Turfloop), Polokwane, South Africa

T. A. Makhetha Department of Chemical Sciences, University of Johannesburg, Doornfontein, Johannesburg, South Africa

Nompumelelo Malatji Nanotechnology Research Lab, Department of Chemistry, School of Physical and Mineral Sciences, University of Limpopo(Turfloop), Polokwane, South Africa

V. Manju Indian Institute of Technology, Chennai, India

Odwa Mapazi Analytical Services Division, Mintek, Randburg, Johannesburg, South Africa

Phillemon Matabola Advanced Materials Division, DSI/Mintek Nanotechnology Innovation Centre, Mintek, Randburg, Johannesburg, South Africa

Kwena D. Modibane Nanotechnology Research Lab, Department of Chemistry, School of Physical and Mineral Sciences, University of Limpopo(Turfloop), Polokwane, South Africa

R. M. Moutloali Institute for Nanotechnology and Water Sustainability, College of Science, Engineering and Technology, University of South Africa, Florida Science Campus Florida, Johannesburg, South Africa

Jonathan Tersur Orasugh Department of Chemical Sciences, University of Johannesburg, Doorfontein, Johannesburg, South Africa;
Centre for Nanostructures and Advanced Materials, DS1-CSIR Nanotechnology Innovation Centre, Council for Scientific and Industrial Research, Pretoria, South Africa

Sadanand Pandey Department of Chemistry, College of Natural Sciences, Yeungnam University, Gyeongsan, Gyeongbuk, Republic of Korea

Mercedes Guadalupe López Pérez Biotechnology and Biochemistry Department, Center for Research and Advanced Studies of the IPN (Cinvestav-IPN) Irapuato Unit, Mexico City, México

Gubbala V. Ramesh Department of Chemistry, Chaitanya Bharathi Institute of Technology (A), Gandipet, Hyderabad, Telangana, India

Suprakas Sinha Ray Department of Chemical Sciences, University of Johannesburg, Doorfontein, Johannesburg, South Africa;
Centre for Nanostructures and Advanced Materials, DS1-CSIR Nanotechnology Innovation Centre, Council for Scientific and Industrial Research, Pretoria, South Africa

N. Mahendar Reddy Department of Chemistry, Chaitanya Bharathi Institute of Technology (A), Gandipet, Hyderabad, Telangana, India

Gowri Priya Sakala Department of Chemistry, Indian Institute of Science Education and Research, Pune, Maharashtra, India

Soumen Sardar Department of Polymer Science and Technology, University of Calcutta, Kolkata, India

S. V. Sheen Mers Indian Institute of Technology, Chennai, India

Keneiloe Sikhwivhilu Advanced Materials Division, DSI/Mintek Nanotechnology Innovation Centre, Mintek, Randburg, Johannesburg, South Africa

Kiran Kumar Tadi Centre for Healthcare Advancement, Innovation and Research, Vellore Institute of Technology, Tamilnadu, India

Mohamed Zahouily Laboratory of Materials, Catalysis & Valorization of Natural Resources, FSTM, Hassan II University, Casablanca, Morocco;
MASCIR Foundation, VARENA Center, Rabat Design, Rabat, Morocco

Chapter 1
Nanocellulose-Graphene Oxide-Based Nanocomposite for Adsorptive Water Treatment

Jonathan Tersur Orasugh and Suprakas Sinha Ray

Abstract Hazardous contaminating impurities/toxins, such as poisonous metal particles and colors/dyes, are a significant reason for the toxicity of water bodies. These contaminations make an unfriendly impact on sea organisms and immobilize the compounds in plant life. Subsequently, this issue should be moderated as a disturbing natural danger leading to different unsafe sicknesses in humans. Moreover, several waterborne pathogenic microorganisms likewise cause irresistible infections. Numerous techniques are reportedly established to eliminate these toxins and undesirable microorganisms. Adsorptive treatment and/or exclusion of water toxins and microbial sanitization through different nanocellulose (NC)-graphene oxide (GO) nanocomposite (NGON) materials (adsorbents) are introduced in this chapter. As per available literature, these adsorbent materials have shown extraordinary outcomes for the adsorptive exclusion of water contaminants such as poisonous metal ions and colors/dyes along with the removal of aquatic germs, insecticides, etc. Besides, they have numerous other necessities, including ease of preparation, cheap, and eco-friendly, as green composite blends are handily worked, energy-economical, and fit for multifaceted uses. This chapter also focuses on discussing the technologies embraced to fabricate the aforementioned adsorbents, their performance-based response with regards to adsorption capacity (Q). Our article also presents an ephemeral summary of adsorption working principles like isotherms, adsorption affecting parameters, the kinetics, along with the thermodynamics of the adsorption phenomenon. Furthermore, it reconnoiters the current applications, issues of consideration, related to these NGON adsorbents along with future perspectives.

J. T. Orasugh (✉) · S. S. Ray
Department of Chemical Sciences, University of Johannesburg, Doorfontein, Johannesburg 2028, South Africa

Centre for Nanostructures and Advanced Materials, DS1-CSIR Nanotechnology Innovation Centre, Council for Scientific and Industrial Research, Pretoria 0001, South Africa

M. J. Hato and S. Sinha Ray (eds.), *Functional Polymer Nanocomposites for Wastewater Treatment*, Springer Series in Materials Science 323,
https://doi.org/10.1007/978-3-030-94995-2_1

1.1 Introduction

The humanoid developments towards suburbanization are causing quick expansion in a number of enterprises and varying rural procedural practices, especially agriculture; in this way, all kinds of related contamination such as air, soil, water, sound, electromagnetic, etc., have gained a significant boost. The utilization of cellulose especially in its nanometer form in diverse niches has gained prominence within the recent decades [1–91]. Though nanocellulose utilization in its virgin form or as composites/hybrids in diverse areas of environmental remediation purposes is still new. Nevertheless, the water bodies particularly affected are fresh water leading to worldwide fresh/clean water scarcity [84, 85]. This challenge is of concern more in developing countries seeing more than 3.4 million individuals who are mostly kids, are deceased annually because of the presence of diverse contaminants (such as diverse organic [26], inorganic [53], and biological impurities [47] in water [4, 14].

Industrial wastes primarily hold a high concentration of dyes, pesticides, toxic metals, and metal oxides which possess the tendency to assemble themselves into tissues within the food cycle chain, resulting in a serious threat to aquatic life and/or ecological disturbance. Even though these metals or some of their oxides are not degradable biologically, they remain in living tissues for a very long time, causing severe health challenges to both animal and human life [65]. In this regard, the predisposal treatment of industrial-based effluents is required to remove these contaminants, chiefly zinc (Zn), cadmium (Cd), copper (Cu), mercury (Hg), arsenic (As), lead (Pb), chromium (Cr), nickel (Ni), manganese (Mg), and so on [65], even as shown in Table 1.1, along with other poisonous contaminants including europium (Eu), uranium (U), titanium (Ti), etcetera [83]. For metropolitan contaminated water, a huge quantity of mercury has been reported, whereas coal-utilized power plants and refineries hold other heavy metals, along with a large quantity of Cd which releases from stabilizers, Cd–Ni power storage devices, phosphate fertilizers, along with pigments, while copper contamination comes from electronics waste, tanneries, and/or mining operations [4]; manganese release into the environment is from metal smelters, ceramics, and/or paints; also, the presence of zinc in effluents is from pesticides/insecticides, textiles, dyeing/pigments, electroplating, pharmaceuticals, cosmetics, galvanizing, brass & bronze, microelectronics, plastics, and/or paints industries; lead on the other hand is connected to wood preservatives, textiles, microelectronics, and plastics industries waste [1].

Pesticides such as a triazine (TZ)-based pesticides have been broadly adopted for agricultural practices in recent decades for weed control in diverse crops. Even though they assume an important part in the tilling of cereals, like rice and/or maize, their remains have posed a harmful source of contaminants to the ecosystem. Harmful pesticides residues present themselves as a potential hazard to humans and other animals, resulting in health challenges such as birth defects, cancers, hormone disorders, etc. [29]. Table 1.1 presents some pesticides, their sources, and posed a risk and also their permissible limits are presented in Fig. 1.1.

Table 1.1 Harmful dyes, metals, pesticides, and waterborne bacteria and their adverse effect

Category	Contaminant	Origin/source	Side effect(s)
Dyes	Basic Red-9	Industrial wastes	Carcinogenic, dermatitis, teratogenicity, histopathological effects
	Congo Red	Industrial wastes	May be carcinogenic, dermatitis, irritant to the eye, skin, mucus membrane, mutagenic, etc.
	Crystal Violet	Industrial wastes	Lethal to renal and respiratory system develops chemical cystitis, etc.
	Malachite Green	Industrial wastes	Extremely carcinogenic, histopathological effect, mitotic poisoning, mutagenic, teratogenic, etc.
	Methyl Blue	Industrial wastes	Causes hemolytic anemia, breast cancer, hyperbilirubinemia, respiratory challenges
	Rhodamine-8	Industrial wastes	Eyes irritant, carcinogenic to animals (both marine and land)
Heavy metal ions & oxides	As	Pesticides, Chemical wastes, Bi-products from mines,	Enzyme-inhibitor, Carcinogenic
	Be	Nuclear plants, space productions, coal plants, etc.	Poisonous, cancer-causing
	B	Industrial bi-products, cleansing agents, etc.	Deadly to florae and algae
	Cd	Industrial ejection, metal electroplating, Ni–Cd from batteries, etc.	One of the origins of high blood pressure, kidney disorder, anemia, illness, etc.
	Cr	Metal electroplating industries, mining, tanning, etc.	Cancer-causing

(continued)

Table 1.1 (continued)

Category	Contaminant	Origin/source	Side effect(s)
	Cu	Metal electroplating industries, mining, etc.	Deadly to florae and algae
	Fluorine (F)	Natural ecological sources, manufacturing bi-products	Causes bone impairment, dappled teeth
	Pb	Drains, crude oil, coal, mining, etc.	Causes anemia, kidney malfunction, Neurological disarrays
	Mn	Mining and manufacturing bi-product, the bacteriological act of Mn minerals of low-slung pH	Deadly to florae
	Hg	Mining and manufacturing bi-product, coal, etc.	Extremely deadly in its form as CH_3Hg^-, Hg^{2+}
	Molybdenum (Mo)	Natural and manufacturing surplus	Noxious to faunae
	Selenium (Se)	Natural and coal sources	Poisonous
	Zn	Metal coating companies, manufacturing waste	Poisonous to ecological plants
Insecticides/ pesticides	Atrazine	Agricultural weed control sprays	Cause endocrine disruption, hormonal disorder, fetotoxicity, skin irritant, an increased relative risk of ovarian neoplasia, can induce mammary tumors in rats, immunotoxicity, behavioral alterations
	Cyromazine	Agricultural weed control sprays	Causes serious irritation to the skin and eye irritation. It can also cause respiratory aggravation. It is harmful to oceanic life, presenting lasting impacts

(continued)

Table 1.1 (continued)

Category	Contaminant	Origin/source	Side effect(s)
	Hexazinone	Agricultural weed control sprays	The nervous system, immune system, endocrine function, development or reproduction, and carcinogenicity or mutagenicity
	Metribuzin	Agricultural weed control sprays	Central nervous system damage, kidney and liver damage, narcosis and labored breathing, deficiency or excess of the human growth hormone
	Prometon	Agricultural weed control sprays	Discreetly exasperating to the skin, eyes, and respiratory expanse, liver, and heart to animals
	Prometryn	Agricultural weed control sprays	Nausea, Sore throat, Respiratory, depression, Muscle weakness
	Simazine	Agricultural weed control sprays	Trouble in strolling, quake, seizures, loss of motion, cyanosis, eased back breath, miosis, stomach agony, looseness of the bowels, and impeded adrenal capacity, lower food admission, higher water consumption, incoordination, quakes, and shortcoming, harm to the testicles, kidneys, liver, and thyroid, unsettling influences in sperm creation, and gene mutations

(continued)

Table 1.1 (continued)

Category	Contaminant	Origin/source	Side effect(s)
	Desethylterbutilazine	Agricultural weed control sprays	Hormonal disorder, fetotoxicity, skin irritant, an increased relative risk of ovarian neoplasia, can induce mammary tumors in rats, immunotoxicity, behavioral alterations
	Terbuthylazine	Agricultural weed control sprays	Mildly to moderately irritating to the eyes and slightly irritating to the skin
Waterborne bacteria	Bacillus cereus		Vomiting, nausea, diarrhea, mucus
	Enterococcus faecalis		Shortness of breath, fever, bleeding gums, chest pain, diarrhea, fatigue, stiff neck, and abdominal pain
	Escherichia coli		Abdominal pain, watery diarrhea, intestinal toxin damage, nausea, vomiting, fever, and fatigue
	Pseudomonas aeruginosa		Dermatitis, gastrointestinal infection, soft tissue contamination, urinary expanse contagion, bone, and joint infection
	Salmonella typhimurium		Diarrhea, Vomiting, abdominal cramps, and fever
	Staphylococcus		Bloodstream, bone, and joint infections, pneumonia, scalded skin syndrome, toxic shock syndrome, etc.
	Shigella flexneri		Dysentery, drug resistance, joint pains, painful urination, virulence, and eye irritation

(continued)

Table 1.1 (continued)

Category	Contaminant	Origin/source	Side effect(s)
	Vibrio		Abdominal cramps, fever, nausea, decreased blood pressure, skin lesions, etc.

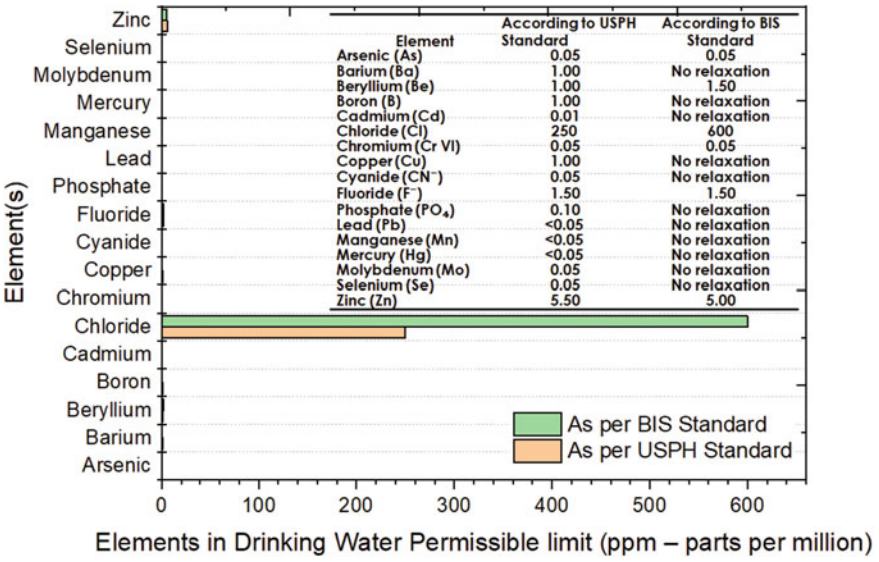

Fig. 1.1 Permissible limits of diverse toxic elements in consumable H_2O acceptable limit (ppm)

Additionally, synthetic dyes-based organic pollutants are primarily fabricated from multifaceted organic compounds containing azo bonds, which result in extremely oncogenic features. They are not usually biodegraded and/or unreactive to other chemicals [84]. Dyes are the most important constituent of agricultural, food technology, photo-electrochemical cells, light-harvesting arrays, textile, hair colorings, Kraft bleaching, paper/pulp, pharmaceuticals, tannery productions waste, dye/their intermediates, etc. [1, 4, 75, 84] In this manner, these ventures uncommonly add to water contamination with different manufactured coloring matter and make the water sullied. Therefore, unique physical, synthetic, and natural strategies have been advanced like oxidation, photocatalytic degradation [55], adsorption [84], substance precipitation, layer filtration, electrochemical treatment, ion exchange, coagulation & flocculation, flotation, and a number of biological techniques within the recent years to remediate the contaminated aquatic bodies. Amongst these approaches, the adsorption method is preeminent as an effective tool in water purification because of its facile functional phenomenon with great execution, magnificent decontamination,

and sustainable results properties. Further, adsorption measure has ended up being best for removal of heavy metals/metal-oxides, along with adsorptive removal of azo-based dyes known to be cancer-causing, a portion of the colors along with their antagonistic impacts are displayed in Table 1.1. The afore-conversed inorganic and organic pollutants can readily remove via diverse commercialized practices and more efficiently by adsorption technique; although waterborne pathogens remain a challenge, a number of common waterborne bacteria are presented in Table 1.1. On the contrary, conventional water treatment approaches such as adsorption techniques are limited in removing all of the wastewater impurities (pathogens, organic, and inorganic). Whenever any one of the above-conversed methods is adopted for dyes, metal ions, water-borne microorganisms, etc. removal. remain and/or vice-versa, owning to the fact that no single approach eliminates the entire category (three major) contaminations. Nevertheless, several pieces of literature are available with regards to diverse cellulose (CEL) graphene-based adsorbent materials, and some of them even demonstrate the excellent potential for antimicrobial activities [24, 52, 57, 64, 70, 84, 85]. Therefore, scientists are currently putting in predetermined efforts towards the development of suitable multifunctional CEL graphene-based advanced materials like adsorbents, photocatalyst, membranes, etcetera, specifically nanomaterials based [52, 64], which are capable of removing all kinds of wastewater contaminants.

This chapter focuses on discussing the technologies adopted for the preparation of the aforementioned adsorbent materials and their response with regard to adsorption capacity (*Q)*. The present study also presents an ephemeral summary of adsorption working principles like isotherms, adsorption affecting parameters, the kinetics, or thermodynamics of the adsorption phenomenon. Furthermore, it reconnoiters the current applications, challenges, and/or barriers associated with these NGON adsorbents along with future perspectives.

The uniqueness of this chapter article is its focus on multifunctional CEL graphene-based synthesized materials significant for wastewater remediation. The foremost measurable intimidate factor for these systems' performance is the adsorptive exclusion of harmful ecological contaminants from H_2O along with the deactivation of waterborne germs. A careful clarification of resistances in the existing adsorption systems and required forthcoming lightening is likewise embodied in this paper. This clever component focuses on excellent qualities for future improvements in the high-level engineered CEL graphene-based materials for wastewater remediation, which are depicted deliberately in the current chapter.

1.2 Water Treatment and Approaches

Among the diverse wastewater contaminants, manufactured dyes are the entities majorly ejected in enormous amounts yearly. These dyes are chiefly organic compounds made up of multifaceted aromatic compounds encompassing two main components: (I) The portion that imparts color referred to as chromophores (such as

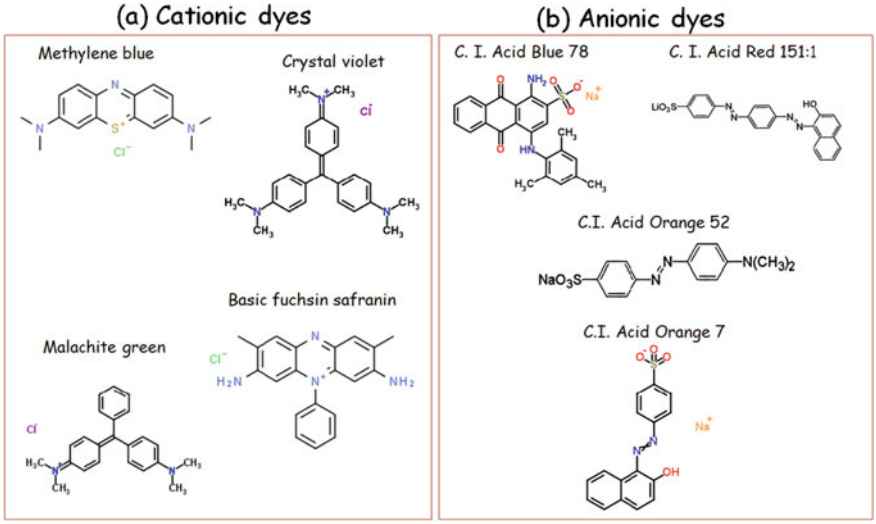

Fig. 1.2 Structural (molecular) representation of a variety of conventional cationic (**a**) and anionic (**b**)

–OH, $–NH_2$, $–NR_2$, –NHR, and –COOH) and auxochromes (like $–NO_2$, –NO, $–N_2$, etc.).

Chromophores are the basic entity of all categories of dyes like reactive, azo, basic, vat, acidic, and disperse dyes [57]. The molecular structures of a variety of conventional anionic and cationic dyes are shown in Fig. 1.2. These colored materials have diverse applications in several industries, including food, printing, paper, plastic, textiles, cosmetics, etc. About 7 × 105 tons and ~ 10,000 categories of dyes and/or pigments used by industrial dyeing and printing processes have been reported [57]. ≥ 10,000 tons of colorants are expended worldwide, each year for which ~10 − 15% are released together with industrial effluents to diverse aquatic environments [57]. The released dyes are known to be nondegradable, meaning they can't be degraded even in sludge pretreatment units, owning to their extremely extraordinary solubility in H_2O, making them hard to be remediated via conventional approaches. Furthermore, dyes used in textile chemical processing departments are hypothetically carcinogenic and genotoxic, triggering environment degradation and diverse lethal ailments in animals or humans [5–7]. These textile dyes do as well compromise the inherent value of aquatic environments by raising BOD and COD (biochemical and chemical oxygen demand); hence, hindering photosynthesis, plant growth, aquatic food-sequence/cycle alteration, and/or resulting in bio-obduracy or bio-accumulation [57], which of great concern globally.

A broad range of biological/biochemical and physicochemical techniques (Fig. 1.3), such as coagulation [55], flocculation [55], photocatalytic degradation [55], chemical electrolysis [57], biodegradation [34], oxidation [55], membrane separation (reverse osmosis (RO) and/or filtration) [55, 57], adsorption [5, 6, 84], magnetic

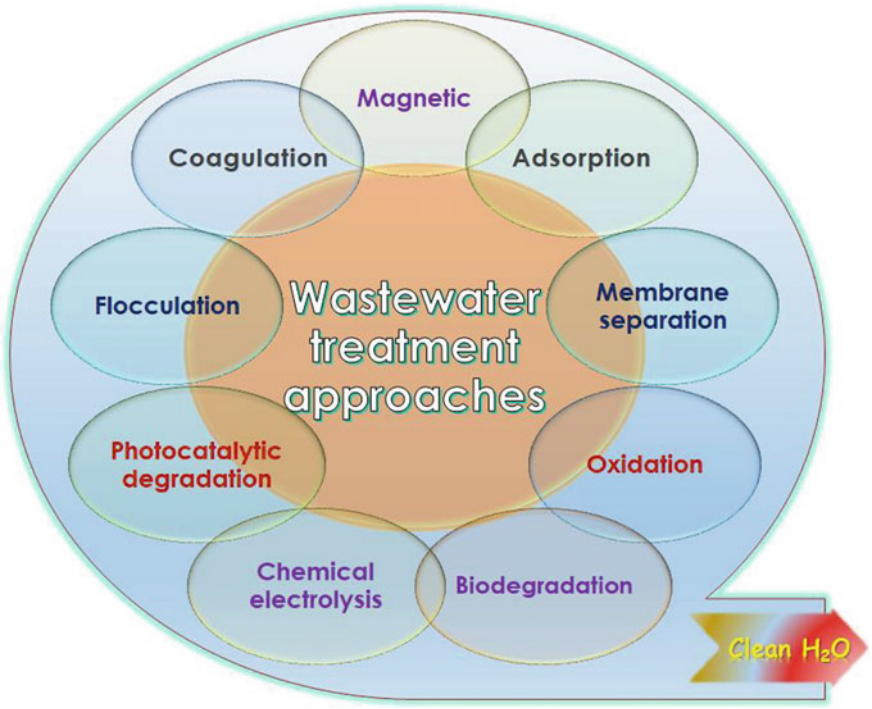

Fig. 1.3 Selected wastewater treatment approaches

[13], etc., is reportedly used for the treatment of waste H_2O. Nevertheless, expensive raw materials and challenges faced in design and/or separation constrain the adoption of the majority of these approaches for extensive applications [57]. Most of these wastewater remediation techniques are ineffective singly to perform at lesser noxious waste percentages. However, certain approaches demand for a high amount of chemicals in addition to input energy plus the generation of an enormous quantity of deadly waste products. Certainly, the adsorption technique is comparatively the most commonly adopted technique due to its cheap, facile, or benign process, ecofriendly approach, and excellent efficacy, along with its distinctive property the recyclability and reuse of the adsorbent after numerous renaissance sequences [84].

1.2.1 Adsorption Wastewater Treatment

1.2.1.1 Adsorption: The Working Notion

Adsorption is a physicochemical phenomenon where the adsorbate matter transfers itself in the form of liquid and/or gas against the adsorbent material surface.

Adsorption phenomenon involves four steps: bulk, film/external mass diffusion, pore/intraparticle diffusion, combined lastly adsorption via physical/chemical reactions. Here, even distributive dispersion of adsorbate or adsorbent limits bulk diffusion, making it negligible. Hence, adsorptive contaminants removal kinetic reaction is controlled through film/pore diffusion, though the sheet(s) surface area fashioned with liquid/its concentration unswervingly impacts diffusion of the film for the reason that liquid concentration and surface area possess a direct relationship with the film diffusion [12]. Conversely, the $\sqrt{t}$ or $t^{0.5}$ (adsorption time square root) presents a direct relationship with the diffusion through the pores for metal oxides, taking into account that this process is affected by the film-based diffusion [12, 84].

1.2.1.2 Adsorption Isotherms

The main process, i.e., adsorption equilibrium, if not known, makes it challenging to comprehend the adsorption phenomenon precisely. The point where a given molecule's adsorption and desorption rate are equal is referred to as adsorption equilibrium [84]. Conversely, there are three types of adsorption equipoise, namely: (i) Adsorption isotherm, (ii) Adsorption isostere, and (iii) Adsorption isobar: furthermore, equilibrium adsorption is characteristically reliant upon the concept of adsorption isotherm, discussed as at steady temperature, the state of equilibrium between the concentration in fluid-phase in bulk as well as adsorbed entities amount. The adsorption isotherms kinds existing include Brunauer–Emmett–Teller (BET), Freundlich, Langmuir, and Temkin, which are typically adopted as per the aforementioned objective [84]. The adsorption approach has been reportedly used in CEL graphene (nano)composites for the remediation of water [84].

1.2.2 Filtration Wastewater Treatment

Filtration technology adoption for wastewater treatment by membrane technology relics the utmost energy-efficient approach aimed at separating pollutants (μm-sized adsorbates even to the Å-sized hydrous ions) from wastewater [59]. Nevertheless, the current conventional membrane systems, including comparatively high-priced synthetic substances, are often non-sustainable for the neediest communities in the societies of the world. Emerging bioderived NC-based membrane systems centered upon nanoscale-CEL fibres that could be isolated from nearly all lignocellulosic biomaterials are the solution to the challenge(s) with their synthetic counterparts. It's plausible that NC-based membranes prepared from low-cost, abundantly available, and sustainable resources could reduce the cost of filtration-based membrane separation, seeing these membranes provide the capability of removing a broad variety of contaminants in a single phase by size segregation seizing or adsorption. These bioderived NC-based membrane technology couldn't only suit solving consumable

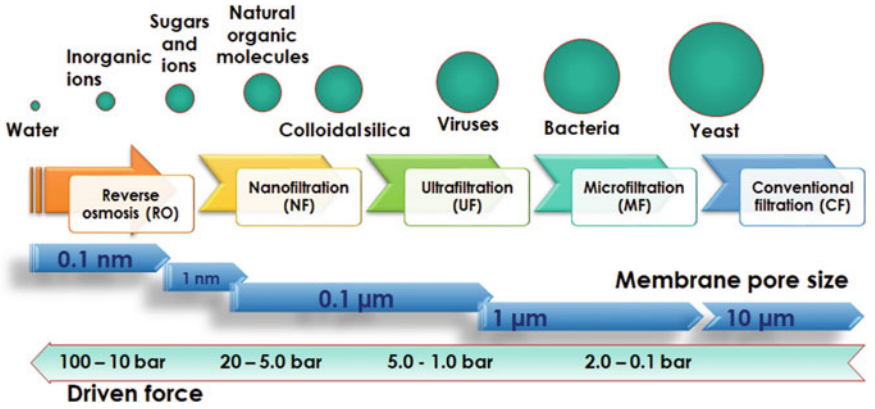

Fig. 1.4 Classification of pressure-driven membrane filtration, pore size, and pressure relationship

H_2O challenges globally, but it could also present a facile and novel cheap platform for diverse pressure-driven filtration approaches, such as nanofiltration (NFL), microfiltration (MF), ultrafiltration (UF), RO, etc. [59].

Pressure-driven filtration (filter/membrane) technologies, from MF to RO, continue to be the most energy-efficient routes for water remediation. The working phenomenon of these separation techniques is uncomplicated: characteristically, pollutants such as molecules/metal ions transit certainly from high concentration regions to regions of low-slung concentration, and so with the application of external pressure, these contaminants are made to then flow from lower concentration regions to higher concentration regions; the approach could be used in water remediation. The cataloging of pressure-driven filtration-membrane approaches, their pore sizes along with their correlated pressure is presented in Fig. 1.4. Commonly, small pore-sized filtration membranes demand for very high pressure for effective performance [59]. Running a membrane filtration set-up utilizing higher pressure demands an unfailing energy supply (such as electrical/mechanical or both (hybrid)) along with the usage of robust/strong equipment (like pump equipped for high pressure). These collective prerequisites are regularly past the range of the neediest neighborhoods that require cheap and clean drinking water at the maximum. Nevertheless, a pressure-driven system is gravity-driven. It could be very cheap and is facile to maintain, making it exceptionally appropriate for even the poorest communities living below standard. The equivalent membrane filtration operation that is gravity-driven is microfiltration (Fig. 1.4). This is because MF membranes driven by gravity have the smallest average pore size for water, as it remains the major energy-efficient approach towards wastewater remediation; seeing this wastewater purification principle is straightforward.

The combined prerequisites are frequently past the range of the least fortunate groups that need minimal expenditure, safe water for drinking. In any case, a single pressure system, driven by gravity, can have a pitiful expense and isn't difficult to keep up with, making it especially appropriate for helpless communities living

off the lattice. A comparable filtration system that is gravity-driven is microfiltration (Fig. 8.4). This is on the grounds that gravity-driven-MF layers have the littlest average size of the pore for three layers to incorporate (1) non-woven fabric (because of μm-size strands) which could be viewed as a low-end MF film, (2) a permeable ply (formed with phase reversal technique) which could be utilized straightforwardly as a UF film, along with (3) a thickly crosslinked hindrance layer (created by the interfacial polymerization strategy) that delivers the layer helpful for NF and RO systems. The necessity of every part ply is unique: the non-woven fabric ply should be solid to give in general mechanical strength, and as a rule, has the most noteworthy porosity (60–70%); the center permeable ply should possess an even pore dispersion on the surface of the layer (as a supportive layer or the hindrance layer), having a moderately lower porosity; the top boundary layer (regularly an interfacial polymerized cross-connected polyamide grid) has the littlest pore size conveyance just as the least porosity.

1.2.3 Catalytic Wastewater Treatment

The drive towards providing clean water for personal and manufacturing use has resulted in the emergence of several water purification approaches, for which catalytic wastewater purification technique is of great prominence [2, 34, 55]. There is limited literature in this niche regarding NC-GO-based nanocomposites, but we will discuss a few reports.

It has been established by a group of researchers that, in an event where CEL was converted to NC, adsorption efficiency was enhanced as a result of augmented surface area, amount of accessible functional groups/moieties, and crystal-like nature. Thereafter self-cleaning properties were imparted to the NC via incorporating substances that have photo catalytic degradation properties. GO various oxygen function moieties like –OH, phenol, and epoxy surface groups largely at the basal plane along with the R–COOH groups at the boundaries were utilized as reinforcing fillers in the fabrication of nanocomposites with diverse polymeric matrices for the adsorptive exclusion of a number of noxious wastes from effluents, along with nonselective photocatalytic degradation of pollutants [2]. This report proved NC-GO-based nanocomposites to be an effective material for multifunctional adsorbent and/or photocatalytic material.

A novel photocatalyst; nano ZnO/GO/NC nanocomposite aimed at effectual adsorptive take-up followed by photodegradation of ciprofloxacin (CF) (known antibiotic extensively utilized in fowl farming) has been conversed. Self-cleansing characteristics in CEL were also achieved here by introducing nano ZnO incorporated GO into the NC matrix. ZnO incorporation in GO tuned the subsequent band gap to 2.4 eV, and subsequently nanocomposite materialization with NCs, the band gap was further boosted to 2.8 eV, within the UV visible region. Hence, CF degradation (due to electron–hole interaction) was achieved under visible light. The stepwise modification of the synthesis of ZnO-GO/NC resulted in good properties

for pore radius, pore-volume, and surface area, of ~12.5 nm, ~0.026 mL/g, and ~12.68 m^2/g correspondingly. These authors reported that the optimum pH for the effective performance of the nanocomposite was 5.5 at a ZnO/GO/NC dosage of 2.0 g/L, and the attained equilibrium was at ~120 min, while adsorption of the drug followed the second-order kinetics. Their report established that the model best-fitted was Sips isotherm explaining the kind of interface between CF and ZnO/GO/NC. Also, they showed that CF degradation followed first-order kinetics while the degradation process optimal pH was reported as 6.0, and 98.0% maximum degradation efficiency was achieved. The recyclability of the ZnO/GO/NC adsorbate after five successive cycles indicates its potential for removing and degrading CF from the aquatic/wastewater environment [2].

Also, in another study, successful in-situ synthesis of an innovative 3D-photocatalyst comprising of Cu_2O/TiO_2 loaded CNF/rGO via simplistic hydrothermal process and freeze-drying. This 3D formed macro-structure provides the template for anchoring of Cu_2O and TiO_2 while also presenting an efficient pathway for enhanced electron transference and, consequently, the photocatalytic activity of the nanocomposite. Their findings established that the Cu_2O and TiO_2 were uniformly included in the aerogel network structure, resulting in a nanocomposite with a large surface area having highly exposed actives sites. In comparison to unembellished rGH, CNF/ rGH, Cu_2O/CNF/rGH, and TiO_2/CNF/rGH, the Cu_2O/TiO_2/CNF/rGH displayed enhanced photocatalytic activity for the degradation of methyl orange (MO) dye. Their report revealed that enhancement in the photoactivity was credited to charge transfer and electron–hole parting from the synergistic influence of Cu_2O/TiO_2 attached to CNF/rGH. The activity on Staphylococcus aureus and Escherichia coli was also studied, revealing the synergistic influence of the CNF/rGH framework anchored Cu_2O/TiO_2 resulting in excellent anti-bacterial activity [87].

1.2.4 Other Wastewater Treatment Approaches

Other wastewater purification approaches are well known, but the ones used in NC-GO-based nanocomposites materials are solvent-based precipitation and coagulation, distillation, silica gel, ion-exchange/Ion exchange resins, etc.

1.3 Nanocellulose

Within the last few decades, nanocellulose (NC) (Nanostructured CEL) has been proven to be one of the most prominent green/ecofriendly nanomaterials of modern times. These adsorption systems gain of growing attention from researchers and industrialists is due to their attractive and excellent characteristics like sustainability,

abundance, high aspect ratio, excellent mechanical properties, light weight, cytocompatibility, biodegradability, and biocompatibility [24, 66]. The rich functional hydroxyl groups on the surface of NC permit a wide range of functionalization through diverse chemical reactions, leading to the development of various materials having tunable attributes [40, 41, 43–45, 84]. This section will converse on NC, starting from its bioderived sources like plants and animals.

1.3.1 Introduction

The word "Cellulose" was coins from the French word "cellule," signifying a living cell in addition to glucose, initiated by an expert French scientist so-called Anselme Payen, in 1838 [48]. Cellulose is one of the most plentifully accessible biomaterials and is highly involved in research studies on earth. As depicted in Fig. 1.5, CEL is semi-crystalline; hence it possesses crystalline locale and amorphous expanses of diverse kinds relying upon the CEL source [24, 41, 43–45, 52]. CEL is categorized into four unique classes of polymorphs, CEL I, II, III, and IV (Table 1.1) [40, 52].

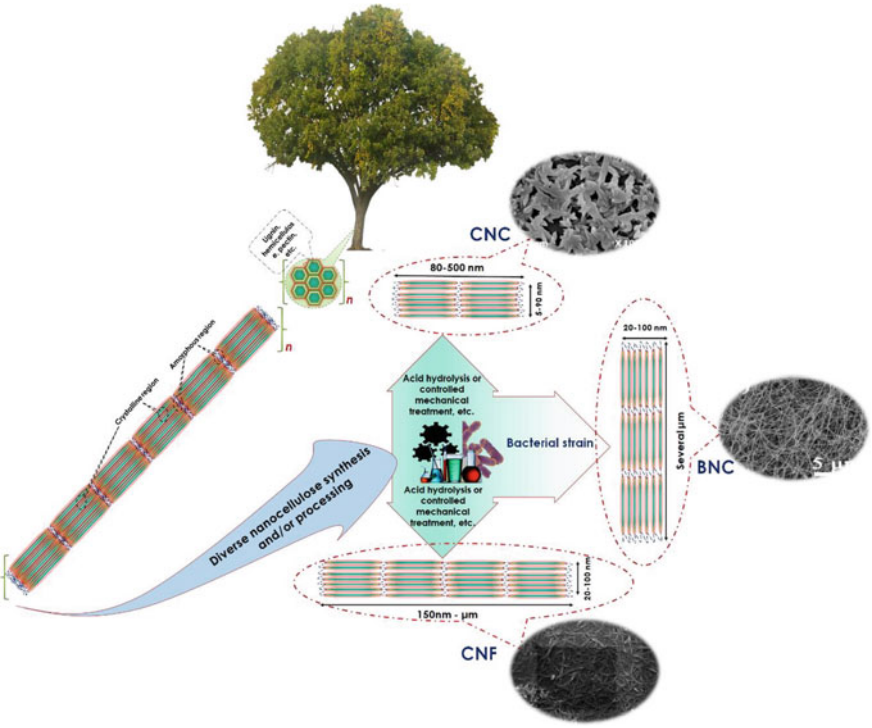

Fig. 1.5 From CEL to nanostructured CEL

At present, CEL-based nanomaterials are a rising category of nanomaterials with such a large amount of appealing properties: that is isolated from property crude raw materials (CEL and/or lignocellulose like jute, hemp, sisal, cotton, wood, etc.) at a comparatively low cost with certain attractive attributes like—biodegradability, biocompatibility, phenomenal mechanical strength, high water absorption ability, and high surface area, etc. NCs have been reconnoitered for their numerous probable uses in the polymer (nano)composites for adsorption, food additives, tin films, aerogels, wound dressings, tissue scaffolding, sustained drug-delivery, reinforcement in hydrogels, rheology modifiers in hybrid films, artificial blood vessels, EMI shields, etc. NC can be defined as a CEL material having dimensions somewhere around one of its measurements in a nano range (≤100 nm) [24, 40, 41, 43, 44, 52].

1.3.2 Structure, Source-Based Overview, and Nomenclature with Categories

Cellulose "$(C_6H_{10}O_5)n$" is a bio-linear polymer made up of β-Dglucopyranose entities joined by β-1,4 glycosidic bonds (Fig. 1.5) [40, 52]. In the natural world, CEL doesn't occur as a discrete entity/compound but rather an assemblage of single molecular chains [24, 48, 52]. In the end, several individual CEL chains agglomerate together to form fibrils/microfibrils owning to the stout intramolecular or intermolecular H-bonds, that provide the CEL molecular chain(s) with a highly fast structure [24, 52, 84], which further results in the formation of a crystal-like structure due to the strong H-bonding because of the –OH functional groups. The molecular structure of CEL is made of three –OH groups: the primary –OH group at its C-6 position or the secondary –OH group at C-2 and at C-3 being all hydrophilic [52]. Nevertheless, CEL is insoluble in water and has a large number of solvents. Owing to cellulose's large number of hydroxyl functional groups on its surface, which binds to diverse materials like dyes, pharmaceuticals, and metal ions, making it a suitable material for the manufacture of adsorbent materials [84] (Table 1.2).

Table 1.2 Diverse crystalline CEL polymorphs

Nanocellulose form	Preparation approach/process	Citations
CEL I/native CEL	Synthesized naturally from bacteria, plants, etc.	[43, 52, 59, 91]
CEL II	Regeneration or mercerization of CEL I -dissolving CEL I in a solvent/swelling it in an acidic/basic solution	[59, 91]
CEL III	Treating CEL I or II with ammonia solution	[52, 91]
CEL IV	High temperature (up to 260 °C) treatment of CEL III in glycerol	[52, 91]

1.3.3 Preparation Approaches for NCs

Nanocellulose is prepared by the fragmentation of native CEL from the lignocellulose biomasses by chemical, mechanical, and biological methods (Fig. 1.6) [4–6, 12, 14, 24, 26, 29, 34, 40, 41, 43–45, 47, 48, 52, 55, 57, 59, 64, 65, 68, 70, 72, 84, 85]. These techniques could be adopted separately or in an amalgamated form in order to achieve the predetermined morphology as well as the structure [43, 52].

NCs' seclusion approach can be realized by either a biosynthesis-based bottom-up or top-down approach by disintegrating lignocellulose plant biomasses [43, 52]. With regards to their seclusion techniques, NC-based materials are categorized into three core categories as presented in Table 1.3: CEL nanocrystals/whiskers/cellulose nanoparticles (CNCs), cellulose nano-fibrils(CNFs)/microfibrillated CEL /nanofibrillated cellulose (CNFs), and bacterial CEL nanofibres (BCNF) [41, 43, 44, 52].

1.3.3.1 Cellulose Nanocrystals/Whiskers/Cellulose Nanoparticles (CNCs)

CNCs are mainly gotten from lignocellulosic biomass like jute, sisal, wood, cotton fibers, etc. through acid-based hydrolysis at well-ordered factors of time, temperature, along with acid:CEL fibers ratio [41, 43, 44, 52]. The extraction of CNCs involves the use of concentrated mineral acids like nitric acid [44], sulfuric acid [44], etc., usually used in the hydrolysis process to eliminate the amorphous expanse containing hemicellulose, pectin, lignin, and other noncellulosic entities [43, 52]. The

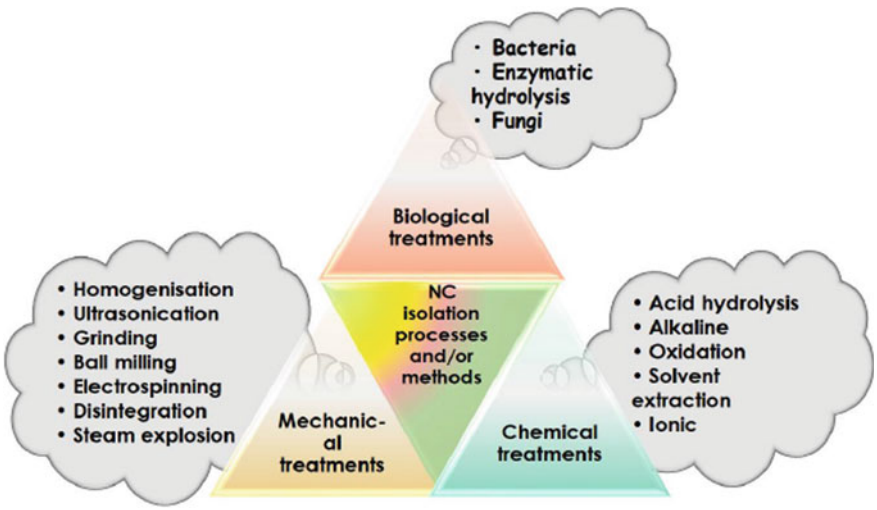

Fig. 1.6 Nanocellulose (NC) isolation processes

Table 1.3 Categories of NCs as per synthesis processes, source, and properties

NCs type	Raw material source	Preparation approach	Properties			References
			Diameter	Length	Architecture	
BC	Bacteria, fungi	Bacterial strain	20–100 nm	Several μm	3D fibrous network	[15, 27, 32, 35, 49, 50, 76]
CNF		Chemical and mechanical techniques (Homogenization/cryo-crushing/steam explosion/grinding etc..)	20–100 nm	150 nm-μm	3D fibrous network	[17, 40, 42, 52, 56]
CNC		Chemical and mechanical techniques	5–90	80–500	Rice/rod-like shaped	[40, 43, 44, 45]

results of sulfonated CNCs are highly crystalline rice/rod-shaped/needle-like shaped nanocellulose (1–90 nm) coupled with a lengthwise dimension of not many100 nm as per CEL derived-source [43–45, 52]. During the acid treatment, the generated hydronium ions "H_3O^+" penetrate the CEL's amorphous zone, aiding the 1,4-glycosidic links cleavage in the CEL structural series and disintegration of the solid inter/intramolecular CEL chains hydrogen bonding network [52]. The CNCs produced using sulfuric acid are proven to possess good thermal stability properties owning to sulfate ester anchorage onto their planes [44]. CNCs also display several exceptional characteristics like high crystallinity index, high strength, along with enormous surface area [43–45].

1.3.3.2 Microfibrillated Cellulose/Cellulose Nanofibrils/Nanofibres (MFCs/CNFs)

MFCs/CNFs are secluded by means of the mechanical fragmentation of nonmodified, modified, and/or well-ordered chemically, enzymatically, and solvent treated CEL fibers [17, 40, 42]. The procedure of preparing MFCs/CNFs mechanically normally encompasses adopting high shear forces/ultrasound like grinding, homogenization, ball milling, ultrasonication, which requires higher consumption of energy along with the involvement of diverse kinds of apparatus along with tedious processes which are expensive [25]. CNFs possess <100 nm along with lengthwise dimensions ranging from hundreds of nm to μm.

1.3.3.3 Bacterial Nanocellulose Fibers (BNCFs)

BNCFs are prepared using aerobic bacteria as extracellular polyose sheath via a bottom-up nanomaterials (NCs) synthesis, which results in 3D networked NFs [32, 49, 52]. Even though bacteria (BC)-based CEL parades similar molecular formulae like plant-derived NCs, it possesses an exceptional 3D micro and nano-porous structural network with high water content (≥90%), high crystallinity (70 ≥ 80%), high purity, a high degree of polymerization, as well as high warm and mechanical dependability [32, 49, 52]; conversely, it is unattractive with regards to economic considerations because of its extremely expensive carbon source.

1.4 Graphene Oxide/Graphite Oxide

Graphene oxide/graphite oxide (GO/GiO) is the oxidized kind of graphene/graphite, which is a recognized raw material for the preparation of reduced GO (rGO), GO/rGO-based composites/hybrids, along with chemically functionalized graphene or its oxides [35, 49, 50, 55, 57, 64, 70, 80, 84, 85, 72]. GO containing oxygen

functional entities enable its interface with several chemical groups through H-bonds, covalent bonds, etc. The additional forces of collaboration, like van der Waals links, π-π interactions, along with ionic interfaces, promotes the noncovalent graphene/graphite, rGO, and GO functionalization [35, 49, 50, 55, 57, 64, 70, 80, 84, 85, 72]. Graphene/ GiO exhibits abundantly available oxygen-containing functional groups like hydroxyl, ether, carbonyl, phenolic, epoxide, and/or –COOH groups [35, 49, 50, 55, 57, 64, 70, 72, 78, 80, 81, 83–85, 90], among which, several hydroxyl, epoxide and ether surface groups are positioned along its basal plane, while the carboxylic functional units are located on graphene/GiO sheets edges [35, 49, 50, 55, 57, 64, 70, 72, 78, 80, 81, 83–85, 90]. GO's chemical reactivity enables its potential for various applications, including adsorption, anticancer treatment, paints, adhesives, bioimaging, lubrication, etc. In this section, the chemical as well as structural characteristics of GO or rGO, and their functionalization, chemically by diverse chemical methods are critically reviewed.

1.4.1 Preparation Approaches for Graphite/Graphene Oxide

Severe oxidation of graphitic materials like graphite powder results in the materialization of oxidized graphite, also known as GiO [12]. The drawn-out interlamellar dispersing in the GiO in light of oxygen functionalities on the basal plane along with entombed water particles enables the adjacent splitting of GiO also with the help of sonication and results in the formation of GO. GiO was found a whole lot sooner, around 1859, compared to graphene, around 2004; the fundamental 1st testimony by the British physicist B. C. Brodie portrayed the fabrication of GiO through oxidation of the graphitic materials by the use of fuming HNO_3 acid and $KClO_3$ as the oxidizing reagent/agent [8]. The author reported the ratio of C:H:O for the prepared GiO as 61.04:1.85:37.11. Staudenmaier has conversed an enhanced oxidation approach by adding a small amount of potassium chlorate. Additional oxidation was executed by acidifying the formulation with concentrated H_2SO_4 [61]. These methodologies were viewed as risky and tedious cycles. In 1958, Hummers and Offerman fostered a quick and moderately more secure strategy for setting up the GiO by reacting graphitic powder with an admixture of H_2SO_4, $KMnO_4$, and $NaNO_3$ (anhydrous) [21]. The Hummers' approaches avoid the utilization of profoundly destructive raging nitric corrosive. The utilization of $KMnO_4$ and $NaNO_3$ admixture resulted in oxygen-rich kind GiO. Afterward, Tour et al. built upon Hummers' technique to boost the oxidation process efficacy. In Tours' method, $NaNO_3$ was excluded, the quantity of $KMnO_4$ was upraised, also, oxidation response was completed in a combination of H_2SO_4/phosphoric acid (9:1 proportion) to manage the cost of oxidizing graphite contrasted with Hummers' approach [21]. Developments over the diverse preparation approaches for GiO are being sought after constantly to yield powerful other options. The GiO is a non-stoichiometric compound, its structure (chemical) as well as composition is principally governed by its synthesis procedure, oxidizing agents' utilization, response factors, along with crude graphite antecedent.

Essentially, there exists no substantial chemical disparity between GiO and GO [8, 10, 20, 21, 61, 84]. GiO is known to be the podium material used in the synthesis of GO via exfoliation. Fundamentally, GO comprises of a reduced number of graphitic carbon lamellae (max 10). In contrast, the GiO has a limitless/endless number of graphitic carbon lamellae having extended interlamellar separating, driven by plentiful oxygen-containing functional groups along its plane parallel to the lateral or horizontal axis and the caught water atoms through the H-holding organization [24, 28]. The GiO arranged by factor oxidation courses as in Fig. 1.7 is shed in the water or other solvents (polar) with the help of ultrasonication and managing the cost of the GO. Sonication, shower sonication, or potentially test sonication, has been grounded and extensively utilized methodology for the peeling of GiO. All things considered, it prompts some underlying breaking in the lamellae of GO. The extent of oxygen-containing functional groups in GiO, ultrasonication standard and process period, ultrasonic recurrence, along with the energy administered for the peeling greatly determine the nature of the consequent GO.

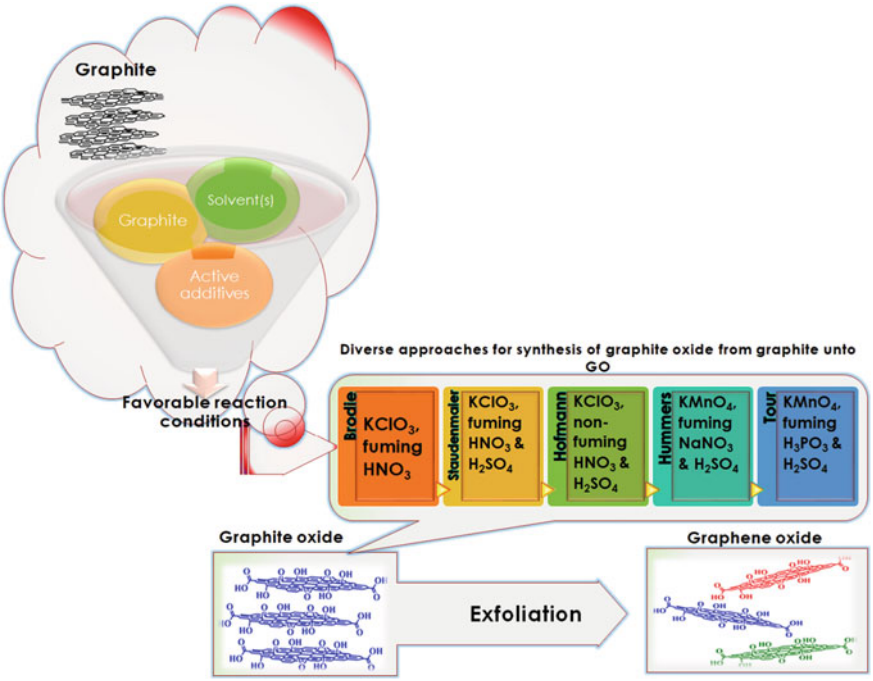

Fig. 1.7 Diverse chemical techniques towards GiO synthesis from graphite via exfoliation unto GO

1.4.2 Structural Properties of GiO/GO

Distinct from graphene, GO is the architecturally altered sheets of sp^2 C in a honeycomb framework/assembly as well as a mix of abundant sp^3 C because of the oxygen-containing functional groups. The GO lamellae (atomic-thick) are interconnected together via a 6 to 9 Å interlamellar spacing. The existence of oxygen-containing functional groups on the plane parallel to the lateral or horizontal axis and entrapped H_2O iotas through hydrogen interface expands GO interlamellae layout. Hence, the interlamellae gaps in GO being 6–9 Å is considered to be ominously higher considering the fact that graphene interlamellar spacing is 3.34 Å. GOs' chemical architecture is as a result been a subject of significant debate owing to the extensive level of structural flaws, non-stoichiometric arrangement, the disparity in oxygen-containing functional groups, along with inconsistency in GO preparation sequences, it remains a challenge. Thus, numerous structural (chemical) models of GiO and/or GO are postulated within the past 80 years [16, 18, 39, 54, 58, 63]. The Hofmann, Ruess, Scholz-Boehm, Nakajima-Matsuo, Lerf-Klinowski, Dekany, and Ajayan models are the much-considered models for GO structure (Fig. 1.8).

1.4.2.1 Hofmann Model

GiO's first model was projected by Hofmann and Holst in the year 1939 for the structure containing repeating units of 1,2-epoxides on the entire sp^2-hybridized plane parallel to the lateral or horizontal axis of graphene (Fig. 1.8a) [69].

1.4.2.2 Ruess Model

Ruess proposed the second model of GiO in the year 1946 for the structure containing 1,3-epoxide and –OH groups on the whole sp^3-hybridized plane parallel to the lateral or horizontal axis (Fig. 1.8b) [54].

1.4.2.3 Scholz-Boehm Model

In 1969, Scholz and Boehm postulated the third structural model for GiO, where the structure architecture was prepared of only –OH and ketone groups as depicted in Fig. 1.8c [58].

1.4.2.4 Nakajima-Matsuo Model

Again, Nakajima and Matsuo, in 1969, proposed the fourth model structure of GiO, which resembled graphite intercalation compound as shown in Fig. 1.8d [39]. The

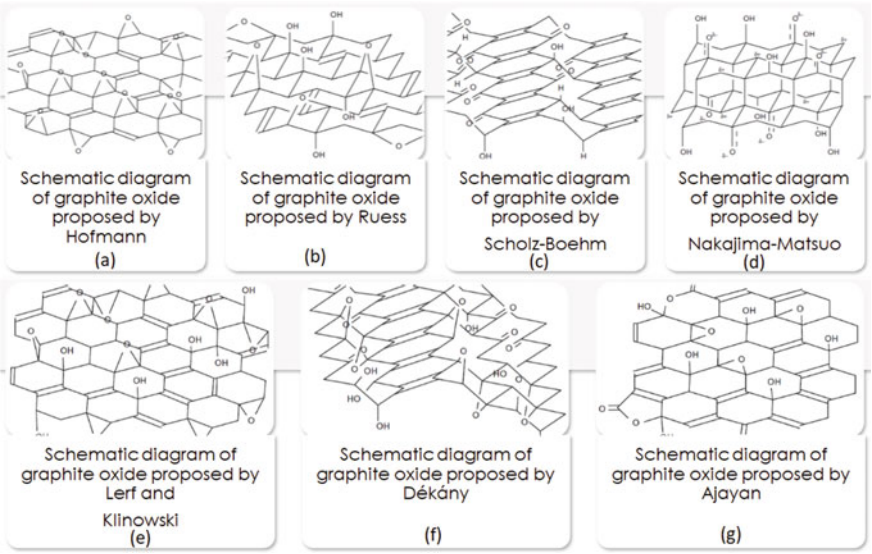

Fig. 1.8 GiO structural models: **a** Hofmann model, **b** Ruess model, **c** Scholz-Boehm model, **d** Nakajima-Mastsuo model, **e** Lerf-Klinowski model, **f** Dekany model, and **g** Ajayan model

GiO models recommended by Hofmann, Ruess, Scholz-Boehm, and Nakajima-Matsuo were mostly derived with regards to the compositions (elemental), chemical reactions, and XRD (X-ray diffraction) results.

1.4.2.5 Lerf-Klinowski Model

Lerf and Klinowski, later in 1998, proposed the fifth model of GiO, derived from NMR (nuclear magnetic resonance). The postulated structure (chemical) of GiO consists of two regions, that is, aromatic expanses having un-oxidized benzene rings as well as regions comprising 6-membered aliphatic rings (Fig. 1.8e) [28].

1.4.2.6 Dékány Model

Dékány proposed the sixth structural model of GiO in 2006, as derived from NMR, XRD, XPS (X-ray photoelectron spectroscopy), FTIR (Fourier transform infrared spectroscopy), TEM (transmission electron microscopy), ESR (electron spin resonance), and elemental analysis. The structure of GiO was proposed to be made of two diverse domains having trans-structured cyclohexane linked chairs along with ridged hexagonal ribbons. These trans-linked cyclohexane chairs were made of 1,3-epoxide and tertiary hydroxyl functionalities, whereas the corrugated hexagonal ribbons were occupied with cyclic ketones and quinones. Additional phenolic groups

were presented into the projected structural model by Dékány to validate the acidity of GiO (Fig. 1.8f) [63].

1.4.2.7 Ajayan Model

The seventh structural model proposed for GiO was by Ajayan in 2009 with relative ratios of functional groups, 115 (hydroxyl and epoxide):3(lactol O–C–O): 63(graphitic sp^2 carbon):10(lactol + ester + acid carbonyl):9(ketone carbonyl) as depicted in Fig. 1.8g [18].

1.4.2.8 Tour Model

The most recent GiO model was referred to as the dynamic structure model by Tour in 2012. As per extensive research work carried out by Tour, GiO exists as a dynamic structure with a certain set of functional groups but persistently changes in the company of non-aqueous solvent seeing GO possess a peculiar property of high acidity in its aqueous solutions, which is problematic to agrees with the existing models and its ability to reduce under strongly alkaline conditions in the absence of a reducing agent [16].

The oxidation conditions principally control the dissemination and plenitude of oxygen functional groups in the GiO. The GiO or potentially GO display magnificent dispersibility in water, and it is credited to high extremity and arrangement of H-bonding by oxygen-containing functional groups with water. The higher polarity further broadens GO compatibility with polar solvents. A wide range of oxygen-containing functional groups in GO accelerates its connection with organic molecules, polymeric matrices, nanoscale materials, and so forth. Thus, GO has been a great forerunner to synthesizing the rGO, graphene functionalization (synthetically), functionalized graphene, graphene-based composites, and their subsidiaries.

1.5 Nanocellulose-Graphene Oxide-Based Nanocomposites

The utilization of NC-based (nano)composites as adsorbents for wastewater treatment has attracted great interest among researchers globally within the recent decades [62, 64, 68, 72, 78, 80–82, 85, 90]. These novel categories of adsorbents have reportedly displayed excellent properties such as biodegradability, sustainability, eco-friendliness, and high adsorption capacity (Q).

1.5.1 NC-GO-Based Nanocomposites

Zaman et al. have described NC-GO nanocomposite synthesis by means of a one-pot facile synthesis approach having excellent properties for use for the exclusion of MB from water [84]. These authors observed that ~98% MB abstraction was attained within 135 min. Also, they stated that, at optimized experimental settings suggested by RSM (response surface methodology), the Q of the (nano)composite was established as ~ 334.19 mg g^{-1} whereas the maximum adsorption capacity (Q_{max}) as estimated by Langmuir isotherm is 751.88 mg g^{-1}. They concluded the phenomenon was steered by Langmuir and Freundlich isotherm as it fitted well with pseudo-second-order kinetics [84].

Also in another study, a group of researchers synthesized an efficient CEL/GO (CGO) composite fibres adsorbent fabricated by wet-spinning approach and studied the experimental conditions (MB concentration temperature, pH, adsorbent dosage, concentration, as well as the contact time) for methylene blue dye (MB) removal. These authors utilized CEL as a support to immobilize and link GO sheets resulting in the formation of CEL/GO fibres. Their results revealed an upsurge in Q with a corresponding increase in the experimental conditions. Nevertheless, a decrease in Q with increased contact time owing to the reduced active sites availability was observed [10]. Their report established a Q of ~ 480.77 mg/g for MB [10]. The adsorption kinetic investigations of the nanocomposites adsorption kinetic data were superlatively defined by a pseudo-second-order model, and the thermodynamic parameters displayed that their studied adsorption phenomenon was found to be endothermic and spontaneous [10]. Also, the adsorbent (CGO) fibers, were much fixed and easily detachable and could be recycled by washing with diluted NaOH solution with the retention of $\geq$93% Q after three recycling times.

Another group of researchers studied CEL-based hydrogel incorporated GO by adopting NaOH/urea as the processing solvent [11]. These authors explored the adsorptive exclusion of Cu^{2+} ions where their results revealed an upsurge in Cu^{2+} ions adsorption with a rise in GO/CEL ratio due to the increased incorporated oxygen functionalities within the hydrogel as the GO/CEL ratio increased [11]; also, resulting in an enhancement in the electrostatic attraction, ion-exchange capability, along with the surface complexation of the fabricated adsorbent. Their report proved that the adsorbent dosage increase resulted in a corresponding decreased adsorption as observed owning to saturation of active sites [11]. An increase of the pH > 5.3 displayed a great decline in the adsorption process owing to declination in the solubility and copper ions precipitation under alkaline conditions. Also, the adsorption process fitted the pseudo-second-order kinetics and Langmuir isotherm model, which depicts mono layer adsorption [11].

For instance, Hussain et al. demonstrate for the 1st time the adsorptive assessment of GO/CNFs monolith for removal of MB dye from wastewater [22]. These authors proposed a strong chemical interaction (chiefly H-bonding) that accounted for the realization of the GO/CNFs monolith hybrid assembly, leading to a mechanically strong structure with adjustable pore-structure or surface properties. The synthesized

GO/CNFs adsorbents may utterly get rid of traces to reasonable concentrations of MB dye, and it followed the pseudo-second-order kinetics model. The adsorption isotherm behaviors of the GO/CNFs were found to be in the following sequence: Langmuir isotherm > Freundlich isotherm > Temkin isotherm model. In contrast, the maximum adsorption capacity (Q_{max}) attained was 227.27 mg g^{-1} [22]. These authors established that the inclusion of NCs follows an exponential correlation with respect to the dye uptake capacities, where specific surface area and high surface charge density were chiefly responsible for the dye adsorptive mechanism [22]. Also, the regeneration efficiency attained was up to four successive cycles at the affordable recollection along with no recontamination of remediated water [22].

1.5.2 Nanocellulose-rGO Nanocomposites

rGO aerogel is among the hot niches in the field of C-based materials systems since its advent because of its highly low density, outstanding porosity, ultrahigh specific surface area, and chemical inertness stability [9, 20]. Furthermore, rGO-initiated composites are at present broadly used for a variety of multifunctional materials in niches like adsorption/adsorbents [20], electromagnetic interference (EMI) shields [71], catalysts [2], capacitors, and sensor [31], etc. In the utilization of rGO for wastewater remediation technologies, adsorption has been considered as probably the best treatment as a result of its high evacuation effectiveness without the age of unsafe side-effects [2]. The spongy structural architecture, the ultrahigh specific surface area of (nano)cellulose-based nanocomposites, and its favorable interaction with organics significantly enhance the removal efficiency and capacity of wastewater pollutants [2].

In another work, with the aim of ameliorating the hydrophobic characteristics as well as Q of NC aerogels, nanochitosan (NCS) and rGO were amalgamated into an NC aerogel to prepare NC/NCS/rGO nanocomposite aerogel via hydrothermal technique in combination with a freeze-drying process [19]. The ideal conditions, including the impact of NC and NCS wt.% for manufacturing the NC/NCS/rGO nanocomposite aerogel having great permeable microstructures and amazing adsorption limits, were assessed. Their results demonstrated that the NC/NCS/rGO nanocomposite aerogel synthesized considered 0.1 wt% NCS and 0.05 wt% NC exhibiting a high hydrophobicity, low density, 9.3 mg cm^{-3}, along with increased water contact angle of 115.26°, outstanding adsorption capacities of 171.85 ± 3.02, 159.64 ± 1.83, 153.22 ± 2.92, 149.60 ± 6.26, 139.93 ± 3.69, 132.47 ± 3.45, 176.82 ± 4.66, 128.70 ± 0.69, and 120.34 ± 5.57 g g^{-1} for mineral oil, sesame oil, acetone, ethyl acetate, thiophene, pump oil, waste pump oil, kerosene, and ethyl alcohol, respectively. Moreover, these aerogel adsorbents may perhaps proficiently and uninterruptedly take away the oil from contaminated water as established by means of the synthesized oil and/or water pump apparatus [19]. As a result, they proposed the prepared NC/NCS/rGO composite of a synthetic ultralight porous

admixture fabricated from a gel as a potential candidate for oil and organic solvent adsorption [19].

Also, in another study, NFC was utilized as a reinforcing component of film-forming in combination with GO. Then the rGO-derived CPFs were fabricated via facile reduction-based reaction of GO/NFC-derived nanocomposite film with no adhesives inclusion, thereby effectively avoiding the challenges of dispersion along with its amalgamation with other constituents triggered by direct use of high graphene content [10]. With the comparison between three reduction techniques for directly reducing GO/NFC composite films, the authors reported that 450 °C thermal reductions and/or reduction using HI acid were more effectual in comparison to ascorbic acid reduction [10]. In this regard, they adopted HI acid (HI) chemical reduction as well as thermal reduction process for the investigative analysis of NFC inclusion to the film conductivity, where they found that rising NFC content inclusion from 10 to 50% led to a decline in the electrical conductivity (EC) of the composite film from HI acid reduction from 153.8 S/m to 22.2 S/m. In contrast, the composite films conductivity increased at first and then declined after thermal reduction both at 450 °C and 550 °C [10]. Interestingly, the authors found that at 16.6% NFC content, the EC reached a high level of 86.21 Sm^{-1} and/or 168.9 Sm^{-1}. This interesting study by Gu et al. presents preliminary studies for additional advancement of rGO/graphene-derived NCs nanocomposite having low resistance value and high EC in large-scale production [9].

With a focus on developing graphene-based materials having multifunctional properties for environmental applications, Minitha et al. utilized/explored the dual functional properties of magnetite ornamented rGO "rGO/Fe_3O_4" nanocomposite, prepared by the solvothermal method for application in superior antibacterial performance towards Escherichia coli and Pb(II) toxic substances removal via aqueous suspension [38]. It is very interesting to know that the rGO/Fe_3O_4 Their examination of autonomous in vitro organic test results uncovers that the bactericidal activity of the synthesized rGO/Fe_3O_4 composite was chiefly initiated by reactive oxygen species (ROS) dependent oxidative stress [38]. With regards to Pb (II) organic metal ion adsorption, the maximum Q of 76.3 mgg^{-1} was reported, and its adsorption isotherms tailored fine with the Freundlich model. The work demonstrates that the preparation and utilization of multifunctional properties nanocomposite materials having superior killing properties for gram-negative pathogenic species along with the effective exclusion of Pb(II) where nanocellulose could be included will make the nanocomposite a perfect biological and chemical adsorptive disinfectant agent for present/future wastewater remediation [38].

Wang et al., in their report of ultralight composite aerogels, fabricated using bio-sustainable BC and GO with the aid of a facile environmentally friendly drying approach for the first time, has been reported [73]. These authors smartly utilized the hydrophilic character of these two composites and the exceptionally permeable construction, BC/GO aerogels postulated to exceptionally retain not just natural fluids, for example, cyclohexane and DMF yet in addition water, to specifically adsorb/absorb organic liquids after GO reduction with the aid of H_2 gas, leading to nanocomposite aerogels of BC and rGO [73]. The reported nanocomposites may

well precisely absorb 135–150 g organic liquids per gram of their weight, even at higher BC inclusion (80%) in the nanocomposite aerogel. Hence, BC nanofibrils' amphiphilic property was postulated to be impacted by its decoration or coating with GO nanoplatelets [73]. Upon reduction, just the hydrophobic property of rGO ruled in the got BC/rGO composite aerogels, showing the achievability to isolate natural fluids from their blends with water by means of retention [73]. This transformation approach of GO in the aerogel structure into rGO presents a general, easy, and successful strategy for the synthesis of innovative materials for the partition of natural fluids and additionally water remediation [73].

TZ pesticides adsorption from wastewater utilizing CEL/graphene nanocomposites (CGC) was researched by Zhang et al. where utilized rGO at a predetermined temperature [85]. In comparison to five other sorbents (graphite carbons, primary secondary amine (PSA), graphite carbon black (GCB), CEL, and graphene), CGC nanocomposite used for the adsorption of six TZ pesticides (simeton, simazine, atrazine, cyprazine, ametryn, and prometryn). They reported that the CGC composite showed higher adsorption efficiency compared to five other sorbents. The adsorption process followed the Langmuir model, which was also endothermic [85]. The composite was reported to be stable and cheap (cost-effective) with an adsorption efficiency $\geq$ 85% after 6 cycles [85].

A report on CMC-rGO aerogel (CMCrGA) was synthesized for the exclusion of organic solvents/liquids and dyes by Xiang et al. [77]. These authors also investigated the adsorption of different organic lipids (acetone, methanol, dimethyl sulfoxide (DMSO), N, N-dimethyl acetamide (DMAC), ethanol, N, N-dimethyl formamide (DMF), colleseed oil and engine oil), and rhodamine B (RhB) dye. Their research findings established that the CMC-rGA absorption capacity for liquid organic compounds was not the same as a result of their different densities, molecular dimension, surface tension, along with hydrophobicity. For the exclusion of RhB dye, the CMC-rGA displayed a maximum Q of ~161.29 mg/g [77].

1.5.3 Adsorption Isotherms

The kinds of adsorption isotherms available, include Freundlich, Brunauer–Emmett–Teller (BET), Langmuir, and Temkin which are typically adopted for the aforementioned purpose.

1.5.3.1 Langmuir Isotherm

Langmuir isotherm usage is majorly in homogeneous adsorbent surfaces where there is no interface between molecules adsorbed, such as conversed adsorption of solid–gas point. Both variation and adsorbents' quantification in terms of the Q is also recognized through Langmuir isotherm [12]. Langmuir isotherm linear form of the is usually expressed as:

$$\frac{C_e}{q_e} = \frac{1}{Q_{max K_1}} + \left(\frac{1}{Q_{max}}\right) C_e \tag{1.1}$$

where C_e meant the balance focus in mg L^{-1}, q_e is the adsorbed sum in mg/g of adsorbent, $Q_{max K_1}$ is mono-layer adsorption capacity consistent, and K_1 is the constant of adsorbent fondness to adsorbate.

1.5.3.2 Freundlich Isotherm

Dilute aqueous solutions with a little scope of concentration are analyzed under Freundlich isotherm. Briefly, the adsorption phenomenon examined with regards to heterogeneous surfaces is expounded by this isotherm [4].

Its linear form representation is thus:

$$log q_e = log K_F + \left(\frac{1}{n}\right) log C_e \tag{1.2}$$

where, K_F denotes adsorption capacity (*L/mg*), while *1/n* reflects the characteristic constant of the system.

1.5.3.3 Brunauer–Emmett–Teller Isotherm

Brunauer–Emmett–Teller isotherm came into consideration on the grounds that the mono-layer created in Langmuir adsorption isotherm will in general uncover itself as a substrate to adsorbate atoms. The quantities of compounds/substances of gas adsorbed as for comparative pressure are determined by BET [4]. The benefit of this isotherm relates the surface area along with pore-size distribution estimations. The numerical portrayal of BET is:

$$q = \frac{q_m K_B C}{C_s - C\left[1 + \frac{(K_B - 1)C}{C_s}\right]} \tag{1.3}$$

where q_m represents the max absorbable value of q, K_B denotes the system constant, and C_s is the solute saturated concentration.

1.5.3.4 Temkin Isotherm

Temkin isotherm is related to an association amid adsorbent(s) and the adsorbate(s) during the process of adsorption [3–5]. The main trademark presumptions of Temkin isotherm is linearly diminished in molecules/particles adsorption heat along with its

suitability towards ion concentration of medium-sized molecules.

$$q_e = \frac{Rt}{b} lnK_T + \frac{RT}{b} lnC_e \tag{1.4}$$

where R denotes the gas constant, b represents the Temkin constant, while KT is linked to the Temkin isotherm constant to L/g.

1.5.4 Vital Parameters in Adsorption Studies

1.5.4.1 Effect of Temperature

Temperature is amongst the major significant adsorption elements that might influence the adsorption phenomenon, emphatically or contrarily. On the off chance that the adsorption increments with an increment in temperature, it alludes to endothermic adsorption, and it occurs, on the grounds that the adsorption forces turn out to be more grounded between the adsorbent essential destinations and particles of the adsorbate. Furthermore, as temperature expands, the arbitrary development of adsorbate molecules likewise increases, subsequently leading to the chance of adsorbate particles to connect with dynamic adsorbent destinations fortifying. Though, if the adsorption cycle is adversely impacted by increasing the reaction temperature, the process is referred to as exothermic adsorption, while the explanation for this is debilitating the adsorption forces within the middle of the fundamental spots existing on the outer layer of the adsorbents and adsorbate molecules [3–5, 20, 22].

1.5.4.2 Effect of pH

The ionization level of ecological contaminations and the existing functional groups' protonation existing upon the adsorbent outer layer are incredibly adjusted by means of pH [3–5, 20, 22]. Subsequently, the pace of the adsorption interaction is fundamentally constrained by solutions' pH. The adsorbent dynamic sites protonation (H+) and deprotonation (OH −) are controlled by means of solutions' pH and based on pH, as different particles are acquired in the solution. Hence, the charged sites on adsorbate and adsorbent are either affected by the forces of electrostatic repulsion/attraction. For example, anionic dyes can't be proficiently adsorbed on adsorbents at higher pH however cationic dyes can. At lower pH, anionic dyes viably adsorbed on the adsorbent however not the cationic ones. essentially being, the raising of pH is likewise helpful for cationic metals adsorption with the reason for desorption of anionic metals or the other way around. Henceforth, the pH enhancement study is an irreplaceable factor in upgrading the adsorption of ecological contaminants with specific qualities.

1.5.4.3 Effect of Concentration

This impact is estimated by utilizing various adsorbate concentrations with consistent adsorbent doses. Further, adsorbate fixation assessment gives the expulsion rate and adsorption potential information [3–5, 20, 22, 29, 33]. The biding sites of the adsorbent and adsorbate concentration have a direct correlation initially, so increased adsorbate concentration leads to a swift increase in adsorption phenomenon after a while, because of the more modest number of accessible binding sites resulting in a decline in the adsorption process. In any case, on increasing the adsorbate percentage at the beginning, the exclusion rate diminishes on account of the main specific number of accessible binding sites. Contrary, in case the adsorbent is accessible substantially more, it results in a sharp decline in the adsorption process. The discussion above proves that the accessible sites available for binding and the % of individual adsorbate have a direct relationship with the adsorption process.

1.5.4.4 Effect of Contact Time

Chemical, as well as physical responses, are especially impacted by adsorbent to adsorbate time of contact. In this way, contact time is a significant part of the specific assurance of the adsorption process [84]. On the record, if adsorption equilibrium has need of additional time, it prompts an improper adsorption process, while a reduced amount of time is required, adsorption equilibrium proposes a lot of adsorbates might be adsorbed on the adsorbent. Subsequently, the short contact time of equilibrium causes the adsorption less expensive, less tedious, and further developed proficiency. What's more, contact time is has a direct relationship with the binding sites of the adsorbent. Before all else, adsorbate particles/particles are fastly connected to the binding sites and contact time reduction. Anon, adsorbent active sites gradually transcend towards equilibrium along with an increment in the contact time.

1.5.5 Kinetics of Adsorption

The rate of adsorption and residual time all fall within the adsorption kinetic studies, as these parametric factors remain indispensable for the demonstration of the design and control of the adsorption process [33, 35, 56, 57, 63, 64, 67, 73, 74, 84, 85, 88]. Moreover, transfer of adsorbate mass along with its intraparticle mass transfer, diffusion, along with adsorption process against the adsorbent are all assessed adopting kinetic studies. Despite the adsorption mechanism along with its determining step towards controlling the adsorption process is performed typically using intraparticle diffusion, pseudo-second-order, as well as pseudo-first-order simulations. A transitory overview of the above-mentioned models is cited thus.

1.5.5.1 Pseudo First Order

This model was first introduced by Lagergren where it was successfully used to study the kinetic of adsorption. As per the Pseudo first-order model, the adsorption sites fill-up rate has a direct relationship with the accessible active binding sites [33, 35, 56, 57, 63, 64, 67, 73, 74, 84, 85, 88]. Hence, the binding sites stuffing rate is directly related to the active binding sites thus:

$$\log(q_e - q_t) = logq_e - \frac{k_1}{2.303} \tag{1.5}$$

Here, q_e stands for the equilibrium adsorption capacity (mg/g), q_t is assigned to the adsorption capacity at time t (mg/g), contact time denoted as t, while k_1 is rate constant (min^{-1}).

1.5.5.2 Pseudo-Second Order

The Pseudo-second-order model provides an appropriate method for determining the adsorbate chemical adsorption onto the surface of the adsorbent [33, 35, 56, 57, 63, 64, 67, 73, 74, 84, 85, 88]. The pseudo-second-order model linear expression is:

$$\frac{t}{q_t} = \frac{1}{k_2 q_{2e}} + \left(\frac{1}{q_e}\right)t \tag{1.6}$$

where k_2 is the reaction constant (g/mg min).

Besides, the constant k_2 is employed to calculate the preliminary sorption rate h at $t \rightarrow 0$:

$$h = k_2 q_{2e} \tag{1.7}$$

1.5.5.3 Intra-Particle Diffusion

The transition of adsorbate entities/ions dissemination on top of the adsorbent material is the primary factor upon which the rate of adsorption could be distinguished [33, 35, 56, 57, 63, 67, 84, 85, 88]. Moreover, the unhurried step is known as the rate recognizing step. That is the reason the controlling stage is sub-atomic dispersion as recommended by the intra-molecule dispersion model, and it very well may be shown in the as:

$$q_t = k_{diff} t^{0.5} + C \tag{1.8}$$

K_{diff} represents reaction constant (g/mgmin), while C signifies intercept (mg/l).

1.5.6 Adsorption Thermodynamics

The Q is significantly influenced by the temperature; thus, the appropriate analysis of the adsorption process can't be performed by putting the thermodynamic findings behind. Also, the feasibility of the adsorption course is examined via Gibb's equation haven been employed for the estimation of the variation in standard adsorption entropy (ΔS°), enthalpy (ΔH°), and Gibb's free energy (ΔG°). Conversely, it is employed for the assessment of endothermic and/or exothermic characteristics, and to determine the spontaneous/nonspontaneous process of adsorption follows [23]:

$$\Delta G^o = \Delta H^o - T\Delta S^o \tag{1.9}$$

Nevertheless, the parameters are offered in the aforementioned expression, i.e., Gibb's free energy (ΔG°), enthalpy (ΔH°), as well as entropy (ΔS°) are clearly assessed via a facile expression earlier expressed by Sen & Gomez in 2011 thus:

$$\log\left(\frac{q_e}{C_e}\right) = \frac{\Delta S^o}{2.3030R} + \frac{-\Delta H^o}{2.303RT} \tag{1.10}$$

where q_e signifies adsorbate equilibrium concentration (mg/L), C_e addresses equilibrium concentration in aqueous solution (mg/L), T mirrors the temperature, while R is the gas constant. In addition, the linear type of Van't Hoff plot between $\log(q_e/C_e)$ versus $1/T$ gives significant results in intercept and slope form, which can be utilized for changing the entropy and enthalpy assessment. The attainability of the process of physical adsorption has Gibb's free energy in the range of 0 to 20 kJ mol^{-1} and for the chemical adsorption, it ranges from − 400 to − 80 kJ mol^{-1}. Also, positive/negative enthalpy esteems propose the exothermic/endothermic adsorption process, and irregularity; that is, the entropy of the adsorption declines as the adsorbate ions/particles/molecules are adsorbed on the surface of the adsorbent. In this way, by utilizing the above condition the total idea of the adsorption cycle can be appropriately distinguished.

1.5.7 Nanocellulose GO-Based Adsorbents Mechanism with Wastewater Pollutants

The nanocellulose-GO-based adsorbents' interaction with the pollutants is referred to as adsorption [77–80, 82, 84, 85]. Adsorbed materials such as wastewater pollutants onto the solid material (termed adsorbate) surface, while the solid material

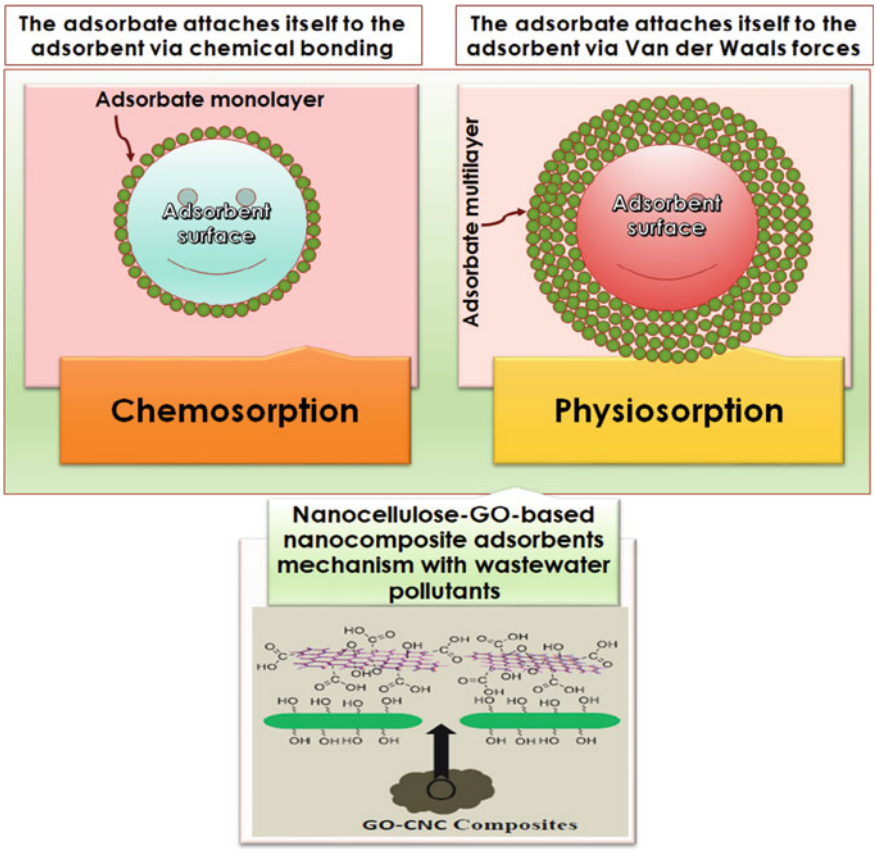

Fig. 1.9 Graphical demonstration of nanocellulose-GO-based nanocomposite adsorbents physisorption and chemisorption mechanism

itself is defined as the adsorbent. The diffused wastewater pollutant molecules are adsorptively held onto the adsorbent surface upon exposing the adsorbent to the pollutant. Figure 1.9 depicts the adsorption mechanism of two categories (Chemisorption and/or Physisorption) for nanocellulose-GO-based adsorbents dependent on the kind of adsorbents and pollutants. One more form of adsorption mechanism that occurs through ions exchange is referred to as ion-exchange adsorption.

1.5.7.1 Nanocellulose-GO-Based Nanocomposite Adsorbents Chemisorption Mechanism

The phenomenon occurs when adsorbate/contaminant's particles are chemically bonded via H-bonds, ionic, etc. to the adsorbent (NC-GO based adsorbent in this wise) called chemisorption. It is also well understood to be chemical adsorption;

this mechanism of adsorption kind is much precise and requires extra energy of ~ 80–240 kJ/mol, is normally, irretrievable and favors raised temperature. Furthermore, chemisorption does majorly follow Langmuir isotherm seeing only monolayer adsorption is fashioned in the adsorption process. Essentially, three kinds of chemical adsorption phenomenon, as discussed in the following subsections. Zaman et al. reported that the activation energy (E_a) of the MB adsorption onto the GO-CNC phenomenon was found to be 49.70 kJ mol^{-1} and confirmed that an E_a value more than 40 kJ mol^{-1} indicates that MB adsorption using GO-CNC was mainly chemisorption [84]. Nanocellulose-GO-based nanocomposite adsorbents adsorption mechanism may be based on precipitation, reduction/oxidation, physisorption mechanism, dipole–dipole interaction, hydrogen bonding, π–π stacking, hydrophobic/oleophilic interaction, pore filling adsorption, and/or ion-exchange adsorption mechanism [1–4, 9, 10, 11, 38, 64, 67, 78–81], Table 1.4.

1.6 Adsorption-Based Water Treatment Application Using Nanocellulose-Graphene Oxide-Based (NGON) Nanocomposites

The application of nanocellulose-graphene oxide-based nanocomposites (NGON) for adsorptive wastewater treatment has been broadly reported by researchers all over the globe owing to its novel, innovative attributes, low-cost, facile synthesis approaches, biocompatibility, sustainability, lightweight, high surface area, and so on. The utilization NGON for wastewater treatment ranges from the removal of dyes [24, 84], antibiotics [37], pesticides [3], heavy metal ions [30, 46, 70, 78, 80, 82, 89, 90], radioactive elements [51, 60, 78], oils [50], etc. as contaminants in the wastewater.

1.6.1 Removal of Heavy Metal Ions

The exclusion of heavy/toxic metal ions from water/wastewater before its consumption has been of high interest to the WHO within the last century. Several works have been investigated and put forward by researchers globally for the remediation of wastewater unto consumption by researchers, industries, and individual bodies owning to the shortage of clean water globally [70, 80, 82, 90]. This is due to the vast surface hydroxyl group coupled with the carboxylic groups on the surface of NC-GO nanocomposites or their hybrids.

In a study on a group of researchers, it has been established that the administration of a thin layer of GO onto CNFs films to fabricate CNF–GO layered-composite membranes showed dramatic enhancement in their wet-mechanical firmness, H_2O

Table 1.4 Diverse NC/graphene-derived composite/nanocomposite/hybrid adsorbents along with their multi-functional usage

Adsorbents/filter material(s)	Multi-functional usage	Adsorption performance				References
	Contaminants removed	Q_{max}	pH	Temp [K]	Mechanism of adsorption	
Nano ZnO incorporated GO/NC "ZnO-GO/NC"	Ciprofloxacin (CF)	8 mg/L	5.5	303.15	Multilayer process (Physisorption)	[2]
Cellulose nanocrystals/graphene oxide composite (CNCs-GO)	Antibiotic levofloxacin hydrochloride (Levo-HCl)	41 mg/g	4 (4–9)	303.15	Chemical reaction, diffusion, or mass transfer-dominate (Chemosorption)	[64]
CNF/GO hybrid aerogel	Tetracyclines	454.6 mg/g	2	298.15	Electrostatic pull, p-π interface, π-π interface or H-bonding (Chemosorption)	[81]
	Quinolones	128.3 mg/g	2	298.15	Electrostatic pull, p-π interface, π-π interface or H-bonding (Chemosorption)	[81]
	Sulfonamides	227.3 mg/g	2	298.15	Electrostatic pull, p-π interface, π-π interface or H-bonding (Chemosorption)	[81]
	Chloramphenicols	418.7 mg/g	2	298.15	Electrostatic pull, p-π interface, π-π interface or H-bonding (Chemosorption)	[81]

(continued)

Table 1.4 (continued)

Adsorbents/filter material(s)	Multi-functional usage	Adsorption performance				References
	Contaminants removed	Q_{max}	pH	Temp [K]	Mechanism of adsorption	
	β-Lactams	230.7 mg/g	2	298.15	Electrostatic pull, p-π interface, π-π interface or H-bonding (Chemosorption)	[81]
	Macrolides	291.8 mg/g	2	298.15	Electrostatic pull, p-π interface, π-π interface or H-bonding (Chemosorption)	[81]
Graphene/TEMPO-Oxidized Cellulose	MB Dye	227.27	6.5	303	Monolayer (Chemosorption)	[22]
Graphene oxide (GO)/nanocellulose aerogel	MB	111.2 mg/g	7		Electrostatic pull, p-π interface, π-π interface or H-bonding (Chemosorption)	[74]
	Tetracycline (TC)	47.3 mg/g	7		Electrostatic pull, p-π interface, π-π interface or H-bonding (Chemosorption)	[74]
GO layer was fabricated on cellulose nanofiber (CNF) membrane	A mixture of Victoria blue B, Methyl Violet 2B and Rhodamine 6 G	8.1	7.17		Electrostatic pull, p-π interface, π-π interface or H-bonding (Chemosorption)	[33]

(continued)

Table 1.4 (continued)

Adsorbents/filter material(s)	Multi-functional usage	Adsorption performance				References
	Contaminants removed	Q_{max}	pH	Temp [K]	Mechanism of adsorption	
	Victoria blue B	3.0	7.17		Electrostatic pull, p-π interface, π-π interface or H-bonding (Chemosorption)	[33]
	Methyl Violet 2B	2.8	7.17		Electrostatic pull, p-π interface, π-π interface or H-bonding (Chemosorption)	[33]
	Rhodamine 6 G	2.3	7.17		Electrostatic pull, p-π interface, π-π interface or H-bonding (Chemosorption)	[33]
Nanocellulose-graphene oxide hybrid aerogel	MB	265.6 mg/g	4–5	Room temperature		[24]
	Congo red (CR)	21.5 mg/g	4–5	Room temperature		[24]
	Waste oil	55.0656 mg/g				[24]

(continued)

Table 1.4 (continued)

Adsorbents/filter material(s)	Multi-functional usage	Adsorption performance				References
	Contaminants removed	Q_{max}	pH	Temp [K]	Mechanism of adsorption	
Graphene oxide cellulose nanocrystals nanocomposite	MB	334.19 mg/g	4–10	20–50 °C	MB Adsorption onto GOCNC partially fitted Langmuir model at the beginning of adsorption and then partway Freundlich model at the later adsorption phase indicative of a steady transition of mono-layer surface adsorption to the diverse electrostatic interface	[84]
Graphene Oxide-Cellulose Composite	U (VI)	3.70–147.80 mg/g	5	298.15	Electrostatic pull, p-π interface, π-π interface or H-bonding (Chemosorption)	[78]

flux, and metal (Ag(I) and Cu(II) Q such as ion pollutants from the water via filtration [70]. These authors observed that the CNF-GO composite, as studied during drying of the pre-wet layers after metal particle adsorption, showed a clear intensity increase in the low q area of the SAXS dissipating profiles proposing the arrangement of nanoparticles (NPs) which did steadily develop as an element of drying time. Likewise, through sub-atomic elements reenactments, the authors announced that the GO sheets are solidly adsorbed on the CNF support through a thick network of intermolecular H-bonds, along with self-interactions, while the carboxyl groups of GO balance out the additional GO layer on CNFs, building up the oxygen–hydroxyl as well as hydroxyl–hydroxyl intermolecular bonds among the composite phases [70].

Some other group of researchers who studied a novel adsorbent based on GO-TETA-DAC, synthesized adopting dialdehyde cellulose (DAC) grafted GO with triethylenetetramine (TETA) acted as the cross-linking reagent [80]. They applied the GO-TETA-DAC nanocomposite for the adsorptive removal of Cu (II) and Pb (II) ions from aqueous solution and attained an outstanding performance where the Q_{max} of 65.1 and 80.9 mg/g for Cu(II) and Pb(II) at a pH of 5.0. The adsorption isotherm and kinetics also showed that the adsorption course conformed to Langmuir and pseudo-second-order-model [80], and adsorption efficiency of $\geq$77% even after four times of recycling. They said, the adsorption processes amid heavy metals and two aspects that could deliberate GO-TETA-DAC: at the initial stage, the ion-exchange reaction amongst ions of heavy metal and –OH, –COOH, or -NH_2 functionalities onto the adsorbent surface; and in addition, the enormous specific surface area of GOTETA-DAC could be another cause for the adsorption phenomenon [80]. The greater specific surface area augments the Q of heavy-metal ions along with the ion-exchange course concerning heavy metal ions and GO-TETA-DAC could be conveyed as in the expression below:

$$\text{GO-TETA-DAC-COOH} + M^{2+} \longrightarrow \text{GO-TETA-DAC-COO}^{-} \cdots\cdots M^{2+} + H^{+}$$

$$\text{GO-TETA-DAC-OH} + M^{2+} \longrightarrow \text{GO-TETA-DAC-CO}^{-} \cdots\cdots M^{2+} + H^{+}$$

We know that the phenomenon expressed by Yao et al. above stands for almost all NC-GO nanocomposites and/or hybrids except for a few [80].

1.6.2 Removal of Toxic Dyes

The exclusion of dyes from wastewater towards the supply of clean water has been researched by several researchers within the last decade [1, 10, 13, 34, 35, 57, 59, 68, 77, 82, 84].

The use of green renewable bioderived resources to address the consumption of non-sustainable resources and the contamination of modern wastewater concurring

with the sustainable development of the ecosystem has been explored [24]. Their study designed a hybrid aerogel using NCs and GO, which served as a purifier for MB, congo red (CR), and waste oil removal from wastewater. They reported that NCs provided abundant –OH groups, a high aspect ratio of approximately 500, and an average thickness of ~30 nm were uniformly distributed on the GO sheets surface with a side length of 1∼3 μm, which resulted in the hybrid aerogel having a porosity of up to 99% [24]. These authors' work revealed that the hybrid aerogel reached the Q_{max} of 265.6 mg/g and 21.5 mg/g for MB and CR. The NC-GO mass ratio was 8:2. Outstanding oil Q up to 25.6 g/g was achieved after further hydrophobic treatment of the hybrid aerogel resulting in beneficial oil/water separation, which is a good strategy for applying the NCs in water remediation [24].

Zaman et el. reported for the first report on the utilization of a cost-effective synthesis route modified Hummers' method for in-situ amalgamation of novel GO-CNCs nanocomposite in a solitary reaction pot [84]. The authors reported removal of ~98% MB within 135 min. The Q of the nanocomposite attained under peak experimental state of affairs as per RSM was ~334.19 mg g^{-1}, whereas the max Q_{max} estimated by Langmuir isotherm was 751.88 mg g^{-1}. The adsorption phenomenon, in this case, established that the process followed Langmuir and Freundlich isotherm as well as followed pseudo-second-order kinetics together: The nanocomposite presented an immense probability for extensive usage in contaminated water remediation [84].

Graphene/CNFs hybrid monolith for MB dye adsorption prepared through urea assisted self-assembly technique has been reported [22]. These authors postulated that a strong chemical interface, chiefly H-bonds interaction was responsible for the hybrid assembly creation, making it possible for the nanocomposite to completely get rid of traces to moderate concentrations of the dye (MB), following the pseudo-second-order kinetics model [22]. The adsorption isotherm characteristics of the hybrids have followed the sequence: Langmuir isotherm > Freundlich isotherm > Temkin isotherm model. In contrast, the Q_{max} achieved was 227.27 mg g^{-1}, where the inclusion of NC followed an exponential correlation with the dye adsorption capacities [22]. The high surface-charge density along with the specific surface area was reported to chiefly contribute to the dye adsorption mechanism, as the renaissance and reutilizing efficiency of the adsorbents was up to four successive cycles with low-cost recollection and no re-pollution of remediated water [22].

Reports on 3D carboxymethyl cellulose (CMC)/rGO nanocomposite aerogel cross-linked via poly (methyl vinyl ether-co-maleic acid)/poly(ethylene glycol) structure by a turning freezing approach, exhibiting high structural stability though concurrently sustaining its outstanding Q for organic dyes removal. The Q_{max} attained was 520.67 mg/g with rGO inclusion [86]. The adsorption kinetics and isotherm displayed that the adsorption process followed the pseudo-second-order and Langmuir adsorption models, while the adsorption was spontaneous. Moreover, the crosslinked nanocomposite aerogel could be easily recycled even after washing with dilute HCl solution, retaining ≥97% of the Q after five recycling, seeing the adsorbents outstanding character perfect for wastewater treatment and environmental remediation [86].

The fabrication of ultrathin GO coating was prepared on CNF membrane aimed at achieving a robust crosslinked system free encrusted membrane with coactive water flux and separation characteristics, where in contrast to pristine cellulosic or GO membranes, GO-CNF hybrid membranes were reported to exhibit a significantly enhanced mechanical stability in both dry and wet states. has been reported [33]. The synthesized ultrathin GO film on the CNF presents an inimitable and effectual for fabricating highly multifunctional, cost-effective, and facile wastewater remediation membranes with a substantial gain with regards to mechanical stability, robustness, flux, and refutation of dyes compared to the isotropic membrane with GO nanosheets randomly dispersed in the CNFs network [33].

GO-NC nanocomposite aerogel synthesized by first dispersing CNFs fibrils in GO nanosheets. CNFs having high aspect ratios and -ve potential facilitated the GO flakes' exfoliation with no need for a chemical cross-linker via steric hindrance and electrostatic repulsion [74]. Water purification analyses were carried out adopting MB and tetracycline (TC) as the model pollutants, where the nanocomposite aerogel adsorption process followed a pseudo-second-order model and Langmuir adsorption isotherm [74]. The Q_{max} attained was ~111.2 mg/g for MB and 47.3 mg/g for TC. The GO-NC nanocomposite aerogel could be simply regenerated/recycled employing ethanol. Even after three cycles, the aerogel maintained a high adsorptive removal efficiency of (98%) for MB and (97%) for TC. The adsorption mechanism was essentially attributed to π-π interactions and electrostatic attraction [74].

The reports on NC-GO-based nanocomposites for adsorptive water purification has established the valuable impact of NC in these materials owning to their large surface area, lightweight, ability to be tuned, highly porous structure leading to the formation of favorable structure for both adsorptive, absorptive, and in some cases antibacterial along with the catalytic activity.

1.6.3 Removal of Radioactive Residues/Element-Ions

Radiological toxins are brought about by radioactive components. Wellsprings of radioactive material could be soils or shake the water travels through or some modern waste. The disintegration of normal stores of specific minerals (radioactive) may discharge radiations (like a, b). Radiological components (viz. U^{226}, Ra^{226}, Ra^{228}, and Rn^{228}) will in general be a more noteworthy issue in groundwater than surface water. A wide range of radiological defilement increment the danger of disease [51, 60]. The challenges of radioactive elements/ions in water are an immense problem globally. Radioactive elements such as U, thorium, etc. in H_2O have gotten more significant owing to the shortage of liquid H_2O for humanoid and industrial consumption, particularly, consent in these areas where, additionally, the minerals comprising of radioactive ions/elements are of great significance as regards groundwater. Typically, radioactive elements like U content in clean water could range from 0.01 ppb to 50 ppb, for surface water, and ~2000 ppb in groundwater, where this quantity depends on factors including leaching contact time with the radioactive element

sources, water flow, evaporation, redox conditions, partial CO_2 compression, the pressure of O_2, and pH. Complex ions (like vanadate, fluorides, phosphates, carbonates, sulfates, silicates) availability as well as the interface amongst these elements, also plays a role in radioactive ions/elements content in environmental H_2O [51].

Adsorption study for novel multi-carboxyl-functionalized NC-GO nanocomposite adsorbent for removing U from wastewater/water along with comparing the selective adsorption behavior for hazardous metal ions U ions has been put forward [55]. It was clear that NC-GO nanocomposites displayed very high adsorption performance when compared to individual NC and/or ZnO-GO, while the kinetic data followed the pseudo-second-order model. The equilibrium attained at 120 min and isotherm followed the sequence Sips > Langmuir > Freundlich. The U adsorbed could be desorbed using 0.1 M HCl conducted more than 6 cycles illustrating the practicality and repeated use of these adsorbents for the removal of U [51].

In order to assess the reliability and possibility of carboxylate-functionalized ethylene glycol dimethacrylate (EGDMA) cross-linked NC/GO polymer nanocomposite "EGDMA-g-nCell/GO" used for Th(IV) removal, adopting a sequence of batch optimized adsorption experimentations was carried out and also recovery where the equilibrium adsorption capacity (Q_0) among the numerous models as reported was 141.21 mg/g at 30 °C which tailored fine with Langmuir isotherm having reduced χ^2 and R^2 values [60]. Their synthesized and used adsorbent could undergo four regeneration cycles with no considerable loss in Q with the aid of a 0.1 M HNO_3 desorption agent, attaining ~ 98.0% recovery [60].

In another work, efficacious fabrication of an effective, cheap nanocomposite "GOC," which presented substantial U (VI) adsorptive character has been explored: the adsorption parameters were optimized through variation of the investigational parameters like the adsorbent dosage, pH, along with the contact time [78]. Their work revealed that GO and/or GOC displayed high U (VI) affinity, which was well explained by the Freundlich adsorption isotherm. These authors realized 97.5% U (VI) removal (dosage = 1.75 g/L at pH 5.0) in 70 min with an initial U solution concentration of 10 mg = L, GOC. GOC has exceptional Q for the actual U liquid waste while the U exclusion rate is reaching ≥99%, thereby making GOC a potent adsorbent for adsorptive removal of U-based manufacturing waste matter [78].

1.6.4 Removal of Oils

Recently, several researchers have been attracted to the nontoxic, sustainable, biocompatible, etc., attributes of NC-GO/rGO nanocomposites in the remediation of wastewater [20, 73, 88].

rGO/amino multi-walled carbon nanotube/NC (rGO/MWCNTs-NH2/NC) nanocomposite aerogel prepared via hydrothermal and freeze-drying along with high-temperature annealing technique has been explored by Hui et al. [20]. These authors established an optimal condition for rGO/MWCNTsNH2/NC nanocomposite aerogel was the mass ratio of GO to MWCNTs-NH_2 of 8:1 with NC wt%of ~0.06%,

which was adopted for adsorption tests and oil/water separation showing outstanding adsorption properties for diverse oil and organic solvents like ethyl acetate (161.76 ± 7.69 g/g), dichloromethane (156.14 ± 8.24 g/g), cyclohexane (92.73 ± 5.22 g/g), acetone (103.87 ± 7.83 g/g), and sesame oil (124.09 ± 6.64 g/g), and attained an oil/water separation in just 20 s [20]. Effectively facilitation of the hydrophobicity of rGO aerogel attained by both MWCNTs-NH_2 and NC could, for oil and/or organic solvents adsorption: The Q of 161.76 ± 7.69, 156.14 ± 8.24, 92.73 ± 5.22, 103.87 ± 7.83, and 124.09 ± 6.64 g g-1 for the rGO/MWCNTs-NH2/NC nanocomposite aerogel for ethyl acetate, dichloromethane, cyclohexane, acetone, and sesame oil was reported in these work [20].

1.6.5 Residual Antibiotics

CN-GO-based nanocomposites composed of several ethers, ester, and –OH functionalities, which added to the high adsorption % of these composites for antibiotics and other pharmaceutical drugs through mechanisms including:

- Dipole–dipole intermolecular forces.
- H-bonding.
- π-π interfaces/interactions.

A report supporting this phenomenon has been conversed recently by Luo et al. who synthesized chitosan/CEL composite microspheres graphene embedded adsorbent system based on activated carbon (CCM-AC) aimed at tylosin (TYL) antibiotic adsorptive exclusion [36]. They reported that the adsorbent surface consists of –OH and –CO functional groups and the nanocomposites adsorption approach for tylosin was based on physical and/or biochemical interactions, which included H-bonding, electrostatic and π-π interactions (Fig. 1.10) [36]. Their analysis also established that the adsorption performance of the CCM-AC nanocomposites on tylosin was defined by batch and fixed-bed adsorption experiments. At the same time, their adsorption mechanism was also studied. The composites' Q_{max} was found to be 59.26 mg g^{-1}, and the adsorption performance was in harmony to Langmuir and pseudo-second-order kinetics [36].

There are literature reports on NC-GO-based nanocomposites or hybrids for the adsorption mediated wastewater treatment aimed at antibiotics removal within the last decades [2, 37, 64, 81].

Yao et al., in their work, synthesized CNFs/GO hybrid aerogel through a one-step ultrasonication technique aimed at adsorption-based exclusion of 21 varieties of antibiotics from wastewater [81]. They revealed that as-prepared CNF/GO nanocomposite aerogel has interconnected 3D architectural network morphology, where GO nanoplatelets/sheets with 2D architecture were closely engineered along the CNFs via H-bonds prompting the aerogel to exhibit superior Q in regard to the selected antibiotics [81]. The antibiotics exclusion percentages (R%) were recorded to be ≥

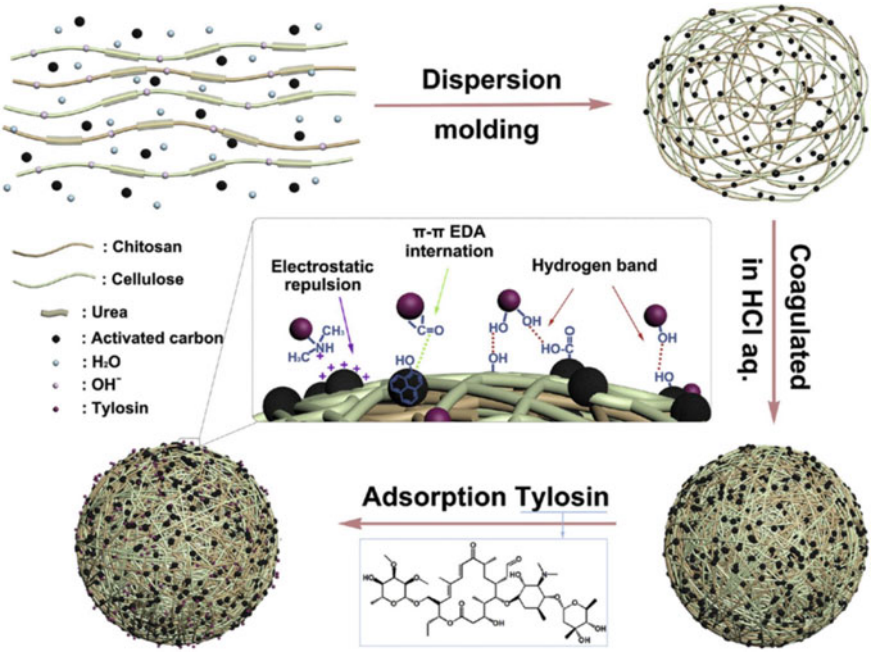

Fig. 1.10 The scheme for fabrication CCM-AC and the adsorption mechanism of TYL on CCM-AC. Reproduced with permission from [36]. Copyright 2019, Elsevier Science Ltd

69%, and the order of selected six sets of antibiotics as per their adsorption proficiency was as thus: Tetracyclines > Quinolones > Sulfonamides > Chloramphenicol > β-Lactams > Macrolides. They established that the adsorption process was based on the electrostatic pull, p-π interaction, π-π interface, as well as H-bonding [81]. Comprehensively, they stated the composites (CNF/GO aerogel) adsorption capacities as 418.7 mg · g^{-1} (chloramphenicol); 291.8 mg · g^{-1} (macrolides), 128.3 mg · g^{-1} (quinolones), 230.7 mg · g^{-1} (β-Lactams), 227.3 mg · g^{-1} (sulfonamides), and 454.6 mg · g^{-1} (tetracyclines) estimated by the Langmuir isotherm models [81], and even the rejuvenated nanocomposite aerogels could still over and over again be utilized after ten cycles with sustained adsorption performance.

Tao et al. in their study aimed at the removal of residual levofloxacin hydrochloride (Levo-HCl) antibiotics in wastewater using a CNCs-GO composite with a 3D structure revealed that the nanocomposite material possessed a high surface area and electrostatic attraction, resulting in enhanced Q of the CNCs-GO for the aimed Levo-HCl [64]. They adopted a simulation approach based on the Box–Behnken design to study the effects of the diverse factors on the elimination of Levo-HCl by the CNCs-GO and observed that the nanocomposite material exhibiting excellent antibiotic Q, having an exclusion percentage of $\geq$80.1% at a maximized pH of 4; the adsorbent dosage of 1.0 gl^{-1}, at an initial contaminant concentration of 10.0 mgl^{-1} and contact time of 4 h [64]. Sips model adsorption isotherm was reported to fit

well, while the kinetics studies revealed the phenomenon of adsorption matches the quasi-second-order kinetics model [64].

1.6.6 Pesticide Adsorption

As per available literature, NC-GO-based adsorbents for pesticides removal from wastewater have been of growing interest within the last two decades [3, 25, 62, 79, 85]. Nayak et al. has reported the successful fabrication unto application of CEL/nanocellulose/graphene nanocomposites using an innovative approach: adopting covalent and non-covalent coupling approaches; the authors showed that nanocellulose surface could be modified, which was further utilized to avoid self-aggregation and promote efficient dispersion in nonaqueous media [25]. Studies on superhydrophilic GO/electrospun CNF synthesis and its successful use in solid-phase film tip adsorption (SPMTA) as an efficient adsorbent for the concurrent study of polar organophosphorus pesticides (OPPs) in more than a few foods and water samples have been exploited [3]. These authors studied the impact of more than a few parameters like sample pH, adsorbent dosage, adsorption time, and initial adsorbent concentration and established that the SPMTA was linear within 0.05 and 10 mg l^{-1} for ideal conditions of adsorption: pH 12; 5 mg of adsorbent measurements and adsorption season of 15 min for methyl parathion, sulfotepp, ethoprophos, as well as chlorpyrifos having extraordinary relationship coefficients of 0.994 to 0.999. Satisfactory precision (RSDs) was attained with respect to intraday (n = 3, 0.06–5.44%) along with interday (n = 3, 0.17–7.76%) analyses [3]. Modest detection limits: 0.01–0.05 mg l^{-1} and acceptable adsorption reliability "71.14–99.95%" were also achieved in their study for the spiked OPPs [3].

1.7 Conclusions, Limitations, and Future Perspectives

Nanocellulose-based composite systems have demonstrated boundless ability for adsorptive exclusion of diverse wastewater pollutants because of their great surface tunable properties. Organic and inorganic wastewater pollutants have reportedly shown a high affinity with regards to NC-GO-based (nano)composite adsorbents surface, which is largely credited to the existence of diverse surface functionalities, including amino, epoxy, hydroxyl, carboxyl, and thiol on these NC-GO-based materials. In this chapter, we here considered assorted NC-GO-based (nano)composites and their explored adsorption competence for the exclusion of diverse noxious waste from wastewater and how the interface between the adsorbates and adsorbents impacts adsorption process efficiency. It has been established through the reviewed works that most of the adsorption process for NC-GO-based nanocomposites/hybrids

involves the interface between contaminants and the adsorbent via diverse mechanisms including H-bonding, van der Waals forces, electrostatic interaction, along with π-π interactive forces.

The increasing quantity of harmful materials such as synthetic dyes, metals ions, and/or waterborne pathogens/bacteria/viruses in surrounding water day-after-day degraded its quality causing contamination in the water, and consequently grave water challenges.

Water necessity and its wellbeing measures are principal worries to the entire world, including individuals. Comprehensive water remediation requires the adopted adsorbent, which is equipped to eliminate all kinds of contaminations (poisonous metals, engineered colors, and waterborne microorganisms); in like manner, numerous adsorbents, as well as their hybrids/composites, are herewith conversed in this chapter for wastewater remediation. Uncommon capacities/properties in regards to ecofriendly synthesis/preparation, reusability, cost-effectiveness, straightforward handling/operation, facile fabrication approach, along with eco-friendly nature are together with this discussed. The alteration typically trails these capacities and multifunctional applications of these nanocellulose-graphene composites compresses its high porosity, even passage of porosity, huge explicit surface area, minimal surface energy, as well as higher absorption. These distinctive adsorbents present a decision for optional properties like mechanical characteristics, chemical stability, thermal protection, and electrical shielding. The uses and characteristics of NC-graphene composites adsorbents aimed at water remediation are hereby generally tended in this article; in spite of, there are as yet a few demands that ought to basically be thought of and request more enhancement in future multifaceted NC-graphene composites adsorbents, like: (a) the design and development of NC-GO-based adsorbent constituents having acceptable amalgamated adsorption/antibacterial performance for exclusion of various kinds of contaminants inclusion in wastewater ought to be sensibly researched and conversed for improvement; (b) the rudimentary correlation of diverse NC-GO-based adsorbents materials for business standpoint most be considered for adsorptive remediation percentage along with the antibacterial action against monetary effectiveness; (c) at the initial stage, almost all the material utilized for the preparation of conventional adsorbents were not founded upon the idea of green chemistry/materials, feasible, ecofriendly, and sustainable, etc. Focus on the design and fabrication of NC-GO-based adsorbent materials will largely fill this gap; (d) also, the dearth of genuine tests conditions (like adsorption and antibacterial tests) for NC-GO-based adsorbents at the moment makes it hard for the assessment of genuine practice and advancement in this regard. (e) With respect to business development for NC-GO-based adsorbents, the adsorbent materials that are effectively accessible in abundant quantity, minimal expense, and nearby business sectors should be selected; for example, nanocomposite adsorbents (NC-GO-based) display great adsorption proficiency; however, nanomaterials, in general, are not effectively accessible in the business sectors, (f) large scale manufacturing of specific purposes adsorbents such as NC-GO-based adsorbent in the market at the moment isn't well understood. Also, a high surface area of NC-GO-based adsorbents is likewise needed

to get a high adsorption capacity (Q). However, the huge surface area of NC-GO-based adsorbents influences their mechanical strength. Accordingly, detail, profound insight on adsorbent mechanical properties study is a fundamental part, (g) the compelling partition of NPs lingering from NC-GO-based adsorbent treated water is exceptionally essential and requires further investigation to comprehend foresee their buildup and potential dangers on human wellbeing and the climate. Correspondingly, the attractive NC-GO-based nanocomposites/hybrids usage can fundamentally isolate the remaining NPs from the NPs-based adsorbent treated water. Furthermore, natural risks of the got away nanoparticles could be assessed by biocompatibility arrangement of adsorbents, (h) recovery also, reusability of adsorbents are additionally involved strides for the research and business sectors. It very well may be remembered for additional examination, (i) as this review shows the utilizations of NC-GO-based adsorbents yet restricted somewhat. In reality, wastewater contains different contaminations including alkaline, acids, and salts; NC-GO-based multifunctional adsorbents should be designed and fabricated in such a manner, all pollutants related to water could be removed, and finally (j) slight harms and bio-fouling (on the surfaces of adsorbents because of harmfulness and microorganisms in water) are fundamental sources to make the entire adsorbent nonfunctional. Examination of the recycling of the adsorbents besides such little challenges should be deemed fit for additional exploration.

Frantically, these CEL-graphene-based adsorbent materials structures with multifaceted uses are favorable and dependable to take for enormous scope; while looking for additional benefits of such multifunctional adsorbents-based applications are attractive at the same time challenging.

Acknowledgements The authors wish to acknowledge the Department of Chemical Sciences, University of Johannesburg, Doorfontein, Johannesburg 2028, South Africa, and DST-CSIR National Centre for Nanostructured Materials, Council for Scientific and Industrial Research, Pretoria 0001, South Africa.

Declaration of Competing Interest The authors declare that there is no competing interest in whatsoever form.

References

1. S. Afroze, T.K. Sen, A review on heavy metal ions and dye adsorption from water by agricultural solid waste adsorbents. Water Air Soil Pollut. **229**, 1–50 (2018)
2. T.S. Anirudhan, J.R. Deepa, Nano-zinc oxide incorporated graphene oxide/nanocellulose composite for the adsorption and photo catalytic degradation of ciprofloxacin hydrochloride from aqueous solutions. J. Colloid Interface Sci. **490**, 343–356 (2017)
3. N.I.F. Aris, N.A. Rahman, M.H. Wahid et al., Superhydrophilic graphene oxide/electrospun cellulose nanofibre for efficient adsorption of organophosphorus pesticides from environmental samples. R. Soc. Open Sci. **7**, 192050 (2020)
4. U. Baig, M. Faizan, M. Sajid, Effective removal of hazardous pollutants from water and deactivation of water-borne pathogens using multifunctional synthetic adsorbent materials: a review. J. Clean Prod. 126735 (2021)

5. A. Bhattacharyya, B. Banerjee, S. Ghorai et al., Development of an auto-phase separable and reusable graphene oxide-potato starch based cross-linked bio-composite adsorbent for removal of methylene blue dye. Int. J. Biol. Macromol. **116**, 1037–1048 (2018)
6. A. Bhattacharyya, S. Ghorai, D. Rana et al., Design of an efficient and selective adsorbent of cationic dye through activated carbon - graphene oxide nanocomposite: study on mechanism and synergy. Mater. Chem. Phys. 260 (2021)
7. A. Bhattacharyya, D. Mondal, I. Roy et al., Studies of the kinetics and mechanism of the removal process of proflavine dye through adsorption by graphene oxide. J. Mol. Liq. **230**, 696–704 (2017)
8. B.C. Brodie, On the atomic weight of graphite. Philos. Trans. R. Soc. Lond. **149**, 249–259 (1859)
9. J. Chen, H. Li, L. Zhang et al., Direct reduction of graphene oxide/nanofibrillated cellulose composite film and its electrical conductivity research. Sci. Rep. **10**, 3124 (2020)
10. L. Chen, Y. Li, S. Hu et al., Removal of methylene blue from water by cellulose/graphene oxide fibres. J. Exp. Nanosci. **11**, 1156–1170 (2016)
11. X. Chen, S. Zhou, L. Zhang et al., Adsorption of heavy metals by graphene oxide/cellulose hydrogel prepared from NaOH/urea aqueous solution. Materials (Basel) 9 (2016)
12. Y. Chen, Synthesis and characterization of novel functional materials based on cellulose and graphene oxide (2020)
13. E. Chibowski, A. Szczes, Magnetic water treatment-a review of the latest approaches. Chemosphere **203**, 54–67 (2018)
14. A. Chiori, Urban water planning in Lagos, Nigeria: an analysis of current infrastructure developments and future water management solutions (2018)
15. P. Dhar, B. Pratto, A.J. Gonçalves Cruz et al. Valorization of sugarcane straw to produce highly conductive bacterial cellulose/graphene nanocomposite films through in situ fermentation: kinetic analysis and property evaluation. J. Clean Prod. 238 (2019)
16. A.M. Dimiev, L.B. Alemany, J.M. Tour, Graphene oxide. Origin of acidity, its instability in water, and a new dynamic structural model. ACS Nano **7**, 576–588 (2012)
17. K. Dutta, B. Das, J.T. Orasugh et al., Bio-derived cellulose nanofibril reinforced poly(N-isopropylacrylamide)-g-guar gum nanocomposite: an avant-garde biomaterial as a transdermal membrane. Polymer **135**, 85–102 (2018)
18. W. Gao, L.B. Alemany, L. Ci, P.M. Ajayan, New insights into the structure and reduction of graphite oxide. Nat. Chem. **1**, 403–408 (2009)
19. H. Gu, C. Gao, X. Zhou et al., Nanocellulose nanocomposite aerogel towards efficient oil and organic solvent adsorption. Adv. Compos. Hybrid Mater. 1–10 (2021)
20. Y. Hui, W. Xie, H. Gu, Reduced Graphene oxide/nanocellulose/amino-multiwalled carbon nanotubes nanocomposite aerogel for excellent oil adsorption. ES Food Agrofor. (2021)
21. W.S. Hummers, R.E. Offeman, Preparation of graphitic oxide. J. Am. Chem. Soc. **80**, 1339 (1958)
22. A. Hussain, J. Li, J. Wang et al., Hybrid monolith of graphene/TEMPO-oxidized cellulose nanofiber as mechanically robust, highly functional, and recyclable adsorbent of methylene blue dye. J. Nanomater. (2018)
23. W.B. Jensen, Vignettes in the history of chemistry. 1. What is the origin of the Gibbs–Helmholtz equation? ChemTexts **2** 1 (2016)
24. W. Jei, S.-H. Gui, J.-H. Wu, D.-D. Xu, Y. Sun, X.-Y. Dong, Y.-Y. Dai, Y.-F. Li, Nanocellulose-graphene oxide hybrid aerogel towards water purification. Appl. Environ. Biotechnol. 4 (2019)
25. N.A.V Jitendra, Synthesis, characterization and preparation of nanocellulose and different cellulose/nanocellulose/graphene composites from cassava root and its potential application for pesticide adsorption from water. Int. J. Res. Anal. Rev. (IJRAR) 5 (2018)
26. R. Kant, Textile dyeing industry an environmental hazard. J. Nat. Sci. **4**(1), 22–26 (2012)
27. P. Kotcharat, P. Chuysinuan, T. Thanyacharoen et al., Development of bacterial cellulose and polycaprolactone (PCL) based composite for medical material. Sustain. Chem. Pharm. 20 (2021)

28. A.H. Lerf, H. He, M. Forster, J. Klinowski, Structure of graphite oxide revisited. J. Phys. Chem. B **102**, 4477–4482 (1998)
29. P. Li, X. Yang, H. Miao et al., Simultaneous determination of 19 triazine pesticides and degradation products in processed cereal samples from Chinese total diet study by isotope dilution–high performance liquid chromatography–linear ion trap mass spectrometry. Anal. Chim. Acta **781**, 63–71 (2013)
30. W. Li, L. Zhang, D. Hu et al., A mesoporous nanocellulose/sodium alginate/carboxymethyl-chitosan gel beads for efficient adsorption of Cu(2+) and Pb(2). Int. J. Biol. Macromol. **187**, 922–930 (2021)
31. D. Liao, Y. Guan, Y. He et al., Pickering emulsion strategy for high compressive carbon aerogel as lightweight electromagnetic interference shielding material and flexible pressure sensor. Ceram. Int. **47**, 23433–23443 (2021)
32. J. Liu, S. Wang, L. Jiang et al., Production and characterization of antimicrobial bacterial cellulose membranes with non-leaching activity. J. Ind. Eng. Chem. **103**, 232–238 (2021)
33. P. Liu, C. Zhu, A.P. Mathew, Mechanically robust high flux graphene oxide - nanocellulose membranes for dye removal from water. J. Hazard. Mater. **371**, 484–493 (2019)
34. W. Logrono, M. Perez, G. Urquizo et al., Single chamber microbial fuel cell (SCMFC) with a cathodic microalgal biofilm: A preliminary assessment of the generation of bioelectricity and biodegradation of real dye textile wastewater. Chemosphere **176**, 378–388 (2017)
35. H. Luo, J. Xie, J. Wang et al., Step-by-step self-assembly of 2D few-layer reduced graphene oxide into 3D architecture of bacterial cellulose for a robust, ultralight, and recyclable all-carbon absorbent. Carbon **139**, 824–832 (2018)
36. X. Luo, L. Liu, L. Wang et al., Facile synthesis and low concentration tylosin adsorption performance of chitosan/cellulose nanocomposite microspheres. Carbohyd. Polym. **206**, 633–640 (2019)
37. X. Luo, L. Liu, L. Wang et al., Facile synthesis and low concentration tylosin adsorption performance of chitosan/cellulose nanocomposite microspheres. Carbohydr. Polym. **206**, 633–640 (2019)
38. C.R. Minitha, K. Rajavel, R.T. Rajendra Kumar, Magnetite decorated reduced graphene oxide: a study of multifunctional antibacterial and removal of lead ion properties for water disinfection applications. Adv. Eng. Mater. 22 (2020)
39. Y. Nakajima TaM, Formation process and structure of graphite oxide. Carbon **32**, 469–475 (1994)
40. J.T. Orasugh, S. Dutta, D. Das et al., Sustained release of ketorolac tromethamine from poloxamer 407/cellulose nanofibrils graft nanocollagen based ophthalmic formulations. Int. J. Biol. Macromol. **140**, 441–453 (2019)
41. J.T. Orasugh, S.K. Ghosh, D. Chattopadhyay, Nanofiber-reinforced biocomposites, in *Fiber-Reinforced Nanocomposites: Fundamentals and Applications* (2020), pp. 199–233
42. J.T. Orasugh, N.R. Saha, D. Rana et al., Jute cellulose nanofibrils/hydroxypropylmethylcellulose nanocomposite: A novel material with potential for application in packaging and transdermal drug delivery system. Ind. Crops Prod. **112**, 633–643 (2018)
43. J.T. Orasugh, N.R. Saha, G. Sarkar et al., Synthesis of methylcellulose/cellulose nano-crystals nanocomposites: material properties and study of sustained release of ketorolac tromethamine. Carbohydr. Polym. **188**, 168–180 (2018)
44. J.T. Orasugh, N.R. Saha, G. Sarkar et al., A facile comparative approach towards utilization of waste cotton lint for the synthesis of nano-crystalline cellulose crystals along with acid recovery. Int. J. Biol. Macromol. **109**, 1246–1252 (2018)
45. J.T. Orasugh, G. Sarkar, N.R. Saha et al., Effect of cellulose nanocrystals on the performance of drug loaded in situ gelling thermo-responsive ophthalmic formulations. Int. J. Biol. Macromol. **124**, 235–245 (2019)
46. K. Ozge, C. Hande, Chitosan/graphene oxide/nanocellulose composites for removal of Cu(II) and Pb(II) Ions in aqueous solution. Polym. Sci. Ser. A (2021)

47. P. Pandey, P. Kass, M. Soupir et al., Analysis and application of Bacillus subtilis sortases to anchor recombinant proteins on the cell wall. AMB Expr. **4**, 1–16 (2014)
48. A. Payen, Mémoire sur les Applications Théoriques et Pratiques des Propriétés du Tissu Élémentaire des Végétaux. Compt. Rendus **8**, 59–61 (1839)
49. S.C. Pinto, G. Goncalves, S. Sandoval et al., Bacterial cellulose/graphene oxide aerogels with enhanced dimensional and thermal stability. Carbohydr. Polym. **230** 115598 (2020)
50. Y. Qin, S. Li, Y. Li et al., Mechanically robust polybenzoxazine/reduced graphene oxide wrapped-cellulose sponge towards highly efficient oil/water separation, and solar-driven for cleaning up crude oil. Compos. Sci. Technol. 197 (2020)
51. A. Radhakrishnan, J. Nahi, B. Beena, Synthesis and characterization of multi-carboxyl functionalized nanocellulose/graphene oxide-zinc oxide composite for the adsorption of uranium (VI) from aqueous solutions: Kinetic and equilibrium profiles. Mater. Today: Proc. **41**, 557–563 (2021)
52. S.S. Ray, A.O.C. Iroegbu, Nanocellulosics: benign, sustainable, and ubiquitous biomaterials for water remediation. ACS Omega **6**, 4511–4526 (2021)
53. E. Rosenberg, Heavy metals in water: presence, removal and safety. Johns. Matthey Technol. Rev. **59**, 293–297 (2015)
54. G. Ruess, Über das graphitoxyhydroxyd (graphitoxyd). Monatshefte für Chemie **76**, 381–417 (1746)
55. S. Sadhukhan, A. Bhattacharyya, D. Rana et al., Synthesis of RGO/NiO nanocomposites adopting a green approach and its photocatalytic and antibacterial properties. Mater. Chem. Phys. **247**, 122906 (2020)
56. G. Sarkar, J.T. Orasugh, N.R. Saha et al., Cellulose nanofibrils/chitosan based transdermal drug delivery vehicle for controlled release of ketorolac tromethamine. New J. Chem. **41**, 15312–15319 (2017)
57. L. Saya, D. Gautam, V. Malik et al., Natural polysaccharide based graphene oxide nanocomposites for removal of dyes from wastewater: a review. J. Chem. Eng. Data **66**, 11–37 (2020)
58. W. Scholz, H.P. Boehm, Untersuchungen am graphitoxid. VI. Betrachtungen zur struktur des graphitoxids. Z. Anorg. Allg. Chem. **369**, 327–340 (1969)
59. P.R. Sharma, S.K. Sharma, T. Lindström et al., Nanocellulose-enabled membranes for water purification: perspectives. Adv. Sustain. Syst. 4 (2020)
60. R. Sreenivasan, S. Suma Mahesh, V.S. Sumi, Synthesis and application of polymer-grafted nanocellulose/graphene oxide nano composite for the selective recovery of radionuclides from aqueous media. Sep. Sci. Technol. **54**, 1453–1468 (2018)
61. L. Staudenmaier, Verfahren zur darstellung der graphitsaure. Berichte Der Deutschen Chemischen Gesellschaft (A and B Series) **31**, 1481–1487 (1898)
62. F. Suo, G. Xie, J. Zhang et al., A carbonised sieve-like corn straw cellulose–graphene oxide composite for organophosphorus pesticide removal. RSC Adv. **8**, 7735–7743 (2018)
63. T. Szabó, O. Berkesi, P. Forgó, K. Josepovits, Y. Sanakis, D. Petridis, I. Dékány, Evolution of surface functional groups in a series of progressively oxidized graphite oxides. Chem. Mater. **18**, 2740–2749 (2006)
64. J. Tao, J. Yang, C. Ma et al., Cellulose nanocrystals/graphene oxide composite for the adsorption and removal of levofloxacin hydrochloride antibiotic from aqueous solution. R. Soc. Open Sci. **7**, 200857 (2020)
65. P. Tchounwou, C. Yedjou, A. Patlolla et al., Heavy metal toxicity and the environment in Molecular, clinical and environmental toxicology, ed. by A. Luch, vol. 101 (Springer, Berlin, 2012), pp. 133–164
66. J. Tersur Orasugh, S. Dutta, D. Das et al., Utilization of cellulose nanocrystals (CNC) biopolymer nanocomposites in ophthalmic drug delivery system (ODDS). J. Nanotechnol. Res. 01 (2019)
67. D. Trache, V.K. Thakur, R. Boukherroub, Cellulose nanocrystals/graphene hybrids-a promising new class of materials for advanced applications. Nanomaterials (Basel) 10 (2020)

68. A. Tshikovhi, S.B. Mishra, A.K. Mishra, Nanocellulose-based composites for the removal of contaminants from wastewater. Int. J. Biol. Macromol. **152**, 616–632 (2020)
69. Ulrich Hofmann uRH Uber die Saurenatur und die Methylierung von Graphitoxyd. Berichte Der Deutschen Chemischen Gesellschaft (A and B Series) **72**, 754–771
70. L. Valencia, S. Monti, S. Kumar et al., Nanocellulose/graphene oxide layered membranes: elucidating their behaviour during filtration of water and metal ions in real time. Nanoscale **11**, 22413–22422 (2019)
71. Y.-J. Wan, P.-L. Zhu, S.-H. Yu et al., Ultralight, super-elastic and volume-preserving cellulose fiber/graphene aerogel for high-performance electromagnetic interference shielding. Carbon **115**, 629–639 (2017)
72. J. Wang, X. Li, L. Tang et al., Synthesis approaches to magnetic graphene oxide and its application in water treatment: a review. Water Air Soil Pollut. 232 (2021)
73. Y. Wang, S. Yadav, T. Heinlein et al., Ultra-light nanocomposite aerogels of bacterial cellulose and reduced graphene oxide for specific absorption and separation of organic liquids. RSC Adv. 4 (2014)
74. Z. Wang, L. Song, Y. Wang et al., Construction of a hybrid graphene oxide/nanofibrillated cellulose aerogel used for the efficient removal of methylene blue and tetracycline. J. Phys. Chem. Solids 150 (2021)
75. P. Wexler, *Encyclopedia of Toxicology* (Elsevier/Academic Press, 2014)
76. Y. Wu, T.Y. Huang, Z.X. Li et al., In-situ fermentation with gellan gum adding to produce bacterial cellulose from traditional Chinese medicinal herb residues hydrolysate. Carbohydr. Polym. **270**, 118350 (2021)
77. C. Xiang, C. Wang, R. Guo et al., Synthesis of carboxymethyl cellulose-reduced graphene oxide aerogel for efficient removal of organic liquids and dyes. J. Mater. Sci. **54**, 1872–1883 (2018)
78. A. Yang, J. Wu, C.P. Huang, Graphene oxide-cellulose composite for the adsorption of uranium(VI) from dilute aqueous solutions. J. Hazard. Toxic Radioact. Waste 22 (2018)
79. J. Yang , C. Ma, J. Tao et al., Optimization of polyvinylamine-modified nanocellulose for chlorpyrifos adsorption by central composite design. Carbohydr. Polym. **245**, 116542 (2020)
80. M. Yao, Z. Wang, Y. Liu et al., Preparation of dialdehyde cellulose graftead graphene oxide composite and its adsorption behavior for heavy metals from aqueous solution. Carbohydr. Polym. **212**, 345–351 (2019)
81. Q. Yao, B. Fan, Y. Xiong et al., 3D assembly based on 2D structure of cellulose nanofibril/graphene oxide hybrid aerogel for adsorptive removal of antibiotics in water. Sci. Rep. **7**, 45914 (2017)
82. H. Yu, S. Zhang, Y. Wang et al., Covalent modification of Nanocellulose (NCC) by functionalized Graphene oxide (GO) and the study of adsorption mechanism. Compos. Interfaces **28**, 145–158 (2020)
83. S. Yu, D. Wei, L. Shi et al., Three-dimensional graphene/titanium dioxide composite for enhanced U (VI) capture: insights from batch experiments, XPS spectroscopy and DFT calculation. Environ. Pollut. **251**, 975–983 (2019)
84. A. Zaman, J.T. Orasugh, P. Banerjee et al., Facile one-pot in-situ synthesis of novel graphene oxide-cellulose nanocomposite for enhanced azo dye adsorption at optimized conditions. Carbohydr. Polym. **246**, 116661 (2020)
85. C. Zhang, R.Z. Zhang, Y.Q. Ma et al., Preparation of cellulose/graphene composite and its applications for triazine pesticides adsorption from water. ACS Sustain. Chem. Eng. **3**, 396–405 (2015)
86. M. Zhao, S. Zhang, G. Fang et al., Directionally-grown carboxymethyl cellulose/reduced graphene oxide aerogel with excellent structure stability and adsorption capacity. Polymers (Basel) 12 (2020)
87. A.L.T. Zheng, S. Sabidi, T. Ohno et al., Cu2O/TiO2 decorated on cellulose nanofiber/reduced graphene hydrogel for enhanced photocatalytic activity and its antibacterial applications. Chemosphere **286**, 131731 (2021)

88. X. Zhou, Q. Fu, H. Liu et al., Solvent-free nanoalumina loaded nanocellulose aerogel for efficient oil and organic solvent adsorption. J. Colloid Interface Sci. **581**, 299–306 (2021)
89. C. Zhu, P. Liu, A.P. Mathew, Self-assembled TEMPO cellulose nanofibers: graphene oxide-based biohybrids for water purification. ACS Appl. Mater. Interfaces **9**, 21048–21058 (2017)
90. C. Zhu, S. Monti, A.P. Mathew, Cellulose nanofiber-graphene oxide biohybrids: disclosing the self-assembly and copper-ion adsorption using advanced microscopy and reaxff simulations. ACS Nano **12**, 7028–7038 (2018)
91. A. Ishikawa, T. Okano, J. Sugiyama, Fine structure and tensile properties of ramie fibres in the crystalline form of cellulose I, II, IIII and IVI. Polymer **38**(2), 463–468 (1997). https://doi.org/10.1016/S0032-3861(96)00516-2

Chapter 2
Recent Progress in Polysaccharide-Based Hydrogel Beads as Adsorbent for Water Pollution Remediation

Dalia Allouss, Edwin Makhado, and Mohamed Zahouily

Abstract This chapter briefly reviews the recent developments on polysaccharide-based hydrogel beads for water pollution remediation. The deployment of polysaccharide-based adsorbent materials in treating wastewater is challenging since they are very soluble in the aqueous medium. To date, modification of natural polysaccharides has attracted extensive attention because their functional groups changes, imparting a high binding affinity for various pollutants in water. In the same vein, this work covers recent advancements in the modifications and progresses in the domain of hydrogel technology with particular attention on polysaccharide-based hydrogel beads and their composites. These materials have been employed in removing various organic dyes and heavy metals from wastewater. Different types of polysaccharide-based hydrogel beads, as well as polysaccharide-based hydrogel beads composites used for the treatment of wastewater, are discussed in this chapter. Furthermore, the reader is provided with comprehensive experimental findings regarding the adsorption mechanisms and capacities of such hydrogel adsorbents for adsorbing contaminants from aquatic liquids. Lastly, we end this chapter with a look into some existing challenges and prospects of the polysaccharide-based hydrogel beads in water pollution remediation.

D. Allouss (✉) · M. Zahouily
Laboratory of Materials, Catalysis & Valorization of Natural Resources, FSTM, Hassan II University, Casablanca, Morocco
e-mail: allouss-dalia@hotmail.fr; dalia.allouss@etu.fstm.ac.ma

E. Makhado (✉)
Department of Chemistry, School of Physical and Mineral Sciences, University of Limpopo, Polokwane, South Africa
e-mail: edwin.makhado@ul.ac.za

M. Zahouily
MASCIR Foundation, VARENA Center, Rabat Design, Rabat, Morocco

M. J. Hato and S. Sinha Ray (eds.), *Functional Polymer Nanocomposites for Wastewater Treatment*, Springer Series in Materials Science 323,
https://doi.org/10.1007/978-3-030-94995-2_2

2.1 Introduction

An increase in industrialization has led to a substantial rise in environmental pollution. Both organic and inorganic contaminants arise from a diverse group of industries, including textile, leather, drug, food processing, cosmetic, battery, smelting, mining, printing, ceramic, and glass manufacturing [20, 72, 92]. Organic and inorganic contaminants pose drastically a weighty risk for the aquatic ecosystem. In addition, these contaminants, especially organic dyestuffs and severe heavy metal ions, are viewed as very risky since they are non-biodegradable, extremely harmful, and persistent and tend to be bioaccumulating [67, 69]. The complex structure of organic dyes prevents light penetration and photosynthesis, allowing them to accumulate in an aquatic environment [12]. Additionally, the ions of heavy metals present a public health concern, e.g. exposure to arsenic affects all organ systems (e.g. cardiovascular, renal, nervous as well as respiratory systems) [88]. Similarly, the majority of the dyes utilized in the textile industry are toxic and potentially carcinogenic [17]. Lately, emergent pollutants are occupied a colossal interest in the wastewater research field because of their poisonous feature, and they are unknown products or chemicals without regulatory status [25]. The treatment of these noxious contaminants in an aqueous medium is crucial. Based on the above-stated increasing material resources production inflicts the influx of anthropogenic pollutants into the aqueous environment, engendering a potential menace to people's health and the ecosystem. For these reasons, several nations and the World Health Organization (WHO) have formulated life-threatening levels of heavy metals contamination in drinking water (Table 2.1) [112]. Accordingly, enormous efforts have been directed towards removing harmful heavy metal ions and organic dyestuffs from wastewater. Including electrocoagulation/degradation process, membrane filtration [33], electrocoagulation [7], chemical coagulation [102], chemical precipitation [122], advanced oxidation process [28], and adsorption system [6] that have shown off a good performance in wastewater remediation.

The adsorption method has been recognized as an encouraging process due to its simplicity, feasibility and it is relatively inexpensive compared to other conventional techniques. Therefore, the flexibility of adsorption makes it largely utilized while removing contaminants from wastewater [4]. Principally, an adsorption system is

Table 2.1 The standard level of certain heavy metal ions in drinking water set by the WHO and various countries (μg/L)

Heavy metals	WHO	USA	European Union	Canada	Japan	China	Australia
Pb	10	15	10	10	50	10	50
Cr	50	100	50	50	50	50	50
Cd	3	5	5	5	10	5	2
As	10	10	10	25	10	10	7
Hg	6	2	1	1	0.5	1	1

applied to remove highly toxic or low concentrated pollutants, which are not freely treated by other conventional techniques. It also inhibits the generation of harmful and hazardous waste and is viewed as an eco-friendly solution, with widespread potential for industrial applications [75]. Typically, two modes of adsorption are used, namely the continuous [26] and the discontinuous modes [104]. The discontinuous or batch system operates in a controlled environment containing the desired dose of adsorbent in contact with the defined volume of effluent. The continuous flow column adsorption is designed as a dynamic adsorption process where the influent (pollutant or adsorbate solution) is continuously fed into the column and discharged [34]. Furthermore, any adsorption process may be economical when low-cost adsorbents are employed or when regeneration is achievable [46]. Dynamic adsorption technology tends to be preferred at the industrial level since it is convenient for large-scale water purification.

The selection of the adsorbent presents a decisive part in the implementation/design of any adsorption mode. In the recent era, academics have focused their attention on producing affordable, efficient, eco-friendly, and renewable adsorbents. Polymeric materials are the most promising and gained considerable attention in the field of separation technology. Within this context, the use of polysaccharide-based adsorbents has drawn a surge of attention as an emerging technology due to the use of natural resources. Several researchers revealed that polysaccharide-based adsorbents are favorable materials to uptake organic dyestuffs and metallic ions from polluted water [10, 17, 36, 44]. Polysaccharides belong to the group of materials known as carbohydrates. They are a class of natural polymers that are available in high quantities from sustainable sources and exhibit certain key properties, including nontoxicity, degradability, and compatibility with the environment [59]. Among polysaccharides, alginate [127], chitosan [47], cellulose [15], and starch [114] have been drawn exceptionally spotlight for wastewater treatment as sustainable adsorbents. The practical applications of the aforementioned natural polysaccharide as adsorbents are limited because these materials cannot achieve desirable adsorption performance. For this reason, natural polysaccharides are used as coagulants and flocculants for wastewater treatment [124].

In the last few years, academic and industrial communities have devoted special attention to the development of modified polysaccharides-based adsorbents. It is well documented that most polysaccharides have immense structural as well as abundant reactive hydroxyl (–OH), amine, carboxyl (–COOH), amino ($–NH_2$), acryl amino ($–NH_2$) and sulfonic ($–SO_3H$) groups which provide possibilities for physical and chemical modification to generate novel materials. Modification of polysaccharides led to improved properties without changing the fundamental backbone of polysaccharides [82]. Various polysaccharides-based adsorbents have been prepared and applied as adsorbents for removing dyes and metal ions from wastewater. According to the literature, numerous types of polysaccharides-based adsorbents have been investigated including the grafting process, hydrogel, hydrogel composite, and hydrogel beads [5, 6, 48, 64, 65, 91].

Hydrogels represent three-dimensional (3D) soft polymeric materials, which can imbibe a substantial amount of liquids [70]. In this direction, their innate ability to

retain and absorb a high quantity of liquid makes them ideal candidates for the adsorption of aquatic pollutants. Hydrogels attracted a great deal of regard in numerous interests owing to their permeability, biocompatibility, relatively cheap, and nontoxicity. Hydrogels have found fruitful utilization in several fields, such as biomedical materials, drug delivery, biosensors, wound dressing, agriculture, wastewater treatment, personal hygiene, diapers, cosmetic products, etc. Hydrogels are developed according to their intended application and they can be prepared in different forms such as hollow fiber, ring, film, beads, and powder [48, 76, 126]. Recently, polysaccharide-based hydrogel beads have been devised as adsorbents to adsorb pollutants from aqueous solutions. Numerous researchers applied hydrogels to uptake noxious heavy metal ions including arsenic (As (V)), copper (Cu (II)), lead Pb (II), chromium (Cr (VI)) as well as cadmium (Cd (II), and organic dyes (i.e. methylene blue (MB), Congo red (CR), Rhodamine blue (RhB), malachite green (MG), crystal violet (CV) and methyl orange (MO)) from the aquatic ecosystem. The recyclability of hydrogels for repeated cycles makes them attractive for practical application in environmental remediation. On the other side, Fakir and co-authors reviewed the use of fabricated hydrogel beads for organic pollutants degradation [2].

In recent years, the ongoing attention in this domain of technology has incited the elaboration of polysaccharide-based hydrogel composite. This approach has broadened the use of hydrogel beads in various application fields. In this direction, various inorganic materials such as titanium dioxide (TiO_2), iron oxide (Fe_2O_3), graphene oxide (GO), clay minerals, and carbon materials have been incorporated into the polymeric hydrogel networks [5, 6, 21, 63–66, 68, 71, 103]. Studies have shown that incorporating inorganic materials into polymeric hydrogel matrices is a promising approach for enhancing their performance when contrasted with hydrogel without inorganic components. For example, hydrogels incorporated with inorganic materials exhibited improved properties like thermal stability, mechanical strength, and important capacity of adsorption; it is noteworthy to mention that the applicability of hydrogels is strongly influenced by the stability of integrated inorganic materials in the polymeric hydrogel networks. Hong and co-authors compared the adsorption capacity of the prepared MnO_2-alginate beads and alginate beads as adsorbents for adsorption of strontium from seawater from real seawater [41]. Their outcomes displayed that the capacity of adsorption of the MnO_2-alginate bead composite was about four times greater than the alginate beads [41].

In this chapter, the ambition is to study the ongoing progress in applying polysaccharide-based hydrogel beads as adsorbents for remediating contaminated water containing organic dyestuffs and/or heavy metal ions. Moreover, recent advancements in the development of polysaccharide-based hydrogel beads have also been reviewed in this chapter. The adsorption of the abovementioned aqueous pollutants by employing polysaccharide-based hydrogel beads through batch/dynamic adsorption systems has been comprehensively discussed with their comparative sorption capacity. Lastly, the future challenges of the use of polysaccharide-based hydrogel beads for wastewater are considered.

2.2 Polysaccharides

Polysaccharides are usually derived from plants (i.e., cellulose, alginate, guar gum, etc.), animals (e.g., chitosan, chitin and heparin), and microorganisms (e.g., pullulan, xanthan gum and gellan). These biopolymers are of great value thanks to their outstanding and unique characteristics, namely their hydrophilic character, their biodegradability, and their high biocompatibility.

Moreover, polysaccharides may be obtained from sustainable sources, which is economically advantageous over traditional synthetic polymers [89]. In addition, they show biological and chemical features such as being non-toxic, biologically compatible, fully biodegradable, having functionality, with high chemical reactivity, chirality, chelation characteristics and adsorption properties. Cellulose, chitosan, alginate, and starch represent the most typical polysaccharides that will be discussed in the following sections.

2.2.1 Sodium Alginate

Alginate is a sodium salt of alginic acid, which is usually extracted out of the cell walls of brown algae. It is a polyelectrolyte, hydrophilic biopolymer, extensively employed in cosmetics, medical products, pharmaceuticals, textiles, food additives, and wastewater treatment [131]. As a linear water-soluble polysaccharide, alginate comprises linear blocks of β-D-mannuronic acid (M) and α-L-guluronic acid (G) monomers linked via (1 → 4) in the structural arrangement. Hence, the skeleton of alginate is made up of sequences of mannuronic acid blocks (M blocks, etc.) or guluronic acid blocks (G blocks), and alternating sequence regions (i.e., MG, MMG, GGM). Alginates exhibit a broad variation in the distribution of molecular weight and are charged polysaccharides with electrostatic forces resulting from the carboxylic groups in the biopolymer skeleton (Fig. 2.1a). Accordingly, their solubility is very sensitive to the pH and to the ion strength of the solvent, as well as to the existence of ions in the solution. Monovalent metal ions (e.g., Na^+) create soluble salts with alginate while divalent or multivalent cations produce gels. Cations show a distinct affinity to alginates, albeit the degree of cross-linking may also be impacted by the chemical composition (M/G ratio). The model (Fig. 2.2), whereby the existence of cross-linking cations drives interactions between alginate chains, has described the gelation of alginates [14].

2.2.2 Starch

Starch is a botanical polysaccharide that is mostly found in wheat, roots and tubers like potatoes, cassava, and manioc, and legumes such as peas, chickpeas, and beans.

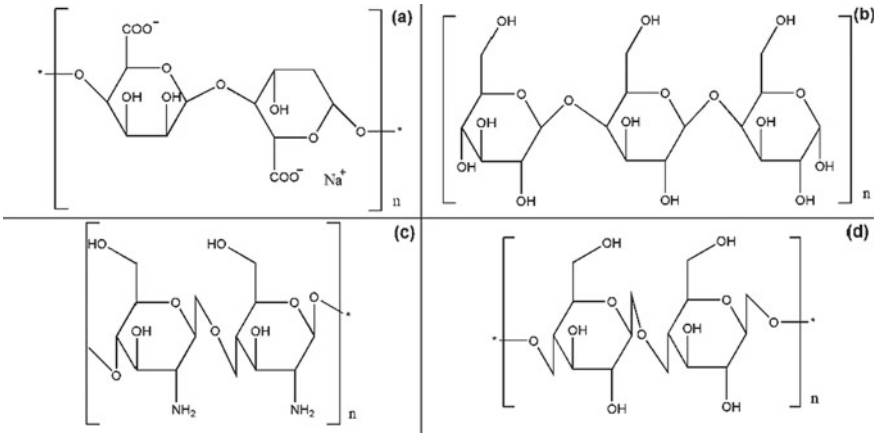

Fig. 2.1 Chemical structure of Polysaccharides **a** sodium alginate, **b** starch, **c** chitosan, and **d** cellulose

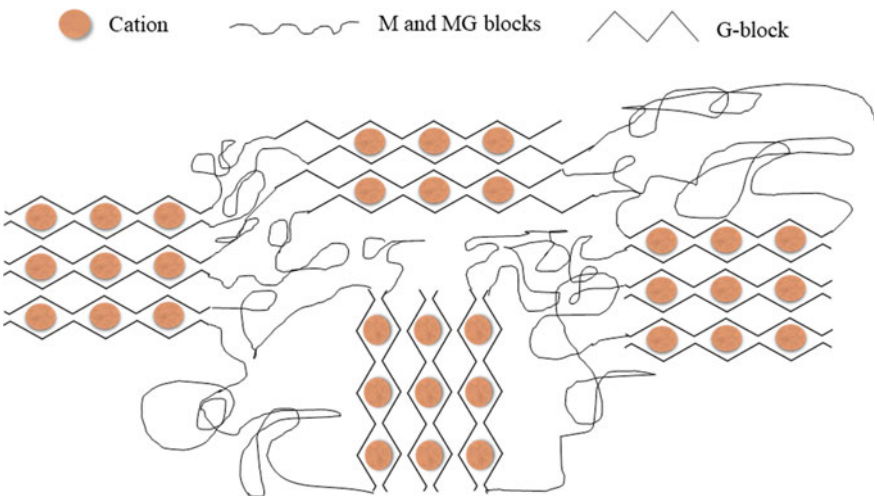

Fig. 2.2 Egg-Box model representation

Starch is one of the richest natural polymers on earth. Starches are blends of two polyglucanes, amylopectin and amylose; however, they only have one kind of carbohydrate that is glucose. Amylose is a mainly linear polymer of linked α-D-glucopyranosyl units (1 → 4). Amylopectin is a heavily ramified polymer of α-D-glucopyranosyl units that contain 1 → 4 linkages with 1 → 6 ramification points. The relative ratio of these components varies according to the source of the starch (for instance, tapioca, corn, wheat, and potato) and the influences on the molecular order and crystallinity of the starch polysaccharide (Fig. 2.1b). Approximately 70% of the

mass of the starch pellet is classed as amorphous and around 30% as crystalline. The amorphous areas are made up of most of the amylose and a considerable quantity of amylopectin. The crystalline part is mainly composed of amylopectin [42]. Starch has been widely utilized to produce biocompatible hydrogels owing to its low-priced, tremendous natural richness, biodegradability/biocompatibility, recyclability, and safe properties [79].

2.2.3 Chitosan

Chitosan (Fig. 2.1c), derived from the N-deacetylation of chitin, a natural polymer from crustaceans and fungi biomasses. It can also be prepared cheaply from chitin that is the second more abundant biopolymer in nature (after cellulose) and is freely obtainable from seafood processing debris. Chitosan shows a great capacity to remove metallic ions because it has a couple of functional groups (hydroxyl and amine groups) that can serve as active sites for metal ions uptake [109]. Chitosan is very versatile when it comes to development. The processing of chitosan could be in various ways, as follows hydrogels, films, micro-and nanoparticles, porous scaffolds, micro-and nanofibers, and meshes for a variety of practical utilizations. It is insoluble in water and organic solvents. Nevertheless, after protonation of the amine functionalities of the glucosamine units by acid, electrostatic repulsions between the NH_3 groups will destroy the attractive interchain interactions, like hydrogen bonds and hydrophobic interactions, and thus the solubility of chitosan. At pH lower than its pK_a, which may be between ~6.5 and ~7 chitosan is a polycation, and at pH 4.0 and less, it is protonated [87]. Chitosan exhibits an intrinsic anti-microbial ability, preventing the development of bacteria and fungi. Chitosan-coated surfaces have been demonstrated to be immune to the formation of biofilm generated by bacteria and yeast [37].

2.2.4 Cellulose

Cellulose remains the dominant glucose polymer found in nature. It is the principal component of plants and natural fibers such as linen and cotton. Cellulose is a straight chain of ring-shaped glucose molecules and has a flat, ribbon-like configuration. The monomer (Fig. 2.1d) is composed of two anhydroglucose rings, $[(C_6H_{10}O_5)_n$; n = 10.000 to 15.000, where n is a function of the cellulosic source material]. It is joined by oxygen covalently bonded to C1 of a glucose ring and C4 of the adjacent ring ($1 \rightarrow 4$ bonds) and therefore referred to as the glucoside bond $\beta 1 \rightarrow 4$ [80]. Cellulose and its derivatives are green polymers because they are degradable by various bacteria and fungi existing in the air, water, and soil. It has gained attention in water remediation owing to its outstanding adsorptive performance [18]. Cellulose hydrogels, reversible or stable, may be produced through suitably cross-linking aqueous

solutions of cellulose ethers, such as methylcellulose (MC), hydroxypropyl methylcellulose (HPMC), ethyl cellulose (EC), hydroxyethylcellulose (HEC), and sodium carboxymethyl cellulose (CMC), which are amongst the highest frequently operating cellulose derivatives.

2.3 Polysaccharide-Based Hydrogel Beads Preparation

Polysaccharides have outstanding physical and chemical properties coupled with bio-resource properties such as abundance, biocompatibility, and sustainability. The most used techniques to prepare polysaccharide beads are emulsion cross-linking [57] and ionic crosslinking [84]. In the water treatment and purification domain, polysaccharide-based hydrogel beads are very effective in capturing a broad selection of aqueous contaminants including metallic ions, harmful dyestuffs, and harmful pharmaceutical wastes [95].

2.3.1 Dropping Method: Ionic Cross-Linking

The beads are obtainable by forming rounded droplets of a polysaccharide gel and solidifying these droplets in a cationic curing solution, such as Ca^{2+}, Al^{3+}, Ba^{2+}, Fe^{3+}, etc. By squeezing the polymeric gel through a thin opening, such as a syringe nozzle (Fig. 2.3), a droplet is produced when the connected forces of gravity and pressure used for ejection exceed a certain value that is determined by the surface tension of the solution and the capillary forces at the exit [8]. Typically, the diameter of the polysaccharide-based hydrogel beads prepared using the dripping method is limited to a range of about 0.5 to 3 mm. Furthermore, the droplets needed time to change completely from a "teardrop" form, directly after their ejection from the solution to a spherical shape. The optimization of dropping speed, drop height, and gel viscosity is therefore of great importance for preparing hydrogel polysaccharide beads via ionotropic drip gelation technique.

2.3.2 Emulsion Solidification Method

The dispersion of a natural polymer containing a source of calcium in an immiscible solvent of opposite polarity at high speed of rotation forms an emulsion that can be stabilized with surfactants [57]. The resulting emulsion consists of droplet particles of the dissolved polysaccharide, which can solidify to beads of identical size by adding acidic solution, as illustrated in Fig. 2.4. The size of the beads in the suspension ranges from about 10 to about 100 μm in diameter and it is dependent on the rate of stirring, the class and amount of surfactant, the proportion of hydrophobic to

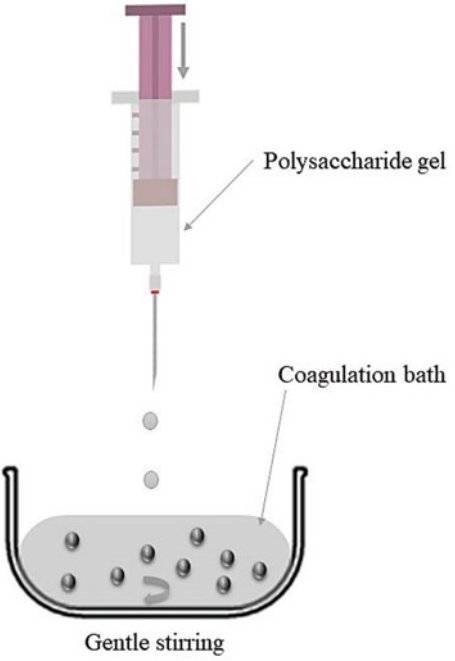

Fig. 2.3 Preparation of hydrogel polysaccharide beads by ionotropic gelation method

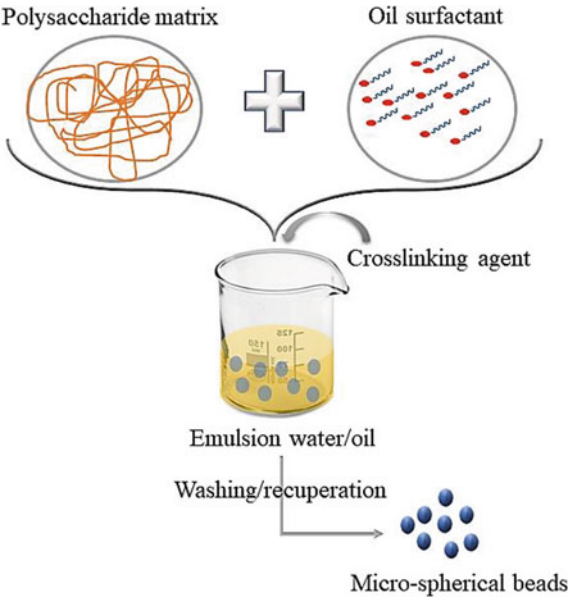

Fig. 2.4 Production of polysaccharide beads by emulsion solidification method

hydrophilic solvent, and the viscosity of the dispersion medium and the gel [52]. Therefore, polysaccharide beads made by emulsion cross-linking are about 10 times smaller than beads made by ionic cross-linking.

2.4 Water Purification Through Adsorption Systems

Adsorption is a surface process that takes place when a gaseous or liquid solute becomes concentrated on the surface of a solid or liquid (adsorbent), creating a molecular or atomic film (adsorbate). This system is a cost-effective and proven technique, which may be adopted for water purification. More particularly, the process is applicable as a tertiary treatment to reduce and remediate the contaminated water by decreasing the concentrations of a wide range of pollutants found in concentrations from ppm to ppb. This technique of uptake/purification offers the simplicity of design and operation, high versatility of performance and the potential to regenerate and recycle the adsorbent and collect the adsorbate. The present section highlights the principles and fundamentals of each adsorption process, including continuous and discontinuous systems.

2.4.1 Batch/Discontinuous Adsorption System

The batch adsorption process is implemented in agitated tanks containing a volume of adsorbate and a certain quantity of adsorbent beads under specific agitation conditions (Fig. 2.5). Batch stirred adsorbents are used for identifying the kinetics and

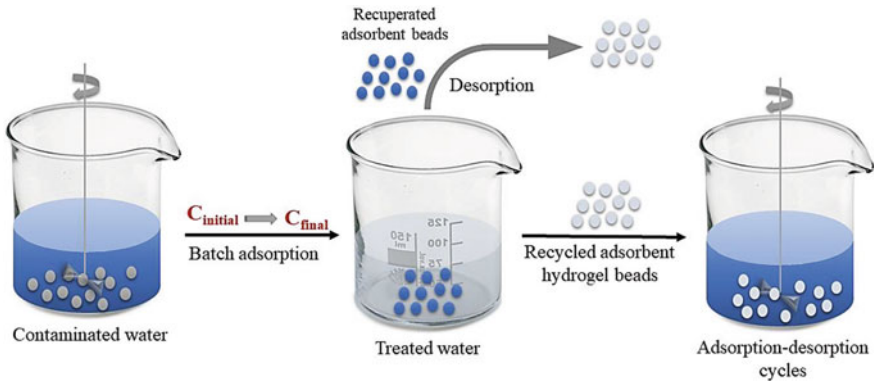

Fig. 2.5 Batch adsorption process for the removal of pollutants using polysaccharide-based hydrogel beads

isotherms for the adsorption process. The kinetic studies are quantified to calculate the adsorption rates, equilibrium time and mass transfer parameters, in contrast, isotherm studies are employed in determining the maximum capacity of adsorption at equilibrium, plus estimating the thermodynamic parameters.

2.4.1.1 Solid–Liquid Isotherms of Adsorption System

An adsorption isotherm is a plot that describes the phenomenon controlling the uptake of a substance from aqueous media to the surface of a solid adsorbent at fixed temperatures and pH [38]. It helps identify the adsorption mechanism as well as in determining the adsorption distribution sites and in the adsorption of pollutants on the surface of the adsorbent. Adsorption equilibrium is reached if an adsorbate phase is kept in contact with the adsorbent for a long duration. The most commonly used equilibrium isotherm models are shown in Table 2.2. The Langmuir isotherm frequently refers to a uniform adsorption surface, where all adsorption sites have a similar affinity to the adsorbate [60]. The Freundlich isotherm model that assumes a heterogeneous adsorption surface [60]. The Temkin isotherm focuses on adsorbent-adsorbate interactions and their effect on the linear reduction of the heat of adsorption with coverage (Temkin 1941). The Dubinin-Radushkevich (D-R) Isotherm model is applied to determine whether the adsorption process is chemisorption or physical adsorption [60].

2.4.1.2 Solid–Liquid Adsorption Kinetics

The kinetic studies are extremely beneficial in evaluating the effectiveness of a given adsorbent and in understanding, the fundamental mechanisms involved. Batch processing is an advantageous approach to studying the underlying kinetics. Several references are available on the kinetics of adsorption, and a variety of mathematical models has been developed for describing the reaction and diffusion processes during adsorption [56, 101]. Adsorption diffusion models have been built on three consecutive stages [94]. (i) diffusion by way of the liquid film that surrounds the particles of the adsorbent, i.e., external or film diffusion; (ii) diffusion within the liquid containing the pores and/or along the pore boundaries, which is known as internal or intra-particle diffusion and (iii) adsorption/desorption between the adsorbate and the active sites, i.e., mass action. To date, adsorption reaction patterns have been greatly employed to explain the adsorption kinetic processes, namely the pseudo-first-order, pseudo-second-order and Elovich models. The nonlinear and linear forms of different mathematical kinetic models for batch/discontinuous adsorption are given in Table 2.3. Lagergren suggested the pseudo-first order equation in 1898 to deal with the adsorption of oxalic and malonic acid on charcoal [90]. This model is regarded as suitable for long adsorption processes where the system is close to equilibrium. The pseudo-second-order model presupposes that the rate of adsorption is second-order relative to the vacant surface sites. The Elovich model is the most commonly used

Table 2.2 Mathematical models of adsorption isotherms

Isotherm models	Non-linear form	Linear form	Plot	References
Langmuir	$qe = \frac{q0KLCe}{1+bCe}$	$\frac{Ce}{qe} = \frac{1}{qmKL} + \frac{Ce}{qm}$	$\frac{Ce}{qe}$ *vs* C_e	[54]
Freundlich	$qe = KF\,Ce1/n$	$\ln qe = lnKF + \frac{1}{n}lnCe$	$\ln q_e$ *vs* $\ln C_e$	[5]
Dubinin-Radushkevich	$qe = (qs)\exp(-Kad\varepsilon^2)$	$\ln qe = lnqs - \beta\varepsilon^2$	$\ln q_e$ *vs* ε	[6]
Temkin	$qe = \frac{RT}{b}\ln(KTCe)$	$qe = \frac{RT}{b}lnKT + \frac{RT}{b}lnCe$	q_e *vs* $\ln C_e$	[31]

Where C_e is the concentration of the adsorbate at equilibrium (mg/L), q_e is the adsorption capacity at equilibrium (mg/g), q_m is the monolayer adsorption capacity per unit of adsorbent (mg/g) and K_L is Langmuir constant related to the free energy of adsorption–desorption. K_f is the Freundlich equilibrium constant (mol g^{-1})/(mol $L^{-1})^{1/n}$, and 1/n is the adsorption intensity. β is the activity coefficient related to mean sorption energy (mol^2 J^{-2}) and ε is the Polanyi potential (J/mol). K_T is the Temkin isotherm equilibrium binding constant (L g^{-1}), b is Temkin isotherm constant, R is the universal gas constant (8.314 J mol^{-1} K^{-1}), and T is the specific temperature (K).

Table 2.3 Batch adsorption kinetic models

Kinetic models	Nonlinear form	Linear form	Plot	References
Pseudo-first-order	$q\mathrm{t} = q\mathrm{e}(1 - e^{-k1t})$	$\ln(q\mathrm{e} - q\mathrm{t}) = lnq\mathrm{e} - K1t$	$\ln(q\mathrm{e} - q\mathrm{t})$ *vs* t	[101]
Pseudo-second-order	$q\mathrm{t} = \frac{k2q\mathrm{e}^2t}{1+k2q\mathrm{e}t}$	$\frac{t}{q\mathrm{t}} = \frac{1}{K2q\mathrm{e}^2} + \frac{t}{q\mathrm{e}}$	$\frac{t}{q\mathrm{t}}$ *vs* t	
Elovich	$q\mathrm{t} = \frac{1}{a}\ln(1 + abt)$	$q\mathrm{t} = \frac{1}{b\ln(ab)} + \frac{1}{b\ln(t)}$	$\mathrm{q_t}$ *vs* ln(t)	[19]
Intra-particle diffusion	$q\mathrm{t} = kit0.5 + c$	$q\mathrm{t} = kit0.5 + c$	$\mathrm{q_t}$ vs $\mathrm{t}^{0.5}$	[39]

Kinetic parameters: q_e (mg/g) is the adsorption capacity at equilibrium, q_t (mg/g) is the adsorption capacity at time *t*, and $\mathrm{K_1}$ (min^{-1}) is the rate constant of pseudo-first-order and $\mathrm{K_2}$ (g mg^{-1} min^{-1}) is the pseudo-second-order rate constant. The integration Elovich equation is described as follows: $q_t = (1/\beta)\ln(\alpha\beta) + (1/\beta)\ln(t + t_0)$ where α (mg g^{-1} min^{-1}) is the initial adsorption rate, β (g mg^{-1}) is a constant related to the surface coverage and the activation energy for the chemisorption. If t» $\mathrm{t_0} = 0$, this equation can be simplified in a linear form as $q_t = (1/\beta)\ln(\alpha\beta) + (1/\beta)\ln(t)$. $\mathrm{K_i}$ is the intra-particle diffusion rate constant (mg g^{-1} $\mathrm{min}^{-0.5}$), and C is a constant related to the extent of the boundary layer effect.

model when the adsorption processes are based on chemisorption at the surface of the solid and the adsorption rate drops with time due to the coverage of the surface layer [19].

2.4.2 Dynamic/Continuous Adsorption System

2.4.2.1 Fixed-Bed Adsorption

Fixed bed systems are commonly applied in drinking water purification, as well as in wastewater treatment, swimming pool water treatment, groundwater treatment, and, in combination with membrane processes, in the preparation of ultrapure water for industrial usages. The fixed-bed continuous adsorption system is a complex mode of operation and an environmentally efficient treatment process compared to the batch/discontinuous process. It can handle vast volumes of contaminant aqueous solution and provide high removal performance. Furthermore, the process can be efficiently scaled up from a laboratory to an industrial implementation [83]. To design and optimize adsorption processes, it is essential to have basic kinetics data represented as breakthrough curves. An inlet/outlet concentration rate (C_t/C_o) as a function of time (t) or flow volume (V_{eff}) is the breakthrough curve of adsorbate in a continuous system that describes the characteristics of the dynamic mode. The behavior of the breakthrough curve is related to the form of the adsorption isotherm and is influenced by the diffusion steps within the fixed bed [100]. A solution tank, a peristaltic pump, as well as a packed column are used to complete the continuous system (Fig. 2.6). In the continuous adsorption system, each adsorbent particle in the bed accumulates the adsorbate from the percolation solution until saturation

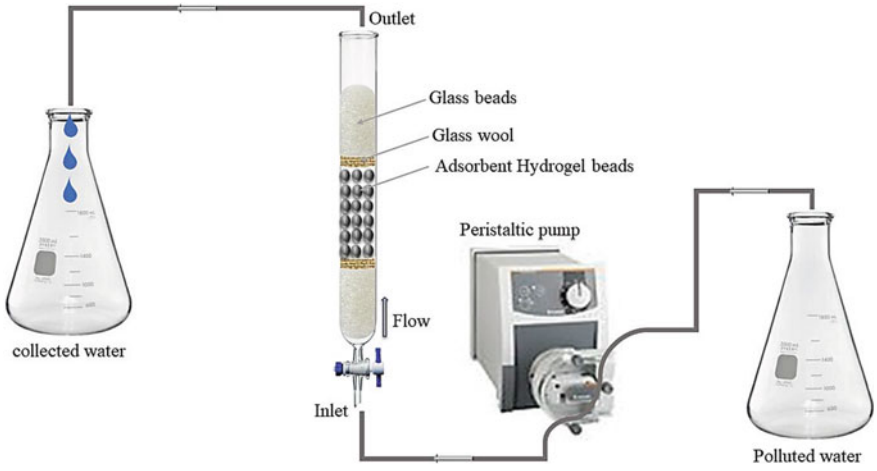

Fig. 2.6 Laboratory setup for breakthrough curve determination

is reached. Breakthrough performance is given through several parameters, such as breakthrough time (t_b, min); the volume of effluent treated to t_b (V_b, L); breakthrough adsorption capacity (q_b, mg/g); saturation/exhaustion time (t_s, min); the volume of effluent treated to t_s (V_{eff}, L); saturation adsorption capacity (q_s, mg/g) and mass transfer zone length (Z_{MTZ}, cm) [100].

2.4.2.2 Process Variable for Fixed-Bed Adsorption

To investigate the experimental breakthrough, or to adjust the experimental data with a breakthrough model, three critical process parameters need to be controlled (Table 2.4), including flow rate, bed height, and inlet concentration [1]. Based on the published data, slower exhaustion and breakthrough times have been noted by increasing the bed height and volume of effluent treated. This occurs because of a boost in the surface area and several binding sites available for adsorption [86]. Furthermore, previous studies have found that breakthrough and exhaustion times are faster with increasing the initial inlet concentration of the adsorbate, owing to a more significant number of empty sites on the surface of the adsorbent at the beginning of the adsorption process [32]. In addition, the breakthrough time was observed to be faster at higher flow rates, and the exhaustion time was expanded with decreasing flow rates. This is due to the increase in the quantity of adsorbate adsorbed per unit

Table 2.4 The effect of fixed-bed process variables on dynamic performance

Adsorbent hydrogel beads	Adsorbate	Process variables effect	References
Cellulose nanocrystal-alginate	Methylene blue	• Initial dye concentration: Lower dye concentration, more time needed to reach saturation zone	[77]
		• Bed height: An efficient dye removal was achieved at high bed height	
		• Flow rate: The adsorbed amount of MB decreased with increasing the flow rate	
PVA-alginate encapsulated Prussian blue-graphene oxide	Cesium	• Initial metal concentration: The breakthrough time decreased with increasing initial influent concentration	[45]
		• Flow rate: The breakthrough time and saturation time decreased with an increased flow rate	
		• Bed height: Breakthrough time and saturation time increased with an increase of the bed height	

Table 2.5 Mathematical models for continuous adsorption modeling

Continuous modelling	Non-linear form	Model parameters	Reference
Thomas model	$\frac{C}{C0} = \frac{1}{1+\exp(k_{\mathrm{TH}q0}\frac{x}{v} - k_{\mathrm{THC}0t})}$	k_{TH} (mL/min/mg): Thomas rate constant	[45]
		q_0 (mg/g): Adsorption capacity	
		x (g): Mass of adsorbent in the fixed-bed column	
		ν (mL/min): Volumetric flow rate	
Adams-Bohart model	$\frac{C}{C0} = \exp(k_{\mathrm{AB}}C0t - k_{\mathrm{AB}}N0\frac{Z}{U0})$	k_{AB} (L/mg/min): Kinetic constant	
		N_0 (mg/L): Saturation concentration	
		Z (cm): Bed height	
		U_0 (cm/min): Superficial velocity	
Yoon-Nelson model	$\frac{C}{C0} = \frac{\exp(k_{\mathrm{YN}}t-\tau k_{\mathrm{YN}})}{1+\exp(k_{\mathrm{YN}}t-\tau k_{\mathrm{YN}})}$	k_{YN} (min^{-1}): Rate constant	
		τ (min): Time needed for 50% adsorbate breakthrough	

of bed height as the flow rate increases, leading to rapid saturation [32]. Besides, the adsorbate has more contact time with the adsorbent at a slower flow rate, allowing for more removal of the adsorbate in the column.

2.4.2.3 Fixed-Bed Adsorption Modelling

To better understand the breakthrough curve behavior, mathematical models were applied to examine the dynamic performances of the continuous system (Table 2.5). The Thomas model affirms that adsorption is instantaneous. It is based on the theory, which the adsorption follows pseudo-second-order kinetics, and that electrostatic interactions and axial dispersion are insignificant [45]. Otherwise, the Adams-Bohart model is usually used to describe the initial part of the breakthrough curve [115]. The Yoon-Nelson model allows no need for detailed data on the physical properties of the adsorbent in the fixed bed column system.

2.5 Application of Polysaccharide-Based Hydrogel Beads in Wastewater Treatment

There are various organic and inorganic pollutants in an aqueous environment. Among these pollutants, organic dyes and heavy metal ions account for most of the research. In this direction, the adsorption of these pollutants has spurred great

interest in the remediation of wastewater, and this has led to a rise in the development of different adsorbents. Several studies have been focused on the removal of organic dyes and heavy metal ions from aquatic media. The excellent water affinity, tunable structure, high porosity and high recovery capacity of hydrogels have gained popularity for the removal of organic dyes, heavy metal ions as well as emerging contaminants from wastewater. The additional benefit lies in the fact that hydrogels are readily prepared from naturally occurring polysaccharides. In the past decades, the use of hydrogels for the removal of organic dyes and heavy metal ions from aqueous media has increased considerably. In the past 10 years, a developing trend of publications in hydrogel beads for the removal of organic dyes and heavy metal ions is shown in Fig. 2.7. The literature survey statistics show an exponential increase in the number of publications per year considering hydrogel beads for water remediation. The next section discusses the use of various types of hydrogel beads as well as hydrogel beads composite for the uptake of organic dyes and heavy metal ions from an aqueous environment. The following subsections depict some of the polysaccharide-based hydrogel beads and their composite, which have been employed for the removal of organic dyes and heavy metal ions that are reported in the literature.

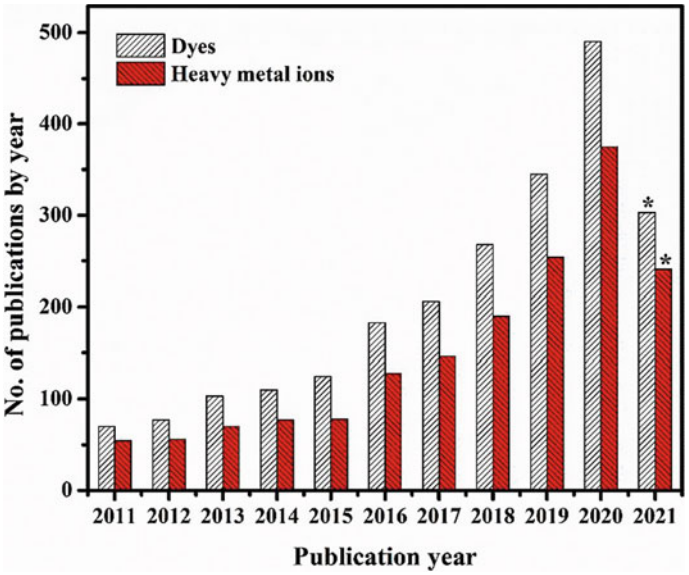

Fig. 2.7 The total number of publications per year on hydrogel beads for removal of dyes and heavy metal ions during the period 2011–2021 (using science direct database). *Data collected in April 2021

2.5.1 Polysaccharide-Based Hydrogel Beads

As described in the preceding section, the interest in the development of hydrogel beads for water remediation has increased significantly in recent years. [55], prepared a series of κ-carrageenan/poly-(glycidyl methacrylate) hydrogel beads via free radical polymerization and the ionic gelation method. According to their characterization results, the prepared κ-carrageenan hydrogel beads with integrated poly-(glycidyl methacrylate) showed the enhanced gel strength, thermal stability, swelling capacity as well as recyclability compared to κ-carrageenan homopolymeric. Moreover, the adsorbent was evaluated for the removal of MB dye from an aqueous solution. The experimental data showed that this adsorbent effectively removed MB dye and recycled for several cycles with high efficiency [55]. Studies have shown that the porosity of hydrogels plays a vital role in improving their aptitude for the adsorption of water as well as contaminants. Hydrogels incorporated surfactants have led to the enhanced porous structure and swelling ability. Several researchers prepared porous polysaccharides-based hydrogels by this method, which is cost-effective and feasible, that allows the control of pores size by changing the surfactant quantity [30, 98]. In this context, polysaccharides-based hydrogels beads have been prepared using surfactant and employed for water treatment. For example, Vakili et al., synthesized novel chitosan hydrogel beads with a cationic surfactant (hexadecyl amine) and investigated the adsorptive performance of the prepared absorbent for the removal of reactive blue 4 (RB4) from aqueous solution [105].

The chitosan hydrogel beads incorporated with hexadecyl amine exhibited enhanced adsorption capacity (454 mg/g) in comparison to chitosan beads (317 mg/g). The improved adsorption capacity towards an anionic dye was attributed to the impregnation of hexadecyl amine into CS [105]. In another study, [16], compared the adsorption behavior of chitosan hydrogel beads and chitosan hydrogel beads incorporated with a cationic surfactant (cetyl trimethyl ammonium bromide). They found that the impregnation of cetyl trimethyl ammonium bromide onto chitosan hydrogel beads enhanced the adsorption of Congo red from the aqueous phase [16]. Kumar and co-authors prepared biopolymer hydrogel beads with Ca^{2+} and Zn^{2+} via an anionic polymerization approach and studied their sorption behavior for MB dye from aqueous media [53]. Zhao et al. [128], prepared porous cellulose nanofiber-sodium alginate hydrogel beads for Pb (II) sorption from the aqueous phase. The prepared adsorbent in their study demonstrated high removal percentage of 82% within 40 min and this adsorbent maintained the adsorption rate (80%) after five regeneration cycles [128].

A one-pot method was explored to prepare arginine cross-linked chitosan/carboxymethyl cellulose hydrogel beads for the removal of metal ions. The adsorption of Pb (II) and Cd (II) ions was investigated via batch mode. The synthesized adsorbent removed Pb (II) and Cd (II) ions at an optimum pH of 6.5 and the maximum adsorption capacity were found to be 182.5 mg/g and

168.5 mg/g, respectively. The adsorption kinetic studies revealed that pseudo-second-order models govern the sorption process, whereas Langmuir best described the adsorption isotherm model for both Pb (II) and Cd (II) ions [73].

On the other side, modifications of chitosan hydrogel beads have been achieved by incorporating carboxyl groups onto polymer networks, which are known to have great chelating effects with many metal ions. For that reason, several carboxylated chitosan hydrogel beads have been reported [27, 116]. Zhang et al., modified the chitosan hydrogel beads via grafting with malic acid and subsequently employed the prepared material as adsorbent for the removal of Cr (VI) and Cu (II) from the aqueous phase [125]. On the other side, Dai et al., prepared poly(acrylic acid) blended with chitosan hydrogel beads via a one-step process and subsequently cross-linked with glutaraldehyde (CS/PAA-GLA) hydrogel beads [22]. The prepared CS/PAA-GLA hydrogel beads demonstrated enhanced mechanical strength and adsorption performance towards Cu (II) ions than CS-GLA hydrogel beads without PAA. In addition, the adsorption capacity of the regenerated CS/PAA-GLA hydrogel beads showed satisfactory recyclability without a significant loss of adsorption efficiency for over five cycles [22]. In another study, Yan and co-authors enhanced the adsorption of Cu (II), Pb (II) and Mg (II) ions from aqueous solution by employing carboxymethylated chitosan hydrogel beads [119].

On the other hand, [44], recently prepared chitosan hydrogel beads and applied this material as an adsorbent for Cu (II) uptake from wastewater. The adsorption kinetic studies showed that the equilibrium was reached within 30 min of contact time. According to their experimental finding, the synthesized chitosan hydrogel beads were efficient in removing copper ions from an aqueous solution and recyclable [44]. Moreover, they constructed a prototype machine aimed for large-scale production of hydrogel beads, chitosan hydrogel beads used for sorption of Cu (II) were fabricated by their newly developed prototype machine shown in Fig. 2.8a, the prepared

Fig. 2.8 **a** Digital image of prototype machine for manufacturing of hydrogel beads and **b** the produced chitosan hydrogel beads. Reproduced with permission from [44], Copyright 2021, Elsevier Science Ltd.

chitosan hydrogel beads by this machine are also presented in Fig. 2.8b. Chitosan-pectin hydrogel beads were prepared by a facile and green method. The as-prepared hydrogel beads were employed for removing Pb (II), Hg (II), Cd (II), and Cu (II) from an aqueous solution. According to the authors, the addition of pectin enhanced the stability, porosity, and adsorption performance of chitosan-pectin hydrogel beads. The experimental data fitted well to the pseudo-second-order and the Langmuir isotherm models. These results confirmed that the chemisorption was the main rate-controlling step in removing heavy metals by chitosan-pectin hydrogel beads and heavy metals were adsorbed on the surface of hydrogel beads by monolayer adsorption. The maximum adsorption capacities of Pb (II), Hg (II), Cd (II), and Cu (II) were found to be 266.5, 208.5, 177.6, and 169.4 mg/g, respectively. Regeneration studies revealed that the chitosan-pectin hydrogel beads exhibited high adsorption–desorption efficiency [97]. The comparative study of the equilibrium adsorption capacity of polysaccharide-based hydrogel beads in removing organic dyes and heavy metal ions is presented in Tables 2.6 and 2.7, respectively. Moreover, adsorption kinetic

Table 2.6 Comparison of some of the reported polysaccharide-based composite hydrogel beads for adsorption of organic dyes

Adsorbent	Target pollutant	Kinetics model	Isotherm model	qmax (mg/g)	References
CTS-HMP beads	MG	PSO	Freundlich	333	[93]
	RR-195	PSO	Freundlich	200	
CG/PG hydrogel beads	MB	PSO	Langmuir	166.6	[55]
Chitosan/tripolyphosphate beads	BB4	PFO & mixed order	R&P	232	[81]
	BB7	PFO &	R&P	259	
CRG-TTX CRG-SDBS	MB	PSO	Langmuir	482.2	[50]
		PSO	Langmuir	469.6	
Alg/GA/RCE hydrogel beads	BB9	PFO	Langmuir, R&P	1442	[9]
Nonporous CMC-based hydrogel beads	MB	PSO	Langmuir	82.3	[13]
CS/STPP hydrogel beads	IC	PSO	Langmuir	500	[49]
CS/β-CD/STPP hydrogel beads	IC	PSO	Langmuir	1000	[49]
κ–Carrageenan/poly (glycidyl methacrylate) hydrogel beads	MB	PSO	Langmuir	166.6	[55]
Single network hydrogel beads Double network hydrogel beads	MB	PSO	Langmuir	1255.7	[51]
	MB	PSO	Langmuir	1437.4	

Table 2.7 Comparison of some of the reported polysaccharide-based hydrogel beads for adsorption of heavy metal ions

Adsorbents	Target pollutants	Kinetics model	Isotherm model	qmax (mg/g)	References
NCS/SA/MC bead	Pb(II)	PSO	Freundlich	114.5	[107]
Saccharomyces cerevisiae/alginate beads	Pb(II)	–	Langmuir, R&P	179.1	[24]
	Cr(VI)	–	Langmuir, R&P	72.1	
	Cd(II)	–	Freundlich, R&P	30.7	
P-CNF-SA hydrogel beads	Pb(II)	PSO	Langmuir	318.4	[128]
P(VBC) beads	Cr(VI)	–	Langmuir	147.1	[3]
	AS(V)	–	Langmuir	95.2	
mGO/beads	Cr(VI)	PSO	Freundlich	14.9	[108]
	AS(V)	PSO	Langmuir	6.9	
NCS/SA/MC beads	Cu(II)	PSO	Freundlich	43.3	[106]
Straw cellulose hydrogel beads	Cd(II)	PSO	Langmuir	95.6	[111]
CYCS/CNC Beads	Pb(II)	PSO	Langmuir	334.9	[117]
Nanochitin-contained chitosan hydrogel beads	Cu(II)	PSO	Langmuir	100.9	[113]
$Fe_3O_{4/EDTA/CS}$ gel beads	Pb(II)	PSO	Langmuir	368.3	[99]
	Cu(II)	PSO	Langmuir	267.9	
	Ni(II)	PSO	Langmuir	220.3	
Chitosan-pectin gel beads	Pb(II)	PSO	Langmuir	266.5	[97]
	Hg(II)	PSO	Langmuir	208.5	
	Cd(II)	PSO	Langmuir	177.6	
	Cu(II)	PSO	Langmuir	169.4	

Pseudo-first-order (PFO), Pseudo-second-order (PSO), and Redlich and Peterson (R&P)

models, isotherm models and maximum adsorption capacity of adsorbents are shown in the tables.

2.5.2 Polysaccharide-Based Hydrogel Composite Beads

Based on the above-stated background, polysaccharide-based hydrogel beads adsorbents showed excellent characteristics, including tailored functionality, low production cost, renewable, and high adsorption capacity [119]. Although polysaccharide-based hydrogel beads adsorbents exhibit the aforementioned properties due to their poor mechanical strength, chemical stability, and recyclability, these materials may dissatisfy the applicability to meet the particular desires of water remediation. In the

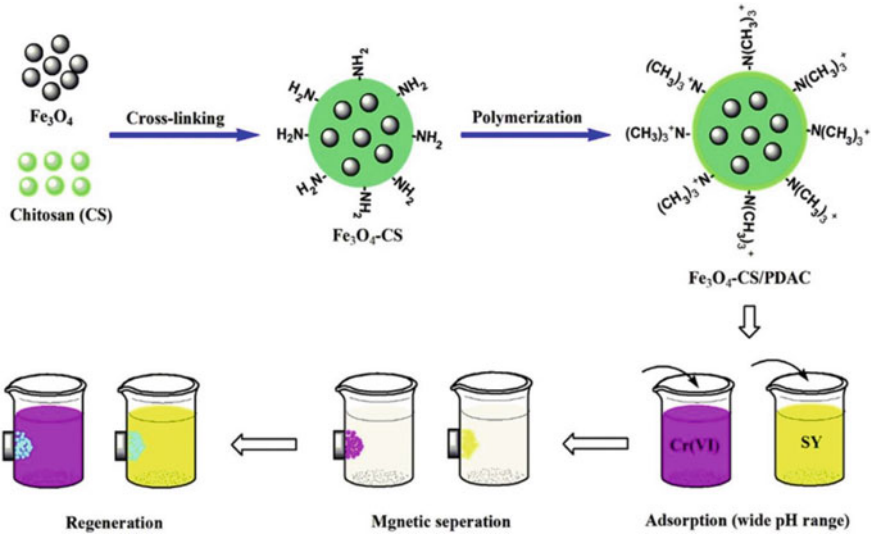

Fig. 2.9 Schematic diagram for the synthesis and application of the as-prepared magnetic chitosan hydrogel beads. Reproduced with permission from [126]. Copyright 2021, Elsevier Science Ltd

recent era, the use of polysaccharide-based hydrogel has been the focus of considerable research. Since the first report on the development of hydrogel nanocomposites in 2002 by Haraguchi and Takehisa, the incorporation of inorganic components onto the hydrogel network revolutionized the use of hydrogels for various applications [40]. This subsection highlights the recent developments in polysaccharide-based hydrogel composite beads with emphasis on the adsorption of organic dyes and heavy metal ions. Magnetic Fe_3O_4 nanoparticles were incorporated into the chitosan hydrogel beads to ease the recovery of adsorbents after adsorption. The prepared magnetic chitosan hydrogel beads were used for removing heavy metal chromium (Cr) and organic dye sunset yellow (SY) from an aqueous solution. Figure 2.9 shows a schematic diagram for the synthesis as well as application of magnetic chitosan hydrogel beads. The batch adsorption experiments demonstrated that the as-prepared magnetic chitosan hydrogel beads exhibited maximum adsorption capacities of 163.93 mg/g and 769.23 mg/g for Cr and SY, respectively. According to their findings, magnetic chitosan hydrogel beads hold great potential for practical application in water treatment due to their high adsorption capacity, easy regeneration, and fast separation [126]. A novel magnetic poly(vinyl alcohol)/modified katira/graphene oxide hydrogel beads were prepared by gelation in the presence of acetone solution of boric acid. The as-prepared adsorbent was employed for the removal of anionic CR as well as cationic CV dyes and heavy metal ions (Pb (II) and Cu (II)) from an aqueous solution. The pseudo-second-order model better described the adsorption kinetics of both dyes and metal ions, while the Langmuir isotherm model was best fitted to experimental adsorption data. The maximum adsorption capacities were

found to be 101.74, 94.0, 69.67, and 81.78 mg/g for CR, CV, Cu (II), and Pb (II), respectively [96].

Daradmare et al. [23], reported the synthesis of UIO-66-alginate composite beads and applied the prepared material as an adsorbent for the removal of Cr (VI) from aqueous media. The prepared adsorbent demonstrated the Cr (VI) adsorption percentage of 98% and satisfactory recyclable efficiency [23]. Peng and co-authors studied new nanocomposite hydrogel beads prepared by phase inversion method for adsorption of MB and MG dyes from wastewater [85]. According to their adsorption studies, MB exhibited fast equilibrium adsorption (40 min) than MG (~7 days). In another study, [110], prepared poly (vinyl alcohol)/sodium alginate/chitosan/montmorillonite (PVA/SA/CS/MMT) hydrogel beads for the removal of MB dye from aqueous media. They investigated the effect of MMT content on the removal of MB dye. Their sorption studies showed that increasing MMT loading up to 29.7% enhanced the MB uptake due to the increment of electrostatic attraction between positively charged MB and negatively charged MMT, high porosity, surface area, which provide accessibility of MB dye molecules to active sites on the PVA/SA/CS/MMT hydrogel beads [110].

The adsorption kinetic models, isotherm models, and adsorption capacities of various polysaccharide-based hydrogel beads composite for the removal of different organic dyes and metal ions from aqueous solutions are tabulated in Tables 2.8 and 2.9, respectively.

The synthesis of dithiocarbamate-decorated poly(vinyl amine) hydrogel beads was achieved via a water droplet templating polymerization approach. The adsorption capacity of the prepared hydrogel beads for the removal of heavy metal ions was evaluated via batch adsorption experiments. The effect of equilibrium concentration on the adsorption capacity of (a) Cu (II), (b) Pb (II) and, (c) Cd (II) ions along with the corresponding fitting plots for the Langmuir model. The adsorption of metal ions exhibited a sharp increase at initial concentrations and then attained a plateau. The maximum adsorption capacities obtained from the Langmuir isotherm model were found to be 2.22, 1.28, and 1.09 mmol/g for Cu (II), Pb (II) and Cd (II), respectively.

Moreover, the Langmuir isotherm model was found to describe the adsorption process better. Therefore, the adsorption of the above-studied metal ions onto hydrogel beads was monolayer coverage. The average free energy of adsorption was estimated by Dubinin-Radushkevich (D-R) isotherm model; the adsorption average free energy for Cu (II), Pb (II), and Cd (II) were 12.35, 11.56, and 11.17 kJ/mol, respectively. These results showed that an exchange of electrons occurred during the adsorption process [110]. Recently, Jamali et al. [43], fabricated chitosan/GO/Fe_3O_4 hydrogel beads by the in-situ co-precipitation methods. The as-synthesized chitosan/GO/Fe_3O_4 hydrogel beads were used for the removal of MB and Eriochrome Black T (EBT) from an aqueous solution. The adsorption data process for both dyes was best correlated to the pseudo-second-order and the Langmuir isotherm model. The authors reported that the theoretical maximum adsorption capacities for MB and EBT were 289 and 292 mg/g, respectively [43]. Other researchers prepared hydrogel composite beads by loading graphene nanoplatelets onto cellulose beads via a physical gelation method. The as-prepared adsorbent

Table 2.8 Comparison of some of the reported polysaccharide-based hydrogel beads for adsorption of organic dyestuffs

Adsorbents	Target pollutants	Kinetics model	Isotherm model	qmax (mg/g)	References
Chitosan-HNTs composite hydrogel beads	MG	PSO	Langmuir & Freundlich	72.6	[85]
	MB	PSO	Langmuir & Freundlich	270.3	
m-CS/PVA hydrogel beads	CR	PSO	Langmuir	470.1	[129]
Porous graphene/CNTs hybrid beads	MB	PSO	Langmuir	521.5	[121]
Chitosan-magadiite hydrogel beads	CR	PSO	Langmuir	135.8	[78]
	MB	PSO	Langmuir	45.25	
PVC-SA-CS-MMT hydrogel beads	MB	Elovich & PSO	Freundlich, R&P, & Sips	137.2	[110]
Graphene Oxide/ Alginate Gel Beads	MB	PSO	Langmuir	357.1	[61]
Magnetic poly(vinyl alcohol)/modified gum Katira/graphene oxide hydrogel beads	CV	PSO	Langmuir	94.0	[96]
	CR	PSO	Langmuir	101.7	
Gum Ghatti-alginate hybrid bead derived titania spheres	RBV	PSO	Langmuir	44.7	[11]
Porous magnetic cellulose / Fe_3O_4 beads	RhB	PSO	Langmuir	151.8	[58]
	MB	PSO	Langmuir	1186.8	
CTS-HMP beads	MG	PSO	Langmuir	333.0	[93]
	RR-195	PSO	Langmuir	200.0	
Magnetic zeolite polyanetholesulfonic/alginate acid gel beads	MB	PSO	Langmuir	400.0	[74]
	MG	PSO	Freundlich	164.0	

Pseudo-first-order (PFO), Pseudo-second-order (PSO), Redlich and Peterson (R&P), Remazol Brilliant Violet (RBV), and Reactive red (RR195).

beads were employed for the removal of CR dye using a differential column batch reactor. The authors showed that the incorporation of graphene nanoplatelets onto the cellulose enhanced the CR dye uptake. Cellulose exhibited a maximum adsorption capacity of 98.1 mg/g whereas cellulose-nanoplatelets hydrogel beads showed a higher maximum adsorption capacity of 139.6 mg/g for the removal of CR dye from aqueous solution [35].

Table 2.9 Comparison of some of the reported polysaccharide-based hydrogel beads for adsorption of heavy metal ions

Adsorbents	Target pollutants	Kinetics model	Isotherm model	qmax (mg/g)	References
MKa@CB	Pb(II)	PSO	Langmuir	90.9	[29]
	Cd(II)	PSO	Langmuir	88.5	
CYCS/CNC Beads	Pb(II)	PSO	Langmuir	334.9	[118]
La-MMT hydrogel beads	AS(V)	PFO	Langmuir	58.8	[120]
Fe_3O_4-ATP/EDTA/CS gel beads	Pb(II)	PSO	Langmuir	368.3	[99]
	Cu(II)	PSO	Langmuir	267.9	
	Ni(II)	PSO	Langmuir	220.3	
Alginate/graphene composite hydrogel beads	Cu(II)	–	Langmuir	169.5	[130]
	Cr(VI)	–	Langmuir	72.5	
Ca-ALg_2 gel beads ALg_2/GO gel beads	Cu(II)	PSO	Langmuir	42.7	[4]
	Cu(II)	PSO	Langmuir	60.2	
GA-grafted CS/PEI/Fe_3O_4 composite beads	Cr(VI)	PSO	Langmuir	476.2	[62]
MOFs/alginate beads	Cr(VI)	PSO	Langmuir	20.0	[23]
CCM composite hydrogel beads	Cu(II)	PSO	Langmuir	143.2	[123]
	U(VI)	PSO	Langmuir	392.6	
Magnetic poly(vinyl alcohol)/modified gum Katira/graphene oxide hydrogel beads	Pb(II)	PSO	Langmuir	81.7	[96]
	Cu(II)	PSO	Langmuir	69.6	

Pseudo-first-order (PFO), Pseudo-second-order (PSO), and Redlich and Peterson (R&P).

2.6 Conclusion and Future Outlook

The impressive quantity of publications in recent two decades related to the elaboration and utilization of polysaccharide-based hydrogel beads as adsorbents indicates the potential significance of these improved materials in the environmental field, including water pollution remediation. The present chapter focuses on the utilization of polysaccharide-based hydrogel adsorbent beads to uptake organic and/-or inorganic contaminants from aqueous solutions using batch and dynamic adsorption systems. The adsorption capacities recorded in the published research papers prove the performance of natural polymer adsorbent beads towards metal ions and dyes, depending on several experimental parameters. As mentioned, incorporating inorganic materials into polysaccharide-based hydrogel beads can considerably affect the enhancement of the adsorption capacity and, consequently, an emerging area

of research is the elaboration of unique composite materials with a strong adsorption capacity. Looking to the near future, polysaccharide-based hydrogel materials applied for water pollution remediation have the potential to progress drastically. Progress in this area will require dedication to developing cost-effective and recoverable/reusable hybrid polysaccharide-based beads.

Acknowledgements The authors immensely acknowledge the financial support from the National Research Foundation (NRF) (Grant No:116679). The authors acknowledge Hassan II University, Casablanca, Morocco, and the University of Limpopo, South Africa.

Declaration of Competing Interest No competing interest to declare.

References

1. I. Agani et al., Removal of atrazine from aqueous solutions onto a magnetite/chitosan/activated carbon composite in a fixed-bed column system: optimization using response surface methodology. RSC Adv. **10**(68), 41588–41599 (2020). https://doi.org/10.1039/d0ra07873e
2. A. Ait El Fakir et al., Engineering of new hydrogel beads based conducting polymers: metal-free catalysis for highly organic pollutants degradation. Appl. Catal. B: Environ. Elsevier B.V. 286(January) (2021). https://doi.org/10.1016/j.apcatb.2021.119948.
3. M. Ajmal, S. Demirci, Y. Uzun, M. Siddiq, N. Aktas, N. Sahiner, Introduction of double amidoxime group by double post surface modification on poly(vinylbenzyl chloride) beads for higher amounts of organic dyes, As (V) and Cr (VI) removal. J. Colloid Interface Sci. **470**, 39–46 (2016). https://doi.org/10.1016/j.jcis.2016.02.040
4. W.M. Algothmi et al., Alginate-graphene oxide hybrid gel beads: an efficient copper adsorbent material. J. Colloid Interface Sci. **397**, 32–38 (2013). https://doi.org/10.1016/j.jcis.2013.01.051
5. D. Allouss, Y. Essamlali, A. Chakir et al., Effective removal of Cu (II) from aqueous solution over graphene oxide encapsulated carboxymethylcellulose-alginate hydrogel microspheres : towards real wastewater treatment plants. Environ. Sci. Pollut. Res. **27**, 7476–7492 (2019)
6. D. Allouss, Y. Essamlali, O. Amadine et al., Response surface methodology for optimization of methylene blue adsorption onto carboxymethyl cellulose-based hydrogel beads: adsorption kinetics, isotherm, thermodynamics and reusability studies. RSC Adv. **9**(65), 37858–37869 (2019). https://doi.org/10.1039/c9ra06450h
7. M. Amarine et al., Nitrate removal from groundwater in Casablanca region (Morocco) by electrocoagulation. Groundw. Sustain. Dev. Elsevier B.V. **11**, 100452. (2020) https://doi.org/10.1016/j.gsd.2020.100452.
8. B. Ambravaneswaran, E.D. Wilkes, O.A. Basaran, Drop formation from a capillary tube: Comparison of one-dimensional and two-dimensional analyses and occurrence of satellite drops. Phys. Fluids **14**(8), 2606–2621 (2002). https://doi.org/10.1063/1.1485077
9. A. Andreas, Z.G. Winata, S.P. Santoso, A.E. Angkawijaya, M. Yuliana, F.E. Soetaredjo, S. Ismadji, H.-Y. Hsu, Alchris Woo Go, Yi-Hsu. Ju, Biocomposite hydrogel beads from glutaraldehyde-crosslinked phytochemicals in alginate for effective removal of methylene blue. J. Mol. Liquids **329**, 115579 (2021). https://doi.org/10.1016/j.molliq.2021.115579
10. M.M.A. Aslam, W. Den, H.W. Kuo, Removal of hexavalent chromium by encapsulated chitosan-modified magnetic carbon nanotubes: fixed-bed column study and modelling. J. Water Process. Eng. Elsevier Ltd, **42**(April), 102143 (2021). https://doi.org/10.1016/j.jwpe.2021.102143
11. S. Banerjee, A. Debnath, V. Singh, Gum ghatti-alginate hybrid bead derived titania spheres for deep removal of toxic dye Remazol Brilliant Violet from aqueous solutions. Environ. Nanotechnol. Monitor. Manag. **15**, 100459 (2021)

12. T. Benhalima, H. Ferfera-Harrar, Eco-friendly porous carboxymethyl cellulose/dextran sulfate composite beads as reusable and efficient adsorbents of cationic dye methylene blue. Int. J. Biol. Macromol. **132**, 126–141 (2019). https://doi.org/10.1016/j.ijbiomac.2019.03.164
13. T. Benhalima, H. Ferfera-Harrar, D. Lerari, Optimization of carboxymethyl cellulose hydrogels beads generated by an anionic surfactant micelle templating for cationic dye uptake: Swelling, sorption and reusability studies. Int. J. Biol. Macromol. **105**, 1025–1042 (2017). https://doi.org/10.1016/j.ijbiomac.2017.07.135
14. I. Braccini, S. Pérez, Molecular basis of Ca2+-induced gelation in alginates and pectins: the egg-box model revisited. Biomacromol **2**(4), 1089–1096 (2001). https://doi.org/10.1021/bm010008g
15. Y. Cai et al., Synthesis of core–shell structured Fe 3 O 4 @carboxymethyl cellulose magnetic composite for highly efficient removal of Eu(III). Cellulose Springer, Netherlands **24**(1), 175–190 (2017). https://doi.org/10.1007/s10570-016-1094-8
16. S. Chatterjee et al., Enhanced adsorption of congo red from aqueous solutions by chitosan hydrogel beads impregnated with cetyl trimethyl ammonium bromide. Bioresour. Technology. Elsevier **100**(11), 2803–2809 (2009). https://doi.org/10.1016/J.BIORTECH.2008.12.035
17. S. Chatterjee, M.W. Lee, S.H. Wooa, Adsorption of congo red by chitosan hydrogel beads impregnated with carbon nanotubes. Bioresour. Technology. Elsevier Ltd **101**(6), 1800–1806 (2010). https://doi.org/10.1016/j.biortech.2009.10.051
18. L. Chen et al., Removal of methylene blue from water by cellulose/graphene oxide fibres. J. Exp. Nanosci. Taylor & Francis **11**(14), 1156–1170 (2016). https://doi.org/10.1080/17458080.2016.1198499
19. S.H. Chien, W.R. Clayton, Application of Elovich equation to the kinetics of phosphate release and sorption in soils. Soil Sci. Soc. Am. J. **44**(2), 265–268 (1980). https://doi.org/10.2136/sssaj1980.03615995004400020013x
20. G. Crini, Non-conventional low-cost adsorbents for dye removal: a review. Biores. Technol. **97**(9), 1061–1085 (2006). https://doi.org/10.1016/j.biortech.2005.05.001
21. N.A. Dahlan et al., Developing of a magnetite film of carboxymethyl cellulose grafted carboxymethyl polyvinyl alcohol (CMC-g-CMPVA) for copper removal. Carbohyd. Polym. (2017). https://doi.org/10.1016/j.carbpol.2017.06.008
22. J. Dai et al., Simple method for preparation of chitosan/poly(acrylic acid) blending hydrogel beads and adsorption of copper(II) from aqueous solutions. Chem. Eng. J. Elsevier **165**(1), 240–249 (2010). https://doi.org/10.1016/J.CEJ.2010.09.024
23. S. Daradmare et al., Metal–organic frameworks/alginate composite beads as effective adsorbents for the removal of hexavalent chromium from aqueous solution. Chemosphere, Pergamon **270**, 129487 (2021). https://doi.org/10.1016/J.CHEMOSPHERE.2020.129487
24. A. De Rossi, C.V.T. Rigueto, A. Dettmer, L.M. Colla, J.S. Piccin, Synthesis, characterization, and application of Saccharomyces cerevisiae/alginate composites beads for adsorption of heavy metals. J. Environ. Chem. Eng. **8**(4), 104009 (2020). https://doi.org/10.1016/j.jece.2020.104009
25. T. Deblonde, C. Cossu-Leguille, P. Hartemann, Emerging pollutants in wastewater: a review of the literature. Int. J. Hyg. Environ. Health Elsevier GmbH. **214**(6), 442–448 (2011). https://doi.org/10.1016/j.ijheh.2011.08.002
26. C. Djelloul, O. Hamdaoui, Dynamic adsorption of methylene blue by melon peel in fixed-bed columns. Desalin. Water Treat. **56**(11), 2966–2975 (2015). https://doi.org/10.1080/19443994.2014.963158
27. B. Doshi et al., Partially carboxymethylated and partially cross-linked surface of chitosan versus the adsorptive removal of dyes and divalent metal ions. Carbohydr. Polym.. Elsevier Ltd (2018). https://doi.org/10.1016/j.carbpol.2018.06.032
28. J. Du et al., (2020) 'Decontamination of heavy metal complexes by advanced oxidation processes: a review.' Chin. Chem. Lett. Chin. Chem. Soc. (2019). https://doi.org/10.1016/j.cclet.2020.07.050
29. S.S.D. Elanchezhiyan, P. Karthikeyan, K. Rathinam, M. Hasmath Farzana, C.M. Park, Magnetic kaolinite immobilized chitosan beads for the removal of Pb(II) and Cd(II) ions

from an aqueous environment. Carbohydr. Polym. **261**, 117892 (2021). https://doi.org/10.1016/j.carbpol.2021.117892
30. F.I. El-Dib et al., Enhancing the porous structure of swellable poly(acrylic acid-co-acrylamide) crosslinked by N-Maleyl chitosan via introducing foaming agents and non-ionic surfactant. Adv. Ind. Eng. Polym. Res. Elsevier **4**(1), 9–18 (2021). https://doi.org/10.1016/J.AIEPR.2020.12.001
31. M. Erfani, V. Javanbakht, Methylene Blue removal from aqueous solution by a biocomposite synthesized from sodium alginate and wastes of oil extraction from almond peanut. Int. J. Biol. Macromol. **114**, 244–255 (2018). https://doi.org/10.1016/j.ijbiomac.2018.03.003
32. G.R. de Freitas, M.G.A. Vieira, M.G.C. da Silva, Fixed bed biosorption of silver and investigation of functional groups on acidified biosorbent from algae biomass. Environ. Sci. Pollut. Res. **26**(36), 36354–36366 (2019). https://doi.org/10.1007/s11356-019-06731-5
33. K. Furuya et al., Development of novel polysulfone membranes with embedded zirconium sulfate-surfactant micelle mesostructure for phosphate recovery from water through membrane filtration. Water Res. Elsevier Ltd **124**, 521–526 (2017). https://doi.org/10.1016/j.watres.2017.08.005
34. C.M. Futalan et al., Fixed-bed column studies on the removal of copper using chitosan immobilized on bentonite. Carbohydr. Polym. Elsevier Ltd. **83**(2), 697–704 (2011). https://doi.org/10.1016/j.carbpol.2010.08.043
35. M.E. González-López et al., Congo red adsorption with cellulose-graphene nanoplatelets beads by differential column batch reactor. J. Environ. Chem. Eng. Elsevier **9**(2), 105029 (2021). https://doi.org/10.1016/J.JECE.2021.105029
36. T. Gotoh, K. Matsushima, K.I. Kikuchi, Preparation of alginate-chitosan hybrid gel beads and adsorption of divalent metal ions. Chemosphere **55**(1), 135–140 (2004). https://doi.org/10.1016/j.chemosphere.2003.11.016
37. R.C. Goy, D. De Britto, O.B.G. Assis, A review of the antimicrobial activity of chitosan. Polimeros **19**(3), 241–247 (2009). https://doi.org/10.1590/S0104-14282009000300013
38. X. Guo, J. Wang, Comparison of linearization methods for modeling the Langmuir adsorption isotherm. J. Mol. Liq. Elsevier Ltd **296**, 111850 (2019). https://doi.org/10.1016/j.molliq.2019.111850
39. K. Haitham, S. Razak, M.A. Nawi, Kinetics and isotherm studies of methyl orange adsorption by a highly recyclable immobilized polyaniline on a glass plate. Arab. J. Chem. **12**(7), 1595–1606 (2019). https://doi.org/10.1016/j.arabjc.2014.10.010
40. K. Haraguchi, T. Takehisa, Nanocomposite hydrogels: A unique organic-inorganic network structure with extraordinary mechanical, optical, and swelling/De-swelling properties. Adv. Mater. **14**(16), 1120–1124 (2002). https://doi.org/10.1002/1521-4095(20020816)14:16%3c1120::AID-ADMA1120%3e3.0.CO;2-9
41. H.J. Hong et al., Enhanced Sr adsorption performance of MnO_2-alginate beads in seawater and evaluation of its mechanism. Chem. Eng. J. **319**, 163–169 (2017). https://doi.org/10.1016/j.cej.2017.02.132
42. H. Ismail, M. Irani, Z. Ahmad, Starch-based hydrogels: present status and applications. Int. J. Polym. Mater. Polym. Biomater. **62**(7), 411–420 (2013). https://doi.org/10.1080/00914037.2012.719141
43. M. Jamali, A. Akbari, Facile fabrication of magnetic chitosan hydrogel beads and modified by interfacial polymerization method and study of adsorption of cationic/anionic dyes from aqueous solution. J. Environ. Chem. Eng. Elsevier **9**(3), 105175 (2021). https://doi.org/10.1016/J.JECE.2021.105175
44. T. Jamnongkan et al., Green adsorbents for copper (II) biosorption from waste aqueous solution based on hydrogel-beads of biomaterials. S. Afr. J. Chem. Eng. Elsevier B.V. **35**(2020), 14–22 (2021). https://doi.org/10.1016/j.sajce.2020.10.005.
45. J. Jang, D.S. Lee, Enhanced adsorption of cesium on PVA-alginate encapsulated Prussian blue-graphene oxide hydrogel beads in a fixed-bed column system. Bioresour. Technol. Elsevier Ltd **218**, 294–300 (2016). https://doi.org/10.1016/j.biortech.2016.06.100

46. J. Jang, D.S. Lee, Effective phosphorus removal using chitosan/Ca-organically modified montmorillonite beads in batch and fixed-bed column studies. J. Hazard. Mater. Elsevier **375**, 9–18 (2019). https://doi.org/10.1016/j.jhazmat.2019.04.070
47. A.H. Jawad et al., Adsorptive performance of carbon modified chitosan biopolymer for cationic dye removal: kinetic, isotherm, thermodynamic, and mechanism study. Int. J. Environ. Anal. Chem. Taylor & Francis **00**(00), 1–15 (2020). https://doi.org/10.1080/03067319.2020.1807966
48. X. Jiang et al., Versatile core/shell-like alginate@polyethylenimine composites for efficient removal of multiple heavy metal ions (Pb2+, Cu2+, CrO42−): batch and fixed-bed studies. Mater. Res. Bull. Pergamon **118**, 110526 (2019). https://doi.org/10.1016/j.materresbull.2019.110526
49. T. Kekes, C. Tzia, Adsorption of indigo carmine on functional chitosan and β-cyclodextrin/chitosan beads: Equilibrium, kinetics and mechanism studies. J. Environ. Manag. **262**, 110372 (2020). https://doi.org/10.1016/j.jenvman.2020.110372
50. S.M. Khoshkho, B. Tanhaei, A. Ayati, M. Kazemi, Preparation and characterization of ionic and non-ionic surfactants impregnated κ-carrageenan hydrogel beads for investigation of the adsorptive mechanism of cationic dye to develop for biomedical applications. J. Mol. Liquids **324**, 115118 (2021). https://doi.org/10.1016/j.molliq.2020.115118
51. Y. Kong, Y. Zhuang, Z. Han, J. Yu, B. Shi, Kun Han, Haotian Hao, Dye removal by eco-friendly physically cross-linked double network polymer hydrogel beads and their functionalized composites. J. Environ. Sci. **78**, 81–91 (2019). https://doi.org/10.1016/j.jes.2018.07.006
52. C. Kotoulas, C. Kiparissides, A generalized population balance model for the prediction of particle size distribution in suspension polymerization reactors. Chem. Eng. Sci. **61**(2), 332–346 (2006). https://doi.org/10.1016/j.ces.2005.07.013
53. M. Kumar et al., 'Optimization of methylene blue using Ca2+ and Zn2+ bio-polymer hydrogel beads: a comparative study. Ecotoxicol. Environ. Saf. Academic Press **121**, 164–173 (2015). https://doi.org/10.1016/J.ECOENV.2015.04.007
54. I. Langmuir, The adsorption of gases on plane surfaces of glass, mica and platinum. J. Am. Chem. Soc. **40**(9), 1361–1403 (1918). https://doi.org/10.1021/ja02242a004
55. S. Lapwanit, T. Sooksimuang, T. Trakulsujaritchok, Adsorptive removal of cationic methylene blue dye by kappa-carrageenan/poly(glycidyl methacrylate) hydrogel beads: preparation and characterization. J. Environ. Chem. Eng. Elsevier **6**(5), 6221–6230 (2018). https://doi.org/10.1016/J.JECE.2018.09.050
56. L. Largitte, R. Pasquier, A review of the kinetics adsorption models and their application to the adsorption of lead by an activated carbon. Chem. Eng. Res. Des. Inst. Chem. Eng. **109**, 495–504 (2016). https://doi.org/10.1016/j.cherd.2016.02.006
57. B.Z. Li et al., Fabrication of starch-based microparticles by an emulsification-crosslinking method. J. Food Eng. Elsevier Ltd **92**(3), 250–254 (2009). https://doi.org/10.1016/j.jfoodeng.2008.08.011
58. B. Li, Q. Zhang, Y. Pan, Y. Li, Z. Huang, M. Li, H. Xiao, Functionalized porous magnetic cellulose/Fe3O4 beads prepared from ionic liquid for removal of dyes from aqueous solution. Int J Biol Macromol **163**, 309–316 (2020). https://doi.org/10.1016/j.ijbiomac.2020.06.280
59. N. Lin, J. Huang, A. Dufresne, Preparation, properties and applications of polysaccharide nanocrystals in advanced functional nanomaterials: a review. Nanoscale **4**(11), 3274–3294 (2012). https://doi.org/10.1039/c2nr30260h
60. Y. Liu, Y.J. Liu, Biosorption isotherms, kinetics and thermodynamics. Sep. Purif. Technol. **61**(3), 229–242 (2008). https://doi.org/10.1016/j.seppur.2007.10.002
61. X. Liu, B. Cui, S. Liu, Q. Ma, Methylene Blue removal by graphene oxide/alginate gel beads. Fibers Polym. **20**(8), 1666–1672 (2019). https://doi.org/10.1007/s12221-019-9011-z
62. T. Lü, R. Ma, K. Ke, D. Zhang, D. Qi, H. Zhao, Synthesis of gallic acid functionalized magnetic hydrogel beads for enhanced synergistic reduction and adsorption of aqueous chromium. Chem. Eng. J. **408**, 127327 (2021). https://doi.org/10.1016/j.cej.2020.127327
63. E. Makhado, M.J. Hato, Preparation and characterization of sodium alginate-based oxidized multi-walled carbon nanotubes hydrogel nanocomposite and its adsorption behaviour for

methylene blue. Dye' Front. Chem. **9**, 576913 (2021). https://doi.org/10.3389/fchem.2021.576913
64. E. Makhado et al., Fast microwave-assisted green synthesis of xanthan gum grafted acrylic acid for enhanced methylene blue dye removal from aqueous solution. Carbohydr. Polym. Elsevier Ltd. **176**, 315–326 (2017). https://doi.org/10.1016/j.carbpol.2017.08.093
65. E. Makhado et al.,'Xanthan gum-cl-poly (acrylic acid)/reduced graphene oxide hydrogel nanocomposite as adsorbent for dye removal, in *Int'l Conference on Advances in Science, Engineering & Technologyand Waste Management (Asetwm-171)* (2017), pp. 159–164. https://doi.org/10.17758/EARES
66. E. Makhado, S. Pandey, J. Ramontja, 'Microwave assisted synthesis of xanthan gum-cl-poly (acrylic acid) based-reduced graphene oxide hydrogel composite for adsorption of methylene blue and methyl violet from aqueous solution. Int. J. Biol. Macromol. Elsevier B.V **119**, 255–269 (2018). https://doi.org/10.1016/j.ijbiomac.2018.07.104
67. E. Makhado, S. Pandey, M. Kang, - E. Kanke, Microwave assisted synthesis of xanthan gum-cl-Dimethyl acrylamide hydrogel based silica hydrogel as adsorbent for cadmium (II) removal' . *Int'l Conference on Advances in Science, Engineering & Technologyand Waste Management (Setwm-19)* 1 (2019), pp. 1–6. https://doi.org/10.1016/j.ijbiomac.2018.07.104
68. E. Makhado et al., Preparation and characterization of xanthan gum-cl-poly(acrylic acid)/o-MWCNTs hydrogel nanocomposite as highly effective re-usable adsorbent for removal of methylene blue from aqueous solutions. J. Colloid Interface Sci. **513**, 700–714 (2018). https://doi.org/10.1016/j.jcis.2017.11.060
69. E. Makhado et al., Microwave-assisted green synthesis of xanthan gum grafted diethylamino ethyl methacrylate: an efficient adsorption of hexavalent chromium. Carbohydr. Polym. Elsevier Ltd. **222**, 114989–114999 (2019). https://doi.org/10.1016/j.carbpol.2019.114989
70. E. Makhado et al., Sequestration of methylene blue dye using sodium alginate poly(acrylic acid)@ZnO hydrogel nanocomposite: kinetic, isotherm, and thermodynamic investigations. Int. J. Biol. Macromol. Elsevier B.V, **162**, 60–73 (2020). https://doi.org/10.1016/j.ijbiomac.2020.06.143
71. N. Malatji et al., Synthesis and characterization of magnetic clay-based carboxymethyl cellulose-acrylic acid hydrogel nanocomposite for methylene blue dye removal from aqueous solution. Environ. Sci. Pollut. Res. **27**, 44089–44105 (2020). https://doi.org/10.1007/s11356-020-10166-8
72. N. Malatjiet al., Removal of methylene blue from wastewater using hydrogel nanocomposites: a review. Nanomater. Nanotechnol. **11**, 11 (2021). https://doi.org/10.1177/18479804211039425
73. K. Manzoor et al., Removal of Pb(ii) and Cd(ii) from wastewater using arginine cross-linked chitosan-carboxymethyl cellulose beads as green adsorbent. RSC Adv. R. Soc. Chem. **9**(14), 7890–7902 (2019). https://doi.org/10.1039/C9RA00356H
74. A.Ü. Metin, D. Doğan, M. Can, Novel magnetic gel beads based on ionically crosslinked sodium alginate and polyanetholesulfonic acid: Synthesis and application for adsorption of cationic dyes. Mater. Chem. Phys. **256**, 123659 (2020). https://doi.org/10.1016/j.matchemphys.2020.123659
75. R. Mofidian et al., Fabrication of novel agarose–nickel bilayer composite for purification of protein nanoparticles in expanded bed adsorption column. Chem. Eng. Res. Design. Inst. Chem. Eng. **159**, 291–299 (2020). https://doi.org/10.1016/j.cherd.2020.03.024
76. N. Mohammed et al., Cellulose nanocrystal–alginate hydrogel beads as novel adsorbents for organic dyes in aqueous solutions. Cellulose. Springer Netherlands **22**(6), 3725–3738 (2015). https://doi.org/10.1007/s10570-015-0747-3
77. N. Mohammed, N. Grishkewich, H.A. Waeijen, R.M. Berry, K.C. Tam, Continuous flow adsorption of methylene blue by cellulose nanocrystal-alginate hydrogel beads in fixed bed columns. Carbohydr. Polym. **136**, 1194–1202 (2016). https://doi.org/10.1016/j.carbpol.2015.09.099

78. A. Mokhtar, S. Abdelkrim, A. Djelad, A. Sardi, B. Boukoussa, M. Sassi, A. Bengueddach, Adsorption behavior of cationic and anionic dyes on magadiite-chitosan composite beads. Carbohydr. Polym. **229**, 115399 (2020). https://doi.org/10.1016/j.carbpol.2019.115399
79. H Mondal et al., Starch-g-tetrapolymer hydrogel via in situ attached monomers for removals of Bi(III) and/or Hg(II) and dye(s): RSM-based optimization. Carbohydr. Polym. Elsevier Ltd, **213**(Iii), 428–440 (2019). https://doi.org/10.1016/j.carbpol.2019.02.035
80. R.J. Moon et al., Cellulose nanomaterials review: structure, properties and nanocomposites. Chem. Soc. Rev. (2011). https://doi.org/10.1039/c0cs00108b
81. P.M. Morais da Silva, N.G. Camparotto, T. de Figueiredo Neves, K.T. Grego Lira, V.R. Mastelaro, Carolina Siqueira Franco Picone, Patrícia Prediger, Effective removal of basic dye onto sustainable chitosan beads: Batch and fixed-bed column adsorption, beads stability and mechanism. Sustain. Chem. Pharm. **18**, 100348 (2020). https://doi.org/10.1016/j.scp.2020.100348
82. P. Pal, A. Pal, Surfactant-modified chitosan beads for cadmium ion adsorption. Int. J. Biol. Macromol. Elsevier B.V. **104**, 1548–1555 (2017). https://doi.org/10.1016/j.ijbiomac.2017.02.042
83. H. Patel, Fixed-bed column adsorption study: a comprehensive review. Appl. Water Sci. Springer International Publishing **9**, 45 (2019). https://doi.org/10.1007/s13201-019-0927-7
84. S.N. Pawar, K.J. Edgar, Alginate derivatization: a review of chemistry, properties and applications. Biomaterials. Elsevier Ltd 3279–3305 (2012). https://doi.org/10.1016/j.biomaterials.2012.01.007
85. Q. Peng et al., Adsorption of dyes in aqueous solutions by chitosan–halloysite nanotubes composite hydrogel beads. Microporous Mesoporous Mater. Elsevier **201**(C), 190–201 (2015). https://doi.org/10.1016/J.MICROMESO.2014.09.003
86. B. Perez Mora et al., Response surface methodology and optimization of arsenic continuous sorption process from contaminated water using chitosan. J. Water Process Eng. Elsevier **32**, 100913 (2019). https://doi.org/10.1016/j.jwpe.2019.100913
87. C.K.S. Pillai, W. Paul, C.P. Sharma, Chitin and chitosan polymers: chemistry, solubility and fiber formation. Prog. Polym. Sci. (Oxford) **34**(7), 641–678 (2009). https://doi.org/10.1016/j.progpolymsci.2009.04.001
88. L. Pontoni, M. Fabbricino, Use of chitosan and chitosan-derivatives to remove arsenic from aqueous solutions - a mini review. Carbohydr. Res. Elsevier Ltd **356**, 86–92 (2012). https://doi.org/10.1016/j.carres.2012.03.042
89. X. Qi et al., Salecan polysaccharide-based hydrogels and their applications: a review. J. Mater. Chem. B **7**(16), 2577–2587 (2019). https://doi.org/10.1039/c8tb03312a
90. H. Qiu et al.,'Critical review in adsorption kinetic models. J. Zhejiang Univ.: Sci. A 716–724 (2009). https://doi.org/10.1631/jzus.A0820524
91. M. Rajiv Gandhi et al., Sorption behaviour of copper on chemically modified chitosan beads from aqueous solution. Carbohyd. Polym. **83**(3), 1082–1087 (2011). https://doi.org/10.1016/j.carbpol.2010.08.079
92. K.R. Ramakrishna, T. Viraraghavan, Dye removal using low cost adsorbents. Water Sci. Technol. **36**(2–3), 189–196 (1997). https://doi.org/10.1016/S0273-1223(97)00387-9
93. N.P. Raval, S. Mukherjee, N.K. Shah, P. Gikas, M. Kumar, Hexametaphosphate cross-linked chitosan beads for the eco-efficient removal of organic dyes: Tackling water quality. J. Environ. Manag. **280**, 111680 (2021). https://doi.org/10.1016/j.jenvman.2020.111680
94. Ravi and Pandey, L. M., Enhanced adsorption capacity of designed bentonite and alginate beads for the effective removal of methylene blue. Appl. Clay Sci. **169**, 102–111 (2019). https://doi.org/10.1016/j.clay.2018.12.019
95. H. Ren et al., Efficient Pb (II) removal using sodium alginate – carboxymethyl cellulose gel beads : preparation, characterization, and adsorption mechanism. Carbohydr. Polym. Elsevier Ltd. **137**, 402–409 (2016). https://doi.org/10.1016/j.carbpol.2015.11.002
96. R. Sahraei, Z. Sekhavat Pour, M. Ghaemy, Novel magnetic bio-sorbent hydrogel beads based on modified gum tragacanth/graphene oxide: Removal of heavy metals and dyes from water. J. Clean. Prod. Elsevier **142**, 2973–2984 (2017). https://doi.org/10.1016/J.JCLEPRO.2016.10.170

97. Z. Shao et al., Novel green chitosan-pectin gel beads for the removal of Cu(II), Cd(II), Hg(II) and Pb(II) from aqueous solution. Int. J. Biol. Macromol. Elsevier **176**, 217–225 (2021). https://doi.org/10.1016/J.IJBIOMAC.2021.02.037
98. X.N. Shi, W.B. Wang, A.Q. Wang, Effect of surfactant on porosity and swelling behaviors of guar gum-g-poly(sodium acrylate-co-styrene)/attapulgite superabsorbent hydrogels. Colloids Surf. B: Biointerfaces. Elsevier **88**(1), 279–286 (2011). https://doi.org/10.1016/j.colsurfb.2011.07.002
99. P. Sun, W. Zhang, B. Zou, L. Zhou, Z. Ye, Q. Zhao, Preparation of EDTA-modified magnetic attapulgite chitosan gel bead adsorbent for the removal of Cu(II), Pb(II), and Ni(II). Int. J. Biol. Macromol. **182**, 1138–1149 (2021). https://doi.org/10.1016/j.ijbiomac.2021.04.132
100. A.L. Taka et al.,Chitosan nanocomposites for water treatment by fixed-bed continuous flow column adsorption: a review. Carbohydr. Polym. Elsevier Ltd. **255**, 117398 (2021). https://doi.org/10.1016/j.carbpol.2020.117398
101. K.L. Tan, B.H. Hameed, Insight into the adsorption kinetics models for the removal of contaminants from aqueous solutions. J. Taiwan Inst. Chem. Eng.. Elsevier B.V. **74**, 25–48 (2017). https://doi.org/10.1016/j.jtice.2017.01.024
102. X. Tang et al., Chemical coagulation process for the removal of heavy metals from water: a review. Desalin. Water Treat. **57**(4), 1733–1748 (2014). https://doi.org/10.1080/19443994.2014.977959
103. T. Tatarchuk et al., A review on removal of uranium(VI) ions using titanium dioxide based sorbents. J. Mol. Liq. Elsevier B.V. **293**, 111563 (2019). https://doi.org/10.1016/j.molliq.2019.111563
104. P. Tripathi, V.C. Srivastava, A. Kumar, Optimization of an azo dye batch adsorption parameters using Box-Behnken design. Desalination. Elsevier B.V. **249**(3), 1273–1279 (2009). https://doi.org/10.1016/j.desal.2009.03.010
105. M. Vakili et al., Chitosan hydrogel beads impregnated with hexadecylamine for improved reactive blue 4 adsorption. Carbohydr. Polym. Elsevier **137**, 139–146 (2016). https://doi.org/10.1016/J.CARBPOL.2015.09.017
106. K. Vijayalakshmi, T. Gomathi, S. Latha, T. Hajeeth, P.N. Sudha, Removal of copper(II) from aqueous solution using nanochitosan/sodium alginate/microcrystalline cellulose beads. Int. J. Biol. Macromol. **82**, 440–452 (2016). https://doi.org/10.1016/j.ijbiomac.2015.09.070
107. K. Vijayalakshmi, B.M. Devi, S. Latha, T. Gomathi, P.N. Sudha, J. Venkatesan, S. Anil, Batch adsorption and desorption studies on the removal of lead (II) from aqueous solution using nanochitosan/sodium alginate/microcrystalline cellulose beads. Int. J. Biol. Macromol. **104**, 1483–1494 (2017). https://doi.org/10.1016/j.ijbiomac.2017.04.120
108. H.C. Vu, A.D. Dwivedi, T.T. Le, S.-H. Seo, E.-J. Kim, Yoon-Seok. Chang, Magnetite graphene oxide encapsulated in alginate beads for enhanced adsorption of Cr(VI) and As(V) from aqueous solutions: Role of crosslinking metal cations in pH control. Chem. Eng. J. **307**, 220–229 (2017). https://doi.org/10.1016/j.cej.2016.08.058
109. W.S. Wan Ngah et al., Utilization of chitosan-zeolite composite in the removal of Cu(II) from aqueous solution: adsorption, desorption and fixed bed column studies. Chem. Eng. J. **209**, 46–53 (2012). https://doi.org/10.1016/j.cej.2012.07.116
110. W. Wang et al., Methylene blue removal from water using the hydrogel beads of poly(vinyl alcohol)-sodium alginate-chitosan-montmorillonite. Carbohydr. Polym. Elsevier **198**, 518–528 (2018). https://doi.org/10.1016/j.carbpol.2018.06.124
111. F. Wang, J. Li, Y. Su, Q. Li, B. Gao, Q. Yue, W. Zhou, Adsorption and recycling of Cd(II) from wastewater using straw cellulose hydrogel beads. J. Ind. Eng. Chem. **80**, 361–369 (2019). https://doi.org/10.1016/j.jiec.2019.08.015
112. P. Wongsasuluk et al., 'Heavy metal contamination and human health risk assessment in drinking water from shallow groundwater wells in an agricultural area in Ubon Ratchathani province, Thailand. Environ. Geochem. Health **36**, 169–182 (2014). https://doi.org/10.1007/s10653-013-9537-8
113. J. Wu, X. Cheng, Y. Li, G. Yang, Constructing biodegradable nanochitin-contained chitosan hydrogel beads for fast and efficient removal of Cu(II) from aqueous solution. Carbohydr. Polym. **211**, 152–160 (2019). https://doi.org/10.1016/j.carbpol.2019.01.004

114. W. Xia et al., Fabrication, characterization and evaluation of myricetin adsorption onto starch nanoparticles. Carbohydr. Polym.. Elsevier **250**(July),. 116848 (2020). https://doi.org/10.1016/j.carbpol.2020.116848
115. Z. Xu, J.G. Cai, B.C. Pan, Mathematically modeling fixed-bed adsorption in aqueous systems. J. Zhejiang Univ. Sci. A **14**(3), 155–176 (2013). https://doi.org/10.1631/jzus.A1300029
116. X. Xu, X. Ouyang, L.Y. Yang, Adsorption of Pb(II) from aqueous solutions using crosslinked carboxylated chitosan/carboxylated nanocellulose hydrogel beads. J. Mol. Liq.. Elsevier B.V. **322**(xxxx), 114523 (2021). https://doi.org/10.1016/j.molliq.2020.114523
117. X. Xu, X. Ouyang, L.-Y. Yang, Adsorption of Pb(II) from aqueous solutions using crosslinked carboxylated chitosan/carboxylated nanocellulose hydrogel beads. J. Mol. Liquids **322**, 114523 (2021). https://doi.org/10.1016/j.molliq.2020.114523
118. X. Xu, X. Ouyang, L.-Y. Yang, Adsorption of Pb(II) from aqueous solutions using crosslinked carboxylated chitosan/carboxylated nanocellulose hydrogel beads. J. Mol. Liquids **322**, 114523 (2021). https://doi.org/10.1016/j.molliq.2020.114523
119. H. Yan et al., Enhanced and selective adsorption of copper(II) ions on surface carboxymethylated chitosan hydrogel beads. Chem. Eng. J. Elsevier **174**(2–3), 586–594 (2011). https://doi.org/10.1016/J.CEJ.2011.09.064
120. S. Yan, Q. An, L. Xia, S. Liu, S. Song, J.R. Rangel-Méndez, As(V) removal from water using the La(III)- Montmorillonite hydrogel beads. React. Funct. Polym. **147**, 104456 (2020). https://doi.org/10.1016/j.reactfunctpolym.2019.104456
121. T. Yao, L. Qiao, K. Du, High tough and highly porous graphene/carbon nanotubes hybrid beads enhanced by carbonized polyacrylonitrile for efficient dyes adsorption. Microporous Mesoporous Mater **292**, 109716 (2020). https://doi.org/10.1016/j.micromeso.2019.109716
122. L. Ye et al., Chemical precipitation granular sludge (CPGS) formation for copper removal from wastewater. RSC Adv. R. Soc. Chem. **6**(115), 114405–114411 (2016). https://doi.org/10.1039/c6ra11165c
123. X. Yi, J. He, Y. Guo, Z. Han, M. Yang, J. Jin, J. Gu, M. Ou, X. Xu, Encapsulating Fe3O4 into calcium alginate coated chitosan hydrochloride hydrogel beads for removal of Cu (II) and U (VI) from aqueous solutions. Ecotoxicol. Environ. Saf. **147**, 699–707 (2018). https://doi.org/10.1016/j.ecoenv.2017.09.036
124. A.Y. Zahrim, C. Tizaoui , N. Hilal, Coagulation with polymers for nanofiltration pre-treatment of highly concentrated dyes: a review. Desalination. Elsevier B.V. **266**(1–3), 1–16 (2011). https://doi.org/10.1016/j.desal.2010.08.012
125. Y. Zhang et al., Malic acid-enhanced chitosan hydrogel beads (mCHBs) for the removal of Cr(VI) and Cu(II) from aqueous solution. Chem. Eng. J. Elsevier **353**, 225–236 (2018). https://doi.org/10.1016/J.CEJ.2018.06.143
126. W. Zhang et al.,Novel pectin based composite hydrogel derived from grapefruit peel for enhanced Cu(II) removal. J. Hazard. Mater.. Elsevier **384**(July 2019), 121445 (2020). https://doi.org/10.1016/j.jhazmat.2019.121445
127. L. Zhao, J.-P. Basly, M. Baudu, Macroporous alginate/ferrihydrite hybrid beads used to remove anionic dye in batch and fixed-bed reactors. J. Taiwan Inst. Chem. Eng. Elsevier **74**, 129–135 (2017). https://doi.org/10.1016/J.JTICE.2017.02.006
128. H. Zhao, X.K. Ouyang, L.Y. Yang, Adsorption of lead ions from aqueous solutions by porous cellulose nanofiber–sodium alginate hydrogel beads. J. Mol. Liq.. Elsevier **324**, 115122 (2021). https://doi.org/10.1016/J.MOLLIQ.2020.115122
129. H.-Y. Zhu, Y.-Q. Fu, R. Jiang, J. Yao, L. Xiao, G.-M. Zeng, Novel magnetic chitosan/poly(vinyl alcohol) hydrogel beads: Preparation, characterization and application for adsorption of dye from aqueous solution. Bioresour. Technol. **105**, 24–30 (2012). https://doi.org/10.1016/j.biortech.2011.11.057
130. Y. Zhuang, F. Yu, H. Chen, J. Zheng, J. Ma, Junhong Chen, Alginate/graphene double-network nanocomposite hydrogel beads with low-swelling, enhanced mechanical properties, and enhanced adsorption capacity. J. Mater. Chem. A **4**(28), 10885–10892 (2016). https://doi.org/10.1039/C6TA02738E

131. X. Zou et al., Preparation and characterization of polyacrylamide/sodium alginate microspheres and its adsorption of MB dye. Colloids Surf. A: Physicochem. Eng. Asp. Elsevier B.V. **567**, 184–192 (2018). https://doi.org/10.1016/j.colsurfa.2018.12.019

Chapter 3
Flocculation of Waste Water Using Architectural Copolymers: Recent Advancement and Future Perspective

Subhadeep Chakraborty, Soumen Sardar, and Abhijit Bandyopadhyay

Abstract The main problem that the world is facing today is the scarcity of natural resources, including freshwater, due to ramping environmental pollution. It is primarily due to rapid industrialization posing a serious threat to the entire ecosystem. Most of the industries discharge effluents to the nearby wetlands and water bodies. As a result, the amount of usable water reduces drastically due to surface and ground waters contamination. The discharged effluents contain various toxic impurities in the form of metals, organic and inorganic particles, suspended solids, etc. If without proper treatment, the water is used, serious health hazards can occur. It is, therefore, necessary to treat the water before it is used for domestic and drinking purposes. There are many stages of treating natural wastewater for removal of organic, inorganic, and suspended loads. The primary process is to remove suspended inorganic solids and for that flocculation is generally used as it is one of the most convenient and cheapest unit operations. At the same time, it has also been found that polymeric flocculants are more effective than conventional inorganic flocculants for settling inorganic suspensions. It works both by charge neutralization and bridging mechanisms to settle the flocs in a reasonably quick time. This chapter vividly described the treatment of wastewater containing suspended inorganic solids with polysaccharide grafted hyperbranched copolymers as flocculants. Hyperbranched polymers have unique properties like higher solubility, higher hydrodynamic volume, more functional ends hence higher zeta potential for charge neutralization and more inner voids for bridging of flocs, which make them a better flocculant than conventional linear polymers. Along with hyperbranched polymer-based natural flocculants, future scope for incorporating various nanoparticles into the polymeric network for further improvement in flocculation efficiency, has also been discussed in this chapter.

S. Chakraborty · S. Sardar · A. Bandyopadhyay (✉)
Department of Polymer Science and Technology, University of Calcutta, 92-APC Road, Kolkata 700009, India
e-mail: abpoly@caluniv.ac.in

M. J. Hato and S. Sinha Ray (eds.), *Functional Polymer Nanocomposites for Wastewater Treatment*, Springer Series in Materials Science 323,
https://doi.org/10.1007/978-3-030-94995-2_3

3.1 Introduction

The natural water bodies are getting increasingly polluted daily due to human activity and industrialization, which leads to tremendous pollution to the environment [28]. Not only surface water but also groundwater are getting contaminated with suspended particles, colloidal substances, and dissolved particles. Among the effluents discharged from various industries, toxic metal ions along with numerous organic and inorganic substances share a considerable part [6, 23]. The water discharged from mines contains negatively charged particles, whereas the effluents from ceramic, paints, cosmetics, ink, etc. industries contain kaolin as the main suspended particles [2]. Due to the smaller size, anisotropic shape, and strong repulsive forces among the particles of kaolin, it forms a stable suspension in water and thus present in huge amount in the sludge getting discharges from the industries as mentioned earlier [62]. These particles get settled down due to the gravitational force, but it occurs over a more extended period, and also, the efficiency is too low. The other conventional methods of treating the effluents are sedimentation, filtration, micro-filtration, ultrasonication, coagulation and flocculation [59]. Among these methods of treating coagulation and flocculation are most commonly in use [57]. Coagulation is achieved by adding coagulants to the wastewater, which are mainly inorganic [7]. Flocculation is somewhat similar to coagulants where the particles are agglomerated by the addition of a foreign substance which causes agglomeration, and thus, the law of gravitation is applied. This substance by which it is done is called flocculants [4]. Flocculants can be natural as well as synthetic in nature, and the synthetic variables are made bio-degradable by incorporating a bio-polymer backbone onto them. Moreover, the commercial coagulants, e.g., poly-aluminium chloride (PAC), alum, etc., can cause a lot of sludge formation and hence making its disposal to the environment a difficult task [17].

On the other hand, flocculation leads to the formation of a lesser amount of sludge, thus making the process eco-friendlier. The inorganic metal ions (mostly the charged ones) can cause various diseases in the body. Al present in PAC causes Alzheimer's disease [41].

The flocculation is achieved by the employment of flocculants which are synthetic as well as natural. The synthetic flocculants are mainly polyacrylamide (PAM), poly (diallyl dimethyl ammonium chloride) (PDADMAC)etc., which are found to be effective in flocculating suspension having a negative surface charge on it. The flocculation occurs following a mechanism called charge neutralization [54]. But acrylamide monomer, when it remains unreacted, leads to carcinogenic diseases, and on the other hand, PAM is found to have good flocculation efficiency [34, 39]. The bio-degradable property can be introduced by introducing a natural polysaccharide backbone into it [5]. This can be done by graft copolymerization, where a free radical initiator is used either thermally or by using a source of radiation. It is due to the grafting of the properties of both natural polysaccharide and its synthetic counterpart hybridized, leading to a mixed property of both the moieties. The graft copolymers can further be modified by nanoparticles to increase their efficiency in flocculation

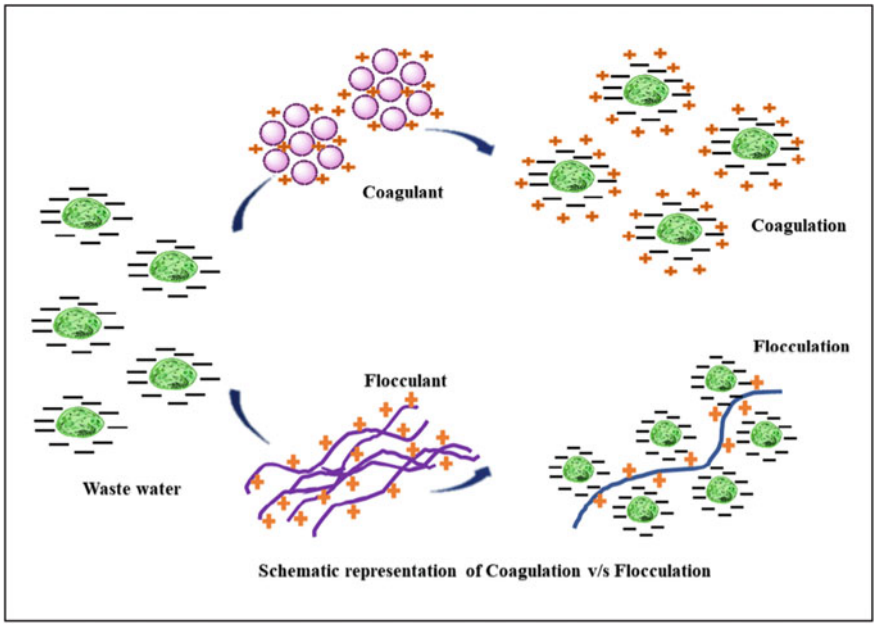

Fig. 3.1 Schematic representation of coagulation versus flocculation

[52]. This chapter elaborates the three types of flocculants, i.e., synthetic, natural, and graft copolymers, which have been used for treating wastewater. Chemical coagulants/flocculants, which are derived from chemical/petroleum-based compounds, are often used in wastewater treatment. Natural bio-flocculants have been thoroughly researched and sourced from natural resources in recent years.

Meanwhile, grafted flocculants have recently been studied and synthesized by mixing chemical and natural flocculants properties [33, 49]. Its flocculating performance, as well as the related flocculating mechanisms for wastewater treatment, are also addressed and discussed. The difference between coagulation and flocculation has been depicted in Fig. 3.1 [55]. Apart from the natural resources nowadays, various synthesized materials are also used for wastewater treatment like graphene oxide, graphene/polymer composite [46], different types of conductive polymers [45], and organic–inorganic hybrid [44].

3.2 Coagulation Versus Flocculation

We have compared the basic difference of coagulation and flocculation in a tabular (Depicted in Table 3.1) form on the basis of the process of work, materials, and application. Inorganic mineral additives/metal salts, which are used as coagulants,

Table 3.1 Difference between coagulation and flocculation

Coagulation	Flocculation
The process of coagulation is chemical in nature	The process of flocculation is physical in nature
Most of the coagulant is a salt of bivalent and trivalent metal ions, which when added in solvent, break down to release charges	The flocculants aremostly polymeric molecule thatinduces the settling of particles and larger floc formation occurs
Mixing is not required for the process of coagulation	In this physical technique, mixing the flocculating agent is a necessary step
In coagulation, the mechanism operating mainly is charge neutralization	In flocculation, there are several operative mechanisms- charge neutralization, polymer bridging, and electrostatic patch mechanism
A higher dosage of coagulant is required due to its low molecular weight	Due to the higher molecular weight of the flocculants, small amount of polymer can bring larger floc formation
Sludge formation is higher	Minimal sludge formation
Non-biodegradable	Synthetic variants are non-biodegradable, but the modified biopolymers are bio-degradable

and organic polymeric compounds, which are used as flocculants, are the two main classes of synthetic chemicals used in commercial wastewater treatment [19].

3.2.1 Inorganic Coagulants

Alum, poly (aluminum) chloride, ferric chloride, ferrous sulfate, calcium chloride, and magnesium chloride are inorganic salts of multivalent metals that have been commonly used as coagulants for decades. It is primarily due to its low-cost benefit, as their selling price is far lower than chemical flocculants [20].

However, owing to a number of drawbacks, inorganic coagulants are still used in a small number of wastewater applications. According to several reports, its application would have two major environmental consequences: the development of vast concentrations of metal hydroxide (toxic) sludge, which would be difficult to dispose of, and a rise of metal (e.g., aluminum) content in the treated water, which may have human health effects. Other disadvantages include the need for a significant volume of material for effective flocculation, sensitivity to pH, inefficiency against microscopic particles, inefficiency in cold water (e.g., polyaluminum chloride), and application of just a few dispersed structures [22]. Many considerations have been considered in order to identify an alternative to lower the dosage of toxic inorganic flocculants in order to reduce the risks of inorganic flocculants [11] (Fig. 3.2).

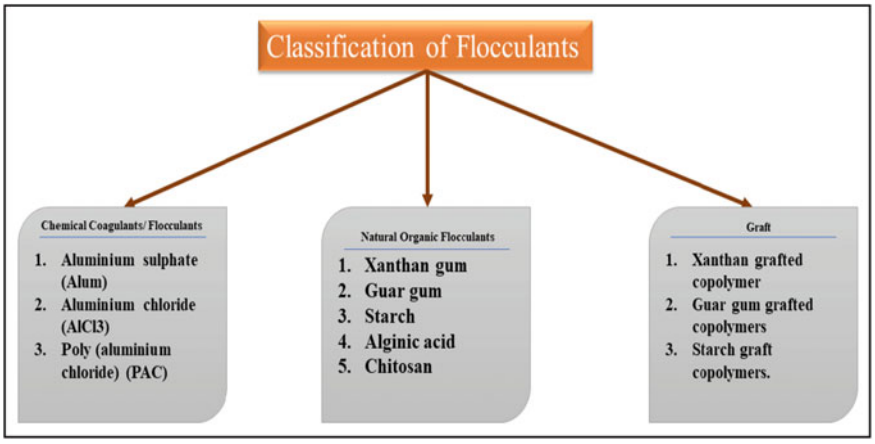

Fig. 3.2 Classification of flocculats

3.2.2 Synthetic Organic Flocculants

Many synthetic polymers have been used as key flocculants (coagulant aids) in recent years to improve coagulation and flocculation performance, with positive results published. The majority of commercial organic flocculants are linear water-soluble polymers made up of repeated units of different monomers, including acrylamide and acrylic acid. They are derived from oil-based and non-renewable raw materials in the majority of cases. Polyacrylamide, polyacrylic acid (PAAc), poly(diallyl dimethyl ammonium chloride) (DADMAC), polyamine, and other polymeric flocculants are often used [51].

The molecular weight, structure (linear versus branched), amount of charge, charge content, and composition of synthetic polymers vary, but they are usually divided into four types: cationic (positively charged), anionic (negatively charged), amphoteric (contains both cationic and anionic groups), and non-ionic (close to neutral).

Water soluble polymers are widely used as flocculants because of their distinct characteristics. The polymers are simple to useand have little effect on the medium's pH [40].

They work well for small amounts (a few mg per liter), and the flocs that develop during flocculation are larger and heavier. In certain cases, a suitable polyelectrolyte can increase floc size, resulting in a solid, compact, regular-shaped floc with good settling characteristics [16].

They work well for small amounts (a few mg per liter), and the flocs that develop during flocculation are larger and heavier. In some instances, a suitable polyelectrolyte can increase floc size, resulting in a solid, compact, regular-shaped floc with good settling characteristics [63].

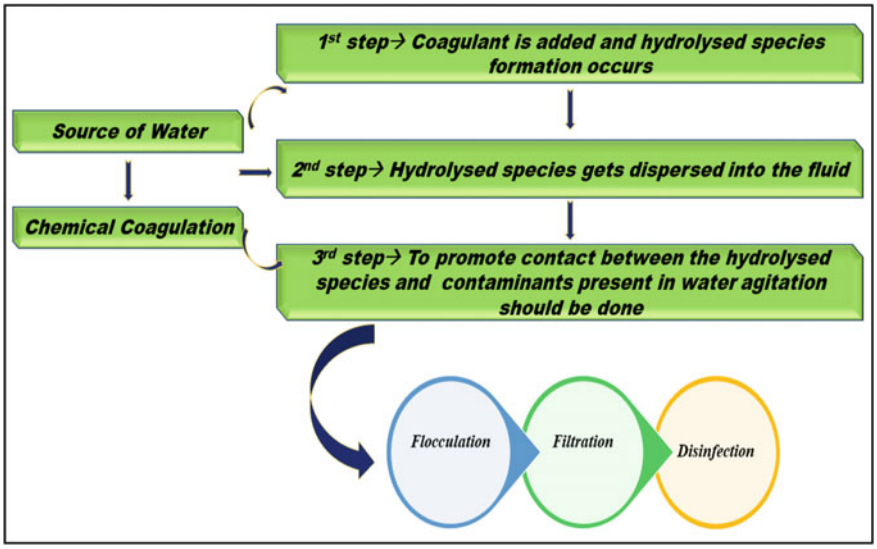

Fig. 3.3 Coagulation—flocculation

3.2.3 Steps Involving Flocculation

The process of coagulation-flocculation involves several steps, which are depicted in Fig. 3.3.

- To the wastewater,a coagulant is added in the first step.
- Formation of hydrolyzedspecies occurs.
- The hydrolyzedspecies gets dispersed into the fluid.
- Vigorous agitation should be done to allow proper mixing of the hydrolyzed species and promote contact between the particles presentwithin the fluid.
- After that, flocculantsare to be added and then filtration and disinfection [25].

3.2.4 Mechanism of Flocculation

The mechanism of flocculation is very important because from the mechanism how the flocculants work to remove the hazardous materials from waste water. Figure 3.4 shows the entire mechanism of the flocculation process.

Floc formation occurs through the following steps taken sequentially:

- The flocculants get dispersed in the solution
- Flocculants diffusion towards the solid–liquid interface
- Adsorption of the flocculants onto the particulate surface

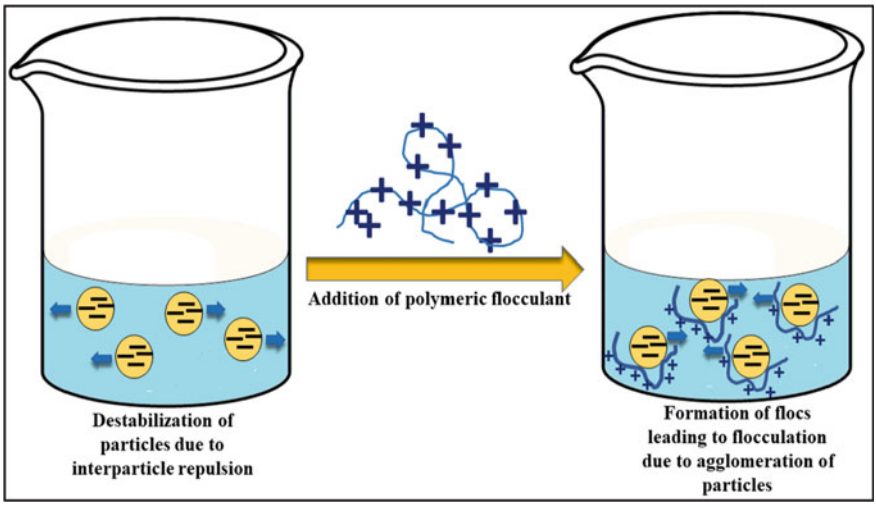

Fig. 3.4 Addition of flocculants and mechanism of flocculation

- Collision with other particles by particles bearing adsorbed flocculants
- In order to form micro-flocs, adsorption of the flocculants to other particles
- Development by successive collision and adsorption of the microflocs to larger and stronger flocs.

Several flocculation processes have been suggested to understand the destabilization of colloids and suspensions by polymers, including polymer bridging, polymer adsorption, and charge neutralization (including electrostatic patch effects), depletion flocculation, displacement flocculation, and so on. Charge neutralization, bridge forming, and electrostatic patch are the three primary processes of coagulation/flocculation involved in the removal of dissolved and particulate pollutants that are often mentioned. The adsorption of flocculants on particle surfaces is important for these processes. The whole flocculation process is depicted in Fig. 3.5.

3.3 Charge Neutralization

Charge neutralization is commonly proposed as the primary process where the flocculants and the adsorption site have opposing charges. Since hydrophobic colloidal particles in wastewater are often negatively charged, inorganic flocculants (metal salts) and cationic polyelectrolytes are preferred in many situations. The development of van der Waals force of attraction to encourage initial aggregation of colloidal and fine suspended materials to form micro-flocculation could occur simply as a result of the particles' reduced surface charge (reduction of zeta potential) and hence a decreased electrical repulsion force between colloidal particles, which causes the

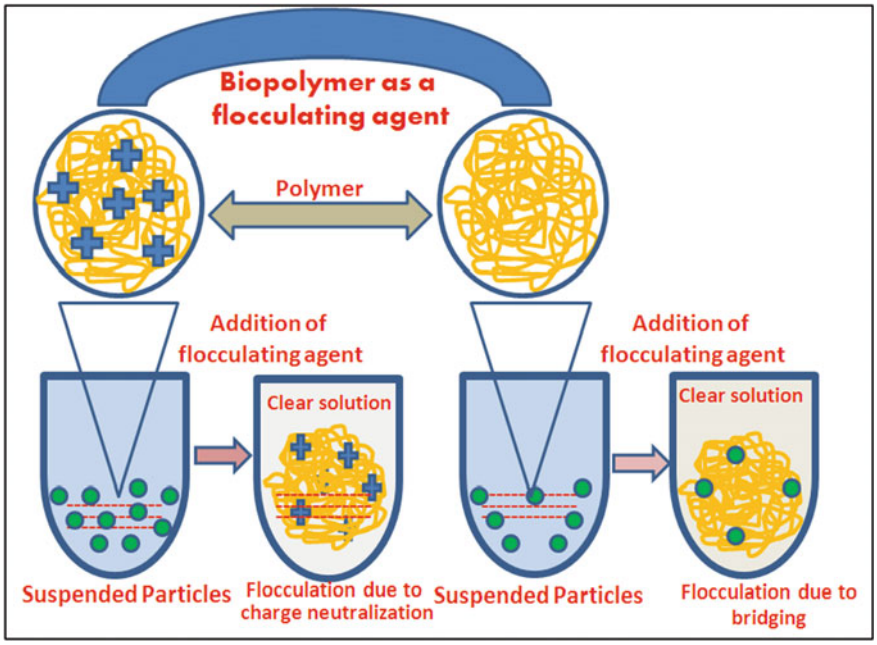

Fig. 3.5 Flocculation process through bio-polymers

formation of van der Waals force of attraction to encourage initial aggregation of colloidal and fine suspended materials to form micro-flocculation. Many experiments have discovered that optimum flocculation occurs at polyelectrolytes dosages around those needed to neutralise particle charge or achieve a zeta potential near zero (isoelectric point). Under the impact of Vander Waals influences, the particles appear to agglomerate at this stage, destabilizing the colloidal suspension. However, if too much polymer is used, a charge reversal will occur, causing the particles to become scattered again, but this time with a positive charge rather than a negative charge. Charge neutralization flocs are often poorly packaged and brittle, and they settle slowly. To cement the micro-flocs together for quick sedimentation and high-water recovery, another high molecular weight polymer with a bridging effect is needed.

3.4 Polymer Bridging

Polymer bridging happens when long-chain polymers with a high molecular weight (up to several million) and low charge density are adsorbed on particles in such a manner that long loops and tails expand or spread well past the electrical double layer into solution. This allows these ‘dangling’ polymer segments to bind and interact with other particles, resulting in ‘bridging’ between particles.

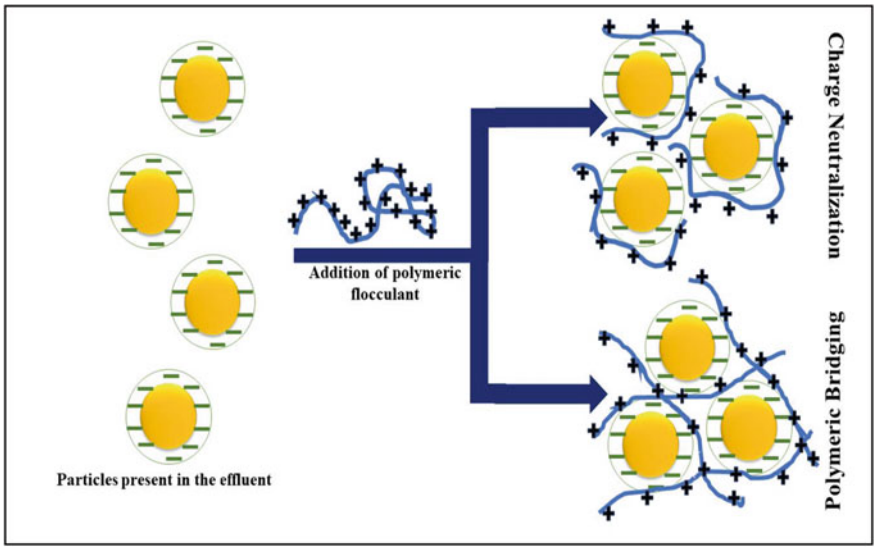

Fig. 3.6 Mechanism of flocculation

The length of the polymer chains must be adequate to stretch from one particle surface to another for successful bridging to occur. As a result, a polymer with longer chains (high molecular weight) should outperform one with shorter chains (low molecular weight). Furthermore, there must be enough unoccupied surface on a particle to attach polymer chain segments adsorbed on other particles. As a result, the amount of polymer used should not be unnecessary (the amount of polymer absorbed should not be excessive). Otherwise, the particle surfaces will be overly saturated with polymer, leaving no sites for other particles to 'bridge' with. Here, the re-establishment of particles occurs.

As a result, only a small amount of adsorbed polymer is required, and excess amounts will cause re-stabilization. Naturally, the adsorbed sum should not be too low; otherwise, insufficient bridging contacts can be created.

As a result of these factors, an optimal dose for bridging flocculation has been proposed. Polymer bridging has long been known to produce much larger and thicker aggregates (flocs) than other methods. Furthermore, at high shear speeds, bridging contacts are more resistant to breakage. This has been depicted in Fig. 3.6 [26].

3.5 Electrostatic Patch

The bridging potential is limited as high charge density polyelectrolytes with low molecular weight adsorb on negative surfaces with a relatively low density of charged areas. Another process known as the "electrostatic patch" mechanism emerges.

The basic concept is that when a strongly charged cationic polymer adsorbs on a weakly charged negative surface to provide total neutrality, each surface charged site cannot be physically neutralized by a cationic polymer segment. Between regions of uncoated negatively charged surfaces cationic 'patches' or 'islands' shape. As particles approach close together, there is an electrostatic attraction between positive patches and negative regions, resulting in particle association and hence flocculation.

These flocs are not as solid as those formed by bridging, but they are stronger than those formed in the presence of metal salts or by basic charge neutralization. For electrostatic patch flocculation to work, polyelectrolytes must have a high charge density. Bridging flocculation becomes more possible as the charge density is reduced [64].

3.6 Mechanism Followed by Natural Bio-Flocculants

Chitosan's properties, such as its cationic activity (reactive amino and hydroxyl groups) and high molecular weight, can be used for charge neutralization and bridging process flocculation. The anionic dye was electrostatically attracted by protonated amine groups from chitosan, leading to neutralization of the anionic charges of dyes. Then the flocculation was further improved by the bridging process, which binds the agglomerates together and settles, in a study that studied coagulation and flocculation of dye-containing solutions using chitosan. Depending on the type of the colloids, chitosan characteristics such as molecular weight and degree of deacetylation, the pH of the suspension, and the experimental conditions, chitosan activity includes two factors: hydrophobic associations and the probability of chain attachment by hydrogen bridges (i.e., concentrations) [5].

Without the aid of a cationic coagulant/flocculants, anionic bio-flocculants (cellulose, tannin, and sodium alginate) are unable to flocculate anionic pollutants from wastewater.As a result, charge neutralization of negatively charged impurities requires the addition of inorganic metal salts (e.g., aluminum and ferric salts) or a cationic polymer (e.g., chitosan) before the addition of bio-flocculants. Anionic cellulose or tannin with negatively charged atoms after charge neutralization the polymer molecules' charged backbone allowed them to be extended into solution and create loops and tails to aid in floc bridging [42, 52].

3.7 Mechanism Followed by Grafted Polymeric Flocculants

Charge neutralization and polymer bridging combine to form the flocculation process for grafted flocculants used in wastewater treatment. At the start of the flocculation phase, charge neutralization predominates, resulting in a large number of insoluble complexes generated quickly. The insoluble complexes then aggregate and form larger net-like flocs due to the bridging effect of the flexible polymeric graft

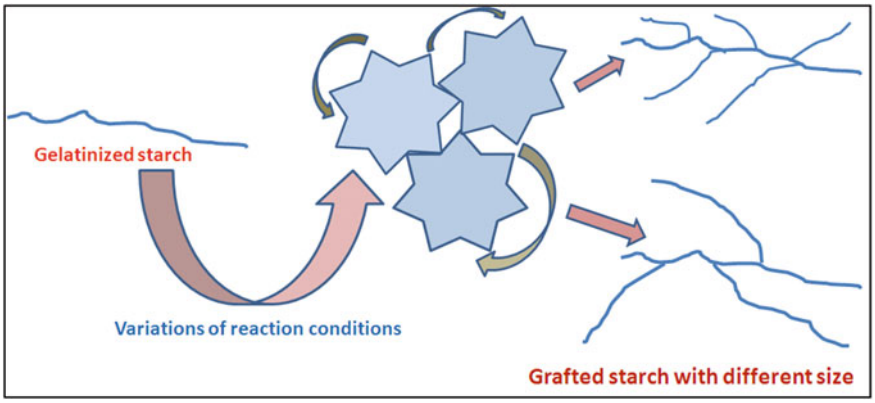

Fig. 3.7 Mechanism of flocculation through bio-materials

chains. Finally, compacted flocs are formed and quickly settled down [47]. Bridging is the most common flocculation pathway, according to other studies. Figure 3.7 demonstrates the flocculation mechanism through bio-polymer.

The polymer bridging process is primarily responsible for graft copolymers' superior flocculation characteristics over linear polymers. Polymer chain segments adsorbed onto the surfaces of various particles, forming bridges between neighboring particles and eventually linking all of the particles together. The polymer bridging process is primarily responsible for graft copolymers' superior flocculation characteristics over linear polymers. Polymer chain segments adsorbed onto the surfaces of various particles, forming bridges between neighboring particles and eventually linking all of the particles together. Since the polymer chains of grafted flocculants are longer, and the gyration radius is greater, the adsorbed polymer molecules appear to follow a more expanded structure when dealing with several particles [3, 37].

3.8 Factors Affecting Flocculation

3.8.1 Molecular Weight of Polymers and Charge Density

As a result of the sequence of incorporating these polymers, each polymer molecule has a propensity to adsorb on a single particle with its low molecular weight, reducing the degree of flocculation. Higher molecular weight polymeric materials can have a greater amount of adsorption to form flocs. For high molecular weight polymers, both the settling rate and the optimal dosage improved. For handling coal washery effluents, extremely high molecular weight anionic flocculants are increasingly crucial for achieving faster sedimentation speeds. Polymers with a lower molecular weight, on the other hand, are sufficient for filtration [31].

3.8.2 Flocculants Dosage and Condition of Mixing

The level of flocculation is influenced by the dosing and mixing sequences. There are no further changes in flocculation of any device above a certain maximal dose of polymers, and adding flocculants reduces competence. At low stirring speeds, the size and settling rate of flocs can be easily controlled after polymer inclusion, at higher speeds, with no subsequent decline at high concentrations, the level of flocculation is reduced, and particles are fully encased by absorbed polymer layers. Hydrodynamic conditions induced by mechanical agitation play a critical role in the flocculation phenomenon [58].

3.8.3 Shear Effect on Flocs

The flocs, which are either produced by bridging flocculation or natural coagulation, are concentrated for breaking with intense shaking. Excess polymer agitation causes formulated flocs to degrade faster than flocs formed with the optimal ratio of polymers. The effective formation of flocs is impossible due to the repulsion of excess adsorbed polymer, so the optimum polymeric dose only grips for a precise agitation degree.

3.8.4 Ionic Strength of the Solution

The configuration of polyelectrolyte is greatly influenced by the ionic strength of every solution, which has an effect on the flocculation phenomenon. The ionic concentration of a solution containing polyelectrolyte reduces as the viscosity of the solution increases due to reciprocal charge repulsion.Increased ionic strength shields the charged areas, allowing polymers to fold and implying a smaller hydrodynamic length, as shown by a decrease in solution viscosity. Ionic strength in solution reduces in a device with high solids for flocculation with a polymer with a higher molecular weight, and bridging is increased by increasing the effective particle radius [38].

3.8.5 Effect of pH

Solvated metal ions can influence the flocculation of inorganic flocculants via Schulze-Hardy effects and double-layer compression in the effective class. These organisms become charged as the pH value rises and their mode of action differs. The presence of an ionizable basic or acidic group influences protonation by pH modifications, which in turn affects colloidal particle surface charge [9].

3.8.6 *Effect of Particle Size*

On the one hand, a brawny relationship occurs between polymer molecular weight and particle size aggregation through the bridging mechanism to form flocs; on the other hand, forces occur to split the flocs, i.e., instability. The charge neutralization potential of a particle's surface is improved by increasing its surface area with polymeric flocculants [60].

3.8.7 *Effect of Temperature*

Temperature fluctuations help with flocculation, but this isn't always the case. With increasing temperature, the rate of particle collision and diffusion increased. On the other hand, adsorption is an exothermic process that has an adverse effect at higher temperatures. The temperature of polymeric chains varies as they extend linearly. Predicting the temperature effect of any device is therefore incredibly difficult [10].

3.9 Flocculation Modeling

The mathematical description of flocculation, or the method of aggregating destabilized suspended objects, has traditionally been focused on thinking of the process as two distinct steps: transport and connection. Local fluctuations in fluid/particle velocities resulting from (a) spontaneous thermal Brownian motion of the particles (perikinetic flocculation), (b) forced velocity gradients from mixing (orthokinetic flocculation), and (c) discrepancies in the settling velocities of individual particles contribute to the collision of two particles. The two precepts can be mathematically interpreted as a probability of effective collision between particles of sizes i and j: The rate of flocculation is simplified in (3.1).

$$\text{Rate of flocculation } = \alpha\, \beta\, (i,\ j)\, n_i n_j \tag{3.1}$$

α is the collision efficiency, β (i, j) is the collision frequency between the two particles of size i and j. n_i, n_j are the concentration of the particles for particles of size i and j, respectively.

The number of collisions is determined by the mode of flocculation, such as perikinetic, orthokinetic, or differential sedimentation. The collision efficiency $\boldsymbol{\alpha}$ (with values ranging from 0 to 1) is a feature of particle destabilization: the higher the degree of destabilization, the higher the value of $\boldsymbol{\alpha}$.Thus, in effect, β is a measure of the transportefficiency leading to collisions, represents the percentage of those collisions leading to attachment [53].

3.10 Kinetics of Aggregation of Particles

The flocculation, deflocculation, and re-flocculation processes follow the kinetics of Smoluchowski's classical model which is based on the existence of two processes that are simultaneously working: the aggregation of particles which follows second order kinetics and the breakage of the aggregate that follows first-order kinetics. Equation 3.2 demonstrated the flocculation kinetics.

$$\frac{d(N_t/N_0)}{dt} = -N_0 k_1 (N_t/N_0)^2 + k_2 (N_t/N_0) \tag{3.2}$$

where N_0 is the number concentration of the particles present in the effluent at time t_0, N_t is the number concentration at time t, k_1 and k_2 are kinetic constants for aggregation of particles and kineticconstants for the aggregate breakage, respectively. The kinetics of aggregation of particlesand aggregate breakage at different initial concentrations can be studied effectively using the above equation. The equilibrium situation can be explained using the relationship of both types of kinetics [57, 24].

3.11 Collision Frequency of Particles

It was well established that the process of flocculation follows bimolecular kinetics. The flocculation kinetics model gives the equation (3.3):

$$\sqrt{\frac{N_0}{N_t}} = 1 + \frac{1}{2} k N_0 t \tag{3.3}$$

where N_0 is the initial number of particles present in the effluent, N_t is the number concentration of theseparticles at time t, and k is the rate constant for collisions betweenthe singlets. Aplot of $(N_0/N_t)^{1/2}$ versus t provides a straight line withan intercept 1 for a bimolecular process, and the rate constant (k)can be obtained from the slope of the curve [8, 12].

3.12 Literature Survey

Till now, several works have been done on flocculation by graft copolymers or other modified versions of the natural polysaccharides. Here a list of such works has been provided to give a better insight into the matter.

Afolabi et al. [1] studied the functional properties and flocculation efficiency of Albizia Saman (AS) and Albizia glaberrima (AG) gum which was modified through

graft copolymerization with acrylamide. The grafting efficiency of AS and AG was 54 and 58%, respectively. The cold-water solubility of AS and AG were increased from 38.23 and 35.55% to 39.75 and 40.55%, respectively. The oil binding and emulsion capacity of AS and AG were decreased from 4.89 and 3.44% to 3.69 and 2.40%, respectively. The flocculation efficiency gets increases from 74% to above 98% for both these polymers after graft copolymerization.

Klein et al. [21] synthesised copolymer of cashew gum with poly(acrylamide) (PAM) using radiation mediated graft copolymerization using potassium persulfate as initiator in aqueous medium. Fourier-transform infrared spectroscopy, nuclear magnetic resonance spectroscopy, and thermogravimetric analysis were used to classify the graft copolymers. The graft copolymers (CG-g-PAM) were tested for their efficacy in flocculating a kaolin suspension.. According to the results, the graft copolymers synthesized with ultrasound energy had greater flocculation properties than those synthesized with microwave energy. Inoculation with the basidiomycete Trametesvillosa in liquid medium was used to assess the biodegradability of the graft copolymers.

Mate et al. [29] synthesized Jhingan-gum grafted acrylamide copolymer by microwave-assisted graft copolymerization technique using potassium persulphate as initiator. Analytical methods were used to validate the synthesized substance, and intrinsic viscosity and grafting percentage were used to determine the best-grafted grade (Jh-g-PAM 3). The efficiency of flocculation under various pH (2–10) and temperature (10–55 °C) conditions revealed that neutral pH and room temperature (25 °C) were optimal for flocculation. Furthermore, as pH was improved, the magnitude of the zeta potential increased from 2.65 to 17.17 mV. However, the particle size declined from 2041 to 1092 dnm, indicating that the kaolin suspension was stable under acidic conditions. The grafted material was found to be capable of removing Cr, Fe, and Pb from 0.004 mg/L to below detection limit (0.003 mg/L), 0.65 mg/L to 0.011 mg/L, and 0.015 mg/L to below detection limit (0.011 mg/L), respectively, in a river sample. With a half-life of 28 days, the grafted material was observed to degrade entirely in 180 days.

Mittal et al. [30] synthesized an environmentally friendly gum ghatti-crosslinked-polyacrylamide (Gg-cl-PAM) from gum ghatti (Gg) and acrylamide (AM) using a microwave-assisted grafting technique and tested it for use in water purification applications as an adsorbent and flocculent. SEM, FTIR, and TGA were used to classify the Gg-cl-PAM, which showed pH-sensitive swelling activity, with the highest swelling observed in neutral pH solution. The flocculation properties of Gg-cl-PAAM in clay solutions were investigated as a function of pH, temperature, and polymer mass filling, with the best results obtained at neutral pH and 40 °C. The adsorption capacities of Gg-cl-PAAM for the removal of various dyes such as brilliant green (BG), rhodamine B (RhB), congo red (CR), and methyl orange (MO) were investigated, and it was discovered that all dyes adopted the Langmuir isotherm model, with qm values of 523.62 mg g^{-1} for BG, 421.60 mg g^{-1} for RhB, 179.09 mg.

Sharma et al. [50] done free radical polymerization in an inert environment using ammonium persulfate (APS) as an initiator and Tetra (ethylene glycol) diacrylate (TEGDA) as a crosslinking agent. Polyitaconic acid (PIA) was grafted onto natural

polysaccharides xanthan gum. Structure was characterized using scanning electron microscopy and Fourier transform infrared spectroscopy (FTIR). The effects of APS, TEGDA, neutralizing degree, kaolinite content, and xanthan gum were studied. The findings show that PIA successfully grafted onto xanthan gum and developed a 3D structure. The weight ratio of Xanthan gum to kaolin, swelling ability, and gel content all increased as the study progressed.

Sand et al. [43] synthesized graft copolymer of sodium alginate and polyacrylamide using a free radical polymerization technique using a potassium bromate/thiourea redox system in an inert atmosphere. Variation of reaction variables such as acrylamide concentration (3.0102–9.3102 mol dm^{-3}), potassium bromates (8×10^{-3}–16×10^{-3} mol dm^{-3}), thiourea (1.6×10^{-3}–4.8×10^{-3} mol dm^{-3}), sulphuric acid (3.0×10^{-3}–7×10^{-3} mol dm^{-3}), alginate (0.6–1.6 g dm^{-3}), period length (60–180 min), and (30–500 C). In comparison to the parent polymer, water swelling potential, metal ion sorption, flocculation, and resistance to biodegradability studies of synthesized graft copolymer were conducted. FTIR spectroscopy and thermogravimetric processing were used to classify the grafted polymers. The flocculation efficacy of the grafted copolymer was found to be much higher compared to its un-grafted analog.

Nandi et al. [32] synthesized polyacrylamide-grafted-tamarind seed gum (PAM-g-TSG) using free radical method assisted with microwave where cerric (IV) ammonium nitrate (CAN) was used as free radical initiator. On grafting, the effects of monomer, CAN, and microwave irradiation time (MIT) were investigated. Several grafting metrics were measured, including percent grafting (percent G), percent grafting quality (percent GE), and percent conversion (percent Cn). MIT may significant contributions to the synthesis. The batch with 10 g acrylamide, 400 mg CAN, and 1 min MIT had the highest percent grafting (890.3%). Elemental research, FTIR, solid-state 13C NMR, DSC, TGA, XRD, viscosity, SEM, acute oral toxicity, and biodegradability studies were used to classify the grafted TSG. The study showed that PAAm-g-TSG is nontoxic and biodegradable. Finally, the grafted gum's flocculating capacity was tested in a paracetamol suspension. The flocculation analysis shows that all batches of graft copolymer have the strong flocculating ability in paracetamol suspension, with capability increasing as concentration and grafting increase. Among others, the batch (highest percent G = 890.3) has the highest degree of flocculation (=5.14 ± 0.26).

Giri et al. [13] synthesized grafted copolymer using kappa-carregeenan and polyacrylamide by microwave-assisted free radical polymerization using ammonium persulfate (APS) as initiator. The effect of reaction variables such as APS, AAm, and KC concentrations, time length, and microwave power was investigated. To classify the graft copolymer, researchers used FT-IR, X-ray diffraction (XRD), differential scanning calorimetry (DSC), and scanning electron microscopy (SEM). The graft copolymer's actions are mildly vulnerable to external pH, and the swelling has adjustable on/off flipping characteristics. The graft copolymer's flocculation efficacy in coal suspension was investigated in order to see whether it could be used as a flocculent. The graft copolymer's acute oral toxicity report was analyzed according to OECD guidance. During the 14-day trial, mice given the graft copolymer showed no

abnormal activity. During the 14 days following therapy with the graft copolymer, no deaths were observed.

Wu et al. [56] and group employed microwave aided initiation to copolymerize AM, DAC, and chitosan (CS) into a novel form of graft modified flocculant (CS-g-PAD), which was employed for sludge conditioning and dewatering. The influence of reaction conditions on microwave-aided copolymerization was examined, and orthogonal experiments were used to determine their ideal values. Microwave aided polymerization can induce the produced side polymer chain of PAD to react with the $–NH_2$ active group in CS, according to the structure and chemical characteristics of CS-g-PAD. As a result, graft copolymerization took place at the amino group linked to the C2 site. In a wide pH range (pH = 3.5–9.5), the synthesized CS-g-PAD outperforms CCPAM, PAD, and CS in sludge dewatering (FCMC: 72.1 percent, SRF: 4.5 1012 m/kg, d50: 679.556 m, Df: 1.72, floc sedimentation rate: 5.72 cm/min).Furthermore, the PAD grafted on CS has a good extension in solution, which increases its adsorption bridging action. The novel grafted CS-g-PAD shows promise and has a wide range of applications in sludge dewatering and conditioning.

Jain et al. [18] discussed the possibility of a polyacrylamide-grafted-polyethylene glycol/SiO_2 nanocomposite as a viable addition for drilling difficult shale deposits that might cause significant wellbore instability in this study. FTIR, Field emission scanning electron microscopy (FESEM), Energy dispersive spectroscopy (EDX), Atomic force microscopy (AFM), and thermogravimetric analyses were used to describe the nanocomposite, which was made using the free radical polymerization process (TGA).It was then used in the development of a water-based drilling mud system. Its impact on the designed mud system's rheological properties and filtration control features was carefully investigated. In addition, hot rolling shale dispersion tests and immersion experiments were used to study its shale inhibition properties. Core flooding experiments were also performed to investigate the formation damage produced by the newly created drilling fluid system. The results of the experiments demonstrated that the synthesized nanocomposite had a better shale inhibition property. The nanocomposite worked in tandem with the other additives in the created system to provide good rheological and filtration capabilities. It also outperformed the partly hydrolyzed polyacrylamide (PHPA) polymer in the designed drilling mud system in terms of formation damage, shale recovery, and thermal stability. As a result, this nanocomposite might be employed as a drilling fluid addition in a water-based shale drilling fluid system.

He et al. [15] was devised and manufactured a novel type of flocculant, a ternary copolymer comprising lignosulfonate, acrylamide, and chitosan. FTIR and XRD elemental analysis and structural characterization revealed that acrylamide effectively grafted onto the two natural polymers, resulting in amorphous macromolecules. The natural polymer-based flocculant was pH-independent and water-soluble. The amphoteric flocculant demonstrated strong color removal efficacy to anionic (Acid blue 113, > 95 percent), neutral (Reactive black 5, > 95 percent), and cationic dyes (Methyl orange, > 50 percent) across a wide range of flocculant dose and pH windows because it possessed several functional groups from the raw materials. From the cost,

source, and performance standpoint, the ternary flocculant based on lignosulfonate, chitosan, and acrylamide might be a promising material in practical applications.

3.13 Selection of Flocculants

The challenge of achieving the optimal clarity or purification will be much simpler if you understand the treatment procedures, such as coagulation-flocculation and direct flocculation, as well as the various forms of flocculants. The flocculants that have been used for the treatment of various forms of wastewaters, based on literature research. The first step in every wastewater treatment is to analyze the properties of the wastewater, which will decide the treatment procedure to be used. Coagulation-flocculation is often used to treat all wastewater with suspended and dissolved constituents, while direct flocculation is only used to treat organic-based effluents of suspended solids. The next step is to decide which flocculants will be used. Cationic coagulants or flocculants are always chosen since the surface charge in colloidal suspensions is almost always negative. Cationic coagulants are often combined with non ionic or anionic flocculants in the coagulation-flocculation process. There are several different flocculants on the market, each with a different molecular weight and charge density. High molecular weight flocculants are typically preferred because they are associated with a better bridging mechanism than other flocculation mechanisms [14].

3.14 Role of Architectural Polymers in Flocculation

The polymeric flocculants were found to have greater flocculating efficiency than that of the coagulants or the commercial flocculants available. Synthetic polymers, on the other hand, have adverse effect on health and the environment. They are non-biodegradable and cause serious health issues for which ETP has not been given the standard for oral toxicity. The natural polysaccharides are biodegradable, but they are much less efficient. The scientists came up with the solution by combining the properties of the natural polysaccharides and the synthetic polymers by graft copolymerization. The graft copolymers contain both properties.

Moreover, due to the increase in porosity, radius of gyration, hydrophilicity, solubility of the graft copolymers increases. As a result, more and more amount of particles get trapped into the cavity and undergo agglomeration and hence flocculation. With increasing factories and health issues, the amount of sludge needed to be deceased to nullify pollution. Architectural polymers, in this regard, play a crucial role. Hyperbranched polymers are architectural polymers that possess high chain-end functionality. They also have high solubility and low viscosity, for which they possess larger hydrodynamic volume. More number of particles get entrapped into the polymer causing greater flocculation due to greater chain-end functionality [27].

3.15 Graft Copolymer Nanocomposite as Flocculants

Graft copolymer nanocomposites are generally used as flocculants. Natural polymers like potato starchwere mostly used to synthesize the nanocomposite on the basis of the application in the flocculation system. Copolymerization enables materials to be created that combine the desired properties of several compounds in a single polymer chain. Copolymerization is a very effective method for the flocculation system. In 2020, Schmidt et al. [48] described the synthesis of graft copolymer between starch and carbon nanotubes for the potential application in flocculation efficiency. They synthesize the material via radical polymerization in an aqueous environment. In the standard jar test, the products were evaluated for their flocculation efficiency in a model aqueous kaolin suspension. For the removal of suspended solids from mine water and pH regulation, a variety of techniques involving inorganic coagulants are frequently used. However, issues such as the large amount of coagulants required, excessive sludge accumulation, aggregate instability and breakage, and the need for water conditioning have prompted research into alternative flocculants or coagulants. Gum karaya (GK) is an anionic polysaccharide derived from trees such as Sterculia urens, Sterculia villosa, and Sterculia setigera, which grow in India and North Africa, respectively. D-galacturonic acid, D-galactose, L-rhamnose, and Dglucuronic acid make up this strongly branched complex with polysaccharides. Considering the structural richness of gum polysaccharides uses in potential in water treatment applications. Hybrid inorganic–organic nanocomposites, which are made up of inorganic nanoparticles and functional polymers, are a new and unusual material type. Water is the most basic need for the survival of our society. One of the most significant conditions for a healthy public health environment is the availability of pure water. For the treatment of textile industry wastewater, various strategies such as reverse osmosis, activated carbon adsorption, and photocatalytic dye degradation have been suggested. The separation of dyes from wastewater can also be accomplished by efficient adsorption of dye molecules into adsorbents. Bio sorbents for dye removal have received a lot of coverage in recent years. Modified polysaccharides, especially polyacrylamide grafted polysaccharides and poly (acrylic acid) grafted polysaccharides, are widely used as flocculants and drag-reducing agents in wastewater treatment [35]. They are effective flocculants at low doses, managed biodegradable, shear resistant, low-cost, and environmentally safe. Graft copolymers made from polysaccharides are also used as adsorbents. In comparison to the individual components, the strong synergistic effect between inorganic nanofiller and modified polysaccharide matrix produces hybrid composite materials with impressive improvements in mechanical, thermal, and surface properties. Hybrid nanocomposite materials have been widely used for the treatment and remediation of toxic wastewater in recent years due to their intriguing properties. However, they have certain drawbacks, such as a limited surface region, a small hydrodynamic radius, and complex diffusion processes. These disadvantages limit their use as effective adsorbents. The direct discharge of industrial wastewater into bodies of water without proper treatment contaminates them with radioactive elements that are highly detrimental to marine life and human health.

Flocculation, precipitation, evaporation, and adsorption are some of the wastewater disposal processes. Flocculation is a cost-effective and reliable method for purifying and recycling manufacturing effluents. The addition of nanoscale filler to a graft copolymer-based matrix will increase surface area and hydrodynamic radius, making it ideal for use as a good adsorbent [36]. Microwave irradiation-based grafting has reformed the area of sustainable green chemistry by reducing the use of non-renewable materials and organic solvents while also reducing the formation of radioactive by-products. As a result, this method is both cost-effective and energy-efficient. Electromagnetic irradiation selectively excites the polar bonds of polysaccharides rather than the non-polar bonds, resulting in polar bond cleavage/breakage. In contrast to traditional chemical grafting techniques, this will produce free radical sites for grafting on the polysaccharide backbone without rupturing the polysaccharide C–C backbone, increasing product selectivity. On the other way cationic polyacrylamide (CPAAm) derivatives have been extensively used in papermaking as preservation and drainage aids, likewastewater and suspension flocculants, water clarification flotation aids, and soil improvers [61]. Biopolymers are distinguished from synthetic polymers by the inclusion of higher-order structures and, in certain cases (as in the case of lignin), the absence of an identifiable repeating unit, as well as a lower polydispersity or even mono-dispersity. Graft copolymers as flocculants have a number of drawbacks, including a low hydrodynamic length, a small radius of gyration, poor thermal stability, and a small surface area. However, there are ways to get around these drawbacks, such as adding nanoscale inorganic fillers on the surface of the polymer matrix, which improves its gyration radius, thermal stability, and surface. In the presence of certain inorganic fillers, such as silica, bentonite, and calcium carbonate, they have been used for papermaking due to their outstanding flocculating properties and special rheological features in aqueous media. CPAAms are primarily responsible for large-scale flocculation in these processes, with charged fillers serving as junctions. Monodisperse silica nanoparticles have been widely used as possible surface modifiers because of their uniform scale, shape, structure, and high specific surface region. Furthermore, polysaccharide hydrogen bonding units can serve as nucleating centers for silica generation and thus as an effective template for the growth of nanoscale silica particles. Biopolymers, especially polysaccharides, have piqued the scientific community's interest because of their supply, biodegradability, and high capacity to absorb contaminants from water. Yoon et al. [61] focused on the effects of the acryl-grafted silica nanoparticles (ASNP) concentration on the flocculation and retention characteristics in papermaking applications. Flocculants are widely used in water and wastewater purification processes to speed up the agglomeration of colloidal particles and the dropping of floc sediments in the water supply, as well as to improve contamination removal quality. Since inorganic flocculants are vulnerable to pH changes, they produce a lot of sludge in the atmosphere. Metal ions from such sludge are a major concern in groundwater [27]. Humans, poultry, and marine species are also highly poisonous to most synthetic flocculants. One example is the carcinogenic effect of acrylamide monomer, which can contaminate the polymer in trace quantities. Limited quantities of polymers can end up in the atmosphere after water treatment in finely divided form or as a diluted solution, posing

an additional challenge. Natural polymer-based flocculants are usually efficient in large concentrations and shear stable. They can also be easily adjusted to improve flocculation performance. According to studies in the literature, the combination of natural and water-soluble synthetic polymer properties allows for the creation of new highly successful flocculants.

3.16 Conclusion

The scope for traditional flocculants, bio flocculants, and grafted flocculants to be used in wastewater treatment has been thoroughly investigated. They also showed remarkable results in reducing or eliminating environmental parameters such as TSS, turbidity, COD, and color, with some studies achieving more than 90% removal. While flocculants have been developed and successfully used in the laboratory to remove contaminants from wastewater, there is still a need to enhance their efficiency in the removal of suspended and dissolved impurities, heavy metals, and color or dye molecules, inorganic or organic pollutants to comply with environmental regulations before the wastewater is discharged into the atmosphere. Given the industrial reliance on cost-effective flocculation technology for wastewater treatment, further potential research into the best flocculants capable of producing very promising results in pollutants removal even at broader pH and other contaminants in wastewater is needed.

Because of the extremely complicated nature of the flocculation process and the wide range of polyelectrolytes required, there are still few flocculation optimization practices in the industry for chemical flocculants. Selecting or regulating the molecular weight and charge density ranges of the polymer is one way to improve the flocculation process. Flocculation pathways vary depending on molecular weight and charge density (neutralization or bridging). In order to produce a better choice of flocculants for particular industrial applications, future research should look at how molecular weight and charge density distribution influence flocculation efficiency. Increasing the effectiveness and lowering the cost of chemicals may be achieved by optimizing these variables.

Furthermore, only a small amount of work has been done on a large scale, with most research focused on laboratory studies. Because of the sophistication of coagulation and flocculation processes, a polymer cannot be chosen for a specific application without extensive research. This testing is divided into two stages: (i) laboratory experiments to determine the form of flocculants and, more specifically, the optimal ionicity, and (ii) industrial trials or practices to validate the flocculants selection as well as the volume and molecular weight. As a result, the applicability and efficacy of most bio-flocculants for wastewater treatment have yet to be determined. More research into the efficacy of natural flocculants is also expected. Last but not least, an effective flocculation procedure requires the use of high-efficiency flocculants that can nearly eliminate or reduce all pollutants in wastewater.Environmentally friendly flocculants that can be manufactured using an easy and cost-effective process and

show high removal efficiencies and significantly denser flocs are seen as a promising commodity in real-world applications from a performance and cost standpoint.

References

1. T.A. Afolabi, D.G. Adekanmi, Characterization of native and graft copolymerized albizia gums and their application as a flocculant. J. Polym. **2017**, 1–8 (2017). https://doi.org/10.1155/2017/3125385
2. M.A. Barakat, New trends in removing heavy metals from industrial wastewater. Arab. J. Chem. **4**, 361–377 (2011). https://doi.org/10.1016/j.arabjc.2010.07.019
3. D.R. Biswal, R.P. Singh, Characterisation of carboxymethyl cellulose and polyacrylamide graft copolymer. Carbohydr. Polym. **57**, 379–387 (2004). https://doi.org/10.1016/j.carbpol.2004.04.020
4. J. Bratby, Coagulation and flocculation: with an emphasis on water and wastewater treatment (1980). https://doi.org/10.1016/0300-9467(81)80062-7
5. W. Brostow, H.E. Hagg Lobland, S. Pal, R.P. Singh, polymeric flocculants for wastewater and industrial effluent treatment. J. Mater. Educ. Pal Singh J. Mater. Educ. **31**, 3–4 (2009)
6. A. Carocci, A. Catalano, G. Lauria, M.S. Sinicropi, G. Genchi, Brief history of the development of the transfusion service. How Recruit Volunt Donors Third World? **238**, 22–28 (2015). https://doi.org/10.1007/398
7. H.W. Ching, T.S. Tanaka, M. Elimelech, Dynamics of coagulation of kaolin particles with ferric chloride. Water Res. **28**, 559–569 (1994). https://doi.org/10.1016/0043-1354(94)90007-8
8. K.K. Das, P. Somasundaran, A kinetic investigation of the flocculation of alumina with polyacrylic acid. J. Colloid Interface Sci. **271**, 102–109 (2004). https://doi.org/10.1016/j.jcis.2003.11.010
9. X. Feng, J. Wan, J. Deng, W. Qin, N. Zhao, X. Luo, M. He, X. Chen, Preparation of acrylamide and carboxymethyl cellulose graft copolymers and the effect of molecular weight on the flocculation properties in simulated dyeing wastewater under different pH conditions. Int. J. Biol. Macromol. (2020). https://doi.org/10.1016/j.ijbiomac.2019.11.081
10. C.S.B. Fitzpatrick, E. Fradin, J. Gregory, Temperature effects on flocculation, using different coagulants. Water Sci. Technol. **50**, 171–175 (2004). https://doi.org/10.2166/wst.2004.0710
11. K. Ghebremichael, J. Abaliwano, G. Amy, Combined natural organic and synthetic inorganic coagulants for surface water treatment. J. Water Supply Res. Technol. - AQUA **58**, 267–276 (2009). https://doi.org/10.2166/aqua.2009.060
12. S. Ghorai, A. Sarkar, A.B. Panda, S. Pal, Evaluation of the flocculation characteristics of polyacrylamide grafted xanthan gum/silica hybrid nanocomposite. Ind. Eng. Chem. Res. **52**, 9731–9740 (2013). https://doi.org/10.1021/ie400550m
13. T.K. Giri, M. Pradhan, D.K. Tripathi, Synthesis of graft copolymer of kappa-carrageenan using microwave energy and studies of swelling capacity, flocculation properties, and preliminary acute toxicity. Turkish J. Chem. **40**, 283–295 (2016). https://doi.org/10.3906/kim-1503-16
14. A.S. Greville, How to select a chemical coagulant and flocculant. Albert Water Wastewater Oper Assoc 24 (1997)
15. K. He, T. Lou, X. Wang, W. Zhao, Preparation of lignosulfonate-acrylamide-chitosan ternary graft copolymer and its flocculation performance. Int. J. Biol. Macromol. **81**, 1053–1058 (2015). https://doi.org/10.1016/j.ijbiomac.2015.09.054
16. Y.C. Ho, I. Norli, A.F.M. Alkarkhi, N. Morad, Characterization of biopolymeric flocculant (pectin) and organic synthetic flocculant (PAM): A comparative study on treatment and optimization in kaolin suspension. Bioresour. Technol. **101**, 1166–1174 (2010). https://doi.org/10.1016/j.biortech.2009.09.064
17. K.O. Iwuozor, Prospects and challenges of using coagulation-flocculation method in the treatment of effluents. Adv. J. Chem. A **2**, 105–127 (2019). https://doi.org/10.29088/sami/ajca.2019.2.105127

18. R. Jain, V. Mahto, V.P. Sharma, Evaluation of polyacrylamide-grafted-polyethylene glycol/silica nanocomposite as potential additive in water based drilling mud for reactive shale formation. J. Nat. Gas Sci. Eng. **26**, 526–537 (2015). https://doi.org/10.1016/j.jngse.2015.06.051
19. J.Q. Jiang, N.J.D. Graham, Pre-polymerised inorganic coagulants and phosphorus removal by coagulation - a review. Water SA **24**, 237–244 (1998)
20. D.J. Joo, W.S. Shin, J.H. Choi, S.J. Choi, M.C. Kim, M.H. Han, T.W. Ha, Y.H. Kim, Decolorization of reactive dyes using inorganic coagulants and synthetic polymer. Dye Pigment. **73**, 59–64 (2007). https://doi.org/10.1016/j.dyepig.2005.10.011
21. J.M. Klein, V.S. de Lima, J.M. da Feira, M. Camassola, R.N. Brandalise, M.M. de Camargo Forte, Preparation of cashew gum-based flocculants by microwave- and ultrasound-assisted methods. Int. J. Biol. Macromol. **107**, 1550–1558 (2018). https://doi.org/10.1016/j.ijbiomac.2017.09.118
22. J.P. Kushwaha, V. Chandra Srivastava, I.D. Mall, Treatment of dairy wastewater by inorganic coagulants: parametric and disposal studies. Water Res. **44**, 5867–5874 (2010). https://doi.org/10.1016/j.watres.2010.07.001
23. D.G.J. Larsson, Pollution from drug manufacturing: Review and perspectives. Philos. Trans. R. Soc. B Biol. Sci. 369 (2014). https://doi.org/10.1098/rstb.2013.0571
24. C.S. Lee, M.F. Chong, J. Robinson, E. Binner, A review on development and application of plant-based bioflocculants and grafted bioflocculants. Ind. Eng. Chem. Res. **53**, 18357–18369 (2014). https://doi.org/10.1021/ie5034045
25. C.S. Lee, J. Robinson, M.F. Chong, A review on application of flocculants in wastewater treatment. Process Saf. Environ. Prot. **92**, 489–508 (2014). https://doi.org/10.1016/j.psep.2014.04.010
26. J. Ma, R. Wang, X. Wang, H. Zhang, B. Zhu, L. Lian, D. Lou, Drinking water treatment by stepwise flocculation using polysilicate aluminum magnesium and cationic polyacrylamide. J. Environ. Chem. Eng. **7**, 103049 (2019). https://doi.org/10.1016/j.jece.2019.103049
27. P. Maćczak, H. Kaczmarek, M. Ziegler-Borowska, Recent achievements in polymer bio-based flocculants for water treatment. Materials (Basel) 13 (2020). https://doi.org/10.3390/ma13183951
28. A. Maria, R. Version, W. Technologies, The costs of water pollution in India (2003)
29. C.J. Mate, S. Mishra, P.K. Srivastava, Design of low-cost Jhingan gum-based flocculant for remediation of wastewater: flocculation and biodegradation studies. Int. J. Environ. Sci. Technol. **17**, 2545–2562 (2020). https://doi.org/10.1007/s13762-019-02587-x
30. H. Mittal, V. Kumar, S.M. Alhassan, S.S. Ray, Modification of gum ghatti via grafting with acrylamide and analysis of its flocculation, adsorption, and biodegradation properties. Int. J. Biol. Macromol. **114**, 283–294 (2018). https://doi.org/10.1016/j.ijbiomac.2018.03.131
31. K.M. Mostafa, A.A. El-Sanabary, Synthesis and characterization of novel smart flocculant based on poly(MAam)-pregelled starch graft copolymers and their degraded products. Adv. Polym. Technol. **32**, 1–10 (2013). https://doi.org/10.1002/adv.21339
32. G. Nandi, A. Changder, L.K. Ghosh, Graft-copolymer of polyacrylamide-tamarind seed gum: synthesis, characterization and evaluation of flocculating potential in peroral paracetamol suspension. Carbohydr. Polym. **215**, 213–225 (2019). https://doi.org/10.1016/j.carbpol.2019.03.088
33. F.E. Okieimen, Preparation, characterization, and properties of cellulose-polyacrylamide graft copolymers. J. Appl. Polym. Sci. **89**, 913–923 (2003). https://doi.org/10.1002/app.12014
34. A.T. Owen, P.D. Fawell, J.D. Swift, J.B. Farrow, The impact of polyacrylamide flocculant solution age on flocculation performance. Int. J. Miner Process **67**, 123–144 (2002). https://doi.org/10.1016/S0301-7516(02)00035-2
35. S. Pal, S. Ghorai, C. Das, S. Samrat, A. Ghosh, A.B. Panda, Carboxymethyl tamarind-g-poly(acrylamide)/silica: A high performance hybrid nanocomposite for adsorption of methylene blue dye. Ind. Eng. Chem. Res. **51**, 15546–15556 (2012). https://doi.org/10.1021/ie301134a

36. S. Pal, A.S. Patra, S. Ghorai, A.K. Sarkar, R. Das, S. Sarkar, Modified guar gum/SiO2: development and application of a novel hybrid nanocomposite as a flocculant for the treatment of wastewater. Environ. Sci. Water Res. Technol. **1**, 84–95 (2015). https://doi.org/10.1039/c4ew00023d
37. S. Pal, G. Sen, S. Ghosh, R.P. Singh, High performance polymeric flocculants based on modified polysaccharides - microwave assisted synthesis. Carbohydr. Polym. **87**, 336–342 (2012). https://doi.org/10.1016/j.carbpol.2011.07.052
38. S.K. Rath, R.P. Singh, Crafted amylopectin: applications in flocculation. Colloids Surf. Phys. Chem. Eng. Asp. **139**, 129–135 (1998). https://doi.org/10.1016/S0927-7757(98)00250-7
39. R.F. Ben, W. Mnif, S.M. Siddeeg, Microbial flocculants as an alternative to synthetic polymers for wastewater treatment: a review. Symmetry (Basel) **10**, 1–19 (2018). https://doi.org/10.3390/sym10110556
40. F. Roselet, D. Vandamme, M. Roselet, K. Muylaert, P.C. Abreu, Effects of pH, salinity, biomass concentration, and algal organic matter on flocculant efficiency of synthetic versus natural polymers for harvesting microalgae biomass. Bioenergy Res. **10**, 427–437 (2017). https://doi.org/10.1007/s12155-016-9806-3
41. M. Rossini, J.G. Garrido, M. Galluzzo, Optimization of the coagulation-flocculation treatment: influence of rapid mix parameters. Water Res. **33**, 1817–1826 (1999). https://doi.org/10.1016/S0043-1354(98)00367-4
42. H. Salehizadeh, N. Yan, R. Farnood, Recent advances in polysaccharide bio-based flocculants. Biotechnol. Adv. **36**, 92–119 (2018). https://doi.org/10.1016/j.biotechadv.2017.10.002
43. A. Sand, A. Vyas, A.K. Gupta, Graft copolymer based on (sodium alginate-g-acrylamide): characterization and study of water swelling capacity, metal ion sorption, flocculation and resistance to biodegradability. Int. J. Biol. Macromol. **90**, 37–43 (2016). https://doi.org/10.1016/j.ijbiomac.2015.11.085
44. S. Sardar, A. Jana, A. Mukherjee, A. Dhara, A. Bandyopadhyay, Bottom-up synthesis of bright fluorescent, moisture-resistant methylammonium lead bromide@poly(3-bromothiophene). New J. Chem. **44**, 2053–2058 (2020). https://doi.org/10.1039/c9nj04734d
45. S. Sardar, R. Koley, U.K. Ghorai, A. Pal, S. Sengupta, I. Roy, A. Bandyopadhyay, Photophysical and electrochemical properties of oligothiophene in non-polymeric and polymeric solvents. J. Mol. Struct. **1168**, 187–194 (2018). https://doi.org/10.1016/j.molstruc.2018.05.037
46. S. Sardar, I. Roy, S. Chakraborty, A.B. Ghosh, A. Bandyopadhyay, A selective approach towards synthesis of poly (3-bromo thiophene)/graphene quantum dot composites via in-situ and ex-situ routes: application in light emission and photocurrent generation. Electrochim. Acta 365 (2021). https://doi.org/10.1016/j.electacta.2020.137369
47. A.K. Sarkar, N.R. Mandre, A.B. Panda, S. Pal, Amylopectin grafted with poly (acrylic acid): development and application of a high performance flocculant. Carbohydr. Polym. **95**, 753–759 (2013). https://doi.org/10.1016/j.carbpol.2013.03.025
48. B. Schmidt, Nanocomposite starch graft copolymers with carbon nanotubes – synthesis and flocculation efficiency. Polimery/Polymers **65**, 226–231 (2020). https://doi.org/10.14314/polimery.2020.3.7
49. G. Sen, R. Kumar, S. Ghosh, S. Pal, A novel polymeric flocculant based on polyacrylamide grafted carboxymethylstarch. Carbohydr. Polym. **77**, 822–831 (2009). https://doi.org/10.1016/j.carbpol.2009.03.007
50. P. Sharma, A. Dagar, V.A. Sapna, A. Sand, Superabsorbent composites (SACs) based on xanthan gum-g-poly (itaconic acid)/kaolinite. Polym. Bull. (2020). https://doi.org/10.1007/s00289-020-03436-5
51. J.J. Shen, L.L. Ren, Y.Y. Zhuang, Interaction between anionic dyes and cationic flocculant P(AM-DMC) in synthetic solutions. J. Hazard. Mater. **136**, 809–815 (2006). https://doi.org/10.1016/j.jhazmat.2006.01.013
52. R.P. Singh, S. Pal, S.A. Ali, Novel biodegradable polymeric flocculants based on cationic polysaccharides. Adv. Mater. Lett. **5**, 24–30 (2014). https://doi.org/10.5185/amlett.2013.6498
53. D.N. Thomas, S.J. Judd, N. Fawcett, Flocculation modelling: a review. Water Res. **33**, 1579–1592 (1999). https://doi.org/10.1016/S0043-1354(98)00392-3

54. R.C. Tilton, J. Murphy, J.K. Dixon, The flocculation of algae with synthetic polymeric flocculants. Water Res. **6**, 155–164 (1972). https://doi.org/10.1016/0043-1354(72)90090-5
55. H.F. Wang, H. Hu, H.J. Wang, R.J. Zeng, Impact of dosing order of the coagulant and flocculant on sludge dewatering performance during the conditioning process. Sci. Total Environ. **643**, 1065–1073 (2018). https://doi.org/10.1016/j.scitotenv.2018.06.161
56. P. Wu, J. Yi, L. Feng, X. Li, Y. Chen, Z. Liu, S. Tian, S. Li, S. Khan, Y. Sun, Microwave assisted preparation and characterization of a chitosan based flocculant for the application and evaluation of sludge flocculation and dewatering. Int. J. Biol. Macromol. **155**, 708–720 (2020). https://doi.org/10.1016/j.ijbiomac.2020.04.011
57. Z. Yang, H. Peng, W. Wang, T. Liu, Crystallization behavior of poly(ε-caprolactone)/layered double hydroxide nanocomposites. J. Appl. Polym. Sci. **116**, 2658–2667 (2010). https://doi.org/10.1002/app
58. Z. Yang, H. Yang, Z. Jiang, T. Cai, H. Li, H. Li, A. Li, R. Cheng, Flocculation of both anionic and cationic dyes in aqueous solutions by the amphoteric grafting flocculant carboxymethyl chitosan-graft-polyacrylamide. J. Hazard. Mater. **254–255**, 36–45 (2013). https://doi.org/10.1016/j.jhazmat.2013.03.053
59. K.-J. Yao, Y.-B. Tang, Synthesis of starch-g-poly(acrylamide-co-sodium allylsulfonate) and its application of flocculation to Kaolin suspension. J. Appl. Polym. Sci. **45**, 349–353 (1992). https://doi.org/10.1002/app.1992.070450217
60. M. Yao, J. Nan, T. Chen, Effect of particle size distribution on turbidity under various water quality levels during flocculation processes. Desalination **354**, 116–124 (2014). https://doi.org/10.1016/j.desal.2014.09.029
61. D.H. Yoon, J.W. Jang, I.W. Cheong, Synthesis of cationic polyacrylamide/silica nanocomposites from inverse emulsion polymerization and their flocculation property for papermaking. Colloids Surf. A Physicochem. Eng. Asp. **411**, 18–23 (2012). https://doi.org/10.1016/j.colsurfa.2012.06.036
62. J. Yu, D. Wang, X. Ge, M. Yan, M. Yang, Flocculation of kaolin particles by two typical polyelectrolytes: A comparative study on the kinetics and floc structures. Colloids Surf. A Physicochem. Eng. Asp. **290**, 288–294 (2006). https://doi.org/10.1016/j.colsurfa.2006.05.040
63. A.Y. Zahrim, C. Tizaoui, N. Hilal, Evaluation of several commercial synthetic polymers as flocculant aids for removal of highly concentrated C.I. Acid Black 210 dye. J. Hazard. Mater. **182**, 624–630 (2010). https://doi.org/10.1016/j.jhazmat.2010.06.077
64. Y. Zhou, G.V. Franks, Flocculation mechanism induced by cationic polymers investigated by light scattering. Langmuir **22**, 6775–6786 (2006). https://doi.org/10.1021/la060281+

Chapter 4
Sustainable Bio-Polymer-Based Nanocomposites for Wasterwater Treatment

S. V. Sheen Mers, V. Manju, Sathish Kumar Kamaraj, and Mercedes Guadalupe López Pérez

Abstract Wastewater treatment includes the removal of undesirable organic and inorganic debris such as dyes and heavy metal ions from wastewater. The recent trend is the usage of green substances for wastewater treatment using the biomaterials such as chitosan, cellulose, starch etc. that are abundantly available in our environment. Using biopolymer-based composites, water treatment can be carried out by a simple adsorption method and it does not require any sophisticated instrumentation to implement the technique which will reduce the cost for commercialization. The efficiency of the adsorbent is improved through surface functionalization thereby tuning its physical and chemical properties interms of stability, dispersibility and specificity. Surface area is another important parameter that can be enhanced by tuning the shape and size of the adsorbent. Understanding the basic process behind the design of adsorbents and the type of interaction between adsorbents and adsorbate enables the calculated invention of new composites. In this chapter, we discuss the type of biopolymers used for treating wastewater, modification of biopolymers for effective adsorption, bionanocomposites used for water treatment, sustainability criteria for using such biomaterials for water purification, the type of interaction between the adsorbent and the pollutant and the practical difficulties in implementing the technique for commercialization.

S. V. Sheen Mers · V. Manju
Indian Institute of Technology, Chennai, India

S. K. Kamaraj (✉)
Instituto Tecnológico El Llano Aguascalientes (ITEL), Tecnológico Nacional de México (TecNM), El Llano, México
e-mail: sathish.k@llano.tecnm.mx

M. G. L. Pérez
Biotechnology and Biochemistry Department, Center for Research and Advanced Studies of the IPN (Cinvestav-IPN) Irapuato Unit, Mexico City, México

M. J. Hato and S. Sinha Ray (eds.), *Functional Polymer Nanocomposites for Wastewater Treatment*, Springer Series in Materials Science 323,
https://doi.org/10.1007/978-3-030-94995-2_4

4.1 Introduction

Water scarcity is a growing global challenge in the twenty-first century and the World Economic Forum rates the water crisis as the number one global threat in terms of societal risks [72]. The total freshwater available on earth is only 0.003% which is being polluted by the rapid growth of industries, accumulation of domestic and sewage wastes due to rising population and intensive agriculture practices. Globally, around one billion people do not have access to safe drinking water and 2.6 billion people have inadequate or inappropriate sanitation services [74]. The most common water pollutants in freshwater sources are heavy metals and metalloids, dyes, pesticides, cosmetics, microplastics, drug residues etc. [13, 34, 56]. Heavy metals and metalloids are discharged from different industries such as metallurgical, electroplating, mining, chemical manufacturing, and battery manufacturing industries. The wastewater containing drugs, metals and dyes are from the pharma, cosmetics textile industries. The wastewater released from the dairy and food processing industries has a high concentration of organic materials, carbohydrates, lipids, proteins etc. This highly nutritious water allows the rapid growth of algae and bacteria which reduces the oxygen in the water environment (eutrophication). The demand for oxygen results in the death of large scale aquatic animals and plants due to the formation of anaerobic conditions. Other important pollutants are the pesticides that are reaching the water bodies because of the inappropriate usage in agricultural practices.

All these pollutants reach the freshwater bodies (lakes, rivers and groundwater) due to the lack of proper disposal of toxic wastes into soil medium and the discharge of wastewater without prior treatment. The discharge of inorganic and organic micropollutants into natural water bodies affects the ecological balance. Some of the pollutants such as heavy metals and anthropogenic components are highly toxic and carcinogenic. Particularly, anthropogenic pollutants may be detrimental not only to human health but also to aquatic organisms. About 8,00,000 people/year are losing life as a consequence of consuming contaminated drinking water [74]. Therefore the treatment of wastewater is essentially important for the safety of the ecosystem and development of human society before when it is discharged into natural bodies [2].

Generally, a few of the main industries in developing countries and small scale industries are not treating the effluents properly because of limited resources and the inadequate guidelines to discharge both primary and secondary wastes. So across the globe, the governments, World Health Organization (WHO), the European Commission and different environmental protection agencies (EPA) have enacted new acts and regulatory guidelines and revised the existing regulatory guidelines to treat wastewater and disposal of toxic wastes [8, 19, 55]. Various guidelines and acts such as the Clean Water Act, the Drinking Water Act and the Protection of Water Sources Act are enacted to monitor the drinking water and to safe-guard water sources [8, 19, 55]. The utmost motives of these regulations are to provide clean and safe drinking water to humans and to provide clean water for irrigation. Most of the studies argue that only a small fraction of the world will have access to clean and safe water by 2050 because

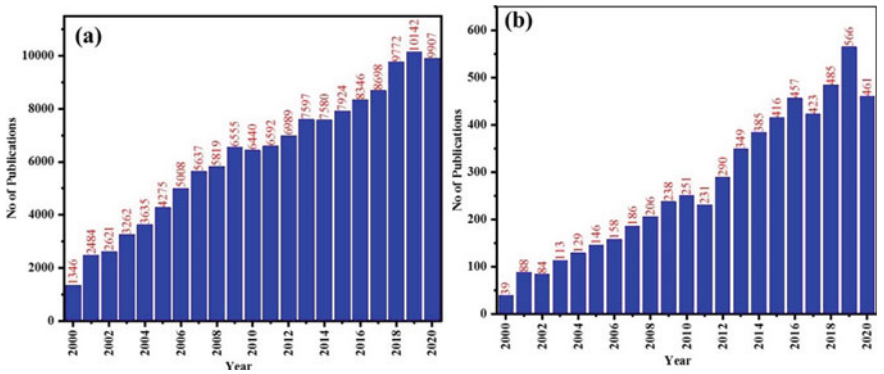

Fig. 4.1 Publication trend in the field of wastewater treatment from 2000 to 2020 and the values are obtained from PubMed using the search words: **a** "wastewater treatment" and **b** "biopolymers for wastewater treatment"

of the large quantity of wastewater that is generated annually [34, 56]. Hence, among scientists and policymakers, developing cost-effective, efficient and sustainable technologies are of major concern to recover wastewaters and have to turn them into safe and reusable. Different wastewater processing methods were developed for this purpose [5, 6, 43, 53]. The literature trend reported in the field of wastewater treatment from 2000 to 2020 is shown in Fig 4.1a. The increasing number of publications indicates the importance of the topic during recent years.

Several methods such as chemical precipitation, complexation, liquid extraction, membrane separation, classical coagulation-flocculation, chemical oxidation and reduction, electrochemical oxidation and reduction, flotation, photocatalytic degradation, reverse osmosis, ion exchange, electrodialysis, biological treatment and adsorption were developed to treat wastewater that is discharged from different industries [7, 91]. Some of these techniques have certain limitations such as poor performance during large-scale applications, low removal efficiency, generation of toxic chemicals and secondary pollutants. The large quantities of sludge and secondary pollutants require post-treatment which increases the cost of the whole process. Also, the current approaches and devices are mostly designed based on synthetic materials which will again increase the cost and often leads to environmental pollution through their disposal. The water treatment methods and devices should be cost-effective, sustainable, viable to scale-up and the resources should be available in abundance. These requirements are perfectly met by biopolymers and their nanocomposites because nature provides us with a large number of biopolymers with excellent physico-chemical properties [7, 35, 53, 70]. The publications trend on the utilization of biopolymers for wastewater treatment was shown in Fig. 4.1b. In this chapter, we discussed the type of biopolymers used for treating wastewater, modification of biopolymers for effective adsorption, bionanocomposites used for water treatment, the criteria for using such biomaterials for water purification, the type of interaction

between the adsorbent and the adsorbate (pollutant), and the practical difficulties in implementing the technique for commercialization.

4.2 Types of Biopolymers Used for Treating Wastewater

There exists a large number of polymers in nature that are abundant, sustainable (because of renewable sources), biodegradable, cost-effective and possess peculiar physicochemical properties [17, 42, 51, 53, 89]. We can tune the flexibility of the devices by forming hybrids/composites with other suitable polymers. For example, chitosan, silk, keratin are flexible while bamboo and wood possess a high combination of roughness and strength. Biopolymers are classified into different ways based on their degradability, based on their polymer backbone and based on the nature of the repeating unit such as polysaccharides, polyproteins, polyphenols and polynucleotides. Based on the type of applications [35, 51, 78, 89], the biopolymers are further classified into bioplastics, biosurfactant, biodetergent, bioadhesive, bioflocculant. The biopolymers are widely used in wastewater treatment not only due to their abundance and sustainable property but also due to their desirable properties such as non-toxicity, poly-functionality, high chemical reactivity, and chelation and adsorption capacities. The biopolymers that are widely used in water treatment can be divided into four classes such as polysaccharides, polypeptides, polyphenols and polynucleotides. The structure and sources of a few sustainable polymers were shown in Fig. 4.2.

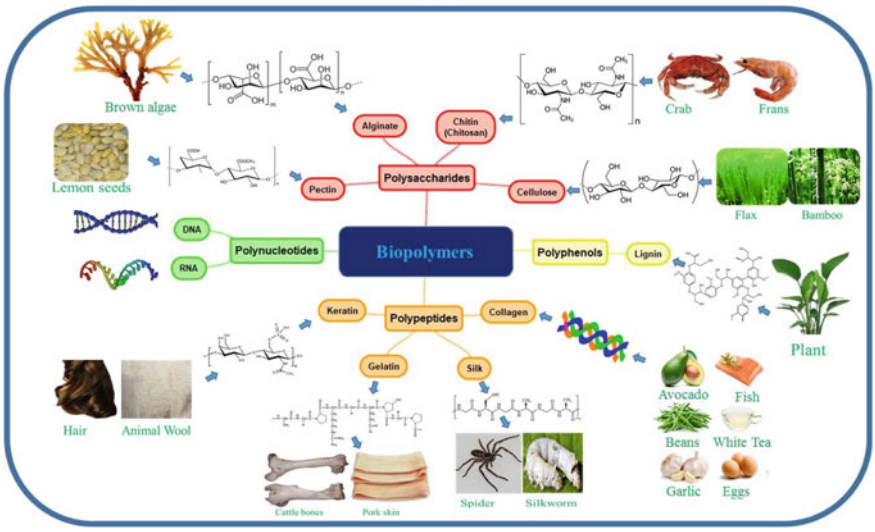

Fig. 4.2 The molecular structure and sources of naturally derived biopolymers for water treatment

4.2.1 Polysaccharides

Polysaccharides are polymeric carbohydrates composed of monosaccharide repeat units bounded together by glycosidic linkage. Natural polysaccharides are simple carbohydrates with a unique monosaccharide repeat unit. The properties of these polymers depend on the sequence of monosaccharide repeat unit, reactive functional groups (–OH, –COOH and $–NH_2$ groups) and its skeletal structure (ranging from linear to highly branched). The widely used organic polymers belonging to the polysaccharides category that are used for wastewater treatment are cellulose, chitosan, starch, alginate, pectin, guar gum and xanthan gum [47, 48, 53]. The polysaccharides and their composites possess excellent adsorption properties due to high hydrophilicity (arises due to the existence of hydroxyl groups), the presence of multiple functional groups (acetamido, primary amino, and/or hydroxyl groups), their high reactivity and chelation ability. Heavy metals can be removed by forming chelates with metals since the functional groups in polysaccharides can bind with metals. On the other hand, the organic molecules, dyes etc. can be removed by electrostatic interaction.

4.2.1.1 Cellulose

Cellulose is the most abundantly available natural polysaccharide and it is composed of β-(1–4) linked D-glucose units. The cellulose materials are derived from the barks of plants, and bacteria [38]. The three general types of cellulose materials are bacterial cellulose (BC), cellulose nanofibers (CNFs, nano fibrillated or micro fibrillated cellulose), cellulose nanocrystals (CNCs, often referred to as cellulose nanowhiskers or nanocrystalline cellulose). The BC is derived from bacteria via a bottom-up approach. Various species of bacteria are capable of fermenting sugars and plant polysaccharides and generating BC. The best-known bacterium is *Komagateibacterxylinus* (previously called *Acetobacter* or *Gluconoacetobacter*). CNFs are obtained from plants sources by a top-down method. The CNCs are prepared by the acid hydrolysis of the CNFs in which the disordered ('amorphous') regions in between the crystalline regions of cellulose fibrils are cleaved, thus liberating only linear, crystalline entities. For example, the lingo-cellulosic raw material (often paper pulp, wood pulp, cotton, animal descent etc.) are used to prepare CNFs. The CNCs are prepared by defibrillation and hydrolysis of CNFs.

The difference between BC, CNFs and CNCs are the differences in dimension, purity and crystallinity. The BC are pure, crystalline, thick (20–100 nm) and have length usually in the micrometre range, while the purity and crystallinity of CNFs are less compared to BC because it contains hemicelluloses and/or lignin residues. Also, the length of CNFs is in the micrometre range while the diameter is very small (4–100 nm). The CNCs are very pure and crystalline but the length (50–500 nm) is much shorter than BCs and CNFs. The cellulose materials possess numerous advantages such as high purity and crystallinity, favourable biocompatibility, low density,

high porosity, durable mechanical properties, high absorption capacity, low cost, and three-dimensional interconnected structures of BC with ultrafine nanofibers. Hence, they find potential applications in different fields such as membranes, nanocomposites, medicine, bioplastics, barrier films, biomedicine, pharmaceutics, electronics etc.

4.2.1.2 Chitin/Chitosan

Chitosan is another member of linear polysaccharides composed of randomly distributed β—linked D—glucosamine and N—acetyl—D–glucosamine. It is generally derived through the deacetylation of the non-toxic polymer chitin which is generally extracted from crustaceans, insects, arachnids, algae, fungi, molluscs, fungi and fishes via several routes of extraction including chemical methods, enzymatic methods, and/or irradiation. The most common method is chemical extraction which involves three basic steps, i.e., deproteinization, demineralization, and deacetylation [6, 48]. Chitosan extracted from different sources have amino ($–NH_2$) and hydroxyl (–OH) functional groups on its polymer backbone. These functional groups have the ability to chelate with metals and hence they can be used to remove metals from the wastewater. The pK_a values mainly depend on the degree of deacetylation in chitosan. The pK_a value of amine groups on chitosan is close to 6.3–6.4 and at pH 5, or below, more than 90% of amine groups get protonated and can attract anionic species [45, 53].

4.2.1.3 Starch

Starch is one of the naturally abundant polysaccharides and it is commonly found in many parts of plants such as stalks, roots, and crop seeds [47, 48]. The main sources of starch are cassava, wheat, rice, maize or corn, and potatoes. Starch consists of D—glucose units linked to macromolecules including amylopectin, branched (1 → 6) −α −D—glucan, amylose, and linear (1 → 4)—linked α −D–glucan. The major component of the starch is the amylopectin polymer. Hence, the primary property of starch depends mainly on the properties of amylopectin. Crystalline and amorphous starch structures (microcrystalline starch, starch nanocrystal, starch crystallite, and hydrolyzed starch etc.) with varying morphologies can be prepared by altering the hydrolysis conditions, sources and the method of extraction. The desirable properties of starch towards water treatment are high abundance, non-toxicity, low cost, renewability and biocompatibility.

4.2.1.4 Alginate

Alginate is a naturally occurring anionic polymer and it is one of the salts of alginic acid. Alginic acid is the only polysaccharide that naturally contains carboxylic

groups. It is a linear copolymer composed of homopolymeric blocks of (1–4)-linked □ −D–mannuronate (M) and its C-5 epimer, α–L–guluronate (G) residues with different sequence or blocks such as consecutive G-residues (G-blocks), consecutive M-residues (M-blocks) or alternating M and G-residues (MG-blocks). The pK_a values of mannuronic acid and guluronic acid are measured to be 3.38 and 3.65 respectively. Alginic acid/alginates are derived from marine brown algae (*Phaeophyceae*) as well as from polysaccharide-based soil bacteria. Alginates are low-cost linear polymers that can form gels when divalent cations are added to them. Also, it can form viscous gum when it is hydrated and it is a superabsorbent (can absorb a large amount of water, as much as hundreds of times equivalent to its mass) [25, 42, 48]. Alginate has been extensively utilized in wastewater remediation due to its stability, high water permeability, biodegradability, and non-toxic nature.

4.2.1.5 Pectin

Pectin is one of the naturally occurring linear polysaccharide-based biopolymer which can be derived from different plant-based sources such as fruit peels and pulp, sugar beet, sunflower heads, lemon seeds, orange pulps etc. [48, 67] Pectin is composed of D–galacturonic acid (GalA) repeating units joined by α−(1−4) glycosidic linkage. It also possesses a number of carboxyl/hydroxyl groups in the polymer backbone and a certain amount of neutral sugar as a side chain. The pK_a of GalA units in pectin is 3.5. Hence, the carboxyl groups are ionized ($–COO^-$) above pH 3.5. The ionized $–COO^-$ can act as a binding site for cationic pollutants and may form ionic cross-linking with divalent cations. In addition to that, the functional groups present on the pectin can form complexes with metals.

4.2.2 Polypeptides

Natural polypeptides are biomaterials composed of repeating amino acids that are linked by peptide bonds. The coupling of a minimum of two or more polypeptides results in specific proteins with unique architecture. Silk, collagen and keratin are three typical proteins consisting of long chains of amino acids and their performance and their application in different fields are due to the hierarchical structure with elongated size. Also, these biopolymers are renewable and can be derived from natural sources such as plants, exoskeletons of arthropods, skin, silkworm cocoon, spider webbing, and hair [20, 77]. The control of structure in polypeptides based materials such as hair or spider silk is exerted at every level of hierarchy and the two most common local conformations are the α-helix and β-sheet structure. Polypeptides also possess different functional groups and polar active sites similar to polysaccharides based materials. Hence, the polypeptides can also adsorb different organic pollutants and metals present in wastewater.

4.2.2.1 Silk

Silk (*Bombyxmori*) is a naturally occurring protein made up of fibroin and glue-like protein sericin, that holds the fibroins together. It is obtained from a variety of species, including silkworms and spiders. Silk fibroins (SF) consist of two polypeptide chains [a heavy H-chain (390 kDa), a light L-chain (26 kDa)] and glycoprotein (P25). Among these, the H–L complex is formed through disulphide bond formation and a glycoprotein (P25) is non-covalently associated with the H– L complex. The H-chain contains the repeating units of Gly-Ala/Ser/Tyr dipeptides while L-chain has the non-repetitive arrangements of amino acids. Silk possesses many ionizable groups on different amino acid residues on the side chain and free carboxyl groups. The carboxyl groups are from different acids i.e. aspartic acid and glutamic acid. These functional groups present on the structure of SF provide the capability to adsorb metal ions at oxygen atoms or on its amide group [20, 38]. Also, it is abundant, low-toxic, biocompatible and exhibits a cationic/anionic nature. Hence, it is used for removing heavy metals, dyes, organic molecules etc. However, the silk exhibits minor mechanical properties and greater unsteadiness. To increase the stability, strength and flexibility, the SF materials are combined with suitable reinforcing fillers.

4.2.2.2 Collagen

Collagen is one of the most abundant proteins in animals (25–35% whole-body protein content). It is one of the main structural proteins in connective tissues [42]. It can be extracted from the skin, bones, and connective tissues of animals such as domesticated cattle, chickens, pigs, and fish. Mostly collagen is derived from the bones of animals. Hence, it is predominantly comprised of 90–95% of organic bone matter. Its primary structure consists of glycine-x–y triads where x is mostly proline and y is probably hydroxyproline. The molecule has 1000 amino acids at 100 kDa molecular weight swirled into a triple helix. We can get multiple forms of collagen from the animal kingdom and its solubility is determined by the age of collagen. The number of free functional groups on collagen decreases with age due to crosslinking of functional groups.

4.2.2.3 Gelatin

Gelatin is a mixture of peptides and proteins and is commonly derived from collagen [42, 77]. It is produced by the partial hydrolysis of collagen extracted from the skin, bones, and connective tissues of animals such as domesticated cattle, chickens, pigs, and fish. It is a translucent, colourless, flavourless food ingredient and its composition mainly depends on its parent collagen. Gelatin is water-soluble and brittle when it is dried. Also, it is non-toxic, biodegradable, biocompatible, low cost and easily available. It also contains various functional groups such as –OH, $–NH_2$, and –COOH which act as the binding sites for various pollutants via interactions such

as polar, ionic interactions or chelation ability thus making gelatin an effective bio adsorbent in wastewater treatment.

4.2.2.4 Keratin

Keratin belongs to the family of fibrous structural proteins (scleroproteins) and it enables animals to protect themselves from predators, competition, and environmental hazards. It is the key structural material making upscales, hair, nails, feathers, horns, claws, hooves, calluses, and the outer layer of skin among vertebrates [15, 18, 62]. Keratin is insoluble in water and organic solvents. Keratin is typically extracted from bovine hooves using the general approach usually applied for collagen production. Keratin has sulphonic acid ($–SO_3H$) in its structure in addition to other generally existing functional groups. The properties of Keratin depend on the sources, structure and crosslinking ability.

4.2.3 Polyphenols

Polyphenols are natural products that consist of multiple phenol units i.e. several hydroxyl groups on aromatic rings. More than 5000 unique categories of polyphenols have been found and they are mostly derived from beverages, vegetables, fruits, cereals, plants and plant metabolites. The properties of the main categories of polyphenols rely on the strength of phenolic rings and the elements attached to these moieties. For example, the main polyphenols are flavonoids, tannins, phenolic acids, lignans and stilbenes. The plant-based polyphenol tannin and complex polysaccharides tannin derivatives are widely used to remove metals, organic molecules and dyes from wastewater and also used to remove oils [4, 17, 27]. The structure of the polyphenols (tannin and lignin) is one of the key factors i.e. they have the ability to form 3D polymer structures and have different functional groups like hydroxyl, methoxyl and phenolic groups. Due to the presence of a large number of hydroxyl groups, polyphenols can chelate with metals and hence, they can be used to remove heavy metals. Also, they can exhibit anionic/cationic character depending on the pH of the solution. By taking advantage of this property, they can be used to remove anionic/cationic molecules from the wastewater.

4.2.3.1 Lignin

Lignin is also one of the organic natural polymers made by cross-linking phenol precursor and it is also the most abundant biomass along with cellulose and chitin. It is usually found in wood and around 50 million tons of lignin are produced annually. Lignin is an amorphous phenolic polymer consist of p-coumaryl alcohol, sinapyl alcohol, and coniferyl alcohol. The structure of the lignin and the repeating units

depend on the plant species, growing location, and growth duration. In addition to that, lignin is further classified as alkaline lignin, lignosulfonate, organosolv lignin, hydrolysis lignin based on the type of separation process. [17, 46] The adsorption capacity of the lignin towards pollutants varies for the above-mentioned lignin. The hydroxyl groups present on the lignin surface plays an important role in the chemical and physical properties of lignin such as reactivity, hydrophilicity, and functionality. Different cross-linking and functionalization methods were developed to improve the adsorption capacity of lignin. Similar to other polymers, lignin and its derivatives can efficiently capture metal ions through chelation, ion exchange, and/or electrostatic interactions.

4.2.3.2 Tannin

Tannins are non-toxic natural polyphenol biomolecules that are widely distributed in roots, barks, stalks and fruits of plants. Also, they are recognized as secondary plant metabolites. Tannin possesses multiple adjacent phenols in its structure [4], [CSL STYLE ERROR: reference with no printed form.]; [27, 53]. The number and the nature of phenol structure determine the physical, chemical, and biological properties of tannin. Since phenol is an excellent hydrogen donor, phenolic groups get deprotonated to form phenoxide which is stabilized via resonance. Hence, tannin usually exhibits anionic behaviour and absorbs cationic molecules. Also, the deprotonated phenolic groups exhibit a strong affinity towards many metal ions. The tannins are classified into two types (1) condensed tannin and (2) hydrolysable tannin or flavonoids. Since tannin contains phenol and –OH in its structure, it can be functionalized with different functional groups using substitution, addition, and coupling and condensation reactions. The specific example for tannin is tannic acid and its pk_a is around 6. However, the pk_a value varies due to the variation in phenolic groups and numbers.

4.2.4 Polynucleotides (DNA)

Polynucleotides are another important class of biopolymers that consist of 13 or more nucleotide monomers that are covalently attached in a chain. DNA and RNA are typical examples of polynucleotides. It is well known that deoxyribonucleic acid (DNA) is a polynucleotide that carries genetic information to instruct the growth, function and reproduction of living organisms and many viruses. Moreover, we can make 2D and 3D nanostructures using DNA origami because the predesigned cocktails of polynucleotide sequences can self-assemble and fold in a self-controlled manner under controlled temperature and chemical conditions [85]. Hence, we can prepare hierarchical 2D and 3D nanostructures for different applications using DNA origami. Interestingly, DNA based nanostructures can be used to remove heavy metals due to their ability to bind with heavy metals [63].

4.3 Application of Biopolymers in Wastewater Treatment

In general, wastewater treatment systems are divided into four main categories: (1) preliminary treatment, (2) primary treatment, (3) secondary and (4) tertiary treatment [7]. The preliminary treatment often consists of physical techniques such as sedimentation, screening, filtration to remove solid physical waste present in the wastewater. The primary treatment methods such as coagulation/flocculation, chemical precipitation, air flotation etc. often involve the addition of chemicals to remove solid and chemical wastes. Secondary treatment methods are used to remove suspended particles and biodegradable organic matter. It consists of several primary approaches and provides a high magnitude of treatment with more specific than primary treatment. Tertiary treatment methods are applied when a high degree of treatment is required and it is often used to remove smaller particles, dissolved dyes, metals, pesticides, dairy products etc. The tertiary treatment method (reverse osmosis, adsorption, filtration etc.) is often pollutant specific and it consists of several primary and secondary treatment methods. Table 4.1 shows the properties of materials to be used as flocculants/coagulants, adsorbents and membrane/filters, and their corresponding process and mechanisms. Statistically, about 54% of the whole processes of water treatment techniques have been carried out using membranes to produce fresh and clean water. Particularly, the filtration techniques such as reverse osmosis (RO), nano-filtration (NF), ultrafiltration, and microfiltration have been carried out using membrane/filters.

The biopolymers, in addition to the properties mentioned in Table 4.1 have added advantages such as hydrophilicity, non-toxicity, biocompatibility, biodegradability, renewable in nature and abundance [35, 78, 82, 89]. Also, biopolymers are flexible that can be reinforced into different structures to improve their properties and possess highly reactive functional groups such as –COOH, –OH, $–NH_2$, $–SO_3H$, phenols, electron-deficient centres, hydrophobic and hydrophilic sites along with different porosity. One can engineer the surface of biopolymer with desired functional groups (–COOH, –OH, $–NH_2$ etc.) [36] to remove specific pollutants by altering the pKa of the polymer backbone. Hence, the biopolymer and its derivatives can be used to remove metals, heavy metals, organic molecules, dyes, pesticides, herbicides, drugs, oil, radionuclides etc. from wastewater. In order to use the biopolymers as coagulants/flocculants and adsorbents, an insoluble species should be formed with the pollutants so that they can be easily removed from the water. The membranes/filters prepared using biopolymers are found to be significant [22, 38, 50]. This is due to the fact that the biopolymers based membranes are flexible, cost-effective, biocompatible, biodegradable, non-toxic and more effectively remove the soluble inorganic and organic species from wastewater. A few examples of the pollutants removed from wastewater using biopolymers, their derivatives and composites are shown in Table 4.2.

As shown in Table 4.2, the cellulose-based materials are used to remove Cr^{6+}, Pb^{2+}, Cd^{2}, Ni^{2+}, Cr^{3+}, Mn^{2+}, Hg^{2+}, Cs^{+}, Fe^{2+}, cationic/anionic dyes, phenols, drugs etc. Also, cellulose has been commonly used as a membrane due to its fascinating properties such as porous nature, semi-permeable, hydrophilic and dimensional strength

Table 4.1 The properties of materials to be used as flocculants/coagulants, adsorbents and membrane/filters, process and mechanisms [38, 41, 53]

Type	Process	Mechanisms	Material Features
Coagulants/Flocculants	Phase transformation	Double-layer compression, adsorption and bridging, charge neutralization, sweep coagulation	High charge density, macromolecular framework, formation of insoluble species with pollutants
Adsorbents	Surface phenomenon	Chelation, ionic interaction, Van der Waal's, ion exchange, hydrogen bonding, physical adsorption and precipitation (depends on surface chemistry and the nature of pollutants i.e. functional groups, cationic/anionic nature and hydrophilic/hydrophobic parts present on them)	Poly-functionalities and their high chemical reactivity, chelation ability, ease of functionalization and high adsorption capacity, tuning of adsorption capacity by different modifications
Membranes/ Filters	Pure water permeance, size exclusion regime, affinity regime (i.e. only pure water is passed through the membrane/filter and the pollutant is rejected by size)	Solution-diffusion model for membrane (rejects pollutants smaller than 1 nm), pore flow model for both filter (rejects pollutants with size bigger than micrometres) and membrane (rejects pollutants with size bigger than 1.5 nm)	Flexible, LBL assembly, formation of sheet structure, ability to tune the pore size, pore-volume, ability to pass selective species, has an affinity to bind with different soluble organic and inorganic species
Catalysts/ Biocatalysts	Electrochemical/Photochemical/ biological degradation of organic molecules and proteins	Electrochemical oxidation/reduction, photocatalytic degradation	Conductive, biocompatible, it should have a bandgap to adsorb light for photochemical degradation, it should mimic the enzymes for biological treatment etc.

Table 4.2 The list of few pollutants removed from wastewater using biopolymers, their derivatives and composites

Biopolymer used	Metals	Dyes	Drugs and other compounds	References
Cellulose	Cr^{6+}, Pb^{2+}, Cd^{2+}, Ni^{2+}, Cr^{3+}, Mn^{2+}, Hg^{2+}, Cs^{+}, Fe^{2+}, As^{3+}	MB, RhB, MO, Rh6G, CR, reactive light-yellow K-4G, acid red GR, victoria blue 2B, MV2B, RB 19	sulfa-methoxazole, acetaminophen, and N,N -diethyl-meta-toluamide (DEET), 2-NP, UO_2^{2+}, Oil	[24, 32,38, 48, 69]
Chitosan	Pb^{2+}, Cu^{2+}, Co^{2+}, Ni^{2+}, Zn^{2+}, Cd^{2+}, Cr^{6+}, Cr^{3+}, As, Ag^{+}, Au, Sb^{3+}, Hg^{2+}	MB, MO, MG, BB, orange G, Red 60, CR, RR 141, RR 16, RR 120, RhB 6G, MG, Reactive blue-21, Acid orange 7, direct red 16, rose bengal, brilliant cresyl, safranin,	Levofloxacin, ceftriaxone, diclofenac and ketoprofen, amoxicillin, tartrazine, Fluoride, nitrate, 4-NP, free fatty acids, phenol, aromatic amines and carboxylic acids, oil	[6, 45, 48 91]
Starch	Pb^{2+}, Cu^{2+}, Cd^{2+}, Cr^{6+}, As, Hg^{2+}	MB, MG, MO, golden yellow SNE dye, CR, MV, acid blue-25, safranin, optilan blue	Sulfamethazine, Bisphenol A, nitrate, urea, napthalene	[48]
Alginate	Pb^{2+}, Hg^{2+}, Cu^{2+}, Co^{2+}, Zn^{2+}, Cd^{2+}, Cr^{6+}, As^{3+}, As^{5+}, Cesium, Fe^{2+}, Ni^{2+}	Brilliant cresyl blue, MO, MB, MV, MG, reactive blue 222, indigo, acid red 14, RhB, basic red 46,	Norfloxacin, 4-NP, nitrate, fluoride, iodine, 4-chlorophenol, trichlorophenol, THF, bisphenol	[48]

(continued)

Table 4.2 (continued)

Biopolymer used	Metals	Dyes	Drugs and other compounds	References
Pectin	Pb^{2+}, Cu^{2+}, Co^{2+}, Ni^{2+}, Zn^{2+}, Cd^{2+}, Cr^{6+}, Cesium, Fe^{2+}	MB, MO	Fluoroquinolones, Ciprofloxacin, Moxifloxacin, 4-NP	[32, 48, 67]
Silk	Cr^{6+}, Hg^{2+}, Cd^{2+}, Pb^{2+},Zn^{2+}, Cu^{2+}, Ni^{2+}, Fe^{3+}, Ag^{+}, As^{3+}, Au^{3+}	Orange G, brilliant yellow and blue, RhB, CR, Rh6G, MB, MG	cytochrome c, Gold nanoparticles, oil	[20, 31, 79, 80, 83]
Collagen/Gelatin	Cr^{6+}, Pb^{2+}, Cd^{2+}, Ni^{2+}, Cr^{3+}, Hg^{2+}, As^{3+}, Co^{2+}, Cu^{2+}, Zn^{2+}	MB, bromocresol green, RhB, CR, and thioflavin Tdyes, pyronin Y, RhB, DG 12, brilliant green, xylenol orange, eosin yellow, MV, acid fuchsin,	Uranium, phosphate, nitrate, Oil	[3, 16, 37, 39, 73, 81, 88]
Keratin	Cr^{6+}, Pb^{2+}, Cd^{2}, Ni^{2+}, Cr^{3+}, Hg^{2+}, Cu^{2+}, Zn^{2+}, Ag^{+},	Brilliant blue FCF, erythrosine, tartrazine, MG,	–	[15, 18, 62]

(continued)

Table 4.2 (continued)

Biopolymer used	Metals	Dyes	Drugs and other compounds	References
Lignin	Pb^{2+}, Hg^{2+}, Cu^{2+}, Zn^{2+}, Cd^{2+}, Cr^{6+}, Ni^{2+}, (light metal ions Na^{+}, K^{+}, and Mg^{2+})	ethyl violet, MG, cationic brilliant red, acid blue 92, and direct red 23	Ibuprofen and acetaminophen	[17, 46, 84, 90]
Tannin	Cr^{6+}, Hg^{2+}, Cd^{2+}, Pb^{2+},Zn^{2+}, Cu^{2+}, Fe^{3+}, Ag^{2+}, As^{3+}, Au^{3+}, Mo^{6+}, Pd^{2+}, Pt^{4+}, Rh^{3+}	MB, MG, brilliant red X-3B, acid dye (red 1), DG86,	Trimethoprim, Uranium, boron, Sb, phosphate, CTAB	[3, 4, 27, 29, 65]
DNA	Hg^{2+}, Cd^{2+}, Pb^{2+},Zn^{2+}, Cu^{2+}, Fe^{3+}, Cr^{3+}, As^{2+}	–	Endocrine disruptor	[23, 64, 86, 87]

Methylene blue (MB), methylene orange (MO), Rhodamine B (RhB), rhodamine 6 G (Rh6G), Neutral reactive blue 19 (RB 19), Arsenic, 2-nitrophenol (2-NP), Reactive Red (RR), BB- Bromothymol Blue, CR-congo red, MV-methyl violet, MG-malachite green, DG-direct yellow.

[39]. Similar to cellulose, chitosan and its derivatives have been used to adsorb heavy metals (Cu, Pb, Ag, Cr, Ni, As), precious metals (Pd, Au, Pt, etc.), organic molecules, oils, radionuclides etc. [6, 45] Similar to other polysaccharides, starch also possesses reactive hydroxyl groups with long-chain polymer backbone which can chelate with metals and will generate negative charge at high pH. Hence, starch, its derivatives and composites are also used to remove heavy metals and charged organic molecules from wastewater [48].

Similarly, alginate is used to remove metals, dyes, drugs etc. It has a high affinity and binding capacity towards metal ions. Also, it forms stable hydrogel beads which exhibit high surface area, network structure, and it is enriched with surface functionalities [48]. The interesting properties of alginate-based bio sorbents are their ability to form macromolecular hydrogel to form a 3D network structure, different

morphologies and structures when they interact with multivalent or divalent metal ions Ca^{2+}, Fe^{3+}, Ba^{2+}, Ag^{+}, Al^{3+}, etc. with selective interactions. Mostly it is used to remove cationic species due to its anionic nature. Another interesting polysaccharide is pectin and the pectin based materials have been mostly utilized for the selective elimination of heavy metals from aqueous media with the affinity sequence of $Pb^{2+} > Cu^{2+} > Co^{2+} > Ni^{2+} > Zn^{2+} > Cd^{2+}$.

Similar to polysaccharides, polypeptides have been used for wastewater treatment. The significance of the natural polypeptides is that they are mostly formed of protein sequences. The proteins usually fold and interweave to form secondary structures with ordered components such as beta sheets, turns, and helices, as well as amorphous coils. The lightweight and fibrous nature of natural silk, keratin, collagen and gelatin make them potential candidates to prepare adsorbents, membranes and catalyst support to remove pollutants from wastewater [18, 20, 61]. Few of the pollutants removed using silk, keratin, collagen and gelatin are shown in Table 4.2.

A trace amount of metal ions can also be removed from wastewater when polyphenols are used [4, 27, 54]. Tannin and lignin are widely used for water treatment. The removal of metals, dyes, charged molecules using tannin is drastically increased after the development of tannin foams due to the increase in surface area. The rigid tannin forms and tannin gels were prepared using tannin powder, formaldehyde and furfuryl alcohol in 70%, 5% and 25%. As shown in Table 4.2, the tannin based materials are used to remove heavy metals, precious metals, boron, phosphates, drug and dyes. Lignin, another abundant polyphenol have been used to remove heavy metal ions (Pb^{2+}, Hg^{2+}, Cu^{2+}, Zn^{2+}, Cd^{2+}, Cr^{6+}, Ni^{2+}), light metal ions (Na^{+}, K^{+}, and Mg^{2+}) and toxic dyes.

The polynucleotides are another important class of biopolymers in which the UV-irradiated DNA film and glass beads were used to remove Hg^{2+}, Cd^{2+}, Pb^{2+}, Zn^{2+}, Cu^{2+} and/or Fe^{3+}ions [86]. The DNA trapped inside flavonoid and APTEMS film [23] was used to remove Hg^{2+}, Cd^{2+}, Pb^{2+}, Zn^{2+}, Cu^{2+}, Fe^{3+}, Cr^{3+} and As^{2+}. Despite its natural abundance, DNA is costly due to the extraction process. But, we can make 2D and 3D nanostructures using DNA origami because the predesigned cocktails of polynucleotide sequences can be self-assembled and folded in a self-controlled manner under optimized temperature and chemical conditions.

4.4 Different Methods of Modification and Architecture of Biopolymers

To improve the adsorption efficiency, membrane formation, hydrophilicity, and catalytic activity, biopolymers are further modified by cross-linking, grafting, coupling etc. Also, different composites have been prepared using biopolymers with metals, metal oxides (Fe_3O_4, ZnO etc.), carbon materials (CNTs, graphene etc.), enzymes etc. Different modification techniques and various forms/architecture were developed to improve the adsorption efficiency of biopolymers, their derivatives and

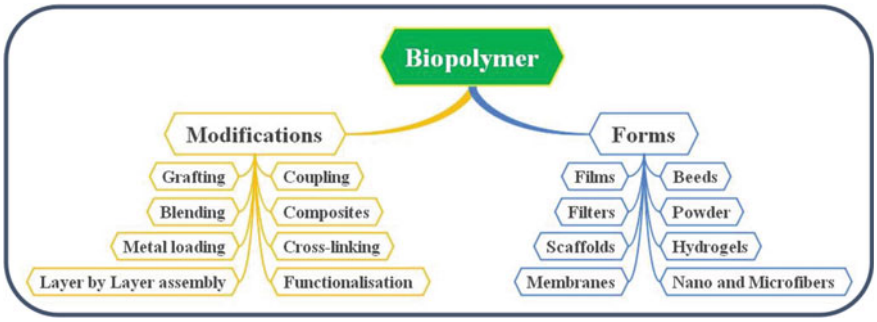

Fig. 4.3 Different modifications of biopolymers and their different forms used for water treatment

composites. The biopolymers are modified by different methods such as cross-linking [14, 71, 73], coupling [69], grafting [33, 42] of biopolymers with other organic molecules or polymers, coupling or grafting of biopolymers on a solid support, forming composites with metals, metal oxides, nanoparticles, polymers etc. [36, 53] Functionalized biopolymer derivatives and their composites with desired functional groups and dimensions can be produced using these modification techniques. Different modification methods and architectures are given in Fig. 4.3. All those methods and architectures are possible due to the highly reactive functional groups and flexible polymer backbone present in biopolymers. Modification of biopolymers will give interesting macromolecular superstructures, e.g. gels and hydrogels networks, polymeric resins, beads, membranes, fibers or composite materials. These biopolymer-based materials can be then used as adsorbents.

Modified biopolymers based adsorbents show an increase in the adsorption capacity, selectivity, recyclability and expand pH range i.e. pK_a of biopolymer-based materials can be altered. For example, chitosan has amine groups in its structure. The pK_a of amine groups on chitosan is close to 6.3–6.4 and the pK_a values are mainly depends on the deacetylation degree of chitosan. However, at pH 5, or below, more than 90% of amine groups get protonated. Hence, they can attract anionic species. Functionalized chitosan (N -carboxymethyl chitosan) contains active hydroxyl (–OH), carboxyl (–COOH), an amine ($–NH_2$) groups. At neutral or alkaline pH, the –COOH groups become negatively charged, which attracts the metal ion or species capable of being positive at the selected pH to adsorb positively charged organic species or metals. The biopolymers are crosslinked with different polymers to form microspheres, hydrogels, aerogels, films etc. For example chitosan-based hydrogels, crosslinked gelatin-starch, nanocellulose-alginate, nanocellulose-chitosan etc. The metal, metal oxides, minerals, clay, carbon nanomaterials and enzymes are dispersed on a biopolymer matrix to form composites. Biopolymer based nanocomposites are getting importance due to their excellent physical and chemical properties. These composites are formed to improve functional properties of biopolymers such as solubility, adsorption capacity, mechanical strength, catalytic activity etc. Also, they

will have functional properties depending on both polymer and nanoparticles present on them.

4.5 Bionanocomposites for Wastewater Treatment

Bionanocomposites (BNCs) are composite materials that contain constituent(s) of biological origin and particles with at least one dimension should be in the range of 10–100 nm. For example, the nanosized inorganic or organic particles are dispersed in an organic polymer matrix. The formation of BNCs is an interesting interdisciplinary area that combines material sciences, biology and nanotechnology. BNCs possess many advantages such as renewable, biocompatible, biodegradable, mechanical-robust, and multifunctional features over synthetic polymer-based composite [11, 70, 85]. The functional properties of BNCs are due to the constituent(s) and size of the nanoparticle present on it. Also, the characteristics of BNCs depend upon the nature of biopolymers, the stoichiometric ratio of constituents, macromolecular skeleton and functional groups. The polymer-based nanocomposites can be divided into different categories. Representative examples of polymer-based nanocomposites are shown in Fig. 4.4.

BNCs have been used in different applications includes drug delivery, bioelectronics, health and environment monitoring, energy generation and storage, and lightweight structural support. It has been encouraged to use BNCs for wastewater treatment due to their excellent mechanical, physical and chemical properties especially the high surface area to volume ratio, interfacial activity, the flexibility of the polymer backbone, functional groups. A few examples of BNCs used for wastewater treatment is given in Table 4.3. The primary constituent of BNCs is either a biopolymer or a nano-sized biopolymer, as shown in figure. The nanosized polymers can be mixed /cross-linked with polymers, metal nanoparticles, metal oxides etc. to form a nanocomposite. For example, cellulose nanocrystals are cross-linked

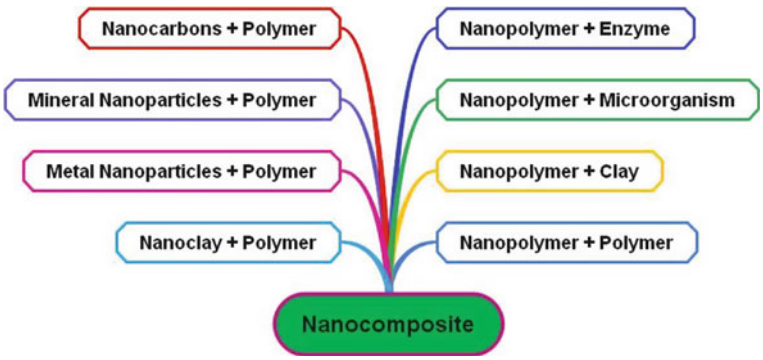

Fig. 4.4 Representative examples of polymer-based nanocomposites

Table 4.3 Few examples of nanocomposite prepared using biopolymer

Nanocomposite	Debris removed from wastewater	Used as	Adsorption capacity	References
NB-DANC-CMC	Bromophenol blue, Direct Blue 6, oil, organic solvents	Focculants	29.842 g g^{-1} and 20.927 g g^{-1} within 5 min, 50 times of its weight for oil and organic solvents	[68]
Cellulose acetate/Graphene Oxide nanocomposite	Ni^{2+}	Adsorbent	75.18 to 86.94% (10 to 40 mgL^{-1})	[76]
Fe_3O_4/CNCs-QXH hydrogel	Zn^{2+}, Pb^{2+}, Cd^{2+}, Cu^{2+}	Adsorbent	0.131, 0.159, 0.136 and 0.15 mmol/g	[60, 69]
CNCs-GQDs	Hg^{2+}, Cu^{2+}, Ni^{2+}, Ag^{+}	Scavenger	–	[1, 69]
Chitosan-derived magnet-sensitive materials	Polycyclic aromatic hydrocarbons	Adsorbent	96%	[52]
Gluten/Pectin/Fe_3O_4 Nano-hydrogel	Sediment contamination in Lake Urmia	Adsorbent	62% for heavy metals and 42% for organic compounds	[57]
Pc-cl-GG/SPION	m-cresol, o-chlorophenol		176.1 and 75.6 mg/g	[67]
SGGO Triple-network Composite Aerogel (3D)	MB and CR dye	Adsorbent	322.6 and 196.8 mg/g	[25]
Saccharomyces cerevisiae/ Fe_3O_4/Calcium alginate	Atrazine		88%	[12]
Au@BSA NCs on CNCs/alginate	Hg^{2+}	Sensor and scavenger	50%	[41]
Gelatin-Zr(IV) phosphate nanocomposite	Methylene blue (MB) and fast green (FG) dyes	photocatalytic degradation	87.81% MB and 89.91% FG were degraded within 5 h	[58]
GA-cl-poly(AAm)/$Ni(OH)_2$/FeOOH NCH	Methylene blue	Photodegradation	75% methylene blue was degraded	[49]
Gelatin-Laccase	Micropollutants	Biocatalysts	–	[21]

with biobased materials and metal oxides, nanoparticles [69]. Metal and metal oxides (Fe_3O_4, CuO, ZnO etc.) are integrated into the biopolymer/nano biopolymers to form BNCs. These BNCs exhibits photocatalytic activity too with other functional properties such as conductivity, catalytic activity, adsorption ability etc. BNCs can also be prepared using 1D, 2D carbon nanomaterials (CNTs, graphene, graphene oxide etc.) and biopolymers. The resulted BNCs exhibits controlled electrical conductivity, thermal conductivity, gas barrier properties, sensing abilities, and controlled molecular porosity, good adsorption capacity, etc.

Fe_3O_4 nanoctahedra in cellulose nanocrstals-Quaternized xylan hydrogel (Fe_3O_4/CNCs-QXH hydrogel), cellulose nanocrystals-graphene quantum dots (CNCs-GQDs), Pectin-crosslinked-guar gum/ superparamagnetic iron oxide (Pc-cl-GG/SPION), Sodium Alginate/gelatin/graphene Oxide (SGGO), Nanobentonite incorporated dialdehyde nanocellulose- carboxymethyl cellulose aerogel

(NB-DANC-CMC), Gum Arabic-crosslinked- poly(acrylamide)/$Ni(OH)_2$/FeOOH nanocomposites hydrogel (GA-cl-poly(AAm)/$Ni(OH)_2$/FeOOH NCH).

The 0D, 1D, 2D and 3D metal nanoparticles are incorporated on the polymer matrix to increase the functional property of the biopolymers such as high electrical conductivity, barrier transport, catalytic ability, and optical activity [58]. For example, bovine serum albumin-protected gold nanoclusters (Au@BSA NCs)-loaded cellulose nanocrystal—alginate hydrogel beads are developed and used for simultaneous sensing and scavenging of heavy metal ions [41]. Similarly, the mineral nanoparticles of different shapes, such as 0D nanoparticles, 1D nanowhiskers and 2D nanoplatelets are also integrated into the biopolymer matrix. For example, the montmorillonite (MTM), $CaCO_3$, hydroxylapatite, and boron nitride were integrated into biopolymers to form BNCs. Chitosan-clay composites are also designed to remove ∼99% of dyes, metals, and harmful negative ions from various solutions and a maximum of ∼94% of the targeted herbicides can be removed from media under investigation. The enzyme/bacteria based BNCs can also prepared using enzymes and biopolymer for biocatalytic applications.

4.6 Adsorption Mechanism

The adsorption (biosorption) is found to be an effective method to treat wastewater using biopolymer-based materials. Also, it is highly attractive for water treatment throughout the world, especially in developing countries. In fact, adsorption is an old drinking water treatment procedure and it is aimed to remove taste and odour imparting compounds from an aqua stream. The advantage of the adsorption method is its capacity to remove both organic, inorganic pollutants, biological species etc. The adsorption phenomenon is broadly classified as chemisorption and physisorption. The physisorption occurs by *Van der Waals* force and electrostatic interaction while chemisorption occurs by mainly chelation, covalent and/or ionic bonding. One can achieve the efficient removal of pollutants using available biopolymers via chemisorption and physisorption due to the presence of a large number of functional groups, charge sites, flexible polymer network etc. in it. Understanding the adsorption kinetics and isotherm is also important to identify the specific adsorbent to remove specific adsorbate and to identify the desorption process. Because the adsorption kinetics and isotherm studies provide information about how the pollutant is bound within or onto the adsorbent. Different adsorption isotherms such as Langmuir, Freundlich, Dubinin-Radushkevich (D–R) model, Temkin model, Toth isotherm, Redlich-Peterson isotherm and Sips (Langmuir–Freundlich) are used to quantify the performance of adsorbent. Among them, the Langmuir and Freundlich isotherms are widely used.

The adsorption capacity is the key parameter to understand the performance of the *adsorbent* for removing the pollutant (i.e. *adsorbate*). The adsorption capacity of the adsorbent depends on solution temperature, nature and concentration of pollutants, presence of other pollutants and other experimental conditions such as pH, contact

time and particle size of the adsorbent. Also, the reported interactions of biopolymers with pollutants are complexation, coordination/chelation, electrostatic interactions, acid–base interactions, hydrogen bonding, hydrophobic interactions etc. However, recent studies have been showing that the adsorption mechanism of biopolymers is complex while the adsorption mechanism of the biopolymers based nanocomposites is even more complex because the mechanism depends not only on the polymer. The adsorption of nanocomposite depends on other components such as metal nanoparticles, metal oxides, mineral metal nanoparticles, clay materials that are incorporated into the biopolymers. Also, morphological features of the nanocomposite (i.e. porosity, pore size, roughness, surface area etc.) plays role in adsorption isotherm.

4.7 Sustainability Criteria for Wastewater Treatment

A systematic strategy is required for reporting water treatment works is mandatory. Generally in literature, the BNCs based reports include the development of new materials, studying their water purification properties, developing different methods such as adsorption, filtration, (photo)electrochemical degradation, photocatalytic degradation, biodegradation, and underlying mechanisms [26, 52, 76] More commonly, a fuzzy-Delphi method was used for screening the criteria required to evaluate certain technology. Several reports are available in the literature about the application of the fuzzy-Delphi methodology for making sustainable decisions. Based on this method, sustainability criteria for wastewater treatment are also divided into four categories [26] (1) technical, (2) environmental, (3) economical and (4) social, as shown in Fig. 4.5. Treatment efficiency, production cost, health and safety risks, environmental safety, ease of implementation are major concerns than other criteria.

4.7.1 Treatment Efficiency

Treatment efficiency of the wastewater treatment method depends on several factors such as the nature of materials, adsorption capacity, catalytic activity, functional

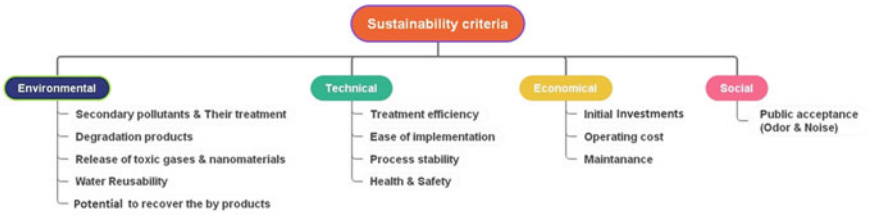

Fig. 4.5 Sustainability criteria for wastewater treatment

groups, morphology, porosity, crystallite structure, hydrophilicity/hydrophobicity, different forms, and biocompatibility, biodegradability and reusability, and treatment techniques [26]. Different methods were reported in the literature such as adsorption, degradation by (photo)electrochemical, biological method, filtration using membranes and filters, conventional coagulation/flocculation for water treatment. Each method has its limitations and evaluation parameters. Hence, one should consider all these factors when the efficiency of the water treatment system has to be reported. For example, the efficiency of the adsorption methods depends on materials adsorption coefficient and their properties while the efficiency of electrochemical methods depends mainly on the electrocatalytic activity. The photocatalysis and (photo)electrochemical methods depend on the bandgap of the material and its light adsorption property. In addition to the above properties, we should require biocompatible and biodegradable materials to improve the efficiency of the adsorbents and catalysts, particularly which are used for biological treatment and microbial fuel cell water treatment.

4.7.2 The Production Cost of Water Treatment

In general, the capital cost includes the cost of raw materials, processing cost, price of materials, utilization of manpower, water transport infrastructure, land required for installation and the cost of instruments used for the water treatment process. Depending on the choice of method of purification, the efficiency and production cost may vary. Adsorption/filtration and ion exchange chelating resins incineration, electrochemistry, membrane filtration, evaporation, liquid–liquid (solvent) extraction based methods are cost-effective methods. In membrane filtration, the cost and sustainability of the membranes decide the cost and in the adsorption method, the cost mainly depends on adsorbents. Like-wise, we need specific catalyst, size and DC source to apply potential/current for large scale electrochemical treatment method. The biological method requires enzymes, microorganisms etc. that are cost-effective. In microbial fuel cell-based water treatment, the cost of electrodes, binders, catalysts, membranes, electron collectors, gas diffusers, and reactors contribute to the production cost. Nowadays, BNCs are found to be cost-effective to make adsorbents, membranes, catalysts and enzyme mimicking materials. However, all those are initial investments. Hence, technically, the capital cost should be normalized with respect to surface area ($/m^2) or volume of wastewater used ($/m^3) or with treatment capacity ($/kg chemical oxygen demand) in addition to the initial investment [66].

4.7.3 Processing Treatment Cost—Spent Money Economy Impact

The metrics used to estimate the profit are net present value (NPV) and internal rate of return (IRR). The profit from a technology depends on the difference between the amount of cash inflow and the amount of cash outflows with respect to time which is known as NPV. For a successful methodology, the amount of cash inflow should be higher i.e., NPV should be positive. NPV can be calculated using the formula:

$$NPV = -A + \sum_{i=0}^{n} \frac{Q_i}{(1+k)^i} + \sum_{i=0}^{n} \frac{Q_i}{(1+k)^i (1+\lambda)^i} \tag{4.1}$$

where A—initial investment, Q—cash flow for a given period (in a year), k—discount rate, n—a lifetime of the plant, r_m—discount rate and λ—annual inflation (price increase per year).

IRR is the discount rate when NPV is zero. When IRR is higher than the minimum required return, then the investment can be done [S14].

$$0 = -A + \sum_{i=0}^{n} \frac{Q_i}{(1+IRR)^i} + \sum_{i=0}^{n} \frac{Q_i}{(1+k)^i (1+\lambda)^i} \tag{4.2}$$

4.7.4 The Production Cost of Biopolymers

Biopolymers are preferentially employed in water treatment with the aim of reducing the cost and it should be less toxic for treating water. Also, they can be discarded into the environment after use. However, the biopolymers should be derived from natural sources to be used as adsorbents. Also, several pretreatments and modification methods were reported in the literature for introducing functional groups, increasing the surface area and tuning the physical properties (such as biocompatibility, biodegradability, reusability etc.). [28, 89] Various chemicals belonging to both hazardous and non-hazardous types are used for the above-mentioned purpose. The cost of production will also increase depending upon the increase in the number of steps involved during the process and the number of chemicals used.

4.7.5 Environment Effect and Eco-Friendly

The effective water treatment method should not affect the environment i.e. there should not be secondary sludge formation. This is because the disposal of secondary

sludge again raises the disposal or treatment issues. Hence, different methods were developed to reuse the adsorbents and catalysts thereby reducing the solid waste generation. Also, biocompatible and biodegradable materials are used which can be degraded when it is discarded into the environment. Moreover, the disposal of nanomaterials is minimized by developing innovative technology for separating the nanomaterials. The separated materials can be reused. For example, magnetic nanomaterials can be removed from sludge by a simple magnetic separation method. In addition to the solid wastes, the soluble byproducts, released toxic gases and released nanomaterials decides the impact of treatment method on the environment [34, 40, 89]. Since, the carbon nanomaterials, CO_2 gas, nanoparticles and radicals disturb the eco-system and cause several diseases, monitoring the products formed and investigating their toxicity is also important. All those above parameters decide the water reuse potential. Basically, the water treatment is carried out based on two purposes (1) potable and (2) non-potable water. Potable water is used for drinking purposes while non-potable water is normally used for non-drinking purposes like washing, agriculture etc. [75]. The water recovery percentage of most of the reports using various purification techniques are in the range of 90–99%.

4.7.6 Health and Safety Risks

The health and safety of workers in the various stages are also important along with the developments in materials, technology and implementation. We need a gigantic infrastructure to treat a large amount of wastewater contains particularly solid wastes. For example, the wastewater treated using coagulation/flocculation methods requires water transport infrastructure, gigantic instruments etc. Additional to instruments, the few processes are dangerous and materials are toxic. To develop BNCs, the workers are exposed to nanomaterials in various stages of manufacturing and handling. Most of the nanomaterials and metal oxides are toxic. For example, TiO_2, ZnO, MgO, noble metal nanoparticles etc. are causing several diseases [26]. We all know that biopolymers are non-toxic. But the extraction methods are hazardous. For example, during the degumming of silk, there are chances for workers to expose to sericin proteins. The sericin protein (hydrophilic adhesive layer) is produced by silkworms. Various laboratory tests have revealed that sericin proteins are the main reason behind causing allergic reactions/infections in humans. Also, to improve the properties of biopolymers, different treatment methods are developed in which hazardous/toxic chemicals are used. Considering the safety and health issues regulatory guidelines need to be created and health should be monitored periodically.

4.8 Practical Snag of Wastewater-Treatment Method

Most of our technologies related to water treatment are at the laboratory level and there will be difficulties while scaling up the processes to the industrial level [9] The main problems are.

(1) nature of wastewater/Mixture of pollutants,
(2) Formation of secondary sludge/disposal,
(3) Long term stability and usage/Fouling of adsorbents and catalysts,
(4) Release of nanomaterials due to the variation in pH and temperature,
(5) Regeneration of adsorbents and catalysts,
(6) Cost of membrane/filters and materials used
(7) Variation in the degree of functional groups and properties of biopolymers,
(8) Long term availability of raw materials.

Different types of wastewater are available and hence, different methods are developed for purification. In addition to that, another issue is the real system where the wastewater contains a mixture of various organic and inorganic pollutants, solid particles, microorganisms. Hence, single adsorbents or catalysts cannot purify the whole system. Most of the treatments are adsorption based methods and many materials are reported in the literature as adsorbents. The sludge formation is also very high in chemical precipitation, chemical oxidation and coagulation/flocculation methods. The secondary sludge formed using BNCs can be disposed into the environment after use. However, the biocompatible and biodegradable nature of BNCs after use and the impact need to be investigated systematically. Further, the corrosive nature of the raw materials will not be a support for long term usage and it will add up expenses at later stages. Hence, highly stable materials are required. BNCs are found to be more effective, biocompatible, biodegradable, renewable and efficient. But, the nanoparticle released from BNCs when the pH of the wastewater is changed.

The regeneration of adsorbents/catalysts plays a major role in addition to their stability when the duration of usage is considered. Several treatment methods like thermal treatment, chemical treatment, supercritical extraction, and photocatalytic and biological degradation are followed to regenerate the used adsorbents. Each of these techniques has its limitations when practically implemented. The thermal treatment method reduces the efficiency of adsorption due to the shrinkage of the spent adsorbent on heating thereby reducing the surface area. High temperatures may alter the functionalities present in the catalysts [59]. The biological degradation method is less effective in the regeneration of catalysts [44]. Understanding the mechanism of adsorption (adsorption isotherm) is a mandate to identify the specific desorption method to regenerate adsorbents [14]. The adsorption mechanism of pollutants on BNCs are complex because adsorption of pollutants on BNCs follows both chemisorption and physisorption. Especially in the case of catalytic degradation followed by adsorption based treatment methods, the mechanism of removing pollutants from wastewater depends on both catalytic and adsorption processes.

While treating the wastewater chemically or photochemically, the possibilities of the formation of toxic and unknown products are the constraints for their practical use.

For example, the release of toxic gases during (photo)electrochemical degradation of dyes. For example, in the Fenton process, the hydroxyl radicals are produced and ferric ion is released into the water. In aerobic and anaerobic processes, the main final product is CO_2. The biological methods are less efficient to dyes, forms uncontrolled degradation products and advanced oxidation processes (AOP) is only at the laboratory scale and it will not be applicable to industries [10] Since the advanced oxidation process forms many radicals which again affect the environment and cause several diseases.

Among different parameters, the '*production cost*' is also important as described under sustainable criteria. The price of raw materials is another constraint for large scale production. The extraction of biopolymers and processing of biopolymers to form BNCs having different architecture such as forms, beads, membranes, gels, aerogels, hydrogels etc. for the effective adsorption of pollutants and durability of the components are other concerns during commercial use. Moreover in biopolymers based MFCs, till now the nafion membrane and platinum cathode were used which enhances the capital cost [30]. The coagulation/flotation method requires high initial capital cost because of large size infrastructure and also the cost of maintenance is also very high.

The source of biopolymers is renewable annually by developing their sustainable sources, so biopolymers can easily be renewable. But the biopolymers are extracted from different sources using different methods owing different properties such as molecular weight, crystallinity, affinity for water, number of functional groups etc. For example, the number of functional groups present on chitosan depends on the deacetylation degree of chitin. The properties of tannic acid depend on the number of phenol groups present in it which varies with the source material. The variation in properties will be reflected in the results. Hence, we should also consider the source and extraction method when selecting biopolymers. Finally, in the laboratory we utilize analytical reagent (A.R) grade chemicals which cannot be available for industrial (large-scale) use or using A.R. grade chemicals increase the cost [9, 66]. Nowadays the noble metal nanoparticles and carbon materials are used to make BNCs based adsorbents. Hence, research should be carried out to understand the toxic nature of these materials even at parts per billion levels.

4.9 Conclusions

In this chapter, we have discussed the types of biopolymers used for developing bionanocomposites, the application of bionanocomposites for wastewater treatment, the environment and the economic impact of the developed catalysts for real-time applications. However, in the actual scenario, the extraction methods, pretreatment procedures, variation in a number of functional groups, release/aggregation of nanomaterials in certain wastewater and the formation of secondary sludge acts as constraints for practical applications.

References

1. M. Alizadehgiashi, N. Khuu, A. Khabibullin et al., Nanocolloidal hydrogel for heavy metal scavenging. ACS Nano **12**, 8160–8168 (2018)
2. P.J.J. Alvarez, C.K. Chan, M. Elimelech et al., Emerging opportunities for nanotechnology to enhance water security. Nat. Nanotechnol. **13**, 634–641 (2018)
3. W.A. Arismendi, A.E. Ortiz-Ardila, C.V. Delgado et al., Modified tannins and their application in wastewater treatment. Water Sci. Technol. **78**, 1115–1128 (2018)
4. H. Bacelo, S. Santos, C. Botelho, Tannin-based biosorbents for environmental applications - A review. Chem. Eng. J. 303 (2016)
5. M.A. Barakat, New trends in removing heavy metals from industrial wastewater. Arab J. Chem. **4**, 361–377 (2011)
6. S. Biswas, J. Fatema, T. Debnath, T.U. Rashid, Chitosan-clay composites for wastewater treatment: a state-of-the-art review. ACS ES&T Water (2021). https://doi.org/10.1021/acsestwater.0c00207
7. X. Bui, C. Chiemchaisri, T. Fujioka, S. Varjani, Water and wastewater treatment technologies
8. N. Carrard, H. Neumeyer, B.K. Pati et al., Designing human rights for duty bearers: making the human rights to water and sanitation part of everyday practice at the local government level. Water 12 (2020)
9. L. Changes, E. Technology, Long-term changes in existing technology 101–106 (2018)
10. G. Crini, E. Lichtfouse, Advantages and disadvantages of techniques used for wastewater treatment. Environ. Chem. Lett. **17**, 145–155 (2019)
11. O.A. Dar, M.A. Malik, I. Ahmed, Bionanocomposites in water treatment 505–518 (2020)
12. A. De Rossi, C.V.T. Rigueto, A. Dettmer et al., Synthesis, characterization, and application of Saccharomyces cerevisiae/alginate composites beads for adsorption of heavy metals. J. Environ. Chem. Eng. **8**, 104009 (2020)
13. T. Deblonde, C. Cossu-Leguille, P. Hartemann, Emerging pollutants in wastewater: a review of the literature. Int. J. Hyg. Environ. Health **214**, 442–448 (2011)
14. S. Dileep, K. Seera, D. Kundu et al., Synthesis and characterization of xylan-gelatin cross-linked reusable hydrogel for the adsorption of methylene blue. Carbohydr. Polym. **256**, 117520 (2021)
15. M.W. Donner, M. Arshad, A. Ullah, T. Siddique, Unravelled keratin-derived biopolymers as novel biosorbents for the simultaneous removal of multiple trace metals from industrial wastewater. Sci. Total Environ. **647**, 1539–1546 (2019)
16. M.Á. Farrán, R.M. Claramunt, C. López et al., Structural characterization of alloxazine and substituted isoalloxazines: NMR and X-ray crystallography. ARKIVOC **2007**, 20–38 (2007)
17. Y. Ge, Z. Li, Application of lignin and its derivatives in adsorption of heavy metal ions in water: a review. ACS Sustain. Chem. Eng. **6**, 7181–7192 (2018)
18. A. Ghosh, S.R. Collie, Keratinous materials as novel absorbent systems for toxic pollutants **64**, 209–221 (2014)
19. J.J. Goddard, I. Ray, C. Balazs, Water affordability and human right to water implications in California. PLoS ONE **16**, 3–5 (2021)
20. P.M. Gore, M. Naebe, X. Wang, B. Kandasubramanian, Progress in silk materials for integrated water treatments: fabrication, modification and applications. Chem. Eng. J. **374**, 437–470 (2019)
21. M. Harguindeguy, C. Antonelli, M.-P. Belleville et al., Gelatin supports with immobilized laccase as sustainable biocatalysts for water treatment. J. Appl. Polym. Sci. **138**, 49669 (2021)
22. Z. Huang, S. Yin, J. Zhang, N. Zhang, Recent advances in membrane hydrophilic modification with plant polyphenol-inspired coatings for enhanced oily emulsion separation. J. Appl. Polym. Sci. **138**, 1–22 (2021)
23. E. Jabeen, N.K. Janjua, S. Ahmed, Removal of metal ions using metal-flavonoid-DNA adduct protocol. J. Saudi Chem. Soc. **23**, 118–126 (2019)
24. A. Jamshaid, A. Hamid, N. Muhammad et al., Cellulose-based materials for the removal of heavy metals from wastewater – an overview. ChemBioEng. Rev. **4**, 240–256 (2017)

25. C. Jiao, T. Li, J. Wang et al., Efficient removal of dyes from aqueous solution by a porous sodium alginate/gelatin/graphene oxide triple-network composite aerogel. J. Polym. Environ. **28**, 1492–1502 (2020)
26. M. Kamali, K.M. Persson, M. Elisabete, I. Capela, Sustainability criteria for assessing nanotechnology applicability in industrial wastewater treatment: current status and future outlook. Environ. Int. **125**, 261–276 (2019)
27. V.U. Kavitha, B. Kandasubramanian, Tannins for wastewater treatment. SN Appl. Sci. 2 (2020)
28. E. Khademian, E. Salehi, H. Sanaeepur et al., Science of the total environment a systematic review on carbohydrate biopolymers for adsorptive remediation of copper ions from aqueous environments-part A: classification and modi fi cation strategies. Sci. Total Environ. **738**, 139829 (2020)
29. A. Koopmann, C. Schuster, J. Torresrodr, Tannin-based hybrid materials and their 1–32
30. T. Krieg, A. Sydow, U. Schröder et al., Reactor concepts for bioelectrochemical syntheses and energy conversion. Trends Biotechnol. **32**, 645–655 (2014)
31. H.W. Kwak, M. Shin, H. Yun, K.H. Lee, Preparation of silk sericin/lignin blend beads for the removal of hexavalent chromium ions. Int. J. Mol. Sci. 17 (2016)
32. E.F. Lessa, A.L. Medina, A.S. Ribeiro, A.R. Fajardo, Removal of multi-metals from water using reusable pectin/cellulose microfibers composite beads. Arab J. Chem. **13**, 709–720 (2020)
33. B. Li, F. Zhou, K. Huang et al., Environmentally friendly chitosan/PEI-grafted magnetic gelatin for the highly effective removal of heavy metals from drinking water. Sci. Rep. **7**, 43082 (2017)
34. B. Liu, S. Zhang, C.-C. Chang, Emerging pollutants—part II: treatment. Water Environ. Res. **91**, 1390–1401 (2019)
35. C. Liu, P. Luan, Q. Li et al., Biopolymers derived from trees as sustainable multifunctional materials: a review 2001654, 1–27 (2020)
36. P. Makvandi, S. Iftekhar, F. Pizzetti et al., Functionalization of polymers and nanomaterials for water treatment, food packaging, textile and biomedical applications: a review 583–611 (2021)
37. P. Makvandi, S. Iftekhar, F. Pizzetti et al., Functionalization of polymers and nanomaterials for water treatment, food packaging, textile and biomedical applications: a review. Environ. Chem. Lett. **19**, 583–611 (2021)
38. A. Mautner, Nanocellulose water treatment membranes and fi lters: a review (2020a). https://doi.org/10.1002/pi.5993
39. A. Mautner, Nanocellulose water treatment membranes and filters: a review. Polym. Int. **69**, 741–751 (2020)
40. E. Methods, Advanced water treatment electrochemical methods
41. N. Mohammed, A. Baidya, V. Murugesan et al., Diffusion-controlled simultaneous sensing and scavenging of heavy metal ions in water using atomically precise cluster − cellulose nanocrystal composites (2016). https://doi.org/10.1021/acssuschemeng.6b01674
42. T.C. Mokhena, V. Jacobs, A.S. Luyt, A review on electrospun bio-based polymers for water treatment. Express Polym. Lett. **9**, 839–880 (2015)
43. T.C. Mokhena, V. Jacobs, A.S. Luyt, A review on electrospun bio-based polymers for water treatment
44. S.M. Momina, S. Isamil, Regeneration performance of clay-based adsorbents for the removal of industrial dyes: a review. RSC Adv. **8**, 24571–24587 (2018)
45. A. Nasar, Chitosan-based adsorbents for wastewater treatment. Mater. Res. Forum LLC (2018)
46. A. Naseer, A. Jamshaid, A. Hamid et al., Lignin and lignin based materials for the removal of heavy metals from waste water-an overview. Zeitschrift für Phys. Chemie **233**, 315–345 (2019)
47. M. Nasrollahzadeh, M. Sajjadi, S. Iravani, R.S. Varma, Materials for sustainable water treatment: a review. Carbohydr. Polym. **251**, 116986 (2021)
48. M. Nasrollahzadeh, M. Sajjadi, S. Iravani, R.S. Varma, Starch, cellulose, pectin, gum, alginate, chitin and chitosan derived (nano)materials for sustainable water treatment: a review. Carbohydr. Polym. **251**, 116986 (2021)
49. M. Naushad, G. Sharma, Z.A. Alothman, Photodegradation of toxic dye using Gum Arabic-crosslinked- poly (acrylamide)/ Ni (OH) 2 / FeOOH nanocomposites hydrogel. J. Clean Prod. **241**, 118263 (2019)

50. R.E. Neisiany, M.S. Enayati, A. Kazemi-Beydokhti et al., Multilayered bio-based electrospun membranes: a potential porous media for filtration applications. Front. Mater. **7**, 67 (2020)
51. T.-D. Ngo, Biobased and Biodegradable Polymers Nanocomposites BT - Handbook of Nanomaterials and Nanocomposites for Energy and Environmental Applications, in *Kharissova OV*. ed. by L.M.T. Martínez, B.I. Kharisov (Springer International Publishing, Cham, 2020), pp. 1–28
52. R. Nistico, F. Franzoso, F. Cesano et al., Chitosan-derived iron oxide systems for magnetically guided and efficient water purification processes from polycyclic aromatic hydrocarbons (2017). https://doi.org/10.1021/acssuschemeng.6b02126
53. N.A. Oladoja, E.I. Unuabonah, O.S. Amuda, O.M. Kolawole, Polysaccharides as a green and sustainable resources for water and wastewater treatment (2017)
54. W.W. Overview, Lignin and lignin based materials for the removal of heavy metals from lignin and lignin based materials for the removal of heavy metals from waste water-an overview (2018). https://doi.org/10.1515/zpch-2018-1209
55. R.C. Palmer, D. Short, W.E.T. Auch, The human right to water and unconventional energy. Int. J. Environ. Res. Public Health 15 (2018)
56. E. Papadopoulos, G. Arsenos, S. Ptochos et al., Pollutants in wastewater effluents impacts. J. Hell. Vet. Med. Soc. **65**, 115–120 (2014)
57. S. Pirsa, F. Asadzadeh, I.K. Sani, Synthesis of magnetic gluten / pectin / Fe 3 O 4 nano - hydrogel and its use to reduce environmental pollutants from Lake Urmia sediments. J. Inorg. Organomet. Polym. Mater. **30**, 3188–3198 (2020)
58. R. Reddy, G. Shimoga, T. June, S. Lee, Fabrication of multifunctional Guar gum-silver nanocomposite hydrogels for biomedical and environmental applications. Int. J. Biol. Macromol. **159**, 474–486 (2020)
59. D.H.K. Reddy, K. Vijayaraghavan, J.A. Kim, Y.S. Yun (2017) Valorisation of post-sorption materials: opportunities, strategies, and challenges **242**, 35–58 (2017)
60. J. Ren, Q. Dai, H. Zhong et al., Quaternized xylan/cellulose nanocrystal reinforced magnetic hydrogels with high strength. Cellulose **25**, 4537–4549 (2018)
61. C.V.T. Rigueto, M.T. Nazari, L.Á. Massuda et al., Production and environmental applications of gelatin-based composite adsorbents for contaminants removal: a review. Environ. Chem. Lett. (2021). https://doi.org/10.1007/s10311-021-01184-0
62. S. Saha, M. Zubair, M.A. Khosa et al., Keratin and chitosan biosorbents for wastewater treatment: a review. J. Polym. Environ. **27**, 1389–1403 (2019)
63. H. Sakai, S. Matsuoka, A.A. Zinchenko, S. Murata, Removal of heavy metal ions from aqueous solutions by complexation with DNA and precipitation with cationic surfactant. Colloids Surfaces A Physicochem. Eng. Asp. **347**, 210–214 (2009)
64. H. Sakai, S. Matsuoka, A.A. Zinchenko, S. Murata, Colloids and surfaces a : physicochemical and engineering aspects removal of heavy metal ions from aqueous solutions by complexation with DNA and precipitation with cationic surfactant **347**, 210–214 (2009)
65. S.C.R. Santos, H.A.M. Bacelo, R.A.R. Boaventura, C.M.S. Botelho, tannin-adsorbents for water decontamination and for the recovery of critical metals : current state and future perspectives **1900060**, 1–12 (2019)
66. E. Science, Y. Zhang, I. Angelidaki, Microbial electrochemical systems and technologies: it is time to report the capital costs (2016). https://doi.org/10.1021/acs.est.6b01601
67. G. Sharma, A. Kumar, C. Chauhan et al., Pectin-crosslinked-guar gum/SPION nanocomposite hydrogel for adsorption of m-cresol and o-chlorophenol. Sustain. Chem. Pharm. **6**, 96–106 (2017)
68. V. Sharma, T. Shahnaz, S. Subbiah, S. Narayanasamy, New insights into the remediation of water pollutants using nanobentonite incorporated nanocellulose chitosan based aerogel. J. Polym. Environ. **28**, 2008–2019 (2020)
69. J. Shojaeiarani, D. Bajwa, A. Shirzadifar, A review on cellulose nanocrystals as promising biocompounds for the synthesis of nanocomposite hydrogels. Carbohydr. Polym. **216**, 247–259 (2019)

70. G. Singh, D. Sharma, T. Stenström, Bio-nanocomposites in water and wastewater treatment 329–353 (2018)
71. P. Sirajudheen, P. Karthikeyan, K. Ramkumar, S. Meenakshi, International journal of biological macromolecules environment responsive Al 3 + networked chitosan-gelatin spherical beads for the effective removal of organic pollutants from aqueous solutions. Int. J. Biol. Macromol. **164**, 3055–3064 (2020)
72. Z. Su, W. Yu, T. Liu et al., Discovery of welcome biopolymers in surface water: improvements in drinking water production (2021)
73. X. Sun, X. Huang, X. Liao, B. Shi, Adsorptive removal of Cu(II) from aqueous solutions using collagen-tannin resin. J. Hazard. Mater. **186**, 1058–1063 (2011)
74. T. Lancet, Water and sanitation: the neglected health MDG. Lancet **368**, 1212 (2006)
75. C. Tortajada, Contributions of recycled wastewater to clean water and sanitation sustainable development goals. NPJ. Clean. Water **3**, 22 (2020). https://doi.org/10.1038/s41545-020-0069-3
76. W. Treatment, A. Aldalbahi, M. El-naggar et al., Development of green and sustainable cellulose acetate / graphene oxide nanocomposite films as 1–16 (2020)
77. C. Vinicus, T. Rigueto, M. Torres et al., Production and environmental applications of gelatin - based composite adsorbents for contaminants removal: a review. Environ. Chem. Lett. (2021). https://doi.org/10.1007/s10311-021-01184-0
78. S. Van Vlierberghe, P. Dubruel, E. Schacht, Biopolymer-based hydrogels as scaffolds for tissue engineering applications: a review 1387–1408 (2011)
79. N. Wahab, M. Saeed, M. Ibrahim et al., Synthesis, characterization, and applications of silk/bentonite clay composite for heavy metal removal from aqueous solution. Front. Chem. **7**, 654 (2019)
80. N. Wahab, M. Saeed, M. Ibrahim et al., Synthesis, characterization, and applications of silk/bentonite clay composite for heavy metal removal from aqueous solution. Front. Chem. **7**, 1–12 (2019)
81. N. Wahlström, S. Steinhagen, G. Toth et al., Ulvan dialdehyde-gelatin hydrogels for removal of heavy metals and methylene blue from aqueous solution. Carbohydr. Polym. **249**, 116841 (2020)
82. W.S. Wan Ngah, M.A.K.M. Hanafiah, Removal of heavy metal ions from wastewater by chemically modified plant wastes as adsorbents: a review. Bioresour. Technol. **99**, 3935–3948 (2008)
83. S. Wang, H. Ning, N. Hu et al., Preparation and characterization of graphene oxide/silk fibroin hybrid aerogel for dye and heavy metal adsorption. Compos. Part B Eng. **163**, 716–722 (2019)
84. Q. Wu, W. Shao, Y. Zhang et al., Use of lignin-based carbons for decolorization of wastewater dyes **15**, 105–116 (2020)
85. R. Xiong, A.M. Grant, R. Ma et al., Naturally-derived biopolymer nanocomposites: interfacial design , properties and emerging applications **125**, 1–41 (2018)
86. M. Yamada, K. Kato, M. Nomizu et al., UV-irradiated DNA matrix selectively accumulates heavy metal ions. Bull. Chem. Soc. Jpn. **75**, 1627–1632 (2002)
87. M. Yamada, K. Kato, M. Nomizu et al., UV-Irradiated DNA matrixes selectively bind endocrine disruptors with a planar structure. Environ. Sci. Technol. **36**, 949–954 (2002)
88. N. Zhang, R. Long, C. Gao, Y. Xiong, Recent progress on advanced design for photoelectrochemical reduction of CO_2 to fuels. Sci. China Mater. **61**, 771–805 (2018)
89. Z. Zia, A. Hartland, M.R. Mucalo, Use of low-cost biopolymers and biopolymeric composite systems for heavy metal removal from water. Int. J. Environ. Sci. Technol. **17**, 4389–4406 (2020)
90. S. Żółtowska-Aksamitowska, P. Bartczak, J. Zembrzuska, T. Jesionowski, Removal of hazardous non-steroidal anti-inflammatory drugs from aqueous solutions by biosorbent based on chitin and lignin. Sci. Total Environ. **612**, 1223–1233 (2018)
91. M. Zubair, M. Arshad, Chitosan-based materials for water and wastewater treatment (Elsevier, 2020), pp. 773–809. https://doi.org/10.1016/B978-0-12-817966-6.00025-X

Chapter 5
Electrospun Nanofiber-Based Composites for Arsenic Removal in Water and Wastewater

Phillemon Matabola, Keneiloe Sikhwivhilu, and Odwa Mapazi

Abstract The growing concern for ground and surface water contamination by arsenic metal has become a serious plight, for it has reportedly affected more than 100 million people worldwide. The increase in the prevalence of arsenic in the environment is reported due to the swift growth of industrial and agricultural activities, leading to the contamination of water resources. Sadly, exposure to environmental arsenic has been known to lead to biological ecosystem disruption in aquatic environments and cancer and death in humans. As a result, various technologies have been developed for arsenic removal, including precipitation, membrane processes, ion exchange, and adsorption. Among these methods, adsorption stands out owing to its high removal efficiency, easy operation, low cost, and absence of toxic sludge. The sorbent materials prepared from electrospun nanofibers have come to the forefront of arsenic uptake on account of the outstanding traits such as high specific surface area; which leads to increased sorption capacity, porosity, reusability, environmental friendliness, flexibility to surface functionalization and potential to conform to a wide range of physical and chemical conditions. This chapter provides an insight into the latest development of nanofiber-based composites as adsorbents for arsenic removal in water.

5.1 Introduction and Background

Water is the most treasured possession in life. Hegel described it in his famous book (philosophy of nature) by saying: "*Water is the element of selfless contrast, it passively exists for others, water's existence is, therefore, an existing for others, its*

P. Matabola (✉) · K. Sikhwivhilu
Advanced Materials Division, DSI/Mintek Nanotechnology Innovation Centre, Mintek, Randburg, Private Bag X3015, Johannesburg 2125, South Africa
e-mail: philemonm@mintek.co.za

O. Mapazi
Analytical Services Division, Mintek, Randburg, Private Bag X3015, Johannesburg 2125, South Africa

M. J. Hato and S. Sinha Ray (eds.), *Functional Polymer Nanocomposites for Wastewater Treatment*, Springer Series in Materials Science 323,
https://doi.org/10.1007/978-3-030-94995-2_5

fate is to be something not yet specialized and thus it soon came to be called the mother of all that special" [10]. Water is a resource of great importance for people and the environment, considering that it is pivotal for everything on our planet to grow and prosper. It covers over 70% of the earth surface and makes up 65% of human bodies. Therefore, it is the most invaluable natural resource on the planet as, without this precious commodity, life on earth would be mythical [12].

Reliable access to clean and low-priced water is deemed one of the basic humanitarian goals and remains a major global challenge for the 21 century [86]. However, globally, water resources are found to be severe risks of over exploitation. This is as a result of the world facing unprecedented adversity of meeting demands for unpolluted water. The accomplishment of the demand is compounded by the deteriorating available supplies of freshwater primarily due to increased population growth, extended droughts, extensive industrialization, improper disposal, and man's undesirable practices. These often affect drinking water, rivers, lakes, and oceans all over the world. This, as a result, compromises human health, the natural environment, and even the global economy.

Among the leading environmental issues of the twenty-first century is the handling of wastewater, particularly because it has a high potential of eventually contaminating the fresh water bodies. All the pollutants present in wastewater are regarded as a serious environmental problem for they affect the quality of drinking water and hence human health. The studies have shown that the major pollutants in raw wastewater streams emanate from intensive anthropogenic activities such as mining, agriculture, and disposal of industrial waste materials [2, 67, 94, 100]. For instance, the mining industries, albeit serving as one of the driving forces of many countries' economies, dump billions of tons of hazardous materials into the environment. As a consequence, the emissions of such pollutants into the air and water are gravely considered as primary factors to the common respiratory, neural and intestinal diseases. To that end, a safe and healthy environment turns out to be a priority that needs immediate intervention in both developing and well-developed countries [16, 76].

The above-mentioned serious concerns call upon novel and effective technologies to address the current environmental issues either by protecting the environment and current water sources or by producing high-quality water from available sources (ocean and wastewater) without harmful by-products. Several different methods have been reported to have the efficacy to remove heavy metals from wastewater. However, they have been found to be inefficient in many ways. That being so, a need to develop an efficient and low-cost technique for the removal of arsenic from contaminated water turned out to be consequential. In this regard, the nanofibers adsorbents were found to be more efficient and suitable in terms of technical and economic feasibility and environmental importance. In recent years, the production of nanofibers has gained a lot more attrition to develop innovative materials with properties that are appropriate to address the challenges related to water treatment.

5.2 Environmental Contamination by Heavy Metals

The pollution of the environment by different pollutants is one of the fundamental issues in human society.

These pollutants are simply described as naturally occurring compounds or foreign matter. When they come into contact with the environment, they bring about dire changes. The literature has indicated that these pollutants exist in different forms, namely, inorganic, organic, and biological. Notwithstanding pollutants falling under different categories, they all bag a great deal of attention due to their impacts on the environment. Inorganic pollutants are metals, salts, acids, and bases [120]. Further, studies have reported that inorganic pollutants as materials found naturally but have been altered by human production to increase their number in the environment [96].

In the group of inorganic pollutants, heavy metals have gained overriding interest to environmental scientists due to their persistence in the environment and toxic nature. They are a part of an ill-defined subset of elements that display metallic properties. These include the transition metals, some metalloids, lanthanides, and actinides. Elements of greatest worry include arsenic, cadmium, cobalt, chromium, copper, mercury, manganese, nickel, lead, tin, and thallium, which are persistent in all parts of the environment. Generally, these metals have densities above 5 g/cm^3, cannot be degraded or destroyed, and have a relative atomic mass of 40 [40].

Fifty three of the ninety naturally occurring elements are heavy metals [118]. Of these, Fe, Mo, and Mn are important as micronutrients, while Zn, Ni, Cu, Co, Va, and Cr are toxic elements but have importance as trace elements. On the other hand, Ag, As, Hg, Cd, and Pb do not have known function as nutrients and seem to be toxic to plants and microorganisms [40, 131]. Heavy metals come from both natural and anthropogenic processes and land in different environmental compartments such as soil, water, air, and their interface. Increasing amounts of heavy metals can account for soil quality degradation, contributing to crop yield reduction, poor quality of agricultural products, posing far-reaching threats to human, animal, and ecosystem health.

5.3 Arsenic Metal

Amongst the heavy metals alluded to, arsenic is characterized as one of the harmful pollutants precisely due to its toxicity, bio accumulating tendency, and threat to human life and environment [37, 53, 101, 119]. It is the twentieth most abundant element in the earth's crust [69] and the forty-seventh most abundant element on earth among the eighty-eight existing elements [66]. It is a metalloid in the constitution of more than 245 minerals [106].

Arsenic has three allotropic forms, namely, grey, black, and yellow. Arsenic and its associated compounds are often used as pesticides and herbicides. This element can flow through arsenic-containing rocks or get into water through the dissolution of

mineral rocks in areas with weathered rocks. Arsenic is also emitted via fossil fuels combustion. Commercially, arsenic is used in alloys and wood preservatives. Also, this element is achieved by heating minerals containing arsenic and re-crystallization of vapors of its sublimation and industrially; it is achieved as an additional product of metal production centers.

Arsenic is traditionally found in a slight quantity on earth. It is in soil and mineral materials, and it gets into air or water through dust or runoff. It is difficult to convert arsenic into liquid or gas states. The metal is mobile naturally, and it is rarely found in one place; this is a good point, but arsenic pollution mostly occurs due to its easy emission. Due to anthropogenic activities such as mining, arsenic can be mobile in most regions. Arsenic cycles are extensive due to anthropogenic activities, and arsenic is found less in the environment and nature. Copper producing industries mostly emit arsenic, but it is also distributed in the lead, zinc production, and agricultural activities. If arsenic gets into the environment, it will not be decomposed, and it gets emitted and causes diseases for humans and animals [106].

Arsenic exists in four valency states, including -3, 0, $+$ 3, and $+$ 5. The elemental state -3 and 0 are extremely rare, whereas $+3$ and $+$ 5 oxidation states are commonly found in groundwater systems, depending on the prevailing redox conditions. Arsenite (As(III)) is dominant under a moderately reducing anaerobic environment, while Arsenate (As(V)) exists in water with abundant dissolved oxygen levels [132, 133]. Arsenite is 25–60 times more toxic than arsenate [61]. Nevertheless, it has been found at 100–200 g/L in groundwater in several countries, notably in Asia, America, Europe, Africa, and the Pacific [132]. Arsenic contamination in drinking water has become a major concern in many regions around the world and has affected more than 100 million people worldwide [87]. Arsenic poisoning of groundwater was first reported in Taiwan in 1968 [77]. It is estimated that there were 19.6 million people at risk of being affected by the consumption of arsenic-contaminated groundwater in China [91]. People drinking arsenic-impacted water greater than 0.05 mg/L are prone to increased risk of lung, bladder cancer, and arsenic-associated skin lesions, as well as other effects such as loss of appetite, muscular weakness, pigmentation changes, and nausea [19]. To minimize the health problems associated with arsenic in water, the World Health Organization (WHO) recommends a strict permissible limit of 10 μg/L as the maximum arsenic contaminant level in drinking water [58].

5.4 Methods for the Removal of Arsenic

As the environmental pollution resulting from discharging wastewater consisting of high concentrations of heavy metals is becoming a pressing issue worldwide, the interest to lower these increased concentrations to below permissible discharge limits has garnered a lot of attention. Accordingly, the development of effective and sustainable purification methods for arsenic removal from water became a matter of

great importance and profound societal value. Nonetheless, in light of the low socio-economic status of the major affected countries, they cannot afford expensive and large-scale treatments to remove arsenic from drinking water to the acceptable levels (10 ppb, as recommended by WHO and US Environmental Protection Agency). Therefore, the development of facile and cost-effective methods, which are easy to handle and can be applied at household and community levels to remediation of arsenic from contaminated groundwater, is of utmost importance.

In consideration of the societal value and critical importance, traditional and different emerging technologies based on chemical, biochemical/biological/biosorption, and physico-chemical treatment processes for arsenic removal from contaminated drinking water have been developed and applied [48]. Many sustainable and naturally abundant materials including waste rice husk [9], iron-based adsorbents such as iron oxy-hydroxides including akaganeite (β-FeOOH), goethite (α-FeOOH), lepidocrocite (ϒ-FeOOH), ferrihydrites ($Fe_{10}O_{14}(OH)_2$), iron-based layered double hydroxides (LDHs), iron oxy-hydroxides doped activated carbon, and iron oxy-hydroxides doped graphene oxide [47, 105], and activated carbon [21] have been examined as efficient adsorbents for arsenic removal. Lately, some novel materials including cellulose-based fibers [25, 102], metal organic framework (MOF), and hydrogel [68], have also been examined. Several of these arsenic removal materials and techniques have also been implemented practically in the affected rural areas. However, most of these methods are unsatisfactory owing to different grounds such as incomplete metal removal (poor efficiency), high reagent and energy requirements, and large quantities of wastes. Furthermore, the type of waste generated is usually toxic and therefore difficult to dispose of. Moreover, other concerns of these processes are largely linked to costs, both initial and operational, as the arsenic problem is mainly in developing or underdeveloped countries and areas. Amongst all these methods, there are some conventional techniques that have been widely applied for arsenic ions removal with some form of merits and demerits.

5.4.1 Conventional Methods

In recent years, conventional methods commonly known as physicochemical methods have been developed for arsenic removal. These are oxidation, precipitation, ion exchange, separation (membrane processes like reverse osmosis, nanofiltration, and electrodialysis), and adsorption [14, 57, 64]. These methods are well recognized for large to medium-scale water treatment plants [28, 65, 88]. These chemical processes can be used individually, sequentially, or in combination for effective As(V) removal [65]. However, As(III) species are poorly removed and require a chemical or physical pre-treatment oxidation to convert it to As(V) for efficient removal [64]. Speciation of arsenic controls its interaction and removal with different environmental materials [22, 57].

Similarly, the presence of different cations, anions, and organic matter affects arsenic removal. These effects grow manyfold at higher concentrations. In Latin

America (LA), many regions are contaminated with additional contaminants along with arsenic. For example, arsenic removal from Argentinian groundwater is complicated due to elevated levels of fluoride and silica. Thus, assessment of different contaminants before treatment technique selection becomes necessary. The advantages and disadvantages of various physico-chemical methods used for arsenic removal are given in Table 5.1. Subsequently, the methods were described briefly in the sections that follow.

5.4.1.1 Adsorption

Adsorption is deemed an efficient and economically practicable method as opposed to other arsenic removal methods [20]. Its efficiency is seen mostly in developing countries faced with unreliable electricity supply and a lack of skilled personnel [22]. Adsorbents with quantitative efficiencies (N95%) are reported for As(III) and As(V) [83]. The adsorption does not generally require chemical addition, as in the case with other techniques [88]. A huge number of adsorbents have been developed and assessed around the world [7, 14] for the removal of arsenic. However, large-scale implementation of these adsorbents is still lacking for this application.

5.4.1.2 Coagulation

Coagulation is a simple method known for treating large volumes of arsenic contaminated water [64]. In this method, the colloidal particles are destabilized by coagulants by particle charge neutralization, causing them to be aggregate, followed by precipitation. During the coagulation-precipitation process, soluble arsenic species are transformed into flocs by the coagulants and can simply be removed by filtration [99]. These processes combine coagulation, adsorption, and sedimentation [108, 25], employing inexpensive chemicals and low installation costs. In consequence, coagulation and filtration have huge application potential for low-cost economies. For the removal of arsenic, arsenite is converted into arsenate, succeeded by its removal via adsorption onto coagulated flocs, and then by filtration [59]. Salts such as $Al_2(SO_4)_3$, $FeCl_3$, and $FeSO_4$ have frequently used coagulants. Among them, ferric chloride is a rather more preferable coagulant since it generates somewhat large flocs [34, 50, 83, 90]. However, the shortcoming of this method is the production of arsenic-containing sludge, which may act as a potential source of arsenic contamination. At present, coagulation technology successfully reduced arsenic from 400 to 10 μg/L under-regulated pH, coagulants, and oxidizing agents with an approximate cost of 2.3 US¢/L of water. It became apparent that the composition of the arsenic-impacted water is the major factor when selecting a specific arsenic removal process [4].

Table 5.1 Advantages and disadvantages of various arsenic removal technologies. Reproduced with permission from [104]. This article has been published under Creative Commons by Attribution (CC-BY) license

Arsenic Removal Technology	Advantages	Disadvantages	Removal Efficiency As $^{(v)}$ (%)
Oxidation	• Low operation cost • Works over a wide pH range	• Very slow process • Drinking water has a bad smell and color in addition to chlorine, permanganate, etc • Sludge formation	>95
Coagulation	• It can be operated within a wide range of pH	• Pre-oxidation ofarsenite required • High arsenic contaminatedsludge production • Expensive process • Additional filtration is required	>90
Adsorption	• Low cost • Ease of operation	• pH, effective surface area and the nature of the adsorbent need to be maintained • Arsenite cannot be removed very well • Post-filtration required • Organic matter, other salts in water decreases the efficiency of the process • Removal of the generated heavy flocs is difficult	100
Ion Exchange Process	• pH-independent process	• Only efficient for arsenite removal • Expensive process • Low capacity • Sludge disposal problem • Resin needs to be replaced again and again	95
Electrocoagulation	• Sustainable technology • Less area requirement	• Sludge production • High investment cost • High energy consumption	>99
Membrane Filtration	• Easy operational technique • High arsenate removal efficiency • No sludge production	• Membrane fouling • High investment cost	>99

5.4.1.3 Oxidation

Arsenic in natural waters, by and large, occurs as arsenite [As(III)] and arsenate [As(V)]. As(III) is more soluble, mobile, and toxic as compared to As(V). As a result, As(III) removal is more challenging than As(V). In light of this, As(III) must be oxidized to As(V) prior to its removal [18]. Thus, it is important amid the arsenic removal process to understand As(III) oxidation and its kinetics in the presence of different oxidants [55]. It was found that the arsenic oxidation in the presence of air or pure oxygen is slow and can be enhanced by using ozone, chlorine, chlorine dioxide, hypochlorite, and H_2O_2 [18].

5.4.1.4 Chemical Oxidation

Chemicals such as Cl_2 (g), ClO^-, O_3, MnO^{-4}, H_2O_2, MnO_2, and H_2O_2/Fe^{2+} (Fenton's reagent) are used to enhance the oxidation kinetics of As(III) [1, 64, 83]. Chlorine shows fast As(III) oxidation kinetics, but on reacting with organic matter it also forms trihalomethanes, which can be awful and some are known carcinogens. Accordingly, potassium permanganate (KMnO4) can be selected as an alternative for chlorine, capitalizing on its wide availability, non-reactivity with filtration membranes, and no formation of disinfection by-products [57, 65].

5.4.1.5 Advanced Oxidation Processes (AOPs)

Advanced oxidation processes (AOPs) generate highly reactive species, including $HO^{\bullet}$, $HO^{\bullet 2}$, and O^{-2} radicals in the aqueous phase. These radicals are produced using chemical oxidants such as H_2O_2, O_3 combined with catalysts or radiation (γ rays or UV irradiation) [82]. The high reactivity of these free radicals makes AOPs suitable for oxidizing many inorganic and organic pollutants, including As(III). AOPs include UV/H_2O_2, O_3/UV, O_3/H_2O_2, Fe^{2+}/H_2O_2, photo-Fenton oxidation, and heterogeneous photocatalysis [82]. AOPs such as heterogeneous photocatalysis can be easily applied in rural and low-income communities [30, 31, 38]. In heterogeneous photocatalysis, aqueous As(III) is oxidized using a semiconductor-like titanium dioxide (TiO_2) as the catalyst [8, 38, 63, 65]. The latter is a widely used photocatalyst owing to its low cost, chemical stability, and outstanding electronic and optical properties. Arsenic-impacted water samples in contact with TiO_2 are exposed to UV light (solar or lamp sources) followed by iron (ferrous) addition to achieving arsenic concentrations below an acceptable level.

5.4.1.6 Ion Exchange

It is a reversible chemical reaction wherein an ion from wastewater solution is exchanged for a similarly charged ion attached to an immobile solid particle. These

solid ion exchange particles are either naturally occurring inorganic zeolites or synthetically produced organic resins [2]. The resins have been successfully used for arsenic remediation in drinking water. Tailored anion exchangers are available, which can reduce the arsenic concentration to < 10 μg/L [63]. Synthetic ion exchange resins normally have quaternary ammonium groups and a polystyrene cross-linked divinylbenzene (polymeric matrix). These resins are particularly efficient for As(V) adsorption. As(V) uptake does not depend on pH and influent concentration. Oxidation is required for As(III) removal via ion exchange resins because neutral H_3AsO_3 is present, and H_2AsO^{-3} is only available at pH > 8 (Fig. 5.2) [83, 90]. The resin surface is loaded with chloride ions via HCl pre-treatment. Chloride ions are easily exchanged by As(III) or As(V) or anions such as $SO_2{}^{-4}$, F^-, and NO^{-3}. Arsenic concentration in water along with the ion-exchange resin type and competing ions, are important factors affecting arsenic removal [99]. High sulfate and total dissolved solids interfere in the process [117]. Ion exchange columns may also be clogged due to suspended solids and iron precipitates [59, 83, 119].

5.4.1.7 Membrane Filtration

Low-pressure (0.069–0.207 MPa) membrane microfiltration or ultrafiltration, high-pressure (0.517–1.72 MPa) membrane nanofiltration and reverse osmosis (RO), or even higher pressure (N1.724 MPa) membranes processes have been probed for aqueous arsenic removal [66, 83, 90]. RO uses pressure to pass water but not solutes through a semipermeable membrane [65]. The micropores allow only water molecules to pass and retain polyvalent ions, including arsenic oxyanions. RO works efficiently in the pH range of 3–11 [65]. For municipal systems or larger scale water remediation applications, multiple membrane units may be connected in series [83]. Low pressure membrane processes, including ultrafiltration or microfiltration are not suitable for arsenic remediation because of the small size of arsenic species that can easily pass the membranes [65, 83] unless pre-treatment with suitable coagulants is implemented prior to membrane filtration. RO is the most suitable option for high salinity water treatment [28]. RO effectively removed As(V), but As(III) removal can only be achieved at pH > 9.0, when As(III) exists as a weak acidic (Fig. 5.2) [80]. This is due to the fact that the neutral form of As(III) cannot be repelled by ionic RO membranes [80]. However, to achieve high removal, As(III oxidation is difficult due to possible membrane damage by residual oxidants [65]. Water hardness, humic acids, organic matter, suspended solids, dissolved solids, and methane interfere with membrane processes. Drinking water's chemical composition is altered when ions other than arsenic are simultaneously eliminated [66]. RO works better in the presence of nitrate and fluoride salt contaminants [64]. However, >70 mg/L silica concentrations can damage the RO membranes. In general, RO efficiently removes arsenic (92%) and fluoride (85–95%) from drinking water [4, 36, 83]. The only limitation with RO is that the safe management of the resultant brine is required in the absence of provisions to treat or dispose of it safely [4, 65]. This increases water treatment costs with RO technology [4, 83].

5.4.1.8 Electrocoagulation

Electrocoagulation is a novel method for arsenic removal with a lot of advantages. It lowers sludge volume; it is quite compact with the trouble-free operation even with high flow rates and has no extra chemicals requirements [97]. The technology utilizes iron and aluminum anodes, which are consumed during the process [97], and is very efficient for both arsenic and fluoride removal.

In electrocoagulation, the coagulant is generated in-situ as electrolytic oxidation of the anode occurs [114]. This process provides improved As(III) removal versus ferric coagulation [46, 114]. Through electrocoagulation, 100 mg/L As(V) was reduced to <2.0 mg/L with a residence time of ~9 min, "current density = 1.2 A/dm^2, liquid flow = 3 L/h., DC current reversed each 2 min [46]". Various articles have reported an arsenic reduction in Latin American groundwater and well water from an initial level of 134 μg/L [5], 50 μg/L [97], 43 μg/L [44], to concentrations well below 10 μg/L. Successful containment of arsenic (As = 106 μg/L) along with fluoride and hydrated silica was achieved from groundwater in a 12 cell electrocoagulation unit [92]. The optimum pH for arsenic removal in electrocoagulation using aluminum electrodes is 7.0, while with iron electrodes, it is 6.5 [109]. The presence of co-existing ions also effects arsenic removal during electrocoagulation. Sandoval and colleagues reported that silicate influences arsenic removal by forming aluminosilicates on aluminumhydroxide flocs [97]. The presence of phosphate and sulfate ions decreases the arsenic removal by competing with arsenic for sorption onto aluminum flocs. Chloride ions favor arsenic removal by enhancing aluminum floc formation by corroding the electrode [97]. Electrocoagulation provides an exciting solution for treating drinking water and groundwater for consumption, but electricity requirements for this treatment limit its application. In urban settings, electrocoagulation usage can be feasible for treating arsenic contaminated water. So far, electrocoagulation application has been limited to laboratory scale and pilot projects, large scale applications of electrocoagulation for providing arsenic-free contaminated water are still lacking [97].

5.5 Electrospun Nanofibers

By and large, the above mentioned methods were found to have had more disadvantages that restricted their thorough potential, and there is a pivotal need for more alternatives to overcome the intricacies of arsenic removal. With that said, electrospun nanofibers came out as ideal materials for the removal of heavy metals ions from drinking water, inclusive of arsenate ions. Nanofibers are a class of nanomaterials with interesting properties unparalleled to other materials. A variety of routes have been employed to fabricate these nanostructured materials from different materials such as drawing, templates synthesis, phase separation, self-assembly, and electrospinning. Amongst these methods, electrospinning emerged greatest in respect of the production of the nanofibers owing to its simplicity, efficiency and its versatility [11,

27, 42]. The technology is described as an easy technique for producing micro- and nanofibers of organic polymers and inorganic oxide materials. With its intriguing traits, the technique finds applications in filters, tissue engineering scaffolds, wound dressing, drug delivery materials, biomimetic materials, composite reinforcement, and many others. A thorough review by [52] showed an unprecedented increase in the number of publications on electrospinning over the past few years. Since electrospun fibers find applications in nanotechnology and biotechnology, this obviously can be seen as a motive force behind the renewed interest in a technique that has been known since the 1930's [39, 52, 107].

The principle behind electrospinning is relatively simple: an electrical field is applied across a polymer solution and a collector plate to force a polymer solution jet out from a small hole. As the solution jet travels, the solvent evaporates and leaves behind a charged polymer fiber [39], which undergoes stretching and thinning as a result of the whipping, and finally collects on the grounded collector as a randomly oriented web of micro- or nanofibers [107]. The operational conditions are known to have a significant influence on the resultant fibers [33, 70]. Previous studies indicate that the development of useful applications of electrospun nanofibers requires a thorough understanding of the electrospinning parameters as the morphology and diameter of the electrospun nanofiber will have an influence on the final product [56, 89, 110, 130].

Nanofibers adsorbents can be used directly and easily separated from aqueous solutions after adsorption due to their long size [62]. Some researchers have prepared modified fibers to remove toxic anions, such as humic acid, fluoride, and phosphate [62, 85], but few studies have been conducted to remove arsenate from wastewater [35, 90, 112]. Sorbents prepared from electrospun nanofibers have come to the front-line of analyte adsorption on the grounds of their interesting attributes such as specific surface are, porosity, high flux, fine pores with interconnected pore structures, and ability to adhere to a wide variety of physical and chemical conditions. However, the relatively low rejection of ions has become a major impediment in the utilization of these membranes. To address this issue, some researchers have modified the structure and surface of electrospun nanofibers by the incorporation of inorganic nanoparticles and specific functional groups [41, 49]. The latter helped achieve the desired functional properties, which improved the removal efficiency and the permeability of membranes [54, 60]. Moreover, the large specific surface offered the nanofibers enhanced sorption capacity [26, 123].

5.6 Reported Work on the Removal of Arsenic Using Nanofibers/Composite Nanofibers

Nanofibers can be electrospun from a host of polymers, if not most. There are a number of factors that influence the choice of polymer for electrospinning nanofibers (NFs) for adsorption purposes. Among these are the availability of the polymer,

process factors such as electrospinnability of the polymer, and the physical and chemical properties of the polymer. This section will explore the polymers or composites that have been used in the fabrication of nanofibers for the removal of arsenic in water.

5.6.1 *Polymers/Composites Used for Fabrication of Nanofibers and Their Properties*

Chitosan has emerged as a popular polymer for the fabrication of nanofibers for the removal of arsenic in water. This is justified by the fact that chitosan is very rich with functional groups that are capable of adsorbing arsenic and heavy metals in general [116, 122, 134], as shown in Fig. 5.1. As a result of this, a number of research papers have been published reporting the removal of arsenic using chitosan nanofibers.

Mokhena et al. [76] prepared blended electrospun nanofibers of chitosan and poly(ethylene oxide) (PEO). The blending with PEO was necessary as pure chitosan proves to be very challenging to electrospin [32, 51], often requiring another polymer to be added [32, 93]. This is due to its rigid chemical structure, polyelectrolyte nature in solution (Mi et al. 1999), and intra- and inter-molecular interactions.

In a subsequent study, [77] produced NFs from a blend of chitosan, PEO, and $FeCl_3$ solutions. The role of $FeCl_3$ (Fe^{3+}) was to enhance the near-neutral (pH 7.0) adsorption of As(V) onto the chitosan nanofibers. Porous, continuous NFs with a typical diameter of 153 nm were obtained (Fig. 5.2).

In yet another study, [73] have retained the synthesis routes of their previous studies [74, 75] to fabricate chitosan NFs doped with Fe^{3+}, however, this time for the removal of arsenite [As(III)]. However, in this study, the NFs were also doped with Zr, Cu, Fe/Zr, and Fe/Cu oxides. These metals have previously been reported to be effective in removing arsenic from water [23, 29, 43, 45].

This chitosan NFs fabrication route involving blending with PEO was also recently explored by [111] to immobilize lanthanum nanoparticles (NPs) for subsequent sequestration of As(V) from water. The previous chitosan NFs modifications by Min et al. [74, 75] involved chitosan modification before the electrospinning process. Herein, lanthanum is deposited on the surface of chitosan NFs post electrospinning.

These studies demonstrate the relative ease with which chitosan NFs can be electrospun and modified with metallic content to produce composite NFs with enhanced properties. Another advantage of having a wealth of functional groups of chitosan is that they also allow for chemical modification of chitosan with organic compounds.

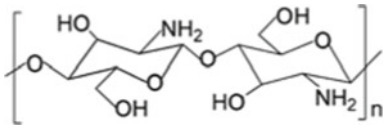

Fig. 5.1 The molecular structure of chitosan

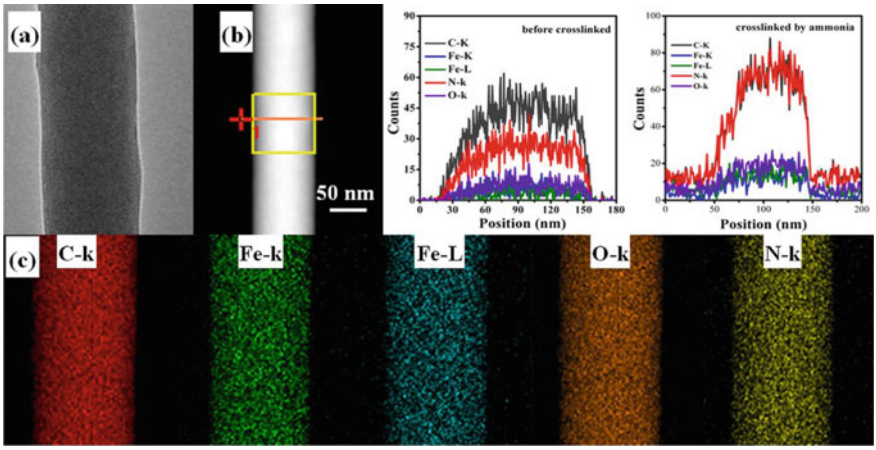

Fig. 5.2 **a** TEM image, **b** line scan, and **c** EDX elemental mappings of C, Fe, O, and N on the surface of ICS-ENF. Reproduced with permission from [77]. This article has been published under Creative Commons by Attribution (CC-BY) license

For instance, poly(vinyl alcohol) (PVA) was used as a modifier for chitosan via cross-linking with glutaraldehyde and assisted in the immobilization of zero-valent iron (ZVI) NPs and improved the porosity of the NFs [24].

Ethylene diamine-modified polyacrylonitrile (PAN) NFs for the removal of arsenic in water have also been reported. Unlike chitosan, PAN has limited functional groups onto which As can be adsorbed. Therefore, it was necessary to modify its EDTA to increase the functional group density on its surface, and the resulting NFs were poly(acrylo-amidino ethylene amine) (PAEA). Transforming PAN microfibers (MFs) into modified NFs enhanced the properties of the fibers. Nitrogen adsorption studies using a Brunauer-Emmet-Teller (BET) analyzer performed on both PAEA NFs and MFs to determine the porosity and specific surface area of the systems revealed an increase from 2.8 m^2/g of PAEA MFs to 10.4 m^2/g of PAEA NFs. This suggests that the introduction of the chelating groups on the NFs surface, together with a reduction in fiber diameter after electrospinning (from 16 μm to 250 nm), enhanced the surface area of the NFs, which is advantageous for adsorption purposes.

Iron was used again in the removal of As(V) from water, this time by [15] in the form of Fe_2O_3 NPs embedded in PAN nanofibers. The presence of Fe_2O_3 NPs in the PAN NFs improved both the porosity and hydrophilicity of the ENMs. The improved interaction with water in the presence of nanoparticles was attributed to the formation of hydroxyl ions at the metal oxide NP-water interface [127].

5.6.2 *Performance Characteristics of NFs in the Removal of Arsenic from Water*

Apart from the properties of the polymer/composite NFs used as adsorbents, water itself has some parameters that influence the performance of adsorbents in adsorbing the targeted pollutant. These include the ionic strength of the solution, the presence of competing ions or interferences, solution pH, and initial analyte concentration [79]. This section discusses the reported performances of NFs in Arsenic removal from water and the influence of solution parameters.

5.6.2.1 Influence of Solution pH

Arsenic commonly exists as arsenate As(V) and arsenite As(III) in the water. Both these arsenic species dissociate in solution to give different ions that interact differently with the adsorbent. The dissociation of arsenic species in water is governed by solution pH. Many studies have identified the dissociation products and the solution pH in which they are dominant [13, 81, 125, 134]. Solution pH also influences the extent of protonation or deprotonation of the adsorbent, which is crucial in the adsorption process. Therefore, the optimal pH for the adsorption of arsenate onto NFs is usually determined by batch adsorption studies.

This was evident from the works of Min et al., who used two chitosan NFs systems to remove As(V) from water [74, 75]. For pure chitosan NFs, adsorption was found to be sharply decreasing as the pH increased until no adsorption took place above pH 10 [74]. Maximum As(V) adsorption was recorded when the initial solution pH was 3.4. Miller et al. [71] explained a similar observation by attributing the decrease in As(V) adsorption onto the surface of TiO_2-impregnated chitosan beads (TICB) to the electrostatic repulsions between the hydroxyl groups of TICB and arsenate, which are both negatively charged. In contrast, at the equilibrium solution pH, chitosan undergoes 99% protonation, which may allow for the adsorption of As(V) onto the positively charged (protonated) amine groups [113], as studies concerning the adsorption of other metal ions by chitosan have proposed [126].

It is fair to link the pH at which maximum adsorption was attained to real-life situations in order to judge the suitability of the adsorbent. Most natural water bodies are close to neutral pH. Therefore, Fe^{3+} was immobilized and dispersed in the chitosan NFs as a means of shifting the pH of maximum adsorption to near neutral [75]. This system was far more superior to the pure chitosan NFs in terms of As(V) adsorption around neutral pH, as it exhibited As(V) removal of $> 90\%$. Adsorption was less than 50% at neutral pH for pure chitosan NFs.

Sorbent materials are associated with a pH at which their surface is neutral. This is called a point-of-zero charge of the material, or pH_{PZC}. Miller and Zimmerman [72] found that a pH above the point-of-zero-charge (PZC) of TICB actually prevented chemisorption of As(V) from occurring. An increase of pH above the pH_{PZC} imparts

an overall negative charge on the surface of the adsorbent. This may lead to electrostatic repulsions between the adsorbent and a negatively charged arsenic species. At pH < $pH_{PZC,}$ the surface of the adsorbent is positive overall, which promotes the electrostatic attraction and adsorption of negatively charged arsenic species. The pH_{PZC} and solution pH dictate how much arsenic can be adsorbed on the surface of NFs. This phenomenon has been observed in several studies.

PAN NFs were impregnated with Fe_2O_3 NPs for removing As(V) in water [15]. The effect of pH on As(V) adsorption was examined where initial pH was varied from 3–11. Maximum adsorption was observed at pH 4–5. Above pH 5 a gradual decline in adsorption was observed. The pH_{PZC} for the composite PAN NFs was determined to be at pH 6.4, below which the composite NFs surface was positively charged and allowed for electrostatic interactions with the negatively charged As(V) species. Above pH_{PZC} 6.4 a dramatic decline was observed. The surface of NFs had assumed a negative charge overall, and less adsorption occurred due to repulsion with As(V).

Poly(acrylo-amidino ethylene amine) (PAEA) NFs were fabricated by modifying PAN NFs with ethylene diamine for As(V) removal [115]. When the effect of pH on As(V) adsorption was studied, pH 3 was found to be the optimum as maximum adsorption took place there. An increase in pH resulted in a decrease in As(V) adsorption. The pH_{PZC} for PAEA NFs was determined to be 7.6. However, a sharp decrease in As(V) adsorption was observed above pH 6. This is because above pH 6, As(V) exists in solution as $HAsO_4^{2-}$, AsO_4^{3-}, as well as $H_2AsO_4^-$, which is dominant at pH < 6 [125]. The presence of the multiple charged As(V) species and decreasing PAEA surface positivity results in greater electrostatic repulsion between As(V) and the adsorbents, hence the decline in adsorption at pH > 6. For this reason, pH 3.0 was adopted as the optimum pH to ensure quantitative As(V) adsorption onto PAEA NFs.

Solution pH played a significant role again in the As(V) removal performance of the chitosan-La NF prepared by Tan et al. [111]. For instance, pure chitosan NFs showed a removal capacity of 33 mg/g at pH 4, which decreased to just 2 mg/g when the pH was adjusted to 11. Meanwhile, chitosan-La NFs exhibited an adsorption capacity of 51–53.5 at a pH range of 4–6. However, a significant drop was observed in adsorption capacity when the pH was above 6. pH influences the form in which As(V) exists in solution, depending on the extent of protonation or deprotonation. [13, 134] explain that at very low pH (~2.2), As(V) exists as the fully protonated H_3AsO_4, while between pH 2.2 and 6.9 $H_2AsO_4^-$ becomes dominant. As the pH increases, As(V) becomes more deprotonated. At pH between 6.9 and 11.5, the $HAsO_4^{2-}$ species is dominant; and, finally, full deprotonation occurs at pH > 11.5 to give AsO_4^{3-} [13, 134]. Chitosan and chitosan-La NFs had pH_{PZC} at 6.5 and 7.8, respectively. Meaning that chitosan was only able to remove $H_2AsO_4^-$, as above pH_{PZC} the chitosan surface becomes negative and repels As(V). However, the extended pH range in which chitosan-La has a positively charged surface allows both $H_2AsO_4^-$ and $HAsO_4^{2-}$ species to be removed from the solution. Hence chitosan-La NFs demonstrated a much higher adsorption capacity than pure chitosan.

Another Fe-doped chitosan electrospun nanofibrous membrane (Fe@CTS ENM) was studied by Min et al. for removing As(III) this time [73]. Fe@CTS ENM demonstrated the ability to consistently remove > 85% As(III) from aqueous solutions of pH varying from 3.3 to 8.0, and after pH 9.0 a sharp decline in adsorption was observed. Unlike in the adsorption of As(V), where at pH 9 H_3AsO_4 has already undergone two deprotonations [13, 134], H_3AsO_3 remains in its neutral form at pH < 9 and only at pH > 9.0 does the deprotonation into $H_2AsO_3^-$ occur [17, 81]. This suggests that the decline observed after pH 9 was caused by electrostatic repulsions between $H_2AsO_3^-$ and the negatively charged surface of Fe@CTS ENM. The authors further explain that the removal of the neutral H_3AsO_3 was not facilitated by electrostatic interactions, as H_3AsO_3 adsorption is not dependent on its deprotonation.

These studies, and many others that have not been discussed, reveal the extent to which solution pH can influence the performance of adsorbents in removing arsenic from water. As shown in the discussions, polymer nanofibers can be modified with organic and/or inorganic substances to manipulate their properties and adjust their ability to perform at various pH points, including at near neutral pH, where the pH of natural waters usually lies. However, this is perhaps one of the areas in which intensive research efforts still need to be focused as far as arsenic removal with NFs or composite NFs is concerned.

5.6.2.2 Influence of Co-existing Ions

It is a common realization that arsenic species are only some of the ions/compounds found in water, especially in wastewater and contaminated natural waters. The ions differ in terms of toxicity, and therefore, the need for their removal. But even those that are not harmful can impact the outcomes of any attempt to remove the harmful ones. Hence it is common practice to study the effect of co-existing ions on the removal of harmful pollutants from water. Selective adsorption of arsenic onto adsorbents is desirable yet difficult to achieve because of the interference caused by co-existing ions. Ionic species such as phosphate, carbonate, sulfate, fluoride, and chloride are common ions in water systems, and their effect on arsenic removal is of interest to researchers. Just like arsenate and arsenite, these ions are negatively charged and can compete with As(V) and As(III) for adsorption sites [3].

The effect of the presence of other anions Cl^- (chloride), NO_3^- (nitrate), and SO_4^{2-} (sulfate) was examined on the removal of As(V) by PAN nanofibers functionalized with Fe_20_3 NPs [15]. It was found that all three anions decreased As(V) adsorption onto the NFs. However, Cl^- and NO_3^- were found to cause less interference than SO_4^{2-}. This was due to the fact that Cl^- and NO_3^- are single charged and smaller in size, compared to the more bulky and double-charged SO_4^{2-}. Because of this, SO_4^{2-} can occupy more of the binding sites of Fe_2O_3 NPs than Cl^- or NO_3^-, resulting in less As(V) adsorbed. This finding is in contrast with the studies by Min et al. where the removal of As(V) by chitosan NFs [74] and Fe^{3+}-immobilized chitosan NFs [75] remained unaffected by small, single charged anions such as Cl^- even if present at very high concentrations compared to that of As(V).

The As(V) removal performance of the chitosan-La NFs fabricated by Tan et al. was compromized by the presence of co-existing anions Cl^-, NO_3^-, SO_4^{2-}, HCO_3^-, and $H_2PO_4^-$, even though to a lesser extent for chitosan-La NFs [111]. In particular, phosphate ions caused the greatest interference on both chitosan and chitosan-La NFs. [74] observed a similar impact of phosphate and sulfate on their chitosan NFs, while carbonate and fluoride had no significant impact. Contrary to that, chloride and carbonate were found to affect the adsorption of As(V) onto even chitosan. This may have been caused by the high concentration of the interferents in the solution (up to 600 mg/L).

The effect of co-existing ions on the adsorption of arsenic species does not seem to be entirely dependent on the nature of the adsorbent; as it can be seen here, chitosan NFs used in two studies were affected differently by the presence of co-existing ions. The presence of co-existing ions CO_3^{2-}, SO_4^{2-}, Cl^-, F^- did not have an impact on the adsorption of As(III) by the Fe-doped chitosan NFs prepared by [73]. The As(III) initial concentration was kept at 1.3 μM, while co-ions varied from 0.1–2 mM (100–2000 μM). The presence of these ions has been found to negatively affect the adsorption of either As(III) or As(V) [79].

5.6.2.3 Nanofiber Capacities and Kinetics and Mechanisms Involved in Arsenic Removal

The performance of the NFs was determined by a combination of adsorption parameters such as equilibrium time, maximum adsorption capacity, adsorbent dosage, and reusability. Theoretical equations have been used to model the adsorption data, viz. the Langmuir and Freundlich isotherms, while the pseudo-first-order and pseudo-second-order kinetic models were applied to analyze the equilibrium data. The reported performances of NFs and NF composites have varied widely in terms of maximum adsorption capacities and equilibrium time, i.e., the time it took the adsorbent to reach equilibrium. Table 5.2 lists the results of some of the studies that are reported in the literature.

The PAEA NFs of Vu et al. required only 15 min to reach equilibrium, while it took 60 min for PAEA MFs to reach As(V) adsorption equilibrium [115]. The difference between the two adsorbents was their specific surface area. PAEA NFs had a surface area of 10.4 m^2/g, while the surface area of PAEA MFs was 2.8 m^2/g. This difference in the surface areas of PAEA NFs and PAEA MFs explains the difference in the As(V) adsorption rates for the two systems. It highlights the advantage of using nanosorbents instead of their bulk counterparts. This is because As(V) was exposed to more adsorption sites when the surface area was higher, thus resulting in faster adsorption and even greater adsorption capacities as calculated from the pseudo-second-order kinetic model. The experimental adsorption capacity from these data was found to be 66.68 and 25.72 mg/g for PAEA NFs and PAEA MFs, respectively, while their respective maximum adsorption capacity was determined from the Langmuir isotherm model to be 76.92 and 27.62 mg/g, which agree with the experimental capacities.

Another strong adsorption performance in terms of adsorption capacity was exhibited by the chitosan-La NFs prepared by [111]. Equilibrium data for the adsorption

Table 5.2 Comparison of reported nanofibrous adsorbents for arsenic adsorption under optimum conditions

Polymer/polymer composite description	Adsorption Capacity (mg/g)	Arsenic Species	pH	Equil. time	Reference
PAN NFs embedded with Fe_2O_3 NPs	82.2	As(V)	3–4	120 min	[15]
Chitosan NFs	30.8	As(V)	3.4	30 min	[74]
Chitosan NFs with Fe^{3+}	11.2	As(V)	7.2	100 min	[75]
PAN NFs modified with ethylenediamine	76.92	As(V)	3	15 min	[115]
Chitosan NFs with La NPs	83.6	As(V)	4–6	350 min	[111]
Chitosan NFs with Fe^{3+}	36.1	As(III)	7	120 min	[73]
Chitosan/cellulose blend	39.4	As(V)		60 min	[84]
Cellulose modified with cysteine	357.14	As(III)	7		[25]
Chitin modified with cysteine	149	As(III)	7		[128]
Chitosan/PVA blend with cerium	18.2	As(III)	6.2–7	60 min	[101]
PVDF with Fe–Mn binary oxide	21.32	As(V)	7	10 h	[6]
PAN with alumina	3.8	As(V)	2	60 min	[103]
PVA/Nafion blend	22.7	As(III)	5.9	5 h	[101]
Chitosan-g-poly(N-vinylcaprolactam) NFs modified with ZIF-8 MOF	258.5	As(V)	3	30 min	[15]

of As(V) onto the surfaces of chitosan NFs and chitosan-La NFs was evaluated using both the Langmuir and Freundlich isotherms. Based on the correlation coefficients obtained for the data, the Langmuir isotherm best fit the data. As calculated from the Langmuir model, the maximum adsorption capacities for chitosan NFs and chitosan-La NFs were found to be 83.6 and 37.8 mg/g, respectively. Chitosan-La NFs owed their higher adsorption capacity to the presence of La-OH NPs on their surface. Figure 5.3 shows the surface of chitosan NFs before and after chitosan modification with La NPs.

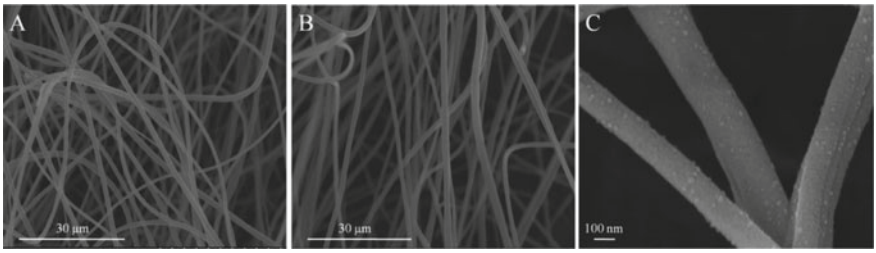

Fig. 5.3 **a** SEM image of chitosan NFs. **b** SEM image of chitosan-La NFs. **c** magnified SEM image of chitosan-La NFs. Reproduced with permission from [111]. Copyright 2020, Elsevier Science Ltd.

The hydroxide form of the NPs is important as it has been reported to improve the hydrophilicity of NFs [15]. ICP-MS studies revealed that the load content of La on the NFs was 13.8 wt%. According to the authors, La was immobilized on the surface of CSN NFs via complexation with amine groups of chitosan, as interpreted from Fourier-transform infrared spectroscopy (FTIR) and XPS data. XPS further revealed that As(V) adsorption also occurred on the amino groups of CSN, which was also reported by [74]. Moreover, a reduction of the La–OH peak (FTIR) upon As(V) adsorption, according to the authors, suggests an adsorption mechanism whereby As(V) substitutes –OH from La the NPs. The equilibrium time for chitosan NFs was found to be 35 min, while that of chitosan-La NFs was 350 min. As explained before, the removal of As(V) using chitosan occurs via electrostatic interaction between the protonated amine groups of chitosan and the negatively charged As(V) [74]. This seems to be the case even for chitosan-La NFs, as rapid uptake of As(V) was observed in the first 40 min, followed by a slow increase until equilibrium at 350 min. This second phase (after 40 min), the authors argue, is likely the complexation of As(V) on the immobilized La-OH NPs via –OH substitution. This two-phase adsorption was responsible for the higher adsorption capacity of chitosan-La NFs than the pure chitosan NFs. However, the high capacity of chitosan-La NFs compromised its equilibrium time. The slow nature of this complexation was attributed to the inner-sphere type of complexation. [74] described this mechanism as one in which an increase in ionic strength does not influence the adsorption of the adsorbate, while describing outer-sphere adsorption as one in which the adsorption of the adsorbate takes place in one plane of the adsorbate surface, and an increase in ionic strength decreases the take-up of the adsorbate.

PAN NFs decorated with Fe_2O_3 NPs were fabricated by [15] for removing As(V) from water. Adsorption equilibrium data was evaluated using the Langmuir and Freundlich models. The Langmuir model was found to return better fitment of the data, indicating monolayer adsorption of As(V) onto a uniform nanofiber surface. The Langmuir model revealed that the maximum adsorption capacities that can be achieved with the composites NFs was 82.2 mg/g, and equilibrium was achieved within 120 min. The authors attributed this to the high porosity and specific surface area (10.37 m^2/g) of the composite NFs. It is important to note that PAN NFs with zero addition of Fe_2O_3 NPs did not exhibit any As(V) adsorption capacity as the As(V) feed solution retained its initial As(V) concentration after being exposed to the PAN NFs. This means that the embedded Fe_2O_3 NPs were solely responsible for all removal of As(V). The adsorption mechanism was said to be a ligand exchange whereby –OH is replaced on the Fe_2O_3 NPs surface by As(V) species.

The results discussed above represent some of the best performances of NFs—in terms of adsorption capacity—applied in the removal of arsenic in water. Others reported 39.4 [84], 36.1 [73], 30.8 [74], 11.2 mg/g [75], etc. Common features about the literature reported on the use of NFs for the removal of arsenic are that the adsorption is reported to almost invariably follow the Langmuir model, assuming monolayer adsorption on a homogeneous surface with no interaction among the adsorbed molecules [84, 95]. Moreover, the kinetic data is reported to follow the pseudo-second-order kinetic model largely. This means that the sorption of arsenic

onto the NF surfaces was more inclined towards chemisorption. The rate of adsorption is not determined by the analyte concentration but rather the adsorption capacity of the adsorbent [121]—the NFs. In this light, it is encouraging to already see high adsorption capacities by some of the NFs reported.

The maximum permissible water level for arsenic is 10 μg/L [124]. Treatment of model water contaminated with arsenic at different concentrations revealed that the Fe^{3+}-modified chitosan NFs could reduce contamination levels to below 10 μg/L when the initial concentration range was 100–750 μg/L [75]. According to the authors, the performance of this Fe^{3+}-modified chitosan NFs on low equilibrium As(V) concentrations renders these NFs suitable candidates for real environmental water treatment, where As(V) concentrations are typically low, including drinking water [75]. Subsequently, Fe-doped chitosan NFs also demonstrated the ability to reduce As(III) in water from 100 μg/L to below the threshold of 10 μg/L [73]. The Fe_2O_3 NP-immobilised PAN NFs fabricated by [15] were able to reduce 5000 μg/L of As(V) to below 10 μg/L in 45 min. These achievements indicate that nanofibrous membranes can be engineered to cater to the removal of arsenic from various water systems, depending on the level of arsenic contamination.

Arguably, the highest maximum adsorption capacity to date on the removal of arsenic from water with NFs was reported by Chen et al. [25]. Cellulose NFs were extracted from wood pulp via the oxidative treatment of the biomass with sodium periodate. The NFs were then imparted with thiol groups, which have been shown to possess a great affinity for As(III) [128] by modifying them with cysteine. The reported maximum adsorption capacity for this system, calculated from the Langmuir adsorption isotherm, was 357.14 mg/g at pH 7. Because of the wide range of As(III) concentrations in which the adsorbent was tested (10–2500 ppm), it was found that the Langmuir model poorly fitted the data. However, when the As(III) concentration range was segmented into three smaller ranges, viz. 10 − 20 ppm, 50 − 250 ppm, and 500–2500 ppm, adsorption data from the 50 − 250 ppm As(III) concentration range was fitted well by the Langmuir isotherm. At the lower concentrations (50 − 250 ppm), low adsorption efficiency was achieved, indicating only partial ionic bonding between the thiol groups and As(III) [25]. The Langmuir isotherm did not suitably fit this data. At the highest concentration range (500–2500 ppm), again, the adsorption data was poorly fitted by the Langmuir isotherm. SEM micrographs (Fig. 5.4a, b) of the functionalized cellulose NFs pre (NDAC−cys) and post As(III) adsorption (NDAC−cys−As(III)-1500) at 1500 ppm are presented in Fig. 5.4 together with accompanying EDX spectra. It can be clearly seen that after adsorption of As(III), arsenic nanoparticles formed on the surface of the adsorbent (Fig. 5.4c) due to As(III) mineralisation into As_2O_3 and were also confirmed by the emergence of a strong arsenic peak in the EDX spectrum (Fig. 5.4d). This explained the poor fitting of the data on the Langmuir isotherm because the mineralization was a multilayer process on a heterogeneous surface. Indeed, adsorption data for the entire As(III) concentration range (without segmenting) was fitted well by the Freundlich adsorption isotherm [25].

Notably, this adsorbent was prepared from cellulose, the most abundant biopolymer on earth, which translates to low production costs and biodegradable.

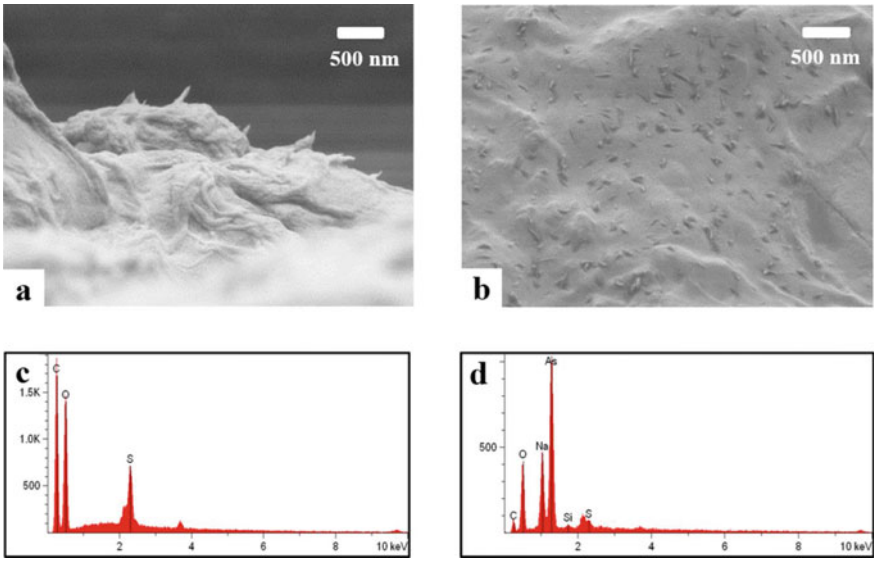

Fig. 5.4 SEM images of **a** NDAC−cys and **b** NDAC−cys−As(III)-1500 (NDAC−cys adsorption with 1500 ppm of As(III)); element mapping spectra of **c** NDAC−cys and **d** NDAC−cys − As(III)-1500. Reproduced with permission from [25]. This article has been published under Creative Commons by Attribution (CC-BY) license

These are some of the most desirable properties of an adsorbent. However, these NFs might be lacking one important thing—the property of being continuous. The oxidation approach produced bundles of agglomerated NFs with diameters averaging 70 nm [25]. The disadvantage of this NF preparation route is that the NFs were not continuous and did not form a mat or membrane, limiting their applicability in modern filtration systems, as they are effectively powder (5 nm width and 150 nm length of individual NF on average). The challenge with powder materials is their difficult recovery and separation of water after the treatment [78]. Nonetheless, considering the performance of these NFs, it would be interesting to see how the NFs would perform if the transformation to NFs were to be conducted by electrospinning to produce a membrane or mat. This is justified by the continued interest shown by researchers in electrospun biopolymeric NFs for wastewater treatment [98] and the already demonstrated potential of electrospun NFs in arsenic removal.

The cysteine-modified cellulose NFs study was preceded by another biopolymer, chitin, underwent a similar extraction process of NFs and modification with cysteine [129]. They reported a maximum adsorption capacity of 149 mg/g at pH 7 from the Langmuir adsorption isotherm. These NFs came in the form of flat ribbons, and like the cellulose-cysteine NFs, they were not continuous and exhibited average width of 24 nm and thickness of 6 nm.

5.7 Conclusion and Perspectives

The environmental degradation by a variety of pollutants is a worldwide scourge destabilizing livelihood. One of the pollutants seriously receiving considerable attrition in the research and academic field is the inorganic arsenic heavy metal precisely due to its toxic nature. The contact with unacceptable quantities of arsenic is in consequence of the geogenic and anthropogenic activities. The latter is of benefit to the economic growth in the world; however, their consequences on the environment are harmful. For instance, the food chain is vehemently and severely disturbed by the arsenic contamination, as evidenced by the deteriorated health conditions of the inhabitants.

In order to contend with the arsenic problem, various physicochemical methods have been intensively probed. The merits and demerits of these technologies have been examined thoroughly. In respect of performance, the technologies displayed modest efficacy in addressing arsenic contamination in wastewater. As a result, low-cost, sustainable, and efficient technologies must be developed at community or household levels to address the arsenic risk in drinking water. That being so, electrospun nanofibrous membranes entrenched themselves as globally recognized filtering media for various applications. This is due to their distinctive and inherent specifications such as high porosity (up to 90%), three-dimensional interconnected pore structure, and functionality that make them highly promising and appealing for both academic and R & D applications. The results that came out upon exploring the nanofiber adsorbents for arsenic removal have indicated that the nanofibers can remove arsenic metals from water. Unfortunately, the technology has not been advanced to large-scale operations. It has only been tested at the laboratory level, so its feasibility for real-world applications is not yet demonstrated. Pilot-scale experimentation and long-term monitoring are therefore recommended. Moreover, estimated treatment costs of these processes are not adequately addressed.

The wide-ranging capabilities and optimal performance conditions of the NFs discussed suggest that no one system is fit for removing arsenic for all water types and arsenic contamination levels. While that may be desirable, it might be challenging to achieve. However, by recommendation, filtration systems can be designed to combine several nanofibrous membranes optimized to perform at different levels of arsenic contamination and their associated water conditions to ensure the complete removal of arsenic or its reduction to acceptable levels.

It is predicted that the growth of the nanofibers global market is anticipated to step up precisely on account of rapid urbanization and industrialization across emerging economies. This is due to the growing rise in demandfor water for domestic and industrial purposes, access to fresh and clean water. Globally, an increasing number of R & D centers are trying hard on industrialization and commercialization of electrospun nanofibrous membranes due to their perceived socio-economic benefits. Thus, adaptations and modifications will be expected in the coming years for a large-scale market of electrospun membranes for water treatment applications.

Notwithstanding that electrospun nanofibers are of use to wastewater treatment, they can also be used in other applications, including cosmetic products, healthcare issues, reinforcement in composites materials, aerospace engineering, and gas/air filtration purposes.

Acknowledgements The authors thank the Department of Science and Innovation/Mintek (DSI/Mintek) Nanotechnology Innovation Centre, South Africa, for financial support.

References

1. M.F. Ahmed, Alternative water supply options for arsenic affected areas of Bangladesh. Arsenic mitigation in *Bangladesh. International Workshop on Arsenic Mitigation in Bangladesh, Dhaka* (2002), pp. 14–16
2. O.B. Akpor, M. Muchie, Remediation of heavy metals in drinking water and wastewater treatment systems: processes and applications. Int. J. Phys. Sci. **5**, 1807–1817 (2010)
3. A. Alam, W.A. Shaikh, O. Alam, T. Bhattacharya, S. Chakraborty, B. Show, I. Saha, Adsorption of As (III) and As (V) from aqueous solution by modified Cassia fistula (golden shower) biochar. Appl. Water Sci. **8**(7), 198 (2018). https://doi.org/10.1007/s13201-018-0839-y
4. M.T. Alarcón-Herrera, J. Bundschuh, B. Nath, H.B. Nicolli, M. Gutierrez, V.M. Reyes-Gomez et al., Co-occurrence of arsenic and fluoride in groundwater of semiarid regions in Latin America: genesis, mobility and remediation. J. Hazard. Mater. **262**, 960–969 (2013). https://doi.org/10.1016/j.jhazmat.2012.08.005
5. R. Alcacio, J.L. Nava, G. Carreño, E. Elorza, F. Martínez, Removal of arsenic from a deep well by electrocoagulation in a continuous filter press reactor. Water Sci. Technol. Water Supply **14**, 189–195 (2014). https://doi.org/10.2166/ws.2013.188
6. P. Aliahmadipoor, D. Ghazanfari, R.J. Gohari, M.R. Akhgar, Preparation of PVDF/FMBO composite electrospun nanofiber for effective arsenate removal from water. RSC Adv. **10**(41), 24653–24662 (2020). https://doi.org/10.1039/D0RA02723E
7. S.S. Alkurdi, I. Herath, J. Bundschuh, R.A. Al-Juboori, M. Vithanage, D. Mohan, Biochar versus bone char for a sustainable inorganic arsenic mitigation in water: what needs to be done in future research? Environ. Int. **127**, 52–69 (2019). https://doi.org/10.1016/j.envint.2019.03.012
8. R. Ameta, A.K. Chohadia, A. Jain, P.B. Punjabi, Fenton and photo-Fenton processes, in *Advanced Oxidation Processes for Waste Water Treatment. Emerging Green Chemical Technology*. (Elsevier , 2018), pp. 49–87. https://doi.org/10.1016/B978-0-12-810499-6.00003-6
9. M.N. Amin, S. Kaneco, T. Kitagawa, A. Begum, H. Katsumata, T. Suzuki, K. Ohta, Removal of arsenic in aqueous solutions by adsorption onto waste rice husk. Ind. Eng. Chem. Res. **45**, 8105–8110 (2006). https://doi.org/10.1021/ie060344j
10. A. Andhale, H. Pawar, S. Zambar, The evaluation of nickel toxicity on Lamellidens Marginalis. Recent Res. Sci. Technol. **3**, 1–5 (2011)
11. A.L. Andrady, *Science and Technology of Polymer Nanofibers*. (Wiley, Hoboken , 2008). https://doi.org/10.1002/9780470229842
12. O.I. Asubiojo, O.B. Ajelabi, Removal of heavy metals from industrial wastewaters using natural adsorbents. Toxicol. Environ. Chem. **91**(5), 883–890 (2009). https://doi.org/10.1080/02772240802614721
13. R. Awual, S. Urata, A. Jyo, M. Tamada, A. Katakai, Arsenate removal from water by a weak-base anion exchange fibrous adsorbent. Water Res. **42**(3), 689–696 (2008). https://doi.org/10.1016/j.watres.2007.08.020

14. S.A. Baig, T. Sheng, Y. Hu, J. Xu, X. Xu, Arsenic removal from natural water using low cost granulated adsorbents: a review. CLEAN–Soil Air Water **43**, 13–26 (2015). https://doi.org/10.1002/clen.201200466
15. P. Bahmani, A. Maleki, H. Daraei, R. Rezaee, M. Khamforoush, S. Dehestani Athar, F. Gharibi, A.H. Ziaee, G. McKay, Application of modified electrospun nanofiber membranes with α-Fe2O3 nanoparticles in arsenate removal from aqueous media. Environ. Sci. Pollut. Res. **26**(21), 21993–22009 (2019). https://doi.org/10.1007/s11356-019-05228-5
16. R. Balamurugan, S. Sundarrajan, S. Ramakrishna, Recent trends in nanofibrous membranes and their suitability for air and water filtrations. Membranes **1**, 232–248 (2011). https://doi.org/10.3390/membranes1030232
17. S. Bhowmick, S. Chakraborty, P. Mondal, W. Van Renterghem, S. Van den Berghe, G. Roman-Ross, D. Chatterjee, M. Iglesias, Montmorillonite-supported nanoscale zero-valent iron for removal of arsenic from aqueous solution: Kinetics and mechanism. Chem. Eng. J. **243**, 14–23 (2014). https://doi.org/10.1016/j.cej.2013.12.049
18. M. Bissen, F.H. Frimmel, Arsenic—a review. Part II: oxidation of arsenic and its removal in water treatment. Acta Hydrochim. Hydrobiol. **31**, 97–107 (2003). https://doi.org/10.1002/aheh.200300485
19. V.M. Boddu, K. Abburi, J.L. Talbott, E.D. Smith, R. Haasch, Removal of arsenic (III) and arsenic (V) from aqueous medium using chitosan-coated biosorbent. Water Res. **42**, 633–642 (2008). https://doi.org/10.1016/j.watres.2007.08.014
20. M. Bryjak, N. Kabay, B.L. Rivas, J. Bundschuh, *Innovative Materials and Methods for Water Treatment: Solutions for Arsenic and Chromium Removal*., vol. 2. (CRC Press , 2016). https://doi.org/10.1201/b19577
21. T. Budinova, N. Petrov, M. Razvigorova, J. Parra, P. Galiatsatou, Removal of arsenic (iii) from aqueous solution by activated carbons prepared from solvent extracted olive pulp and olive stones. Ind. Eng. Chem. Res. **45**, 1896–1901 (2006). https://doi.org/10.1021/ie051217a
22. J. Bundschuh, M. Armienta, P. Birkle, P. Bhattacharya, J. Matschullat, A. Mukherjee, *Natural Arsenic in Groundwater of Latin America 1* (CRC Press. Taylor & Francis, London, UK, 2009)
23. V. Chandra, J. Park, Y. Chun, J.W. Lee, I.-C. Hwang, K.S. Kim, Water-dispersible magnetite-reduced graphene oxide composites for arsenic removal. ACS Nano **4**(7), 3979–3986 (2010). https://doi.org/10.1021/nn1008897
24. D. Chauhan, J. Dwivedi, N. Sankararamakrishnan, Novel chitosan/PVA/zero-valent iron biopolymeric nanofibers with enhanced arsenic removal applications. Environ. Sci. Pollut. Res. **21**(15), 9430–9442 (2014). https://doi.org/10.1007/s11356-014-2864-1
25. H. Chen, S.K. Sharma, P.R. Sharma, H. Yeh, K. Johnson, B.S. Hsiao, Arsenic (iii) removal by nanostructured dialdehyde cellulose–cysteine microscale and nanoscale fibers. ACS Omega **4**, 22008–22020 (2019). https://doi.org/10.1021/acsomega.9b03078
26. S. Chigome, G. Darko, N. Torto, Electrospun nanofibers as sorbent material for solid phase extraction. Analyst (Cambridge, U. K.) **136**, 2879–2889 (2011). https://doi.org/10.1039/C1AN15228A
27. H. Cho, S.Y. Min, T.W. Lee, Electrospun organic nano -fiber electronics and photonics. Macromol. Mater. Eng. **298**, 475–486 (2013). https://doi.org/10.1002/MAME.201200364
28. J.L. Cortina, M.I. Litter, O. Gibert, M. Travesset, A. Ingallinella, R. Fernández, Latin America experiences in arsenic removal from drinking water and mining effluents (2016)
29. R.-M. Couture, J. Rose, N. Kumar, K. Mitchell, D. Wallschläger, P. Van Cappellen, Sorption of arsenite, arsenate, and thioarsenates to iron oxides and iron sulfides: a kinetic and spectroscopic investigation. Environ. Sci. Technol. **47**(11), 5652–5659 (2013). https://doi.org/10.1021/es3049724
30. M.M. de Boggio, I. Levy, M. Mateu, M. Litter, P. Bhattacharya, J. Bundschuh, *Low-cost Technologies for Arsenic Removal in the Chaco-Pampean Plain, Argentina. Natural Arsenic in Groundwater of Latin America,* vol. 1. (CRC Press/Balkema Publisher, Leiden, The Netherlands, 2009), pp. 677–683. https://doi.org/10.1201/b11334-88

31. M.E.M. de Boggio, I.K. Levy, M. Mateu, J.M. Meichtry, S. Farías, G.D. López et al., Low-cost solar technologies for arsenic removal in drinking water, in *Global Arsenic Problem and Challenges for Safe Water Production*, vol. 2. (CRC Press/Balkema Publisher, Leiden, The Netherlands, 2010), pp. 209–218. https://doi.org/10.1201/b10537-21
32. K. Desai, K. Kit, J. Li, S. Zivanovic, Morphological and surface properties of electrospun chitosan nanofibers. Biomacromol **9**(3), 1000–1006 (2008). https://doi.org/10.1021/bm701017z
33. W. Ding, S. Wei, J. Zhu, X. Chen, D. Rutman, Z. Guo, Manipulated electrospun PVA nanofibers with inexpensive salts. Macromol. Mater. Eng. **295**(10), 958–965 (2010)
34. M. Edwards, Chemistry of arsenic removal during coagulation and Fe–Mn oxidation. J. Am. Water Works Ass. **86**, 64–78 (1994)
35. K. Endo, M. Nakagawa, H. Sakanakura, Y. Inoue, I. Masahiro, G. Sugihara, Study on hydrogen sulfide gas production potential test for ground improvement by recycled gypsum and lime. Zairyo **61**, 31–36 (2012). https://doi.org/10.2472/jsms.61.31
36. L. Feenstra, L. Vasak, J. Griffioen, Fluoride in groundwater: overview and evaluation of removal methods, in *International Groundwater Resources Assessment Centre Report nr. SP*, vol. 1 (2007), pp. 1–21
37. Q. Feng et al., Adsorption and desorption characteristics of arsenic on soils: kinetics, equilibrium and effect of Fe(OH)3 colloid, H2SiO3 colloid and phosphate. Proc. Environ. Sci. **18**, 26–36 (2013). https://doi.org/10.1016/j.proenv.2013.04.005
38. K.B. Fontana, G.G. Lenzi, E.C. Seára, E.S. Chaves, Comparision of photocatalysis and photolysis processes for arsenic oxidation in water. Ecotoxicol. Environ. Saf. **151**, 127–131 (2018). https://doi.org/10.1016/j.ecoenv.2018.01.001
39. A. Formhals, US Patent 1,975,504 (1934)
40. J.R. Garbarino, H. Hayes, D. Roth, R. Antweider, T.I. Brinton, H. Taylor, Contaminants in the Mississippi River, U. S Geological Survey Circular 1133, Virginia, U. S. A (1995) ubs.usgs.gov/circ/circ1133
41. R.J. Gohari, W. Lau, T. Matsuura, A. Ismail, Fabrication and characterization of novel PES/Fe–Mn binary oxide UF mixed matrix membrane for adsorptive removal of As (III) from contaminated water solution. Sep. Purif. Technol. **118**, 64–72 (2013). https://doi.org/10.1016/j.seppur.2013.06.043
42. A. Greiner, J.H. Wendorff, Electrospinning: a fascinating method for the preparation of ultrathin fibers. Angew. Chem. Int. Ed. **46**, 5670–5703 (2007). https://doi.org/10.1002/anie.200604646
43. A. Gupta, M. Yunus, N. Sankararamakrishnan, Chitosan- and iron–chitosan-coated sand filters: a cost-effective approach for enhanced arsenic removal. Ind. Eng. Chem. Res. **52**(5), 2066–2072 (2013). https://doi.org/10.1021/ie302428z
44. A. Guzmán, J.L. Nava, O. Coreño, I. Rodríguez, S. Gutiérrez, Arsenic and fluoride removal from groundwater by electrocoagulation using a continuous filter-press reactor. Chemosphere **144**, 2113–2120 (2016). https://doi.org/10.1016/j.chemosphere.2015.10.108
45. C. Hang, Q. Li, S. Gao, J.K. Shang, As(III) and As(V) adsorption by hydrous zirconium oxide nanoparticles synthesized by a hydrothermal process followed with heat treatment. Ind. Eng. Chem. Res. **51**(1), 353–361 (2012). https://doi.org/10.1021/ie202260g
46. H.K. Hansen, P. Núñez, R. Grandon, Electrocoagulation as a remediation tool for wastewaters containing arsenic. Miner. Eng. **19**, 521–524 (2006). https://doi.org/10.1016/j.mineng.2005.09.048
47. L. Hao, M. Liu, N. Wang, G. Li, A critical review on arsenic removal from water using iron-based adsorbents. RSC Adv. **8**, 39545–39560 (2018). https://doi.org/10.1039/C8RA08512A
48. M.A. Hashim, S. Mukhopadhyay, J.N. Sahu, B. Sengupta, Remediation technologies for heavy metal contaminated groundwater. J. Environ. Manag. **92**, 2355–2388 (2011). https://doi.org/10.1016/j.jenvman.2011.06.009
49. T. He, W. Zhou, A. Bahi, H. Yang, F. Ko, High permeability of ultrafiltration membranes based on electrospun PVDF modified by nanosized zeolite hybrid membrane scaffolds under low pressure. Chem. Eng. J. **252**, 327–336 (2014). https://doi.org/10.1016/j.cej.2014.05.022

50. J.G. Hering, P.Y. Chen, J.A. Wilkie, M. Elimelech, Arsenic removal from drinking water during coagulation. J. Environ. Eng. **123**, 800–807 (1997). https://doi.org/10.1061/(ASCE)0733
51. H. Homayoni, S.A.H. Ravandi, M. Valizadeh, Electrospinning of chitosan nanofibers: processing optimization. Carbohyd. Polym. **77**(3), 656–661 (2009). https://doi.org/10.1016/j.carbpol.2009.02.008
52. Z.-M. Huang, Y.-Z. Zhang, M. Kotaki, S. Ramakrishna, A review on polymer nanofibers by electrospinning and their applications in nanocomposites. Compos Sci. Technol. **63**, 2223–2253 (2003). https://doi.org/10.1016/S0266-3538(03)00178-7Get
53. R. Hubner, K.B. Astin, R.J.H. Herbert, 'Heavy metal'-time to move on from semantics to pragmatics. J. Environ. Monit. **12**(8), 1511–1514 (2010). https://doi.org/10.1039/c0em00056f
54. B. Hudaib, V. Gomes, J. Shi, C. Zhou, Z. Liu, Poly (vinylidene fluoride)/polyaniline/MWCNT anocomposite ultrafiltration membrane for natural organic matter removal. Sep. Purif. Technol. **190**, 143–155 (2018). https://doi.org/10.1016/j.seppur.2017.08.026Get
55. S.J. Hug, O. Leupin, Iron-catalyzed oxidation of arsenic (III) by oxygen and by hydrogen peroxide: pH-dependent formation of oxidants in the Fenton reaction. Environ. Sci. Technol. **37**, 2734–2742 (2003). https://doi.org/10.1021/es026208x
56. V. Jacobs, R.D. Anandjiwala, M. Maaza, The influence of electrospinning parameters on the structural morphology and diameter of electrospun nanofibers. J. Appl. Polym. Sci. **115**(5), 3130–3136 (2010). https://doi.org/10.1002/app.31396
57. C. Jain, R. Singh, Technological options for the removal of arsenic with special reference to South East Asia. J. Environ. Manag. **107**, 1–18 (2012). https://doi.org/10.1016/j.jenvman.2012.04.016
58. W. Jiang, X.B. Chen, Y.J. Niu, B.C. Pan, Spherical polystyrene-supported nano-Fe_3O_4 of high capacity and low-field separation for arsenate removal from water. J. Hazard. Mater. **243**, 319–325 (2012). https://doi.org/10.1016/j.jhazmat.2012.10.036
59. E.O. Kartinen Jr., C.J. Martin, An overview of arsenic removal processes. Desalination **103**, 79–88 (1995). https://doi.org/10.1016/0011-9164(95)00089-5
60. S.-M. Kim, Y.-J. Lee, K.-W. Jun, J.-Y. Park, H. Potdar, Synthesis of thermo-stable high surface area alumina powder from sol–gel derived boehmite. Mate.r Chem. Phys. **104**, 56–61 (2007). https://doi.org/10.1016/j.matchemphys.2007.02.044
61. N.E. Korte, Q. Fernando, A review of arsenic (III) in groundwater. Crit. Rev. Environ. Sci. Technol. **21**(1), 1–39 (1991). https://doi.org/10.1080/10643389109388408
62. L. Kuenstl, S. Griesel, A. Prange, W. Goessler, Arsenic speciation in bodily fluids of harbor seals (Phoca vitulina) and harbor porpoises (Phocoena phocoena). Environ. Chem. **6**, 319–327 (2009). https://doi.org/10.1071/EN08079
63. M.I. Litter, M.E. Morgada, J. Bundschuh, Possible treatments for arsenic removal in Latin American waters for human consumption. Environ. Pollut. **158**, 1105–1118 (2010). https://doi.org/10.1016/j.envpol.2010.01.028
64. M.I. Litter, M.T. Alarcón-Herrera, M.J. Arenas, M.A. Armienta, M. Avilés, R.E. Cáceres et al., Small-scale and household methods to remove arsenic from water for drinking purposes in Latin America. Sci. Total Environ. **429**(107–122), 391–416 (2012). https://doi.org/10.1016/j.scitotenv.2011.05.004
65. M. Litter, M. Armienta, S. Farías, Metodologías analíticas para la determinación y especiación de arsénico en aguas y suelos. IBEROARSEN, CYTED, Buenos Aires, Spanish (2009)
66. J.E. Losey, M. Vaughan, The economic value of ecological services provided by insects. Bioscience **56**(4), 311–323 (2006). https://doi.org/10.1641/0006-3568
67. J.F. Liu, Z.S. Zhao, G.B. Jiang, Coating Fe_3O_4 magnetic nanoparticles with humic acid for high efficient removal of heavy metals in water. Environ. Sc.i Technol. **42**, 6949–6954 (2008). https://doi.org/10.1021/es800924c
68. S. Maity, N. Naskar, S. Lahiri, J. Ganguly, Polysaccharide-derived hydrogel water filter for the rapid and selective removal of arsenic. Environ. Sci. Water Res. Technol. **5**, 1318–1327 (2019). https://doi.org/10.1039/C9EW00247B

69. J. Matschullat, Arsenic in the geosphere – a review. Sci. Total Environ. **249**(1–3), 297–312 (2000). https://doi.org/10.1016/S0048-9697(99)00524-0
70. A.V. Melechko, M.A. Guillorn, D.H. Lowndes, M.L. Simpson, Controlled alignment of carbon nanofibers in a large-scale synthesis process. Appl. Phys. Lett. **80**, 4816 (2002). https://doi.org/10.1063/1.1487920
71. S.M. Miller, M.L. Spaulding, J.B. Zimmerman, Optimization of capacity and kinetics for a novel bio-based arsenic sorbent, TiO2-impregnated chitosan bead. Water Res. **45**(17), 5745–5754 (2011). https://doi.org/10.1016/j.watres.2011.08.040
72. S.M. Miller, J.B. Zimmerman, Novel, bio-based, photoactive arsenic sorbent: TiO2-impregnated chitosan bead. Water Res. **44**(19), 5722–5729 (2010). https://doi.org/10.1016/j.watres.2010.05.045
73. L.-L. Min, L.-M. Yang, R.-X. Wu, L.-B. Zhong, Z.-H. Yuan, Y.-M. Zheng, Enhanced adsorption of arsenite from aqueous solution by an iron-doped electrospun chitosan nanofiber mat: Preparation, characterization and performance. J. Colloid Interface Sci. **535**, 255–264 (2019). https://doi.org/10.1016/j.jcis.2018.09.073
74. L.-L. Min, Z.-H. Yuan, L.-B. Zhong, Q. Liu, R.-X. Wu, Y.-M. Zheng, Preparation of chitosan based electrospun nanofiber membrane and its adsorptive removal of arsenate from aqueous solution. Chem. Eng. J. **267**, 132–141 (2015). https://doi.org/10.1016/j.cej.2014.12.024
75. L.-L. Min, L.-B. Zhong, Y.-M. Zheng, Q. Liu, Z.-H. Yuan, L.-M. Yang, Functionalized chitosan electrospun nanofiber for effective removal of trace arsenate from water. Sci. Rep. **6**(1), 32480 (2016). https://doi.org/10.1038/srep32480
76. T.C. Mokhena, V. Jacobs, A.S. Luyt, A review on electrospun bio-based polymers for water Treatment. eXPRESS Polym. Lett. **9**(10), 839–880 (2015). https://doi.org/10.3144/expresspolymlett.2015.79
77. P. Mondal, C.B. Majumder, B. Mohanty, Laboratory based approaches for arsenic remediation from contaminated water: recent developments. J. Hazard. Mater. **137**, 464–479 (2006). https://doi.org/10.1016/j.jhazmat.2006.02.023
78. S. Moosavi, C.W. Lai, S. Gan, G. Zamiri, O. Akbarzadeh Pivehzhani, M.R. Johan, Application of efficient magnetic particles and activated carbon for dye removal from wastewater. ACS Omega **5**(33), 20684–20697 (2020). https://doi.org/10.1021/acsomega.0c01905
79. D. Morillo Martín, M. Faccini, M.A. García, D. Amantia, Highly efficient removal of heavy metal ions from polluted water using ion-selective polyacrylonitrile nanofibers. J. Environ. Chem. Eng. **6**(1), 236–245 (2018). https://doi.org/10.1016/j.jece.2017.11.073
80. R.Y. Ning, Arsenic removal by reverse osmosis. Desalination **143**, 237–241 (2002). https://doi.org/10.1016/S0011-9164(02)00262-X
81. R.S. Oremland, J.F. Stolz, The ecology of arsenic. Science **300**(5621), 939–944 (2003). https://doi.org/10.1126/science.1081903
82. M. Patel, R. Kumar, K. Kishor, T. Mlsna, C.U. Pittman Jr., D. Mohan, Pharmaceuticals of emerging concern in aquatic systems: chemistry, occurrence, effects, and removal methods. Chem. Rev. **119**, 3510–3673 (2019). https://doi.org/10.1021/acs.chemrev.8b00299
83. M. Pirnie, Technologies and costs for removal of arsenic from drinking water, in *Technologies and Costs for Removal of Arsenic from Drinking Water. EPA USA* 284 (2000)
84. D.-N. Phan, H. Lee, B. Huang, Y. Mukai, I.-S. Kim, Fabrication of electrospun chitosan/cellulose nanofibers having adsorption property with enhanced mechanical property. Cellulose **26**(3), 1781–1793 (2019). https://doi.org/10.1007/s10570-018-2169-5
85. G.S. Pokrovski, S. Kara, J. Roux, Stability and solubility of arsenopyrite, FeAsS, in crustal fluids. Geochim. Cosmochim. Acta **66**, 2361–2378 (2002). https://doi.org/10.1016/S0016-7037(02)00836-0
86. X. Qu, P.J.J. Pedro, Q. Qilin Li, Applications of nanotechnology in water and wastewater treatment. Water Res. 4(7), 3931–3946 (2013). https://doi.org/10.1016/j.watres.2012.09.058
87. A.R. Quaff, M.M. Ashhar, Removal of arsenic (III) by activated tea waste and activated charcoal: a comparative study. J. Indian Water Works Assoc. **37**, 63–69 (2005)
88. P. Ravenscroft, H. Brammer, K. Richards, *Arsenic Pollution: A Global Synthesis* (John Wiley & Sons, 2009). https://doi.org/10.1002/9781444308785

89. D.H. Reneker, I. Chun, Nanometre diameter fibres of polymer, produced by electrospinning. Nanotechnology **7**(3), 216 (1996)
90. F. Ren, J. Meng, Y. Wu, L. Hong, Q. Xia, J. Luo, Determination of arsenic speciation in environmental samples by flow injection hydride generation atomic absorption spectrometry. Yejin Fenxi. **29**, 19–23 (2009). https://doi.org/10.1006/mchj.1999.1713
91. L. Rodríguez-Lado et al., Groundwater arsenic contamination throughout China. Science **341**, 866–868 (2013). https://doi.org/10.1126/science.1237484
92. M. Rosales, O. Coreño, J.L. Nava, Removal of hydrated silica, fluoride and arsenic from groundwater by electrocoagulation using a continuous reactor with a twelve cell stack. Chemosphere **211**, 149–155 (2018). https://doi.org/10.1016/j.chemosphere.2018.07.113
93. R. Rošic, P. Kocbek, S. Baumgartner, J. Kristl, Electrospun Chitosan/Peo Nanofibers and Their Relevance in Biomedical Application, in *5th European Conference of the International Federation for Medical and Biological Engineering*. ed. by Á. Jobbágy (Springer, Berlin Heidelberg, Berlin, Heidelberg, 2011), pp. 1296–1299
94. J. Ruparelia, S. DuttaguptA, A. Chtterjee, S. Mukherji, Potential of carbon nanomaterials for removal of heavy metals from water. Desalination **232**, 145–156 (2008). https://doi.org/10.1016/j.desal.2007.08.023
95. R. Saadi, Z. Saadi, R. Fazaeli, N.E. Fard, Monolayer and multilayer adsorption isotherm models for sorption from aqueous media. Korean J. Chem. Eng. **32**(5), 787–799 (2015). https://doi.org/10.1007/s11814-015-0053-7
96. W. Salomons, U. Forstner, P. Mader, M. Heavy, *Problems and Solutions*. (Springer, Berlin, Germany, 1995)
97. M.A. Sandoval, R. Fuentes, J.L. Nava, O. Coreño, Y. Li, J.H. Hernández, Simultaneous removal of fluoride and arsenic from groundwater by electrocoagulation using a filter-press flow reactor with a three-cell stack. Sep. Purif. Technol. **208**, 208–216 (2019). https://doi.org/10.1016/j.seppur.2018.02.018
98. M.N. Sakib, A.K. Mallik, M.M. Rahman, Update on chitosan-based electrospun nanofibers for wastewater treatment: A review. Carbohydrate Polym. Technol. Appl. **2**, 100064–100080 (2021). https://doi.org/10.1016/j.carpta.2021.100064
99. A. Sarkar, B. Paul, The global menace of arsenic and its conventional remediation -a critical review. Chemosphere **158**, 37–49 (2016). https://doi.org/10.1016/j.chemosphere.2016.05.043
100. N. Savag, M. Diallo, Nanomaterials and water purification: opportunities and challenges. J. Nanoparticle Res. **7**, 331–342 (2005). https://doi.org/10.1007/s11051-005-7523-5
101. R. Sharma et al., Electrospun chitosan-polyvinyl alcohol composite nanofibers loaded with cerium for efficient removal of arsenic from contaminated water. J. Mater Chem. A **2**(39), 16669–16677 (2014). https://doi.org/10.1039/C4TA02363C
102. P.R. Sharma, S.K. Sharma, R. Antoine, B.S. Hsiao, Efficient removal of arsenic using zinc oxidenanocrystal-decorated regenerated microfibrillated cellulose scaffolds. ACS Sustain. Chem. Eng. **7**, 6140–6151 (2019). https://doi.org/10.1021/acssuschemeng.8b06356
103. H.H. Shekarabi, P.A. Azar, A. Javid, A. Hasani, Arsenic (V) removal from aquatic media by electrospun alumina nanofiber. Bul. Chem. Commun. **50**, 88–96 (2018)
104. T.A. Siddique, N.K. Dutta, N.R. Choudhury, Nanofiltration for arsenic removal: Challenges, recent developments, and perspectives. Nanomaterials **10**(7), 1323 (2020). https://doi.org/10.3390/nano10071323
105. A. Sigdel, J. Lim, J. Park, H. Kwak, S. Min, K. Kim, H. Lee, C.H. Nahm, P.K. Park, Immobilization of hydrous iron oxides in porous alginate beads for arsenic removal from water. Environ. Sci. Water Res. Technol. **4**, 1114–1123 (2018). https://doi.org/10.1039/C8EW00084K
106. P.L. Smedley, D. Kinniburgh, A review of the source, behaviour and distribution of arsenic in natural waters. Appl. Geochem. **17**(5), 517–568 (2002). https://doi.org/10.1016/S0883-2927(02)00018-5
107. E. Smit, U. Buttner, R.D. Sanderson, Continuous yarns from electrospun fibers. Polymer **46**, 2419–2423 (2005). https://doi.org/10.1016/j.polymer.2005.02.002

108. S. Song, M. Gallegos-Garcia, Arsenic removal from water by the coagulation process, in *The Role of Colloidal Systems in Environmental Protection.* (Elsevier, 2014)), pp. 261–277. https://doi.org/10.1016/j.chemosphere.2016.05.043
109. P. Song, Z. Yang, G. Zeng, X. Yang, H. Xu, L. Wang et al., Electrocoagulation treatment of arsenic in wastewaters: a comprehensive review. Chem. Eng. J. **317**, 707–725 (2017). https://doi.org/10.1016/j.cej.2017.02.086
110. G. Srinivasan, D.H. Reneker, Structure and morphology of small diameter electrospun aramid fibers. Polym. Int. **36**(2), 195–201 (1995). https://doi.org/10.1002/pi.1995.210360210
111. P. Tan, Y. Zheng, Y. Hu, Efficient removal of arsenate from water by lanthanum immobilized electrospun chitosan nanofiber. Colloids Surf. A: Phys.Chem Eng Asp. **589**, 124417 (2020). https://doi.org/10.1016/j.colsurfa.2020.124417
112. K. Toda, T. Ohba, M. Takaki, S. Karthikeyan, S. Hirata, P.K. Dasgupta, Speciation capable field instrument for the measurement of arsenite and arsenate in water. Anal. Chem. **77**, 4765–4773 (2005). https://doi.org/10.1021/ac050193e
113. P. Udaybhaskar, L. Iyengar, A.V.S.P. Rao, Hexavalent chromium interaction with chitosan. J. Appl. Polym. Sci. **39**(3), 739–747 (1990). https://doi.org/10.1002/app.1990.070390322
114. G. Ungureanu, S. Santos, R. Boaventura, C. Botelho, Arsenic and antimony in water and wastewater: overview of removal techniques with special reference to latest advances in adsorption. J. Environ. Manag. **151**, 326–342 (2015). https://doi.org/10.1016/j.jenvman.2014.12.051
115. D. Vu, X. Li, C. Wang, Efficient adsorption of As(V) on poly(acrylo-amidino ethylene amine) nanofiber membranes. Chin. Sci. Bull. **58**(14), 1702–1707 (2013). https://doi.org/10.1007/s11434-013-5717-2
116. X. Wang, Y. Liu, J. Zheng, Removal of As(III) and As(V) from water by chitosan and chitosan derivatives: a review. Environ. Sci. Pollut. Res. **23**(14), 13789–13801 (2016). https://doi.org/10.1007/s11356-016-6602-8
117. L. Wang, K.A. Fields, A.S. Chen, Arsenic removal from drinking water by ion exchange and activated alumina plants. National Risk Management Research Laboratory, Office of Research and Development, US Environmental Protection Agency (2000)
118. R.C. Weast, *CRC Handbook of Chemistry and Physics*, 64th edn. (CRC Press, Boca Raton, 1984)
119. P.N. Williams et al., Occurrence and partitioning of cadmium, arsenic and lead in mine impacted paddy rice: Hunan. China. Environ. Sci. Technol. **43**(3), 637–642 (2009). https://doi.org/10.1021/es802412r
120. M.H. Wong, *Environmental Contamination: Health Risks and Ecological Restoration.* (United States of America: Taylor & Francis Group, 2012). https://doi.org/10.1007/s10646-013-1104-7
121. F.-C. Wu, R.-L. Tseng, S.-C. Huang, R.-S. Juang, Characteristics of pseudo-second-order kinetic model for liquid-phase adsorption: a mini-review. Chem. Eng. J. **151**(1–3), 1–9 (2009). https://doi.org/10.1016/j.cej.2009.02.024
122. F.-C. Wu, R.-L. Tseng, R.-S. Juang, A review and experimental verification of using chitosan and its derivatives as adsorbents for selected heavy metals. J. Environ. Manag. **91**(4), 798–806 (2010). https://doi.org/10.1016/j.jenvman.2009.10.018
123. Y. Wu, R.L. Clark, Electrohydrodynamic atomization: a versatile process for preparing materials for biomedical applications. J. Biomater. Sci. Polym. Ed. **19**, 573–601 (2008). https://doi.org/10.1163/156856208784089616
124. D. Xie, Y. Ma, Y. Gu, H. Zhou, H. Zhang, G. Wang, Y. Zhang, H. Zhao, Bifunctional NH2-MIL-88(Fe) metal–organic framework nanooctahedra for highly sensitive detection and efficient removal of arsenate in aqueous media. J. Mater Chem. A **5**(45), 23794–23804 (2017). https://doi.org/10.1039/C7TA07934F
125. T. Xu, Y. Cai, K.E. O'Shea, Adsorption and photocatalyzed oxidation of methylated arsenic species in TiO2 suspensions. Environ. Sci. Technol. **41**(15), 5471–5477 (2007). https://doi.org/10.1021/es0628349

126. J.S. Yamani, A.W. Lounsbury, J.B. Zimmerman, Adsorption of selenite and selenate by nanocrystalline aluminum oxide, neat and impregnated in chitosan beads. Water Res. **50**, 373–381 (2014). https://doi.org/10.1016/j.watres.2013.10.054
127. L. Yan, Y.S. Li, C.B. Xiang, Preparation of poly(vinylidene fluoride)(pvdf) ultrafiltration membrane modified by nano-sized alumina (Al2O3) and its antifouling research. Polymer **46**(18), 7701–7706 (2005). https://doi.org/10.1016/j.polymer.2005.05.155
128. R. Yang, K.B. Aubrecht, H. Ma, R. Wang, R.B. Grubbs, B.S. Hsiao, B. Chu, Thiol-modified cellulose nanofibrous composite membranes for chromium (VI) and lead (II) adsorption. Polymer **55**(5), 1167–1176 (2014). https://doi.org/10.1016/j.polymer.2014.01.043
129. R. Yang, Y. Su, K.B. Aubrecht, X. Wang, H. Ma, R.B. Grubbs, B.S. Hsiao, B. Chu, Thiol-functionalized chitin nanofibers for As (III) adsorption. Polymer **60**, 9–17 (2015). https://doi.org/10.1016/j.polymer.2015.01.025
130. A.L. Yarin, S. Koombhongse, D.H. Reneker, Bending instability in electrospinning of nanofibers. J. Appl. Phys. **89**, 3015 (2001). https://doi.org/10.1063/1.1333035
131. F. Zhang, X. Yan, C. Zeng, M. Zhang, S. Shrestha, L.P. Devkota, T. Yao, Influence of traffic activity on heavy metal Concentrations of roadside farmland soil in mountainous areas. Int. J. Environ. Res. Public Health **9**, 1715–1731 (2012). https://doi.org/10.3390/ijerph9051715. doi:10.3390/ijerph9051715
132. S. Zhang, H. Niu, Y. Cai, X. Zhao, Y. Shi, Arsenite and arsenate adsorption on coprecipitated bimetal oxide magnetic nanomaterials: mnFe 2 O 4 and CoFe 2O 4. Chem. Eng. J. **158**(3), 599–607 (2010). https://doi.org/10.1016/j.cej.2010.02.013
133. L. Zhang, Y. Zeng, Z. Cheng, Removal of heavy metal ions using chitosan and modified chitosan: a review. J. Molecul. Liquids **214**, 175–191 (2016). https://doi.org/10.1016/j.molliq.2015.12.013
134. A.I. Zouboulis, K.A. Kydros, K.A. Matis, Arsenic(III) and Arsenic(V) Removal from Solutions by Pyrite Fines. Sep. Sci. Technol. **28**(15–16), 2449–2463 (1993). https://doi.org/10.1080/01496399308019748

Chapter 6
Functionalized Biopolymer Nanocomposites for the Degradation of Textile Dyes

Kiran Kumar Tadi, N. Mahendar Reddy, Ch. G. Chandaluri, Gowri Priya Sakala, and Gubbala V. Ramesh

Abstract In recent years, wastewater treatment has been an utmost important endeavor adopted by several researchers around the globe. The alarming level of contamination caused by the continuous release of organic pollutants/effluents into water bodies from various industries such as textile, pharmaceutical, chemical, etc., has adverse effects in day-to-day life. The catalytic degradation of these organic pollutants (dyes) is a promising approach in the treatment of wastewater. The nanocomposites comprising biopolymers decorated with metal and metal oxide nanopaticles offer better applications due to their superior activity, ease of preparation, abundance, and ecological friendliness. Numerous nanocomposite catalysts have been prepared using variety of biopolymers (such as starch, cellulose, lignin, alginate, chitosan, silk, gelatin, gums, and resins) in combination with various metals/metal oxides/metal sulphides (such as Pd, Ag, Cu, CuO, and AgO) have been utilized for degradation of organic dye pollutants. These research findings encouraged us to write this chapter. Here, we include the recent developments in synthesizing novel biopolymer nanocomposites for degradation of a catalytic textile dye in wastewater treatment.

K. K. Tadi
Centre for Healthcare Advancement, Innovation and Research, Vellore Institute of Technology, Tamilnadu 600127, India

N. M. Reddy · G. V. Ramesh (✉)
Department of Chemistry, Chaitanya Bharathi Institute of Technology (A), Gandipet, Hyderabad, Telangana 500075, India
e-mail: venkataramesh_chm@cbit.ac.in

Ch. G. Chandaluri
Faculty of Chemistry, Humanities and Sciences Division, Indian Institute of Petroleum and Energy, Visakhapatnam, Andhra Pradesh 530003, India

G. P. Sakala (✉)
Department of Chemistry, Indian Institute of Science Education and Research, Pune, Maharashtra 411008, India

M. J. Hato and S. Sinha Ray (eds.), *Functional Polymer Nanocomposites for Wastewater Treatment*, Springer Series in Materials Science 323,
https://doi.org/10.1007/978-3-030-94995-2_6

6.1 Introduction

The word polymer originates from the Greek words “Polus” which means “many” and “meros” which means “parts”. Polymers are aggregates of similar macromolecular units known as monomers. Biopolymers are the polymer obtained from plants, animals, or microbes and are easily degradable [7]. Biopolymers contain monomers of a biomolecule, which are linked together to form larger molecules. The prefix “bio” refers to a biodegradable product produced from biological entities. The expression ‘biopolymer’ can be used to describe a wide range of products commonly obtained from biological sources, such as trees, microorganisms, or plants. Few biopolymers can be derived synthetically from biological sources such as amino acids, resins, vegetable oils, protein, sugars, and fats [34]. Conventional methods for synthesizing polymer nanomaterials use chemical compounds which can later cause toxicity because of their long-term stability.

In comparison, biopolymers typically consist of healthy monomers and are climatically carbon neutral. Biopolymers are complex molecular assemblies with preorganized and well-defined 3D structures in contrast to synthetic polymers, which feature random and straightforward structures. This structural contrast plays a significant role in the activity of biopolymers in vivo. For instance, unfolded quaternary form of hemoglobin cannot transport oxygen; rather, folded quaternary hemoglobin efficiently transports oxygen in the bloodstream [58]. The striking features of biopolymers compared to petroleum-based polymers are their sustainability, biodegradability, efficiency, and mechanical properties. Exposure of these biopolymers to microbes in soil, fertilizer, or sea sediment can readily degrade the biopolymers.

Additionally, this feature considerably lowers CO_2 emissions relative to the traditional combustion methods. The use of biodegradable bio-polymers is also highlighted in the context of mitigating global warming. Biopolymers find applications in engineering electronics, food processing, automotive and aerospace technologies.

Research in polymer nanocomposites plays a crucial role in the trending engineering applications [25]. The mutualistic effect of the composites offers variety of materials with unique characteristics such as thermal stability, mechanical strength, and permeability. When biopolymers are combined with inorganic metal/metal oxide nanostructures, nanocomposites are formed, which possess increased mechanical strength in polymer films. Biopolymers, for example, improve the photocatalytic activity of metal oxide nanoparticles (NPs) by separating the electron and hole pairs and also prevent NP agglomeration during the catalytic process, which is a major concern in nanostructures catalysis. Figure 6.1 summarizes multiple biopolymer sources and photocatalytic activity of biopolymer-metal oxide/sulfide nanocomposites.

Water contamination has been an ongoing concern, which has gained considerable attention around the globe. Many sectors, including leather, paints, cosmetics, food, and textiles, contribute to this alarming water contamination. Textile dyeing and finishing is the most significant contributor to water pollution among these industries. Synthetic textile dyes and other dyes are dumped into rivers which contaminate

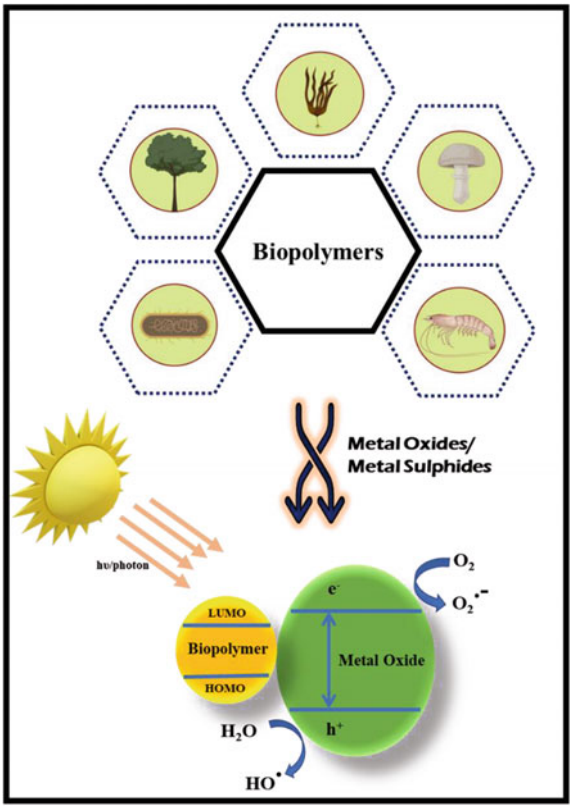

Fig. 6.1 Diagrammatical depiction of multiple biopolymer sources and photocatalytic activity of biopolymer-metal oxide/sulfide nanocomposites

the natural water resources. These dyes lead to a series of problems in the aquatic environment, such as eutrophication, reducing the penetration of sunlight in the water bodies, which affect the photosynthesis of aquatic flora and in turn, hampering the nutrient supply of aquatic organisms. It also gradually increases the bio-oxygen demand for water (BOD) by rising water turbidity and the destruction of the food web [26].

Dyes are incredibly complex, stable, and toxic organic contaminants which can sustain in the atmosphere for a long time. The conventional water treatment processes like adsorption, ultrafiltration, chemical and electrochemical techniques etc., do not readily degrade these pollutants [16]. Although the approaches listed above are not disruptive procedures, they are not called inclusive strategies and transmit water pollutants into the solid phase. Several recent mentions of photocatalysts strategically removing these contaminants as they are eco-friendly, renewable, and generate no toxic by-products. The electron–hole pair is formed upon exposure of the photocatalyst to light, which accelerates the dye degradation reaction. [26] Moreover, inefficient visible light exploitations help restrict practical applications by considering several constraints, including low hydrophobic contaminant adsorption capacity, a

strong aggregation trend, and difficulties in separation and recovery [23]. Therefore, several researchers tried to develop better materials to solve these photocatalyst restrictions by introducing the elementary doping strategy to lessen the band gaps in semiconductors [59], and varying the nanocomposition to extend the rate of recombination with photogenerated carriers [68]. The key goals of this chapter are to provide a detailed introduction to biopolymers, their classification, various sources, and methods of preparation, including various physical and morphological analysis methods used for biopolymers. The synthesis and photodegradation applications of different biopolymer nanocomposites containing metal/metal oxide/metal sulfide will be discussed in the following sections.

6.2 Classification of Biopolymers

The versatility of biopolymers makes them ideal candidates for photocatalytic degradation of dyes in environmental samples. Biopolymers interfaced with nanomaterials and metal-oxides via intermolecular hydrogen bonding. As an example, biopolymeric nanocomposites of starch, alginate, and cellulose incorporated metal-oxides. Moreover, the bandgap of nanomaterials can be easily tuned by various methods. The main advantage of biopolymers capped nanomaterials is that they reduce the bandgap energy and electron–hole recombination rate. Classification of biopolymers is considered based on their origin (natural or synthetic) or their repeating unit (polysaccharides, proteins, nucleotides) or their application (bioplastics, biosurfactant, bioadhesives). Here we consider biopolymers based on their origin of repeating unit and applied for only photocatalytic degradation.

Natural sources such as cotton, wood pulp, silk fabric, and native starch provide various products. Among the various natural biopolymers, cellulose and starches are the most abundant biomass produced. Cellulose is a homopolymer of D-anhydroglucose units (AGU) units linked through 1,4-glycosidic bonds. Interestingly it contains nanodomains crystalline and amorphous regions. Typically chain length of cellulose is expressed in terms of AGU constituents or degree of polymerization (n) that depends on the source and raw materials used during the treatment. The polar groups and molecular structure of cellulose impart hydrophilicity, degradability, chirality, and hydrogen bonding through –OH groups—the ease hydrogen bonding donor activity of cellulose. Moreover, cellulose is relatively stiff and rigid that reflects in its crystallinity and ability to form fibrils.

Chitosan is another important polymer in polysaccharide family and is naturally obtained from shells of crab, shrimp, and krill, by alkaline treatment. Chitosan (2-amino-2-deoxy-ß-D-glucose) has cationic in nature and can be prepared by removing acetyl groups (deacetylation) from chitin in strong alkali. The only difference between chitosan and cellulose is the amine ($–NH_2$) group in position C-2 of chitosan instead of the hydroxyl (–OH) group found in cellulose. Due to the presence of amino functional groups, chitosan is soluble in acidic solvents. The solubility of chitosan

provides an advantage to recycle and reuse the biopolymer nanocomposites. In addition, the positive cation charge of chitosan can easily be electrostatically bound to negatively charged molecules in-particular metal-oxides. Biopolymer composites of chitosan and chitin gained interest in the materials sciences due to their ability to chelate to metal ions, adsorption, and biocompatibility.

An example of a linear polysaccharide is alginate, which is extracted from some species of brown algae. It consists of two uronic acids, namely d-mannuronic acid and 1-guluronic acid. In aqueous solutions, alginate is ionically crosslinked by Ca/Mg divalent cations. When two guluronic acid residues are close enough to make inter- and intra-chain crosslinking is also possible by polyvalent ions. It is reported that alginate embedded with TiO_2 nanocomposites has shown excellent dye degradation properties. Moreover, the nanocomposite was recovered easily from the dyes after treatment due to ease of preparation and its low cost.

Gelatin is a collagen-based biopolymer which used for photocatalytic degradation of dyes. It is biocompatible with ease of chemical modification and crosslinking during preparation of biopolymer nanocomposites. Collagen produces two types of natural gelatin depending on processing conditions. In an alkaline medium, the base attacks the amide groups of asparagine and glutamine and hydrolyses to carboxylic groups. It results in aspartate and glutamate. On the contrary, acidic treatment has no significant effect on the amide linkage. Thus, alkaline treated gelatin contains a higher number of carboxyl groups and, thereby featuring, a low isoelectric point due to negatively charged carboxylic groups. Gelatin nanocomposites also have proven their applications in drug formulations and prostheses.

Guar gum obtained from the ground endosperm of the guar plant (Cyamopsis tetragonolobus). It consists of mannose units attached to galactose. Guar gum is a non-ionic polysaccharide with a d-mannopyranose backbone linked to d-galactose (1–6 linked). It forms a highly viscous gel in water due to its high hydration and swelling rate. Guar gum is used as a liquid oral binder and as a thickening and stabilizing agent in topical pharmaceutical products. It is also for drug delivery, cosmetic formulations, sauces, salad dressing, and other food products. The hydrophilicity of guar agar and thereby its solubility can be tuned for drug releasing capacity to the colons in the large intestine.

Pectin belongs to a non-starch family with linear polysaccharide carbohydrate chains. Its huge structure encompasses an average molecular weight range from 50,000 to 150,000. It is extracted from edible plant materials of citrus fruits and apples. Like guar gum, pectin also forms gels in the presence of acids, sugars, and or calcium ions. Pectin is also used as one of the ingredients in many food products. Pectin is used as an anticoagulant by administered intravenously to control hemorrhage or localized bleeding.

Moreover, it is also used for reducing blood cholesterol. The main advantages of polysaccharides are that they are intact in the physiological environment of the stomach. However, they are degraded by bacteria of the human colon when pectin is administered intravenously.

6.3 Biopolymer Nanocomposites

6.3.1 Introduction to Nanocomposites

Nanocomposites are multiphasic materials comprised of at least two components: a continuous phase and an uncontinuous reinforcement phase. The continuous phase, being a matrix, supports the uncontinuous phase. Generally, polymers are chosen as continuous phase components while nanoparticles with dimensions of the order of 10^{-9} m (10-100 nm) are the components of uncontinuous phase. The recent innovations use a variety of fossil fuel-based, petroleum-based, and synthetic polymers pooled with nanoparticles for several nanotechnological applications [65, 67, 77, 95]. However, these nanocomposites with low biodegradability and inertness pose detrimental effects on the environment. Therefore, substituting the conventional polymers by green materials in these nanocomposites can provide potential applications as they contribute biocompatible, biodegradable, ecofriendly, low dense, and low-cost materials. Furthermore, the biopolymers degrade into biomass, carbon dioxide, or methane which can further serve as a source for carbon and energy in nature.

Biopolymer nanocomposites are typical blends of biopolymers and nanocomposites with significant applications in engineering and technology [58, 89]. The biopolymers are generally obtained from biorenewable resources like plants, animals, bacteria, fungi, algae, etc. Starch, cellulose, lignin, alginate, chitosan, silk, gelatin, gums, resins, etc., are a few examples of biopolymers obtained from biorenewable resources. These biopolymers, upon blending with inorganic metal, metal oxide, metal/metal oxide, metal sulphide, clay nanoparticles etc., result in biopolymeric nanocomposites. Integration of these nanoparticles with biopolymers improves the properties like thermal, mechanical and thermal stability, catalytic, adsorption, the conductivity of the materials, which find applications in water remediation, food packaging, membrane technology, sensors, coatings, adhesives, fuel cells, optic materials, biomedical appliances, tissue engineering, etc. [74]. In this chapter, we will discuss the recent developments in biopolymer nanocomposites used to treat industrial wastewaters.

Water resources, one of the basic needs of life on this earth, are getting contaminated due to rapid industrialization in recent years. As the number of industries increases in leaps and bounds, the water resources are getting contaminated with carcinogenic industrial effluents like dyes, pesticides, heavy metals, etc. Dyes such as rhodamine B (RhB), methyl orange (MO), malachite green (MG), methylene blue (MB), and rose bengal (RB) are released into water resources by textile, paper, leather and cosmetic industries. These dye contaminants influence the color, pH, temperature, chemical oxygen demand (COD), biological oxygen demand (BOD) of water. These organic dye pollutants are resistant to degradation due to the presence of –N = N-,$^{-}$–NO_2, NO, NH_2, NR_2 functionalities. The dye-contaminated water is hazardous to flora and fauna as the dyes restrict the penetration of sunlight, leading to mutagenicity in human beings [4]. Therefore, water remediation becomes essential to obtain clean and safe drinkable water. The common methods for treatment

of industrial wastewaters are filtration, adsorption [63, 90], coagulation and flocculation, membrane separation, oxidation/advanced oxidation, ionic exchange, microbial/enzymatic degradation, catalytic/photocatalytic degradation [20, 30, 60] and other biodegradation processes. These methods have their own merits and demerits, and none of the methods can afford high-quality water. Combining the processes is needed to degrade the contaminants and reduce the sludge formation after their degradation. However, the photocatalytic degradation method provides potential applications [36]. Several polymeric [65, 92], biopolymer materials which include photocatalytic nanoparticles of various metals, are studied for dye degradation applications. In this chapter, we will discuss biopolymeric nanocomposites for water remediation in detail.

6.3.2 Biopolymer-Noble Metal or Metal Nanocomposites

Metal nanoparticles (MNPs) are widely used in nanotechnology. The naked metal nanoparticles with large surface areas can efficiently serve as homogeneous catalysts. However, the formation of agglomerated MNPs reduces the photocatalytic efficacy of these catalysts. Therefore, the immobilization of MNPs into stabilizing matrices can avoid agglomeration and improve photocatalytic efficiency. The matrix-supported MNPs thus serve as heterogenous catalyst systems in electron transfer reactions, attributed to their high fermi potential level and small quantum size effect.

Several noble MNPs like Cu, Ag, Au, and Pd; metals like Fe have been incorporated into various biopolymers through green chemistry strategies for photocatalytic textile dye degradation applications. Copper NPs immobilized on chitosan were fabricated onto cellulose microfibers of a filter paper [39] and cotton cloth [11]. These chitosan-Cu nanocomposites indicated adsorption of Cu^{+2} ions upon treatment with $CuSO_4$ solution on the surfaces. The adsorbed Cu^{+2} ions were converted to Cu^0 NPs by reduction. These Cu NPs in chitosan catalyzed the reductive degradation of methyl orange (MO) and congo red (CR) in the presence of a reducing agent.

Silver (Ag) NPs were incorporated into a conducting polymer, polyaniline (PANI), to enhance the conductivity of the polymer. Further, the Ag doped PANI was grafted onto chitosan to give copolymer nanobiocomposite with enhanced photocatalytic activity towards the degradation of Ponceau BS dye through a mineralization process [82]. The PANI/chitosan/Ag nanobiocomposite was non-toxic, biocompatible as the films clearly showed the growth of food-borne bacteria prominently up to 21 days under a fluorescent microscope. The photocatalytic efficiency and pH dependence of the films in dye degradation was understood by conducting dye degradation experiments under UV light. The films also exhibited good electrical conductivity indicating energy storage applications of films. In another report, Cu, Ag and bimetallic Cu-Ag NPs in varied concentrations were supported by biopolymeric ZCA sheet [42]. The sheet comprised of ZnO-carbon black (ZnO/CB) system embedded in cellulose acetate (CA) polymer. Firstly ZnO/CB nanomaterial was prepared, and then quantitatively varied amounts were dipped into CA solution, which led to the

formation of different ZCA films. These films/sheets were further treated with nitrate salts of Cu, Ag to obtain the MNP adsorbed materials. The catalytic activity of the CuAg/ZCA could be tuned by adjusting the molar concentrations of metal ions. This biopolymer nanocomposite could successfully remove eight pollutants such as o-nitrophenol (ONP), m-nitrophenol (MNP), p-nitrophenol (PNP), 2,6-dinitrophenol (DNP), MO, CR, MB and RB through reduction strategy. Recently, a biopolymer extract, κ-Carrageenan gum (K-CG) was used by a research group for green synthesis of Ag NPs. κ-CG is a polysaccharide gum extracted from seaweeds. The κ-CG, in this case, served as a reducing agent and capping agent for the NPs. Organic dyes, RhB, and MB, were catalytically degraded using this κ-CG-s–Ag NPs [66].

Gold (Au) NPs find applications as visible light-responsive photocatalysts in organic dye degradation processes. Au NPs embedded polymers display enhanced absorption of visible light due to the interband electronic transition from 5d to 6sp. Therefore, the Au NPs serve as active sites on the immobilized polymer support and reduce O_2 and hydroxyl groups. An efficient chitosan/Au nanocomposite, cl-Ch-p(DEAEM)/Au was developed for functional photocatalytic organic dye degradation [56] Fig. 6.2. Chitosan was crosslinked to 2-(diethyl amino) ethyl methacrylate

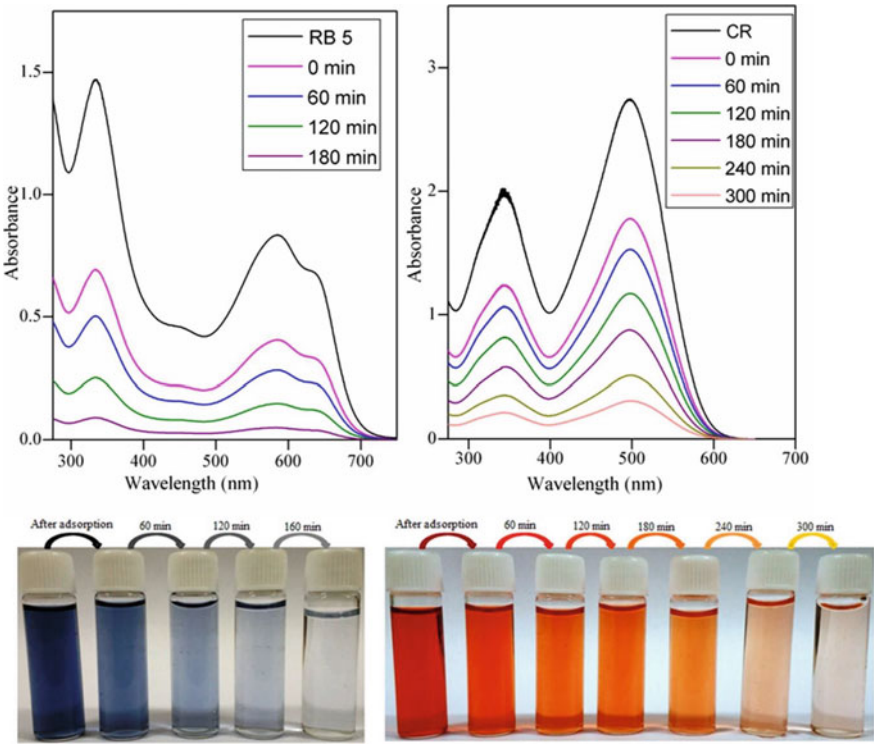

Fig. 6.2 Degradation of dyes (RB5, CR) under sunlight for cl-Ch-p(DEAEM)/Au nanocomposite. Reproduced with permission from [56]. Copyright 2016, Wiley

(DEAEM) through a linker, diethylene glycol. The resultant copolymer is featuring pendant $–NH_2$ groups aided in the reduction Au(III) to Au(0) in situ, which catalyzed the dye degradation process. The nanocomposite readily adsorbed CR and RB 5 dyes at pH 5 due to electrostatic attraction between the cationic adsorbent ($–NH^+$ groups on biopolymer nanocomposite) and anionic adsorbate (SO_3^- groups on dye). Experimental results revealed that cl-Ch-p(DEAEM)/Au nanocomposite could be recycled up to four cycles.

Palladium (Pd) NPs also have been used for photocatalytic dye degradation applications. The incorporation of Pd NPs into carboxymethyl cellulose (CMC) following a green approach, wherein CMC served as both reducing and the stabilizing agent, was reported [46]. Here, Pd NPs were enveloped by CMC thin films and stabilized by ligation of hydroxyl groups present on cellulose. The Pd NPs of desired size and morphology could be achieved by monitoring the concentration of CMC, pH, reaction time and temperatures, through UV–Vis absorption studies. The synthesized Pd-CMC nanocomposite showed good stability for more than a year and high catalytic activity mainly towards azo dyes ($–N=N^-$). The stability of the Pd NPs was evident from the zeta potential measurements of colloidal suspension, which was − 56.2 mV. The specific catalytic activity of the nanocomposite towards azo dyes in the presence of a reducing agent was studied using a model dye, p-Aminoazobenzene (pAAB), which featured a single azo bond.

Further, the nanocomposite was tested for its catalytic activity using acid dyes-acid red 66 (AR66), acid orange 7 (AO7), and two reactive dyes- scarlet 3G (S3G), reactive yellow 179 (RY179), which revealed a promising catalytic activity. Another report by Arslan et al. mentions the use of Pd NPs as a catalyst, supported on chitosan gel-multi walled carbon nanotubes (MWCNT) biopolymer composite [73]. It was used specifically for catalytic degradation of nitro functional pollutants like 4-nitrophenol, 2-nitroaniline, 4-nitro-o-phenylenediamine, and 2,4-dinitrophenol, and azo dyes like CR, MO, MB, and MR in water remediation technology. The authors used chitosan hydrogel-MWCNT, which supported the conversion of Pd(II) to Pd(0) in situ and resulted in Pd(0)-crosslinked chitosan-MWCNT beads or Pd NPs@chitosan-MWCNT. The UV–Vis absorption studies clearly showed that Pd NPs@chitosan-MWCNT catalyzed the reductive degradation of CR, MO, MB, or MR dyes, initiated by reducing agent at room temperature within no time.

Iron (Fe) NPs were synthesized using green tea leaf extracts (GT-Fe). The green tea leaf extracts contain polyphenols, which act as both reducing and capping agents. GT-Fe was used to remove cationic MB and anionic MO dyes through the Fenton-like oxidation method [76]. A comparative study between GT-Fe and non zero-valent (nZVI) iron prepared using a reducing agent by the authors revealed that the performance of GT-Fe was much better than the prepared nZVI in the dye degradation process. Abbasi's research group reported a green method for the synthesis of clay-supported nano iron particles (CnIPs, < 100 nm), which were immobilized into green tea extracts to obtain GT-CnIP [2]. The as-prepared GT-CnIPs were successfully employed in the removal of MG from water. The CnIPs were treated water was further tested for phytotoxicity, which revealed a higher germination percentage with *V. radiata* seeds.

6.3.3 Biopolymer-Nonmetal Nanocomposites

Nonmetal NPs such as carbon black (CB), doped carbon materials, graphene oxide (GO) are also used for textile dye degradation applications. Chitosan/carbon black (Chit/C) and poly(vinyl alcohol)/carbon black (PVA/C) films were compared for photocatalytic degradation of CR [12]. Here, the authors studied the effect of polymeric matrix on the performance of the semiconductor photocatalyst, by choosing a biopolymer, chitosan and a biodegradable polymer, PVA. The polymer-nanocomposite films were prepared by spreading a solution of carbon black NPs (95 nm) on the polymer matrix, followed by evaporating the solvent. Both Chit/C and PVA/C showed similar trends in their photocatalytic degradation of CR in visible light. The efficiency of the catalytic films was observed at pH 6 and 8 mg/L of dye concentration. The rate of degradation was directly proportional to the intensity and time of exposure to light. Chitosan-based graphitic carbon nitride (g-C_3N_4-CS-x) beads, obtained by crosslinking was utilized as a photocatalyst [100]. The authors used g-C_3N_4 which has a narrow bandgap of 2.7 eV and visible absorption capacity, as a catalyst for dye degradation. g-C_3N_4 granules were uniformly distributed on the surface of the chitosan matrix as implied by the characterization techniques-scanning electron microscopy (SEM), diffuse reflectance spectroscopy (DRS), X-ray photoelectron spectroscopy (XPS). Photodegradation of MB under visible light, using g-C_3N_4-CS-3 in appropriate ratio followed first order reaction kinetics. 97% dye degradation was observed even after five cycles which indicates the stability and efficacy of the designed catalyst. Aditionally, the mechanism of photocatalysis was implicit by addition of radical scavengers such as BQ for O_2^-, IPA for. OH and TEOA for holes (h^+), which substantially decreased the rate of dye degradation indicating. O_2^- and h^+ as active species involved in photodegradation of the dye.

6.3.4 Biopolymer-Metal Oxide Nanocomposites

Semiconductor photocatalysts such as TiO_2 (band gap energy: 3.2 eV) [8], V_2O_5 (2.8 eV), $SrTiO_3$ (3.4 eV), Fe_2O_3 (2.2 eV), SnO_2 (3.5 eV), WO_{3-x} (2.6–3.0 eV), Nb_2O_5 (3.4 eV), and ZnO (3.37 eV) are known for applications in wastewater treatment systems [15]. Although several metal oxide NPs are used, biopolymers involving TiO_2 [29] and ZnO NPs play a significant role owing to their low-cost availability and efficiency [48].

6.3.4.1 Biopolymer TiO_2 Nanocomposites

TiO_2 catalyst with a bandgap of 3.2 eV, absorbing a photon act as a semiconductor in dye contaminated water treatment. It effectively degrades toxic pollutant dyes through an auto-oxidation process (AOP) involving chemical, photochemical or

photocatalytic generation of hydroxyl ions (–OH) continuously. The –OH ions are powerful oxidants that degrade the organic molecules into CO_2, H_2O, etc. However, in the absence of dye molecules, recombination of TiO_2 is observed, which reduces the efficiency of the catalyst. Biopolymer supporting matrices like chitosan, cellulose, etc., continuously provide the target dye molecules and avoid recombination of catalyst in photocatalytic conversions.

A report mentions the use of chitosan/TiO_2 (CTC) biopolymer nanocomposite for the degradation of anionic Reactive red 2 (RR 2), cationic MB, and zwitterionic RB dyes under UV light [27]. Using this catalytic system in combination with an oxidant revealed enhanced reaction rates due to in situ capturing of electrons by the oxidant. This process thus avoided the recombination of catalysts. When dye-contaminated water was treated with CTC and irradiated, COD values were significantly reduced. The catalytic system followed pseudo first-order kinetics according to the Langmuir–Hinshelwood model. Similarly, many research groups used a combination of polymer/biopolymers or grafted chitosans to immobilize TiO_2 catalysts. A few examples are listed here, chitosan/poly(methacrylic acid) (PMA) microparticles (Ch/PMA/TiO_2; chitosan grafted to acrylic acid (CA/TiO_2 or CATN) were persistent organic dyes in water [53]. Similarly, sodium alginate-TiO_2 and bentonite-TiO_2 (NaAlg/TiO_2/bentonite), in combination with 9.2 wt% of TiO_2 (35 nm) was used for degradation of MB by 91% at pH 8 in 30 min under UV light [81].

A research group compared the photocatalytic activity of commercially available Degussa P25 TiO_2 (25 nm) and colloidal TiO_2 NPs (6 nm). Both the NPs were immobilized into/onto chitosan either by dip coating or impregnation into chitosan hydrogel. Chitosan hydrogel/TiO_2 nanocomposite obtained by dip-coating method showed better degradation of AO7 under UV conditions [50]. As observed by SEM images, the dip dip-coated nanocomposites indicated smaller pore size with a uniform spread of colloidal TiO2 NPs along the walls. The photodegradation experiments indicated better efficiency of colloidal TiO_2 compared to commercially obtained NPs. In a few cases, modified TiO_2 NPs were grafted onto biopolymer supports to achieve the maximum efficiency of the catalyst. In this line, anatase TiO_2 NPs were grafted to cellulose at low temperatures, and then the NPs were immobilized into clay, i.e., montmorillonite (MMT). Cellulose, in this case, served as an adsorbent and subsequently aided the accumulation of dye on the catalysts surface during photocatalysis of MO. The as-prepared cellulose-g-p4VP/MMT/TiO_2 followed pseudo-first-order kinetics according to the experimental data. It is noteworthy that the addition of clay particles enhanced the adsorption-degradation performance of catalyst and also aided in regeneration of the biopolymer nanocomposite [51]. Meena and coworkers recently reported a sustainable material from seaweed (κ-Carrageenan, ι-Carrageenan and λ-Carrageenan) template, carbon- and sulfur-doped TiO_2. Carrageenans are rich in carbon, sulfur, sodium, and calcium in their matrix. κ-S-TiO_2, ι-S-TiO_2, λ-S-TiO_2 were prepared through hydrothermal calcination. Dye degradation experiments using these modified TiO_2 materials were conducted using solar concentrators. λ-S-TiO_2 showed better photocatalytic performance compared to κ-S-TiO_2 and ι-S-TiO_2 in degradation of MO, MB, and RB [18]. Similarly, a bio nanocomposite hydrogel (TGB-hydrogel) comprised of TiO_2 nanorods and a

biopolymer, gum ghatti (Gg) was used for the removal of a toxic dye, brilliant green (BG). The free radical graft polymerization technique prepared the TGB-hydrogel. The Gg-based TBG-hydrogel showed excellent dye adsorption and degradation. In a circular approach, the bio nanocomposite with the adsorbed dye was processed at high temperature and then used for photocatalytic degradation of ciprofloxacin, a second model pollutant [44], Fig. 6.3.

Interestingly, Krause et al. developed a system with dual properties i.e., biocatalytic and photocatalytic properties for dye degradation. They used bacterial cellulose (BC), a natural polymer obtained by fermentation of *Komagataeibacter xylinus* as

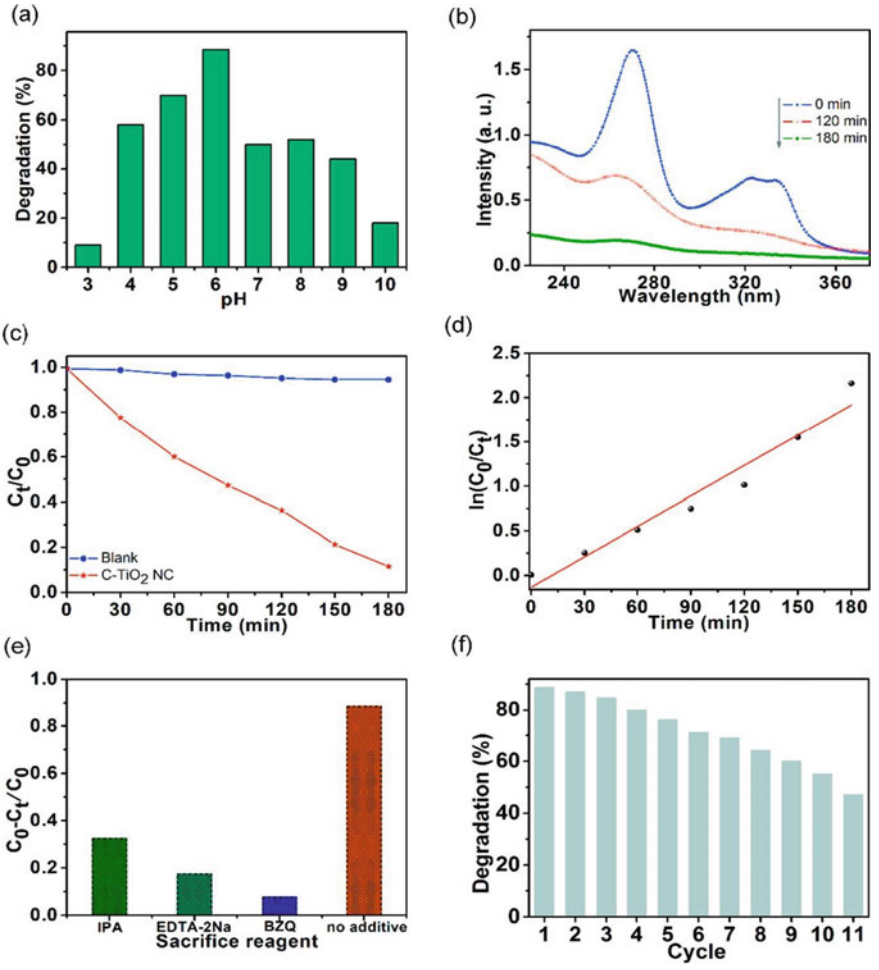

Fig. 6.3 Adsorption and photocatalysis processes using BC/MoS_2 membranes are shown schematically. Reproduced with permission from [44]. Copyright 2018, American Chemical Society

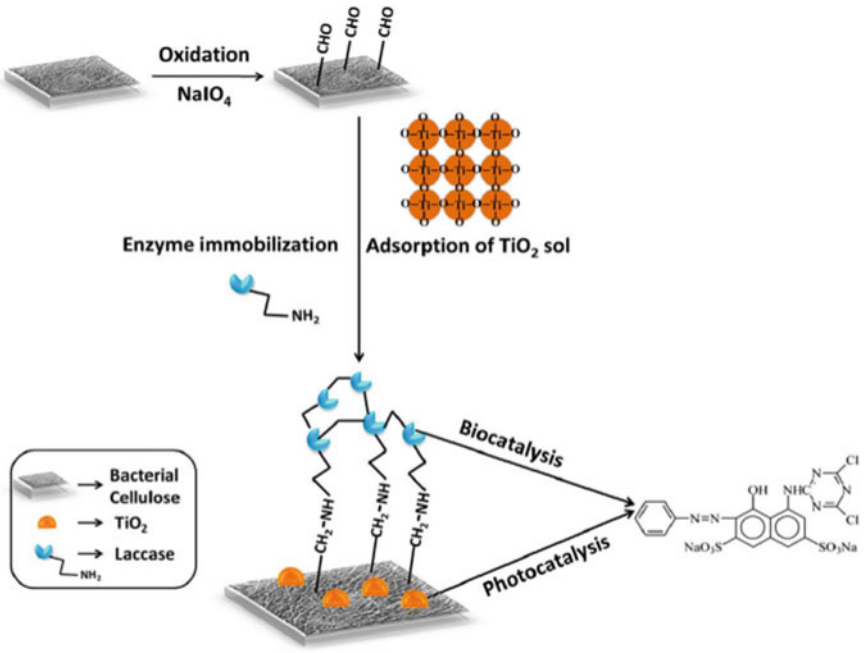

Fig. 6.4 Schematic representation of modification of BC and preparation of OBC/TiO_2-Lac membrane for dye removal applications. Reproduced with permission from [47]. Copyright 2017, Elsevier Science Ltd

matrix; an enzyme, Laccase (Lac) as biocatalyst, and TiO_2 as photocatalyst in their design Fig. 6.4 [47].

BC provides improved mechanical strength by inducing hydrophilicity and surface area to volume ratio, featuring a fibrous network with hydroxyl groups. These hydroxyl groups serve as binding sites for TiO_2 and Lac through hydrogen bonding and crosslinking, respectively. TiO_2 was co-immobilized onto BC-Lac membranes to result in a composite material, i.e., OBC/TiO_2-Lac. The co-immobilization of both Lac and TiO_2 was confirmed by morphological characterization using SEM, AFM, and FTIR. Extensive studies were done, comparing the materials in native state and the bio composite to understand the optimal pH, temperature, thermal stability and reusability of the material which revealed the highest rate of photocatalysis at pH 2.5 and temperature of 50 °C. The OBC/TiO_2-Lac system showed 95% degradation of X-3B dye efficiently under UV light within 3 h with a relative activity of 67% up to ten cycles.

6.3.4.2 Biopolymer-ZnO Nanocomposites

ZnO is an n-type semiconductor with bandgap of 3.37 eV, which shows high electron mobility, good transparency, strong luminescence, and potential photocatalytic dye degradation applications. ZnO, in combination with cellulose nanofibres (CNF), was used as a photocatalyst for the degradation of MB [22]. Derivatives of the composite were prepared by varying the amounts of either ZnO or CNF through in situ precipitation method. The composites were analyzed using SEM, SAXS, zeta potential, FTIR, and XRD techniques. According to SEM, the size of ZnO NPs was distributed between 30 and 500 nm (mostly 200 nm). The SAXS experiment revealed that the composite loaded with higher amounts of ZnO exhibited isotropic scattering, unlike the samples with a lower amount of ZnO, which exhibited anisotropic scattering. An increase in dye adsorption was observed with an increase in the amounts of ZnO and CNF in the samples. Also, an increase in ZnO content resulted in more negative zeta potential values indicating the stability of the system. The photodegradation was fast in case of 0.3 M $Zn(Ac)_2{\cdot}2H_2O$, 1.5 M NaCl, 1 wt % CNF and 0.4 M $Zn(Ac)_2{\cdot}2H_2O$, 2 M NaCl, 1 wt % CNF where the bleaching of MB was observed to be 99% within 20 min. In another way, ZnO NPs were synthesized in the green route using Quince seed mucilage which acted as a reducing and stabilizing agent at calcination temperatures. This material removed over 80% of MB photo catalytically [84].

Alginate/carboxymethyl cellulose (CMC)/ZnO nanocomposite or alginate/CMC/ZnO gel was used for heterogeneous photocatalysis of CR dye. Alginate and cellulose, with porous nature and stability towards the light, improved the photocatalytic activity of ZnO [69]. The gel obtained upon crosslinking was washed thoroughly to remove excess barium ions and was subjected to freeze-drying. Characterization of the gel by SEM, TEM, XRD, FTIR, EDX indicated the attachment of ZnO NPs on the fibrous material of alginate/CMC. The size of these ZnO NPs in the nanocomposite according to the TEM analysis was 28 nm. The optimum condition for photocatalytic degradation of CR was observed when 60 mg of nanocomposite (alginate/CMC:ZnO ratio 1:0.8) was used at pH 3 for 110 min. Reusability of the nanocomposite was observed in 3 cycles which showed the degradation percentage of about 90.12%, 78.82%, and 69.63% in each cycle, respectively.

In a recent report, GO, which has high conductivity (16,000 s/m) and surface area (2600 m^2/g), was used to enhance the photocatalytic efficiency of ZnO. A nanocomposite, ZnO/Ch/GO, was developed for the photodegradation of AO7 [78]. SEM analysis of composites supported the formation of ZnO nanospheres (30–40 nm) on the nonporous and smooth surface of chitosan. In acidic conditions, ready adsorption of negatively charged dye was observed as the bio nanocomposite acquired a positive charge. Efficient photodegradation of AO7 was observed at pH 4, with 20 mg of composite at 20 ppm of dye concentration in 75 min. 97.5% degradation of AO7 was observed using ZnO/Ch/GO which followed pseudo first order kinetics.

Few other metal oxide NPs like Fe_2O_3, MnO_2, and SnO_2, are also used in the following biopolymer nanocomposites for photocatalytic degradation of dyes. A spindle-like Fe_2O_3/C composite was bio templated using agarose for photocatalytic

degradation of MB [98], wherein the carbon acted as an electron transfer channel to improve the conductivity of metal oxide photocatalyst. Another comparative study with Fe_2O_3 nanocomposites using a biopolymer (rice straw)-RSFS and a conducting polymer (polyindole)-PIFS, was attempted to evaluate the photocatalytic performance. Both the materials showed similar degradation of CR dye [55]. A cellulose film containing MnO_2 NPs [64] was used for photobleaching of Indigo carmine in 25 min under ambient light conditions. The film could be reused with high efficiency up to 10 times. Also, Chitosan-SnO_2 nanocomposite (Ch-SnO_2) was used in photocatalysis of MO and RhB in water at different wavelengths of UV light [30].

6.3.5 Biopolymer Metal/Metal Oxide Nanocomposites

Further, another complex hybrid material, CS/AgCl/ZnO hydrogel beads, was prepared by a research group to remove MB and photocatalytic inactivation of *E. coli* and *S. aureus*. from water [85]. AgCl/ZnO nanocomposite suspension was added to chitosan to obtain hydrogel beads. SEM images of these beads indicated the size of ZnO, AgCl ranging between 20 and 40 nm. EDAX, X-ray diffraction, TGA analysis confirmed the immobilization of AgCl/ZnO onto chitosan successfully. The hydrogel beads showed high photocatalytic efficiency at pH 11 with an optimal 1.5 g catalyst with the reusability of up to six cycles. In addition, the composite was able to inactivate microorganisms like *E. coli* and *S. aureus* under visible light conditions. This can be attributed to the fact that AgCl gets activated under visible light and generates charge carriers, i.e., electrons. These electrons get transmitted to the conduction band of ZnO from AgCl, generating holes in the valence band of AgCl, which inactivates the bacteria. Similarly, CS-ZnO/CuO membrane [13] and ZnO/CuO@Alg [32] bio nanocomposites were also prepared for photocatalytic degradation of fast green dye and *p*-nitrophenol, respectively. Silver-nickel oxide/calcium alginate hydrogel beads (Ag@NiO/Alg) were used for the photoreduction of RhB and MO [41]. The authors used Ag NPs here to enhance the catalytic activity of NiO in the biopolymer nanocomposite.

6.3.6 Biopolymer-Metal Sulfide Nanocomposites

Metal sulfides provide promising visible light photocatalytic applications compared to metal oxides as they possess smaller band gaps. CuS is a p-type semiconductor with a bandgap of 1.2–2.0 eV, which finds applications as photocatalyst. A multifunctional composite paper using lignin, xylan or starch biopolymers as stabilizers for the in situ precipitation of CuS nanocomposites on CNF was used for photodegradation [35]. The composite paper with starch, i.e., CuS/starch/CNF, was observed to provide better distribution of CuS revealing high electrical conductivity and photocatalytic activity towards RhB with the highest rate constant. The modified papers

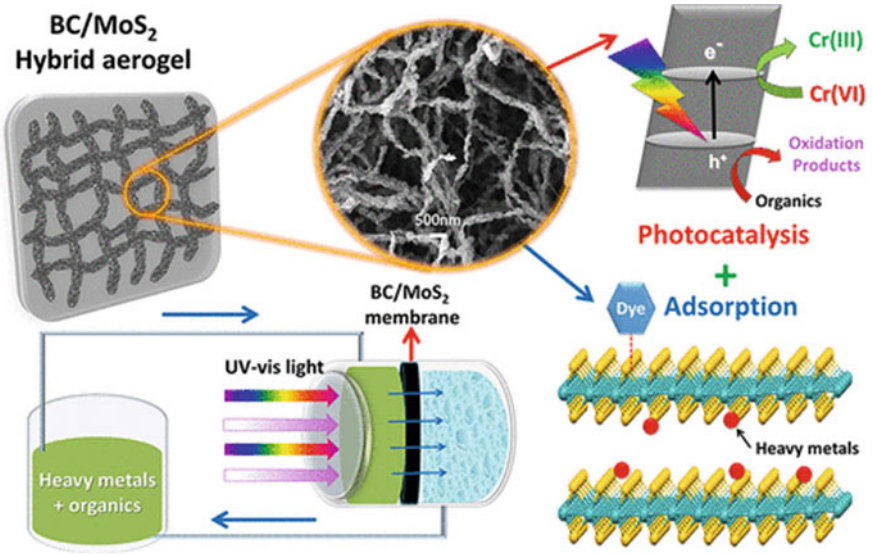

Fig. 6.5 Schematic representation of BC/MoS_2 membrane preparation and its application in adsorption and photocatalysis processes. Reproduced with permission from [28]. Copyright 2020, American Chemical Society

also showed excellent reusability up to at least 10 cycles. Another group reported a cellulose-supported $CuInS_2$ nanocomposites (Cel-CIS) obtained by hydrothermal strategy without using any surfactant or template [86]. Cel-CIS was successful in the degradation of RhB in the presence of visible light.

Rebeiro's group reported bifunctional hybrid aerogel material, BC/MoS_2 membrane that has applications in photocatalysis and heavy metal adsorption, Fig. 6.5 [28]. The smaller bandgap observed for MoS_2, i.e., 1.4–1.9 eV, enables visible light photocatalysis. Also, MoS_2 exhibits a layered structure composed of stacked 2D nanosheets possessing several sulfide sites. These sulfide sites can adsorb organic or inorganic contaminants through hydrophobic, electrostatic, or complexation interactions. The heavy metal adsorption of MoS_2 can be attributed to the soft–soft chemical interactions with heavy metals such as Pb^{+2}, Hg^{+2}, Cd^{+2} (Pearson's soft acids). BC/MoS_2 hybrid aerogel membrane could successfully remove organic pollutants like MB dye up to 99% and inorganic heavy metals such as Cr(VI) in 120 min..

6.3.7 Other Types of Biopolymer Nanocomposites

A nanocomposite with gelatin as biopolymer and Zirconium (IV) phosphate as an inorganic nano photocatalyst was used for dye degradation and antimicrobial applications in water [87]. The nanocomposite was prepared using the sol–gel method and

was well characterized. Dyes like FG, MB were photo reduced by GT/ZP nanocomposite up to 89.91% and 87.81% within five hours. In addition, GT/ZP acted as an antimicrobial material efficiently towards *E. coli*. Khan et al. recently developed a nano photocatalyst which is a ternary metal selenide (TMS), BiCuSe, coated with chitosan. The chitosan coating on TMS resulted in chitosan microspheres (TMS-MS) which prevented the leaching, dispersion, and dissolution of these NPs and avoided the formation of any sludge/ secondary pollutant in dye contaminated water samples [10]. The size of the TMS NPs was observed to be 33 nm. After encapsulation, TMS-MS displayed a porous surface with a pore size of 0.5 μm. This porous material significantly contributed to the photocatalytic activity of TMS-MS by allowing the passage of sunlight through these pores, which led to the activation of the TMS NPs. The chitosan encapsulation also minimized the probability of recombination of the valence band and conduction band, rendering a stable catalyst. The bandgap of TMS-NPs was calculated to be small, i.e., 1.8 eV, when compared to many other catalysts such as ZnO and TiO_2. The photocatalytic activity of the TMS-CM bio nanocomposite was studied using Alizarin red S (ARS) dye. It was observed that the catalyst degraded the dye, following first order kinetics, to a maximum extent of 95% at pH 4 in 180 min. The catalyst was also recyclable up to six times with a maximum efficiency of 86.7%.

The biopolymer nanocomposites reported to date for photocatalytic applications in wastewater treatment are listed in Table 6.1.

6.4 Conclusions

The advantages of catalysts made of both biopolymers and metal/metal oxide nanoparticles are enormous. The research endeavors are progressively increasing to prepare and evaluate these nanocomposites as efficient catalysts for many applications. Herein, the attempt was made to describe the biopolymers, nanoparticles, and importance of wastewater treatment in the introduction part. Then the preparation of various composite catalysts using various biopolymers and metal/metal oxide nanoparticles. The efficacy of these catalysts for the degradation of organic dye pollutants was documented. Both the catalytic reductive and photocatalytic degradation of organic dye pollutants was described with brief mechanisms and various applications. However, still many challenges are to be addressed in turn to transform these catalytic systems for commercial and large-scale applications.

Table 6.1 Comparison of photocatalytic degradation activity of biopolymer nanocomposites

S. No	Type of nanocomposite (Catalyst/ Biopolymer)	Degraded dyes	Time	References
1	Silver nanoparticles/ κ-carrageenan	Rhodamine B, and methylene blue	–	[66]
2	Palladium (Pd)/ chitosan-MWCNT catalyst	Congo red	2 min	[73]
		Methyl orange	1 min	
		Methylene blue	Instantly	
		Methyl red	Instantly	
3	Silver Nanoparticles/ Gelatin	Methyl orange	6 min	[38]
4	Copper Nanoparticles/ Carboxymethyl Cellulose/ Bacterial Cellulose Nanofibers	Methylene blue	6 min	[37]
5	Ag/agar	Methylene blue	20	[24]
		Methyl orange	40	
6	Ag-Au/agar	Methylene blue	20	
		Methyl orange	40	
7	Ag-Au–Pd/agar	Methylene blue	4	
		Methyl orange	4	
8	Copper nanoparticles/Chitosan-coated cotton cloth	Congo red	12	[11]
9	Ag-nano/ polyaniline/chitosan	Poncaeu BS	60	[83]
10	Palladium nanoparticles/glucuronoarabinogalactan	Coomassie brilliant blue G-250	2	[43]
		Methylene blue	2	
		Rhodamine B	2	
11	Palladium nanoparticles/ carboxymethyl cellulose	p-Aminoazobenzene, acid red 66, acid orange 7, scarlet 3G and reactive yellow 179	5 s	[46]
12	Silver nanoparticles/ Guargum	Reactive blue -21,	2	[93]
		Reactive red-141,	30	
		Rhodamine 6G	300	
13	Ag@ anatase TiO_2 nanocomposites/ gum acacia	Malachite Green	30	[70]
14	Cu nanoparticles/ chitosan	Methyl orange	13	[39]
		Congo red	17	
15	Pd/CdS/ wool	Rhodamine B	210	[96]
16	ZnO/Cellulose	Methylene blue	10	[22]
17	Titanium (IV) oxide/ sodium alginate	Basic blue 41	180	[62]

(continued)

Table 6.1 (continued)

S. No	Type of nanocomposite (Catalyst/ Biopolymer)	Degraded dyes	Time	References
18	TiO_2/ chitosan/hydroxyapatite	Methylene Blue,	40	[94]
		Rhodamine B	60	
19	ZnO/chitosan	Crystal violet	210	[1]
20	ZnO/ Quince seed mucilage	Methylene blue	120	[84]
21	Manganese dioxide/ cellulose	Indigo Carmine	25	[64]
22	TiO_2/ Chitosan	Malachite green	240	[17]
23	TiO_2/ polylactic acid	Methyl orange	24 h	[72]
24	Cu_2O/ Graft Gum Ghatti	Naphthol Blue Black	60	[14]
25	TiO_2/ calcium-alginate	Methylene blue	24 h	[45]
26	TiO_2/ chitin	Methylene blue	195	[21]
27	TiO_2/ Chitosan	Methylene orange	180	[3]
28	TiO_2/ Chitosan	C.I. Acid Orange7, C.I. Acid Red18, C.I. Acid Blue113, C.I. Reactive Black5, C.I. Direct Blue78	2–24 h	[50]
29	TiO_2/ bacterial cellulose	Reactive red X-3B	180	[47]
30	CuO/Chitosan	Rhodamine B	60	[75]
31	Niobium (V) oxide/ chitosan	Indigo carmine	30	[91]
32	zinc oxide/ pullulan	Methyl orange	300	[57]
33	ZnO/carbon black/ cellulose acetate/ CuAg nanoparticles	Methyl orange (MO),	12	[42]
		Congo red (CR),	19	
		Methylene blue (MB),	13	
		Rhodamine B (RB)	14	
34	$H4SiW_{12}O_{40}$/cellulose acetate	Methyl orange	120	[49]
35	Fe_2O_3- and Fe_3O_4-modified TiO_2/ Alginate	Methylene blue	120	[19]
36	CeO_2-Bi_2O_3/ chitosan	Acid Blue 113	360	[54]
37	ZnO, AgCl, AgCl/ZnO, / chitosan	Methylene blue	135	[85]
38	Ce(IV)$MoPO_4$/ Gum Acacia	Methyl violet	120	[79]
39	BSA(bovine serum albumin)-Cu complex/ laccase	Malachite green	30	[71]
40	O-carboxymethyl chitosan Schiff bases and their Cu (II) complexes	Methylene blue	90	[52]
41	Co^{2+}@PEM-MSNP, Fe^{2+}@PEM-MSNP Mn^{2+}@PEM-MSNP Polyelectrolyte-coated Mesoporous silica Nanoparticles (Metal@PEM-MSNPs)	Morin dye	5	[99]

(continued)

Table 6.1 (continued)

S. No	Type of nanocomposite (Catalyst/ Biopolymer)	Degraded dyes	Time	References
42	Gelatin-Zr (IV) phosphate	Methylene blue (MB)	5 h	[87]
		Fast green (FG)		
43	Pectin/Graphene Oxide (Pc/GO)	Methylene blue (MB)	25	[40]
		Methyl orange (MO)	90	
44	Multi-walled carbon nanotube coupled β-Cyclodextrin/PANI hybrid	Crystal Violet (CV)	120	[33]
45	C_3N_4 supported on chitosan	Methyl orange (MO)	30	[88]
46	$CoFe_2O_4$@Methylcelloluse	Reactive Blue 19	30	[61]
47	Chitosan-Ascorbic Acid@$NiFe_2O_4$	Malachite green	240	[31]
48	Pd NPs@chitin	Acidic blue 193	15	[6]
49	ZnS/chitosan	Acid brown 5G and acid black 2BNG	120	[9]
50	TiO_2@CS-Hpt	MB ad RhB	60	[94]
51	Iron–bismuth selenide/ chitosan	Crystal violet	150	[5]
52	FeNiSe/ Chitosan	Congo red	140	[97]
53	Chitosan-La^{3+}-graphite	Methylene blue	40	[80]

References

1. B. Abarna, T. Preethi, G.R. Rajarajeswari, Single-pot solid-state synthesis of ZnO/chitosan composite for photocatalytic and antitumour applications. J. Mater. Sci.: Mater. Electron. **30**(24), 21355–21368 (2019). https://doi.org/10.1007/s10854-019-02512-5
2. R. Abbassi, A.K. Yadav, N. Kumar, S. Huang, P.R. Jaffe, Modeling and optimization of dye removal using "green" clay supported iron nanoparticles. Ecol. Eng. **61**, 366–370 (2013). https://doi.org/10.1016/j.ecoleng.2013.09.040
3. S. Afzal, E.M. Samsudin, N.M. Julkapli, S.B.A. Hamid, Controlled acid catalyzed sol gel for the synthesis of highly active TiO2-chitosan nanocomposite and its corresponding photocatalytic activity. Environ. Sci. Pollut. Res. **23**(22), 23158–23168 (2016). https://doi.org/10.1007/s11356-016-7507-2
4. R. Ahmad, R. Kumar, Adsorptive removal of congo red dye from aqueous solution using bael shell carbon. Appl. Surf. Sci. **257**(5), 1628–1633 (2010). https://doi.org/10.1016/j.apsusc.2010.08.111
5. W. Ahmad et al., Photocatalytic degradation of crystal violet dye under sunlight by chitosan-encapsulated ternary metal selenide microspheres. Environ. Sci. Pollut. Res. **28**(7), 8074–8087 (2021). https://doi.org/10.1007/s11356-020-10898-7
6. H.B. Ahmed, N. Saad, H.E. Emam, Recyclable palladium based nano-catalytic laborer encaged within bio-granules for dye degradation. Surfaces Interfaces **25**, 101175 (2021). https://doi.org/10.1016/j.surfin.2021.101175
7. F. Ajalloueian et al., Emulsion electrospinning as an approach to fabricate PLGA/chitosan nanofibers for biomedical applications. BioMed Res. Int. **2014**, 475280 (2014). https://doi.org/10.1155/2014/475280
8. A. Ajmal, I. Majeed, R.N. Malik, H. Idriss, M.A. Nadeem, Principles and mechanisms of photocatalytic dye degradation on TiO2 based photocatalysts: a comparative overview. RSC Adv. **4**(70), 37003–37026 (2014). https://doi.org/10.1039/C4RA06658H

9. A. Alharbi et al., Facile synthesis of novel zinc sulfide/chitosan composite for efficient photocatalytic degradation of acid brown 5G and acid black 2BNG dyes. Alex. Eng. J. **60**(2), 2167–2178 (2021). https://doi.org/10.1016/j.aej.2020.12.025
10. N. Ali et al., Selenide-chitosan as High-performance nanophotocatalyst for accelerated degradation of pollutants. Chem. Asian J. **15**(17), 2660–2673 (2020). https://doi.org/10.1002/asia.202000597
11. N. Ali et al., Chitosan-coated cotton cloth supported copper nanoparticles for toxic dye reduction. Int. J. Biol. Macromol. **111**, 832–838 (2018). https://doi.org/10.1016/j.ijbiomac.2018.01.092
12. M.N. Alshabanat, M.M. Al-Anazy, An experimental study of photocatalytic degradation of congo red using polymer nanocomposite films. J. Chem. **2018**, 9651850 (2018). https://doi.org/10.1155/2018/9651850
13. E. Alzahrani, Chitosan membrane embedded with ZnO/CuO nanocomposites for the photodegradation of fast green dye under artificial and solar irradiation. Anal. Chem. Insights **13**, 1177390118763361 (2018). https://doi.org/10.1177/1177390118763361
14. W.W. Anku, S.K. Shukla, P.P. Govender, Graft gum ghatti caped Cu2O nanocomposite for photocatalytic degradation of naphthol blue black dye. J. Inorg. Organomet. Polym Mater. **28**(4), 1540–1551 (2018). https://doi.org/10.1007/s10904-018-0875-y
15. H. Anwer, A. Mahmood, J. Lee, K.-H. Kim, J.-W. Park, A.C.K. Yip, Photocatalysts for degradation of dyes in industrial effluents: opportunities and challenges. Nano Res. **12**(5), 955–972 (2019). https://doi.org/10.1007/s12274-019-2287-0
16. R.S. Ashraf et al., Methods for the treatment of wastewaters containing dyes and pigments, in *Water Pollution and Remediation: Organic Pollutants*, ed. by Inamuddin, M.I. Ahamed, E. Lichtfouse (Springer International Publishing, Cham, 2021), pp. 597–661
17. M. Bahal, N. Kaur, N. Sharotri, D. Sud, Investigations on amphoteric chitosan/TiO_2 bionanocomposites for application in visible light induced photocatalytic degradation. Adv. Polym. Technol. **2019**, 2345631 (2019). https://doi.org/10.1155/2019/2345631
18. J.P. Chaudhary et al., Fabrication of carbon and sulphur-doped nanocomposites with seaweed polymer carrageenan as an efficient catalyst for rapid degradation of dye pollutants using a solar concentrator. RSC Adv. **6**(66), 61716–61724 (2016). https://doi.org/10.1039/C6RA10317K
19. S. Chkirida, N. Zari, R. Achour, Q. Aek, R. Bouhfid, Efficient hybrid bionanocomposites based on iron-modified TiO2 for dye degradation via an adsorption-photocatalysis synergy under UV-Visible irradiations. Environ. Sci. Pollut. Res. **28**(11), 14018–14027 (2021). https://doi.org/10.1007/s11356-020-11664-5
20. S. Das, H. Mahalingam, Reusable floating polymer nanocomposite photocatalyst for the efficient treatment of dye wastewaters under scaled-up conditions in batch and recirculation modes. J. Chem. Technol. Biotechnol. **94**(8), 2597–2608 (2019). https://doi.org/10.1002/jctb.6069
21. R.S. Dassanayake, E. Rajakaruna, N. Abidi, Preparation of aerochitin-TiO2 composite for efficient photocatalytic degradation of methylene blue. J. Appl. Polym. Sci. **135**(8), 45908 (2018). https://doi.org/10.1002/app.45908
22. M. Dehghani, H. Nadeem, V. Singh Raghuwanshi, H. Mahdavi, M.M. Banaszak Holl, W. Batchelor, ZnO/cellulose nanofiber composites for sustainable sunlight-driven dye degradation. ACS Appl. Nano Mater. **3**(10), 10284–10295 (2020). https://doi.org/10.1021/acsanm.0c02199
23. H. Dong et al., An overview on limitations of TiO2-based particles for photocatalytic degradation of organic pollutants and the corresponding countermeasures. Water Res. **79**, 128–146 (2015). https://doi.org/10.1016/j.watres.2015.04.038
24. H.E. Emam, H.B. Ahmed, Comparative study between homo-metallic & hetero-metallic nanostructures based agar in catalytic degradation of dyes. Int. J. Biol. Macromol. **138**, 450–461 (2019). https://doi.org/10.1016/j.ijbiomac.2019.07.098
25. H. Essabir, M. Raji, S.A. Laaziz, D. Rodrique, R. Bouhfid, Q. Aek, Thermo-mechanical performances of polypropylene biocomposites based on untreated, treated and compatibilized

spent coffee grounds. Compos. B Eng. **149**, 1–11 (2018). https://doi.org/10.1016/j.compositesb.2018.05.020
26. M. Faisal, M. Abu Tariq, M. Muneer, Photocatalysed degradation of two selected dyes in UV-irradiated aqueous suspensions of titania. Dyes Pigm. **72**(2), 233–239 (2007). https://doi.org/10.1016/j.dyepig.2005.08.020
27. M.H. Farzana, S. Meenakshi, Synergistic effect of chitosan and titanium dioxide on the removal of toxic dyes by the photodegradation technique. Ind. Eng. Chem. Res. **53**(1), 55–63 (2014). https://doi.org/10.1021/ie402347g
28. E.P. Ferreira-Neto et al., Bacterial nanocellulose/MoS2 hybrid aerogels as bifunctional adsorbent/photocatalyst membranes for in-flow water decontamination. ACS Appl. Mater. Interfaces **12**(37), 41627–41643 (2020). https://doi.org/10.1021/acsami.0c14137
29. N. Gupta et al., Photocatalytic nanocomposite microsponges of polylactide-titania for chemical remediation in water. ACS Appl. Polym. Mater. **2**(11), 5188–5197 (2020). https://doi.org/10.1021/acsapm.0c00937
30. V.K. Gupta et al., Degradation of azo dyes under different wavelengths of UV light with chitosan-SnO2 nanocomposites. J. Mol. Liq. **232**, 423–430 (2017). https://doi.org/10.1016/j.molliq.2017.02.095
31. I. Hasan, A. Bassi, K.H. Alharbi, I.I. BinSharfan, R.A. Khan, A. Alslame, Sonophotocatalytic degradation of malachite green by nanocrystalline chitosan-ascorbic Acid@NiFe2O4 spinel ferrite. Coatings **10**(12), 1200 (2020)
32. I. Hasan, C. Shekhar, I.I. Bin Sharfan, R.A. Khan, A. Alsalme, Ecofriendly green synthesis of the ZnO-doped CuO@Alg bionanocomposite for efficient oxidative degradation of p-Nitrophenol. ACS Omega **5**(49), 32011–32022 (2020). https://doi.org/10.1021/acsomega.0c04917
33. I. Hasan, S. Walia, K.H. Alharbi, M.A. Khanjer, A. Alsalme, R.A. Khan, Multi-walled carbon nanotube coupled β-Cyclodextrin/PANI hybrid photocatalyst for advance oxidative degradation of crystal violet. J. Mol. Liq. **317**,114216 (2020).https://doi.org/10.1016/j.molliq.2020.114216
34. N. Hernández, R.C. Williams, E.W. Cochran, The battle for the "green" polymer. Different approaches for biopolymer synthesis: bioadvantaged vs. bioreplacement. Org. Biomol. Chem. **12**(18), 2834–2849 (2014). https://doi.org/10.1039/C3OB42339E
35. X. Huang, X. Li, Y. Li, X. Wang, Biopolymer as stabilizer and adhesive to in situ precipitate cus nanocrystals on cellulose nanofibers for preparing multifunctional composite papers. ACS Omega **3**(7), 8083–8090 (2018). https://doi.org/10.1021/acsomega.8b01225
36. G. Jung, H.-I. Kim, Synthesis and photocatalytic performance of PVA/TiO2/graphene-MWCNT nanocomposites for dye removal. J. Appl. Polym. Sci. **131**(17) (2014). https://doi.org/10.1002/app.40715
37. T. Kamal, I. Ahmad, S.B. Khan, M. Ul-Islam, A.M. Asiri, Microwave assisted synthesis and carboxymethyl cellulose stabilized copper nanoparticles on bacterial cellulose nanofibers support for pollutants degradation. J. Polym. Environ. **27**(12), 2867–2877 (2019). https://doi.org/10.1007/s10924-019-01565-1
38. T. Kamal, M.S.J. Khan, S.B. Khan, A.M. Asiri, M.T.S. Chani, M.W. Ullah, Silver nanoparticles embedded in gelatin biopolymer hydrogel as catalyst for reductive degradation of pollutants. J. Polym. Environ. **28**(2), 399–410 (2020). https://doi.org/10.1007/s10924-019-01615-8
39. T. Kamal, S.B. Khan, A.M. Asiri, Synthesis of zero-valent Cu nanoparticles in the chitosan coating layer on cellulose microfibers: evaluation of azo dyes catalytic reduction. Cellulose **23**(3), 1911–1923 (2016). https://doi.org/10.1007/s10570-016-0919-9
40. S. Kaushal, N. Kaur, M. Kaur, P.P. Singh, Dual-responsive pectin/graphene Oxide (Pc/GO) nano-composite as an efficient adsorbent for Cr (III) ions and photocatalyst for degradation of organic dyes in waste water. J. Photochem. Photobiol. A: Chem. **403**, 112841 (2020). https://doi.org/10.1016/j.jphotochem.2020.112841
41. A. Khalil, N. Ali, A. Asiri, T. Kamal, Synthesis and catalytic evaluation of Silver@nickel oxide and alginate biopolymer nanocomposite hydrogel beads. Res. Square (2021)

42. S.A. Khan, S.B. Khan, A. Farooq, A.M. Asiri, A facile synthesis of CuAg nanoparticles on highly porous ZnO/carbon black-cellulose acetate sheets for nitroarene and azo dyes reduction/degradation. Int. J. Biol. Macromol. **130**, 288–299 (2019). https://doi.org/10.1016/j.ijbiomac.2019.02.114
43. A.J. Kora, L. Rastogi, Catalytic degradation of anthropogenic dye pollutants using palladium nanoparticles synthesized by gum olibanum, a glucuronoarabinogalactan biopolymer. Ind. Crops Prod. **81**, 1–10 (2016). https://doi.org/10.1016/j.indcrop.2015.11.055
44. N. Kumar, H. Mittal, S.M. Alhassan, S.S. Ray, Bionanocomposite hydrogel for the adsorption of dye and reusability of generated waste for the photodegradation of ciprofloxacin: a demonstration of the circularity concept for water purification. ACS Sustain. Chem. Eng. **6**(12), 17011–17025 (2018). https://doi.org/10.1021/acssuschemeng.8b04347
45. W.-H. Lam, M.N. Chong, B.A. Horri, B.-T. Tey, E.-S. Chan, Physicochemical stability of calcium alginate beads immobilizing TiO2 nanoparticles for removal of cationic dye under UV irradiation. J. Appl. Polym. Sci. **134**(26) (2017) . https://doi.org/10.1002/app.45002
46. G. Li, Y. Li, Z. Wang, H. Liu, Green synthesis of palladium nanoparticles with carboxymethyl cellulose for degradation of azo-dyes. Mater. Chem. Phys. **187**, 133–140 (2017). https://doi.org/10.1016/j.matchemphys.2016.11.057
47. G. Li et al., Laccase-immobilized bacterial cellulose/TiO2 functionalized composite membranes: evaluation for photo- and bio-catalytic dye degradation. J. Membr. Sci. **525**, 89–98 (2017). https://doi.org/10.1016/j.memsci.2016.10.033
48. K. Li, de Rancourt de Mimérand Y, Jin X, Yi J, Guo J, Metal oxide (ZnO and TiO2) and Fe-based metal–organic-framework nanoparticles on 3D-printed fractal polymer surfaces for photocatalytic degradation of organic pollutants. ACS Appl. Nano Mater. **3**(3), 2830–2845 (2020). https://doi.org/10.1021/acsanm.0c00096
49. W. Li, T. Li, G. Li, L. An, F. Li, Z. Zhang, Electrospun H4SiW12O40/cellulose acetate composite nanofibrous membrane for photocatalytic degradation of tetracycline and methyl orange with different mechanism. Carbohyd. Polym. **168**, 153–162 (2017). https://doi.org/10.1016/j.carbpol.2017.03.079
50. M. Lučić Škorić et al., Chitosan-based microparticles for immobilization of TiO2 nanoparticles and their application for photodegradation of textile dyes. Eur. Polymer J. **82**, 57–70 (2016). https://doi.org/10.1016/j.eurpolymj.2016.06.026
51. X. Man, R. Wu, H. Lv, W. Wang, Synthesis of a montmorillonite-supported titania nanocomposite with grafted cellulose as a template and its application in photocatalytic degradation. J. Appl. Polym. Sci. **132**(41) (2015). https://doi.org/10.1002/app.42627
52. M. Manimohan, S. Pugalmani, K. Ravichandran, M.A. Sithique, Synthesis and characterisation of novel Cu(ii)-anchored biopolymer complexes as reusable materials for the photocatalytic degradation of methylene blue. RSC Adv. **10**(31), 18259–18279 (2020). https://doi.org/10.1039/D0RA01724H
53. L. Marija, M. Nedeljko, R. Maja, Š. Zoran, R. Marija, K.K. Melina, Photocatalytic degradation of C.I. Acid Orange 7 by TiO2 nanoparticles immobilized onto/into chitosan-based hydrogel. Polym. Compos. **35**(4), 806–815 (2014). https://doi.org/10.1002/pc.22724
54. N.U. Mary, M.J. Umapathy, A. Sivasamy, Biomaterial supported binary semiconductor metal oxide nanocomposite for Water remediation under solar irradiation. Optik **208**,164219 (2020). https://doi.org/10.1016/j.ijleo.2020.164219
55. S. Megha, D. Devadathan, V. Baiju, R. Raveendran, Structural, optical and photocatalytic degradation studies of polymer based Fe2o3 nanocomposite. J. Phys.: Conf. Ser. **1172**, 012051 (2019). https://doi.org/10.1088/1742-6596/1172/1/012051
56. L. Midya, A. Pal, S. Pal, Development of crosslinked chitosan/Au Nanocomposite, its characterization and application towards solar light driven photocatalytic degradation of toxic organic compounds. ChemistrySelect **1**(19), 6115–6126 (2016). https://doi.org/10.1002/slct.201601337
57. E.D. Mohamed Isa, N.W. Che Jusoh, R. Hazan, K. Shameli, Photocatalytic degradation of methyl orange using pullulan-mediated porous zinc oxide microflowers. Environ. Sci. Pollut. Res. **28**(5), 5774–5785 (2021). https://doi.org/10.1007/s11356-020-10939-1

58. S. Mohan, O.S. Oluwafemi, N. Kalarikkal, S. Thomas, S.P. Songca, Biopolymers – application in nanoscience and nanotechnology recent advances in biopolymers (2016)
59. A.A. Mohd Yatim et al., Vanadium and nitrogen Co-doped titanium dioxide (TiO2) with enhanced photocatalytic performance: potential in wastewater treatment. J. Nanosci. Nanotechnol. **20**(2), 741–751 (2020). https://doi.org/10.1166/jnn.2020.16946
60. N. Muhd Julkapli, S. Bagheri, S Bee Abd Hamid, Recent advances in heterogeneous photocatalytic decolorization of synthetic dyes. Sci. World J. **2014**, 692307 (2014). https://doi.org/10.1155/2014/692307
61. A. Nasiri, M. Malakootian, M.R. Heidari, S.N. Asadzadeh, CoFe2O4@methylcelloluse as a new magnetic nano biocomposite for sonocatalytic degradation of reactive blue 19. J. Polym. Environ. **29**(8), 2660–2675 (2021). https://doi.org/10.1007/s10924-021-02074-w
62. L. Nouri, S. Hemidouche, A. Boudjemaa, F. Kaouah, Z. Sadaoui, K. Bachari, Elaboration and characterization of photobiocomposite beads, based on titanium (IV) oxide and sodium alginate biopolymer, for basic blue 41 adsorption/photocatalytic degradation. Int. J. Biol. Macromol. **151**, 66–84 (2020). https://doi.org/10.1016/j.ijbiomac.2020.02.159
63. T. Nusrat, S. Sharf Ilahi, R. Geetanjali, C. Saif Ali, Inamuddin, Abdullah MA, Nano-engineered adsorbent for the removal of dyes from water: a review. Curr. Anal. Chem. **16**(1), 14–40 (2020). https://doi.org/10.2174/1573411015666190117124344
64. L.V.F. Oliveira, S. Bennici, L. Josien, L. Limousy, M.A. Bizeto, F.F. Camilo, Free-standing cellulose film containing manganese dioxide nanoparticles and its use in discoloration of indigo carmine dye. Carbohydr. Polym. **230**, 115621 (2020). https://doi.org/10.1016/j.carbpol.2019.115621
65. N. Pandey, S.K. Shukla, N.B. Singh, Water purification by polymer nanocomposites: an overview. Nanocomposites **3**(2), 47–66 (2017). https://doi.org/10.1080/20550324.2017.1329983
66. S. Pandey, J.Y. Do, J. Kim, M. Kang, Fast and highly efficient catalytic degradation of dyes using κ-carrageenan stabilized silver nanoparticles nanocatalyst. Carbohydr. Polym. **230**, 115597 (2020). https://doi.org/10.1016/j.carbpol.2019.115597
67. D.R. Paul, L.M. Robeson, Polymer nanotechnology: nanocomposites. Polymer **49**(15), 3187–3204 (2008). https://doi.org/10.1016/j.polymer.2008.04.017
68. J. Pérez-Obando, D.A. Marín-Silva, A.N. Pinotti, L.R. Pizzio, P. Osorio-Vargas, J.A. Rengifo-Herrera, Degradation study of malachite green on chitosan films containing heterojunctions of melon/TiO2 absorbing visible-light in solid-gas interfaces. Appl. Catal. B **244**, 773–785 (2019). https://doi.org/10.1016/j.apcatb.2018.12.004
69. S. Ramadhani, H. Helmiyati, Alginate/CMC/ZnO nanocomposite for photocatalytic degradation of Congo red dye. AIP Conf. Proc. **2242**(1), 040026 (2020). https://doi.org/10.1063/5.0008095
70. Y.N. Rao, D. Banerjee, A. Datta, S.K. Das, A. Saha, Low temperature synthesis of Ag@anatase TiO2 nanocomposites through controlled hydrolysis and improved degradation of toxic malachite green under both ultra-violet and visible light. RSC Adv. **6**(54), 49083–49090 (2016). https://doi.org/10.1039/C6RA05579F
71. S. Rashtbari, G. Dehghan, Biodegradation of malachite green by a novel laccase-mimicking multicopper BSA-Cu complex: performance optimization, intermediates identification and artificial neural network modeling. J. Hazard. Mater. **406**,124340 (2021). https://doi.org/10.1016/j.jhazmat.2020.124340
72. A. Sangiorgi et al., 3D Printing of photocatalytic filters using a biopolymer to immobilize TiO2 nanoparticles. J. Electrochem. Soc. **166**(5), H3239–H3248 (2019). https://doi.org/10.1149/2.0341905jes
73. I. Sargin, T. Baran, G. Arslan, Environmental remediation by chitosan-carbon nanotube supported palladium nanoparticles: Conversion of toxic nitroarenes into aromatic amines, degradation of dye pollutants and green synthesis of biaryls. Sep. Purif. Technol. **247**, 116987 (2020). https://doi.org/10.1016/j.seppur.2020.116987
74. S. Sarkar, N.T. Ponce, A. Banerjee, R. Bandopadhyay, S. Rajendran, E. Lichtfouse, Green polymeric nanomaterials for the photocatalytic degradation of dyes: a review. Environ. Chem. Lett. **18**(5), 1569–1580 (2020). https://doi.org/10.1007/s10311-020-01021-w

75. P. Senthil Kumar, M. Selvakumar, S.G. Babu, S.K. Jaganathan, S. Karuthapandian, S. Chattopadhyay, Novel CuO/chitosan nanocomposite thin film: facile hand-picking recoverable, efficient and reusable heterogeneous photocatalyst. RSC Adv. **5**(71), 57493–57501 (2015). https://doi.org/10.1039/C5RA08783J
76. T. Shahwan et al., Green synthesis of iron nanoparticles and their application as a Fenton-like catalyst for the degradation of aqueous cationic and anionic dyes. Chem. Eng. J. **172**(1), 258–266 (2011). https://doi.org/10.1016/j.cej.2011.05.103
77. Y. Shen, Q. Fang, B. Chen, Environmental applications of three-dimensional graphene-based macrostructures: adsorption, transformation, and detection. Environ. Sci. Technol. **49**(1), 67–84 (2015). https://doi.org/10.1021/es504421y
78. S. Sheshmani, H. Nejabat Ghamsari, Photodegradation of acid orange 7 from aqueous solution under visible light irradiation using nanosized ZnO/chitosan/graphene oxide composite. Int. J. Environ. Anal. Chem. **100**(8), 912–921 (2020). https://doi.org/10.1080/03067319.2019.1645840
79. V.G. Sirajuddin, G. Sharma, A. Kumar, F.J. Stadler, Inamuddin preparation and characterization of gum acacia/Ce(IV)MoPO4 nanocomposite ion exchanger for photocatalytic degradation of methyl violet dye. J. Inorg. Organomet. Polym. Mater. **29**(4), 1171–1183 (2019). https://doi.org/10.1007/s10904-019-01080-9
80. P. Sirajudheen, S. Meenakshi, Facile synthesis of chitosan-La3+-graphite composite and its influence in photocatalytic degradation of methylene blue. Int. J. Biol. Macromol. **133**, 253–261 (2019). https://doi.org/10.1016/j.ijbiomac.2019.04.073
81. R. Subekti, H. Helmiyati, Sodium alginate-TiO2-bentonite nanocomposite synthesis for photocatalysis of methylene blue dye removal. IOP Conf. Ser.: Mater. Sci. Eng. **763**, 012018 (2020). https://doi.org/10.1088/1757-899x/763/1/012018
82. S. Sultana, N. Ahmad, S.M. Faisal, M. Owais, S. Sabir, Synthesis, characterisation and potential applications of polyaniline/chitosan-Ag-nano-biocomposite. IET Nanobiotechnol. **11**(7), 835–842 (2017). https://doi.org/10.1049/iet-nbt.2016.0215
83. S. Sultana, N. Ahmad, S.M. Faisal, M. Owais, S. Sabir, Synthesis, characterisation and potential applications of polyaniline/chitosan-Ag-nano-biocomposite IET Nanobiotechnology. Inst. Eng. Technol. 835–842 (2017)
84. S.M.T.H. Moghaddas, B. Elahi, V. Javanbakht, Biosynthesis of pure zinc oxide nanoparticles using Quince seed mucilage for photocatalytic dye degradation. J. Alloy. Compd. **821**, 153519 (2020). https://doi.org/10.1016/j.jallcom.2019.153519
85. M.T. Taghizadeh, V. Siyahi, H. Ashassi-Sorkhabi, G. Zarrini, ZnO, AgCl and AgCl/ZnO nanocomposites incorporated chitosan in the form of hydrogel beads for photocatalytic degradation of MB, E. coli and S. aureus. Int. J. Biol. Macromol. **147**, 1018–1028 (2020). https://doi.org/10.1016/j.ijbiomac.2019.10.070
86. N. Tavker, U.K. Gaur, M. Sharma, Highly active agro-waste-extracted cellulose-supported CuInS2 nanocomposite for visible-light-induced photocatalysis. ACS Omega **4**(7), 11777–11784 (2019). https://doi.org/10.1021/acsomega.9b01054
87. M. Thakur, G. Sharma, T. Ahamad, A.A. Ghfar, D. Pathania, M. Naushad, Efficient photocatalytic degradation of toxic dyes from aqueous environment using gelatin-Zr(IV) phosphate nanocomposite and its antimicrobial activity. Colloids Surf. B **157**, 456–463 (2017). https://doi.org/10.1016/j.colsurfb.2017.06.018
88. K. Thiyagarajan, S. Samuel, P.S. Kumar, S.G. Babu, C_3N_4 supported on chitosan for simple and easy recovery of visible light active efficient photocatalysts. Bull. Mater. Sci. **43**(1), 137 (2020). https://doi.org/10.1007/s12034-020-02107-5
89. B. Thomas et al., Nanocellulose, a versatile green platform: from biosources to materials and their applications. Chem. Rev. **118**(24), 11575–11625 (2018). https://doi.org/10.1021/acs.chemrev.7b00627
90. J.N. Tiwari et al., Reduced graphene oxide-based hydrogels for the efficient capture of dye pollutants from aqueous solutions. Carbon **56**, 173–182 (2013). https://doi.org/10.1016/j.carbon.2013.01.001

91. J.D. Torres, E.A. Faria, J.R. SouzaDe, A.G.S. Prado, Preparation of photoactive chitosan–niobium (V) oxide composites for dye degradation. J. Photochem. Photobiol. A **182**(2), 202–206 (2006). https://doi.org/10.1016/j.jphotochem.2006.02.027
92. V. Lp, V. Rajagopalan, A new synergetic nanocomposite for dye degradation in dark and light. Sci. Rep. **6**(1), 38606 (2016). https://doi.org/10.1038/srep38606
93. A. Vanamudan, P.P. Sudhakar, Biopolymer capped silver nanoparticles with potential for multifaceted applications. Int. J. Biol. Macromol. **86**, 262–268 (2016). https://doi.org/10.1016/j.ijbiomac.2016.01.056
94. S. Vigneshwaran, P. Sirajudheen, C.P. Nabeena, S. Meenakshi, In situ fabrication of ternary TiO2 doped grafted chitosan/hydroxyapatite nanocomposite with improved catalytic performance for the removal of organic dyes: experimental and systemic studies. Colloids Surf. A: Phys. Chem. Eng. Asp. **611**, 125789 (2021). https://doi.org/10.1016/j.colsurfa.2020.125789
95. E.Z. Wang, Y. Wang, D. Xiao, Polymer nanocomposites for photocatalytic degradation and photoinduced utilizations of Azo-Dyes. Polymers **13**(8), 1215 (2021)
96. Q. Wang et al., Photodegradation of textile dye Rhodamine B over a novel biopolymer-metal complex wool-Pd/CdS photocatalysts under visible light irradiation. J. Photochem. Photobiol. B **126**, 47–54 (2013). https://doi.org/10.1016/j.jphotobiol.2013.07.007
97. Y. Yang et al., Chitosan-capped ternary metal selenide nanocatalysts for efficient degradation of Congo red dye in sunlight irradiation. Int. J. Biol. Macromol. **167**, 169–181 (2021). https://doi.org/10.1016/j.ijbiomac.2020.11.167
98. Z. Yang, J. Kang, L. Li, L. Guo, A biotemplating route for the synthesis of hierarchical Fe2O3 with highly dispersed carbon as electron-transfer channel. ChemPlusChem **85**(1), 258–263 (2020). https://doi.org/10.1002/cplu.201900641
99. M. Yurdakul, H.A. Oktem, M.D. Yilmaz, Transition metal chelated biopolymer coated mesoporous silica nanoparticles as highly efficient, stable, and recyclable nanocatalysts for catalytic bleaching. ChemistrySelect **4**(7), 2084–2088 (2019). https://doi.org/10.1002/slct.201803783
100. C. Zhao, Q. Yan, S. Wang, P. Dong, L. Zhang, Regenerable g-C3N4–chitosan beads with enhanced photocatalytic activity and stability. RSC Adv. **8**(48), 27516–27524 (2018). https://doi.org/10.1039/C8RA04293D

Chapter 7
Sequestration of Organic Dyes from Wastewater Using Hydrogel Nanocomposites

Nompumelelo Malatji, Edwin Makhado, Kwena D. Modibane, Sadanand Pandey, and Mpitloane J. Hato

Abstract With the growth in civilization and industrialization, there is a rise in the release of organic dyes into water systems, which is causing serious public concern. Although adsorption using biopolymer-based hydrogels has proven to be an ideal technique for treating these dye contaminants from aqueous solutions, these hydrogels suffer from a lack of mechanical stability and recoverability compared to synthetic polymers. Herein, we review the low-cost synthesis of hybrid hydrogel nanocomposites to improve the mechanical stability and separation of the hydrogel in removing dyes from an aqueous solution. The literature reports hydrogels and their nanocomposites as noble adsorbents well-known for addressing water pollution issues. In adsorption technology, hydrogel nanocomposites act as absorbents, prominent to improve the performance of removal efficiency. This current chapter pays particular attention to some recent breakthrough development in water remediation based on hydrogels as efficient adsorbents. In-depth discussions on adsorption and various methods for the synthesis of hydrogels have been devoted to applications of these nanocomposites and are compared in this contribution to the removal efficiency of organic dyes from wastewater.

N. Malatji · E. Makhado (✉) · K. D. Modibane · M. J. Hato (✉)
Nanotechnology Research Lab, Department of Chemistry, School of Physical and Mineral Sciences, University of Limpopo(Turfloop), Sovenga 0727, Polokwane, South Africa
e-mail: edwin.makhado@ul.ac.za

M. J. Hato
e-mail: mpitloane.hato@ul.ac.za

S. Pandey
Department of Chemistry, College of Natural Sciences, Yeungnam University, 280 Daehak-Ro, Gyeongsan, Gyeongbuk 38541, Republic of Korea

M. J. Hato and S. Sinha Ray (eds.), *Functional Polymer Nanocomposites for Wastewater Treatment*, Springer Series in Materials Science 323,
https://doi.org/10.1007/978-3-030-94995-2_7

7.1 Introduction

Water is a vital resource for the survival of living things on earth [40]. Despite the need for this resource, water pollution continues to be a problem in most countries, including South Africa, where the mainstream water supplies are underground and surface water [72]. Water pollution may be defined as any water that is unsafe for drinking by humans and animals [72]. There are two classes of water contaminants, namely, point sources and non-point sources in which they are defined as a source of pollution at a fixed location (mines, industries, power stations, water treatment station, etc. and pollution from moving sources (cars, buses, and trains, respectively [79, 93]. In point source, water pollutants may be classified as either inorganic (fertilizers and toxic metals), organic (dyes), or microbial (viruses and bacteria) [12]. For example, dyes are organic complexes mostly used by textile industries to colour fabrics and contribute mainly to pollution [110]. Other applications may include medical, pharmaceutical, paper, rubber, plastics, leather, food, and cosmetics industries [56]. Dyes contain aromatic rings in their structure and can be either chromophores or auxochromes [23, 56]. Chromophores are responsible for the production of colour (OH, NH_2, NHR, NR_2, Cl, COOH), and auxochromes (NO_2, NO, and N = N) improve chromophores, make molecules soluble in water and improve their affinity to bind materials [23]. The discharging of dye effluents into either surface and/or groundwater sources leads to contamination, resulting in various health and environmental problems [23, 104]. Consumption of contaminated water by humans can lead to vomiting, mutation, cancer, breathing, difficulties, diarrhoea, eyes burn, nausea, shock, cyanosis, jaundice, and tissue necrosis [23, 56, 61, 62, 104]. The environmental issues include the death of aquatic organisms, leading to the development of foul smell [5]. Hence, the need to eliminate dyes from waste effluents before discharging them into rivers and other water streams.

Due to the above-mentioned health and ecological problems, various techniques have been employed for eliminating dyes from wastewater [89]. However, because of the chemical stability and non-biodegradable nature of the dyes, most of these methods are less effective [56]. Additionally, each method has its major disadvantage, as shown in Table 7.1.

The adsorption technique is most favoured owing to its cheap synthesis and operation costs, easy design, and fast removal of dye [48, 66, 88]. Although the adsorption technique is effective for dye removal. Its efficiency is limited by the type of adsorbent used (Gómez et al. 20,107). Various materials have been used for organic dyes removal, which includes; activated carbon, fly ash, graphene, clay, carbon nanotubes, and hydrogels [35, 39, 52, 63, 71, 99, 100, 106, 116]. Among these adsorbents, hydrogels are reported as promising adsorbents for organic dyes removal from aqueous solutions owing to their cheap synthesis, tunable properties, and high removal capacity. This chapter summarises the recent advances and developments of hydrogel adsorbents for wastewater treatment. This is realized by doing a detailed review of various hydrogel adsorbents and their modified systems with great emphasis on the structure and properties of the hybrid hydrogels.

Table 7.1 Removal methods for organic dyes from wastewater

Adsorbent method	Disadvantage	References
Membrane filtration	Membrane fouling and production of concentrated sludge	[88]
Ion-exchange	Ineffective for all dye types	[2, 110]
Photochemical method	Production of by-products	[88]
Electrochemical destruction	Moderately high flow rates that decrease the amount of dye removed	[88]
Anaerobic bioremediation systems	Lead to the production of methane and hydrogen sulphide which are harmful	[2, 78]
Adsorbent using activated carbon	The adsorbent is expensive	[78]

7.2 Hydrogels

7.2.1 Background

Hydrogels are crosslinked gel structured polymers that swell in a liquid medium and can trap liquids for a long time without losing their structural integrity [39, 99]. Hydrogels' swelling capacity and hydrophilicity arise from the presence of hydroxyl, sulfonyl, amide, imide, and carboxylic groups in their 3D backbone [92]. Hydrogels are produced from non-toxic and highly hydrophilic natural polymers called Polysaccharides. Polysaccharides are made by connecting glycosidic bonds between the smaller saccharide units [39, 99, 116]. Polysaccharides provide energy storage and structural support in animals and plants [100]. Examples of these polysaccharides include, alginate, guar gum, locust bean gum, starch, chitosan, carboxymethyl cellulose, carrageenan, and starch [100, 116].

7.2.1.1 Classification of Hydrogels

Hydrogels may well be categorized depending on various characteristics depending on their nature. Hydrogels are classified based on whether they are natural (produced from biological monomers), synthetic (made from artificial monomers), or a combination of natural and synthetic monomers forming a hybrid gel [62] (Table 7.2). The method used for the synthesis of a polymeric composite can also be used to classify hydrogels [62]. These include but are not limited to;

i. Homopolymeric hydrogels: they are hydrogels comprising of a similar kind of monomer.
ii. Copolymeric hydrogels: the polymeric gels contain two or more distinct varieties of monomers resulting in a hydrogel with at least one hydrophilic part.

Table 7.2 Classification of physical and chemical stimuli

Physical	Chemical
Light	Composition of solvent
Magnetic field	pH
Temperature	Molecular species
Sound	Ionic strength
Electric field	
Pressure	

iii. Multipolymer Interpenetrating polymeric hydrogel (IPN): the polymer chain contains two independently cross-linked synthetic and/or natural polymer portions.

Classifications of hydrogels could also be categorized based on the following properties [33],

i. Amorphous,
ii. Crystalline or,
iii. Semicrystallinity: displaying characteristics of both amorphous and crystalline phases.

Moreover, hydrogels can be classified based on whether they are chemically or physically crosslinked. Briefly;

i. The crosslinking of the hydrogel can be achieved physically (1) between oppositely charged groups, (2) by establishing a hydrogen bond, (3) by subjecting gels to freeze and thaw procedure during crystallization using PVA/PVP solution at controlled conditions. Lastly, (4) through hydrophobic connections between polymer chains, the hydrogel strength is improved, and the dissipation energy prevents breakage of bonds. [23].
ii. The crosslinking of hydrogels can be realized chemically through (1) aldehydes, namely; glutaraldehyde, formaldehyde, and acetaldehyde, (2) radiation through ultraviolet rays, gamma rays, an electron beam, or at ambient temperatures to form free radicals where monomers can be added to form or grow the hydrogel chain. Lastly, (3) using MBA crosslinker for free radical polymerization. In this method, an initiator (e.g., potassium persulfate) generates free radicals to interact with monomers in the presence of MBA crosslinks to form the hydrogel [16, 39].

Additionally, the classification of hydrogels could be established according to the charge of the hydrogel polymer chain [21, 55]. Whether the charge is,

i. Non-ionic (neutral).
ii. Ionic (anionic/ cationic)
iii. Zwitterionic (each recurring structural unit has cationic and anionic parts). The overall charge of the polymer chain is zero.
iv. Amphoteric (contains both acidic and basic groups).

Lastly, hydrogels can be categorized depending on whether a chemical or physical stimulus (Table 7.2) encourages their reaction. These hydrogels are sometimes called smart hydrogels [16, 62]. Sometimes environmental conditions can affect the swelling or de-swelling of hydrogels and therefore result in a volume collapse (phase change).

7.2.2 Synthesis of Hydrogels

For application in water remediation processes, the low stability and solubility of hydrogels are improved by developing hybrid hydrogel systems that consist of nanofillers and/or synthetic polymers [21]. Most researches have reported that crosslinking, grafting, and free radical polymerization. Therefore, the type of method used to prepare the hydrogel affects its structural makeup or physical properties. Below are brief descriptions of the methods as mentioned above.

7.2.2.1 Grafting

Grafting uses artificial polymers, namely; methacrylamide, acrylic acid, vinyl alcohol, and acrylamide, to improve the hydrogel backbone [55]. An initiator generates free radical sites to which monomer units are attached [94]. Grafting can initiate through either radiation or chemical stimulus. Chemical grafting makes use of chemicals such as potassium persulfate (KPS), ammonium persulfate (APS) as initiators [68]. Radiation grafting initiates free radicals through microwave or UV visible energy [20].

It was reported in the literature that using a microwave radiation method for synthesizing hydrogels produces sterilized hydrogels [20]. Naturally, polysaccharides have poor mechanical and chemical stability [21]. Grafting solves these problems and improves the biopolymers efficiency by establishing new functional groups from grafted monomers.

7.2.2.2 Crosslinking

Crosslinking process can occur through chemical or physical interaction. During chemical crosslinking, complementary groups within the polymer chain react to form irreversible covalent bonds [91]. In contrast, physical crosslinking occurs through reversible van der Waals forces, hydrogen bonding, and electrostatic reactions [14, 44]. Hydrogels that are crosslinked chemically are mainly applied in the medical field during tissue engineering, wound dressing, wastewater treatment, and drug delivery [57, 105]. Several chemical crosslinkers exist that may be used for hydrogel synthesis. For example, in a study by Mittal et al. hydrogels was produced using a mixture of ascorbic acid and KPS as a redox initiator and MBA as a cross linking

agent in the microwave-assisted graft co-polymerization method (Scheme 7.1) [69]. According to the group, this using MBA as the cross linker to establish links between different polymeric chains. [69].

Chemicals such as tri-propyleneglycol diacrylate (TPGDA) tetra-ethylene glycol dimethyl-acrylate (EGDMA), N, N-methylene-bis-acrylamide (MBA), and ethylene glycol dimethyl-acrylate are the most commonly used as crosslinkers in hydrogel synthesis [96]. However, these crosslinkers produce non-biodegradable hydrogels and are generally toxic [118]. Moreover, the resulting hydrogels are very brittle because of the lack of an effective strategy for energy dissipation and inner structural uniformity [108, 109]. As a solution, hybrid hydrogel systems comprising both physical and chemical interactions have been established by researchers to aid in energy dissipation and improve structural properties, respectively [19, 83]. For example, researchers constructed hybrid polymeric gels using poly(N-isopropyl acrylamide-co-itaconic acid) and non-poisonous octa-vinyl polyhedral oligomeric silsesquioxane (OV-POSS) crosslinkers. The analysis of the SEM and TGA (Fig. 7.1) results demonstrated that the surface of the non-hybridized NIPAM-co-IA (SEM image Fig. 7.1a) was not smooth. However, after crossing with various POSS amounts ((a) 8%, (b), 10%, and (c), 12%), the surface texture changed to a honeycomb-like structure with similar pores of different pore sizes as the POSS amount was raised. The group observed disruption of the honeycomb pattern at higher POSS content (12%), demonstrating that the level of homogeneity in the hybridized gel structure could be manipulated by varying the degree of crosslinking [27]. Their TGA thermogram (Fig. 7.1e) indicated that the thermal stability was enhanced through hybridization with POSS, in which the weight loss obtained for poly(NIPAM-co-IA) from 340 to 500 °C was higher compared to the weight loss achieved for the hybridized hydrogel at the same temperature [27].

7.2.2.3 Free Radical-Polymerization

Free radical polymerization is when free radicals are generated to which monomers bind progressively, and the polymer chain grows [13]. This technique combines crosslinking and grafting methods. In this process, an initiator breaks down by light, photon, or temperature to form a free radical [18]. The advantages of generating free radicals by photon are (1) cost-efficiency, (2) no chemical solvent is required, and (3) it offers improved time-based and spatial control of the reaction procedure [46]. Scheme 7.2 illustrates the synthesis of hydrogels through the free radical polymerization process. Firstly, free radicals are produced through an initiator (initiation). Next, the monomer interacts with the free radicals to create unoccupied functional sites (propagation), and lastly, crosslinking occurs to form a hydrogel (termination) [65].

The most commonly used technique in the polymer industry is free radical polymerization. This technique offers the advantage of easy operation, convenience, and the ability to design and prepare polymers for different uses. Impurities do not easily

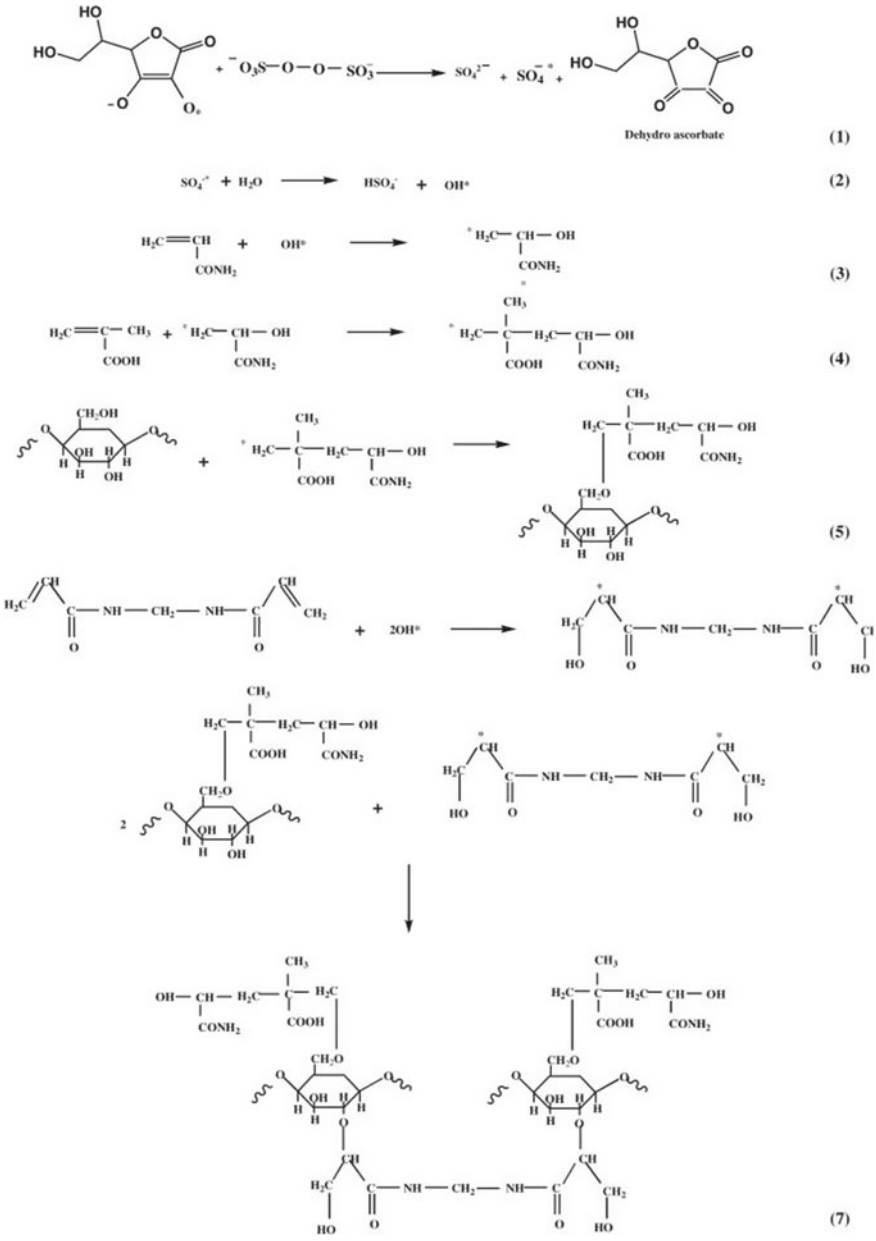

Scheme 7.1 Mechanism for the graft co-polymerization of Gg with P(AAm-*co*-MAA). Reproduced with permission from [69]. Copyright 2015, Elsevier Science Ltd

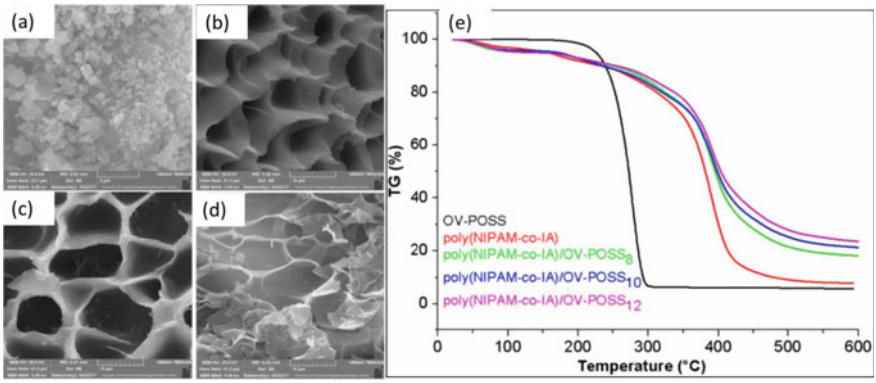

Fig. 7.1 SEM images of poly (NIPAM-co-IA) hydrogel (**a**) and hybrid poly (NIPAM-co-IA)/OV-POSS (8%, 10% and 12% POSS) (**b**–**d**), **e** TGA thermogram. Reproduced with permission from [27]. Copyright 2018, Elsevier Science Ltd

influence it. Free radical polymerization allows the achievement of in situ properties and well-characterized reaction kinetics [84].

7.2.3 Hybrid Hydrogels

It has been reported that hydrogel properties can be improved through generating hybrid hydrogel systems. Recently, many studies have incorporated nanofillers such as metal oxides [63], carbon-based materials [61, 62], and clay-based materials [65] into the hydrogel matrix during the polymerization process to produce a hydrogel nanocomposite with enhanced recovery and stability.

7.2.3.1 Modification of Hydrogels with Inorganic Materials

Depending on the intended application of the hydrogels, their physical properties can be enhanced through the incorporation of inorganic materials. For example, for use in removing contaminants from aqueous solutions, the hydrogel must be mechanically and thermally stable, especially for removing effluents from industries that utilize water for cooling reactions [22, 38]. Wherein the contaminants may be introduced at that point. Additionally, the hydrogels must be easy to recover.

7.2.3.2 Carbon-Based Hydrogels

Carbon-based hydrogel nanocomposites are hydrogels synthesized by incorporating nanofillers such as graphene oxide (GO), biochar, activated carbon, and carbon

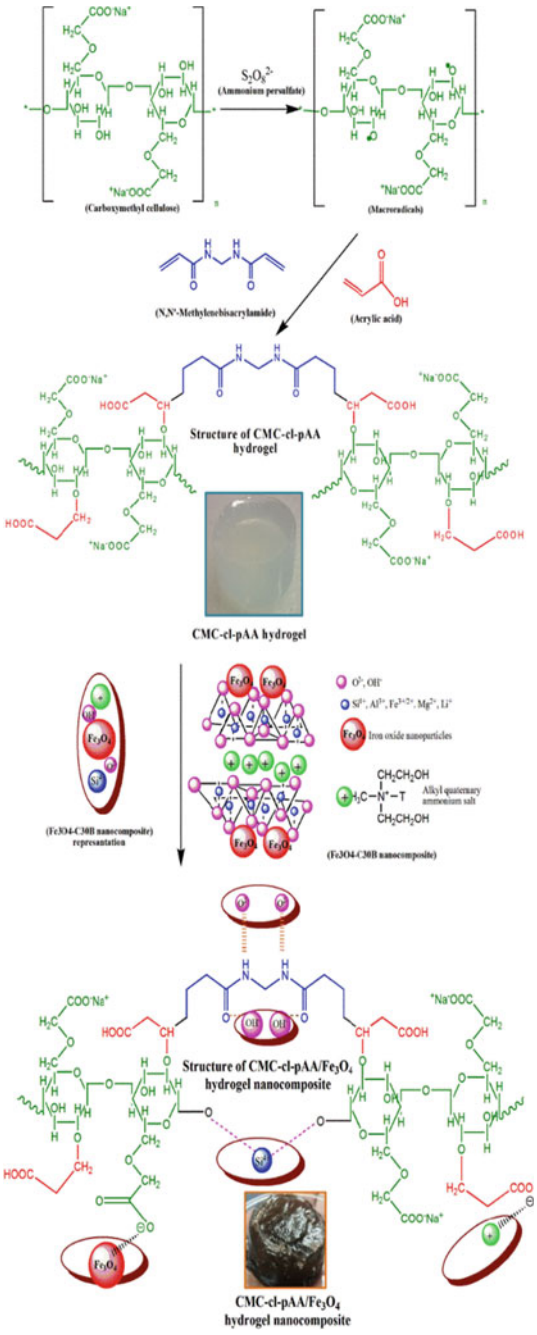

Scheme 7.2 An overview of thermal free-radical polymerization and crosslinking. Reproduced with permission from [65]. Copyright 2020, Springer

nanotubes (CNTs) [11, 64, 95]. GO is a carbon material prepared by oxidizing graphene through chemical or thermal reduction processes. It contains highly hydrophilic groups such as hydroxyl, carboxylic, and epoxy groups that are essential for adsorbing dyes and toxic metals [8]. GO may interact with contaminants through pi-to-pi interactions, electrostatic interactions, or hydrogen bonding [107]. Owing to its outstanding mechanical, electrical and thermal properties, GO has attracted its use in the biomedical, energy and environmental field [31]. An example of a study is by [99]. The group prepared starch hydrogel infused with reduced graphene oxide and reported a high removal capacity of 1106.960 $\mu g\ g^{-1}$ for cationic dyes. The group also reported an improvement in the hydrogel pore size. In another study by [61, 62], xanthan gum-polyacrylic acid hydrogel was modified with reduced GO (XG-cl-pAA/rGO for the removal of MB and MV [28]. The group reported an impressive removal capacity of 1052.63 mg/g and 793.65 mg/g at 25 °C for MB and MV, respectively. Additionally, the XG-cl-pAA/rGO hydrogel nanocomposite was reported to have easy recovery and recyclable.

CNTs are simply graphene sheets rolled up in cylinders of 1 nm in diameter [29]. As a result of their porous structure, large surface area, high tensile strength (0.15 TPa) and elastic modulus (0.91 TPa), CNTs have attracted interest in use for adsorption of pollutants such as dyes, dichlorobenzene, ethylbenzene, and some heavy metals [24, 117]. CNTs can be categorized into two forms, namely, single-walled CNTs (SWCNTs, which are made up of single layers of graphene sheets and multiwalled CNTs (MWCNTs), which are made up of multiple layers of concentric cylinders [4, 29]. Among recent studies that have used carbon-based materials to modify the properties of hydrogels, [62], reported that the incorporation of MWCNT's onto XG/PAA hydrogel improved the surface hydrophilicity and specific area of xanthan gum. The literature reports that although the incorporation of CNTs in gels improves the mechanical properties, the rate of degradation decreases, which is because carbon-based materials have high hydrothermal stability, which makes them resistant to harsh environments [60]. Another widely used carbon-based adsorbent and nanofiller are activated carbon/activated charcoal (AC). This material is reported to improve the surface properties, adsorption capacity, and porosity of adsorbent materials. A study by [45] reported a removal capacity of 60.9 mg/g for TH dye from wastewater using chitosan (CS) hydrogel modified with activated charcoal (CS/AC). Various carbon-based nanocomposite hydrogels and their adsorption properties for the removal of organic dye contaminants from aqueous solutions are listed in Table 7.3.

7.2.3.3 Clay-Based Hydrogels

Natural clays and their improved forms have recently been used for removing pollutants from water [15]. The most commonly used clays, especially for treating toxic metals and dyes, are modified kaolinite and montmorillonite [36]. However, these clays are difficult to regenerate and reuse because of their colloidal dimensions [113]. This prompted the functionalization of these clays—for example, the modification

Table 7.3 Carbon-based adsorbent hydrogels and their adsorption properties in removing contaminants from aqueous solution

Adsorbent	Cross-linker	Dye	Adsorption parameter					References
			q_e (mg/g)	pH	Dosage (mg)	Isotherm models	Kinetics models	
CMC-AAm-GO	MBA	AB-133	185.4	6	100	–	–	[104]
XG-cl-pAA/o-MWCNTs	MBA	MB	521	6	30	Langmuir	PFO	[61]
XG-cl-pAA/rGO	MBA	MV MB	1052.6 793.6	5	10	Langmuir	PSO	[62]
Alg-KBC	Ca^{2+}	CV	2473.0 174.8	10	–	–	PFO and PSO	[77]
CS/CNTs beads	Alkaline mixture	CR	450.4	5	20	Langmuir	PFO	[17]
k-C-g-AA/MWCNT	MBA	CV	118	5–8	200	Langmuir	–	[43]

of montmorillonite (MMT) to form Cloisite 30B. In a study where C30B clay was incorporated onto polypropylene (PP) grafted with maleic anhydride (PP-g-MA) and thermoplastic starch (TPS), it was reported that biodegradation studies performed in compost revealed that the presence of C30B improved the matrix biodegradability [1]. Modification of adsorbents by introducing functionalized clay components may improve both the physical and chemical properties of adsorbents [1, 113]. Other modifications with clay results improve the number of adsorbing active sites, enhanced porosity, and low levels of mineral impurities [1]. In a recent study, C30B was mixed with a culture obtained from an anaerobic sludge to remove hexavalent chromium, where the removal capacity of nearly 100% was obtained [58]. In our recent study, we reported the incorporation of C30B into magnetic carboxymethyl cellulose/poly(acrylic acid) to synthesize the hydrogel nanocomposite [65]. Our findings reported an increased crosslinking density and easy dispersion of magnetite (Fe_3O_4) nanoparticles into the hydrogel matrix due to the presence of the C30B component in the hydrogel. Another study by [81], prepared cellulose-MMT hydrogels for removing MB. The hydrogels had a maximum removal capacity of 1065 mg/g (Table 7.4). Their viscoelasticity studies from the sweep measurements (Fig. 7.2a) showed that when the storage modulus (G') < loss modulus (G"), the cellulose-MMT systems were in a viscous liquid form, however with increasing time when G' > G", the materials were in a gel form. Figure 7.2b in this case revealed that increasing clay content decreased the gel formation. Figure 7.2c revealed that the storage moduli (G') of hydrogels containing clay was higher than that of unmodified hydrogel and was proportional to the clay content from 10 to 15 wt.%. However, the incorporation of clay increased the gel strength from 0.3 kPa to 4.7 kPa, as shown in Fig. 7.2d and e, which was approximately 16 times higher. Furthermore, the study reported that an increase in clay content from 10 to 15 wt.% reduced the swelling capacity of the hydrogel (Fig. 7.2f), reportedly due to a high degree of crosslinking. Furthermore, it was reported that the addition of modified clay containing 2,3-epoxypropyltrimethylammonium chloride increased the crosslinking density of the hydrogel networks, eventually resulting in enhanced storage modulus [81].

7.2.3.4 Metal Oxide-Based Hydrogels

Metal oxide-based nanoparticles have been reported to have a high density and restricted size, which are responsible for their fascinating and unique chemical and physical properties [7, 80]. Examples of metal oxides include titanium dioxide (TiO_2), iron oxide (Fe_3O_4), magnesium oxide (MgO), aluminium oxide (Al_2O_3). Owing to their nontoxic nature, high surface area, high chemical stability, and economical friendliness, Fe_3O_4 nanoparticles are widely used for the removal of toxic metals and organic pollutants from water [7, 80, 85, 97, 119]. Ion-oxide and zinc oxide nanoparticles are some of the most frequently used metal oxides in treating dyes from aqueous solutions [67].

Table 7.4 Clay-based adsorbent hydrogels and their adsorption properties in the removal of contaminants from aqueous solution

Adsorbent	Cross-linker	Dye	Adsorption parameter					References
			q_e (mg/g)	pH	Dosage (mg)	Isotherm models	Kinetics models	
Agar/K-Carra	TEGDVE	MB	242.3	7	–	Langmuir	PSO	[26]
CMC-MMT	ECH	MB	1065	1–10	500	Langmuir	PSO	[81]
P(AA-co-AMPS)/MMT	MBA	MB	192	10	–	Redlich–Peterson	PSO	[42]
CS-g-IA/BT	MBA	MB	500	6	30	Langmuir	PSO	[90]
clay/PNIPAm	LMSH	CV	4.71	8.9	–	–	–	[115]
SH/PAM/clay	MBA	MB	800	–	–	–	–	[111]

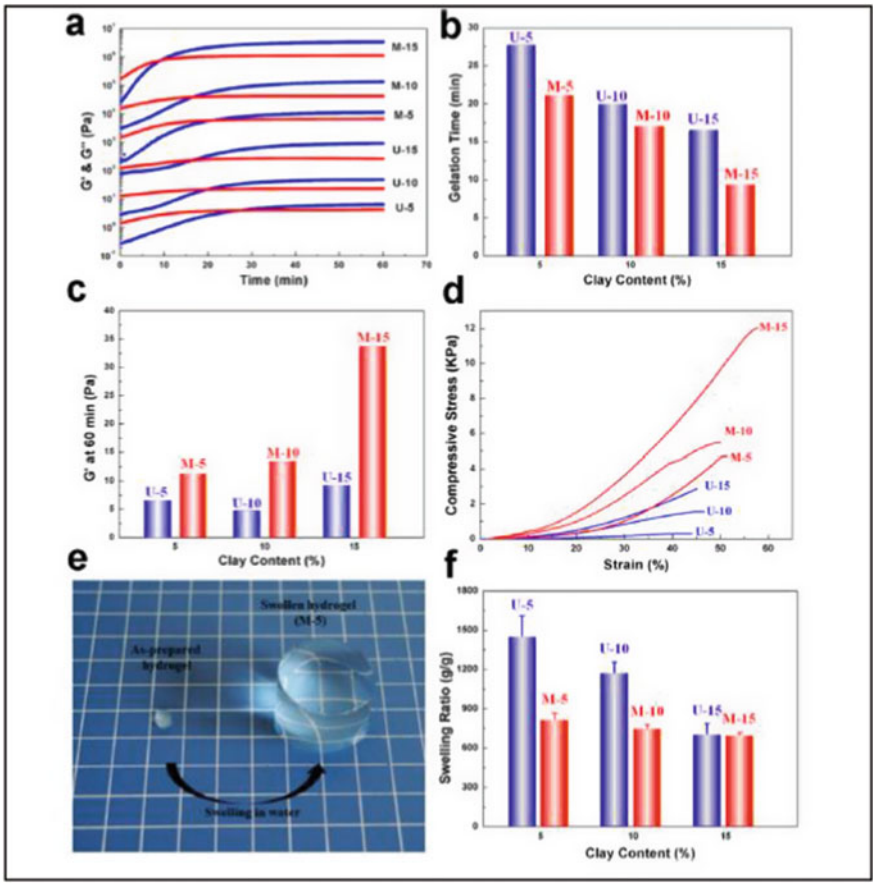

Fig. 7.2 **a** Time dependence of storage modulus (G′) and loss modulus (G″), **b** Gelation time **c** G′ at 60 min **d** Compressive-strain curves **e** Photographs of M-5 **f** The swelling ratio performed using distilled water. Reproduced with permission from [81]. Copyright 2016, American Chemical Society

Amongst the most promising metal-oxides are magnetite (Fe_3O_4) nanoparticles. Magnetite nanoparticles also called black iron oxide amongst other transition metals, have the strongest magnetism and are stable at ambient temperatures [59]. Magnetite is prepared from the coprecipitation of iron oxide salts that result in an inverse spinel crystal structure consisting of half of the Fe^{3+} in tetrahedral coordination and the other half Fe^{2+} ions in octahedral coordination (Fig. 7.3a) [32, 59, 86]. The coprecipitation method is the most useful and suitable technique in preparing magnetite at both lab-scale and industrial scales [53]. Due to their cheap synthesis costs, susceptibility, stability, high porosity, magnetic properties, biocompatibility, and easy chemical modification, MNP's have attracted much use in the wastewater

treatment field [32, 59, 67, 85, 86]). The introduction of MNPs into polymer structures to produce nanocomposite hydrogels leads to a hybrid hydrogel with advantages of both components, thus improved chemical and physical properties. An example of such hybridized hydrogel is Fe_3O_4-g-pAA hydrogel synthesized via radical polymerization in the presence of MBA crosslinker, which resulted in a highly adsorptive hydrogel of 507.7 mg/g removal capacity for MB [82], as shown in Table 7.5. However, according to Flory's theory, the swelling degree of a hydrogel depends on the density of crosslinking, the ionic osmotic pressure, and the attraction of the gel for the liquid [50].

When the crosslinking density is high, the space between the polymer chains decreases, making the gel to be stiff due to tiny nonexpendable pores [50]. Additionally, an increase in the amount of MNPs increases the thermal properties but consequently reduces the swelling capacity as the Fe^{3+} from the incorporated MNPs may act as a physical crosslinking agent [82, 87]. Additionally, in a study by [65] in the removal of MB using CMC-cl-pAA/Fe_3O_4-C30B, the group reported a decreased removal capacity with improved stability for modified HNC compared to non-modified CMC-cl-pAA hydrogel as a consequence of incorporating metal oxide nanoparticles. The most significant advantage of incorporation MNPs into the hydrogel matrix is the improved stability and easy recovery of the material after application [10]. Another prevalent metal oxide is zinc oxide (ZnO) which can be found in nature as a zincite mineral; however, the majority of it is prepared synthetically. Its crystal structure can be found in a hexagonal wurtzite form of cubic zinc blend form (Fig. 7.3b). The form that is most stable and commonly found at ambient temperature is the wurtzite structure Fig. 7.3b [98]. ZnO is commonly used for treating skin-related problems such as nappy rash, dandruff, and incorporation in ointments used in wound dressing [98]. Other applications of ZnO include the use in catalysis, batteries, sensors, and adsorption of contaminants [3, 30, 73, 112]. Their application as adsorbent material was reported in a study by [49], where a guar gum adsorbent hydrogel incorporated with ZnO nanoparticles was used for removing chromium (VI) from water. The group reported that incorporating ZnO nanoparticles improved the recovery of the adsorbent from the aqueous solution after the removal of Cr (VI) [49]. In another study, CMC hydrogel was modified with ZnO for antimicrobial activity, which was influenced by their inexpensiveness and lack of colour [54].

Another widely used metal-oxide is TiO_2, a semiconductor [25, 75]. There exist three forms of TiO_2, namely, anatase, rutile, and brookite. Amongst the three forms, anatase has been reported to be more photoreactive thus its wide use in photocatalytic degradation during water treatment studies [34]. This is because TiO_2 as a photocatalyst is chemically stable, non-toxic, cost-effective, and remains stable during irradiation [9, 47, 74]. Various techniques have been used to synthesize titanium dioxide, namely, low-temperature dissolution-reprecipitation, gas-phase pyrolysis, ultrasonic spray pyrolysis, sol–gel, ultrasonic spray pyrolysis, and combustion synthesis [76]. TiO_2-based nanomaterials have been used in fields such as drug delivery, medical research, self-cleaning, producing antibacterial materials, and energy storage [51, 9]. As nanoparticles for water treatment, TiO_2 offers a high surface area, which is very important in the sorption of contaminants from aqueous solutions [37]. A study

Table 7.5 Metal oxide-based adsorbents for organic dyes removal

Adsorbent	Cross-linker	Dye	Adsorption parameter					References
			q_e (mg/g)	pH	Dosage (mg)	Isotherm models	Kinetics models	
Fe_3O_4/p (Am-co-Na Ac)	MBA	MB	641	7	50	Langmuir	PSO	[7]
pAA-grafted MNPs	MBA	MB	507.7	4	20	Langmuir	PSO	[82]
CMC coated Fe_3O_4@SiO_2 nanocomposite	–	MB	22.7	11	30	Langmuir	PSO	[120]
Fe_3O_4/CA gel beads	$CaCl_2$	MV	713	–	20–40	modified Langmuir–Freundlich	PSO	[6]
ZnO–clay–alginate hydrogel beads	Clay	CR	546.89	5–7	200	Temkin	PFO	[103]
ZnO-PPy nanocomposite	–	BG	140.8	–	50–200	Langmuir	PSO	[114]
Fe_3O_4-CS-Clay	Clay	MB	82	9–12	500	–	–	[10]
chitosan/silica/ZnO NC	–	MB	293.3	–	–	Langmuir	PSO	[41]
SA-poly (AA)/ZnO	MBA	MB	579.2	6	10	Langmuir	PSO	[71]
CMC-cl-pAA/Fe_3O_4-C30B	MBA	MB	1081.6	7	10	Langmuir	PSO	[65]
TiO_2/p(Aam-co-AA)	UV radiation	MB	2.22	–	–	–	PFO	[47]
Gg-cl-PAAm/TiO_2	MBA	MB	1305.5	7	–	Langmuir	PSO	[70]
SA/AA/TiO_2	MBA	MV	1156.6	2–3	–	Langmuir	PSO	[101]

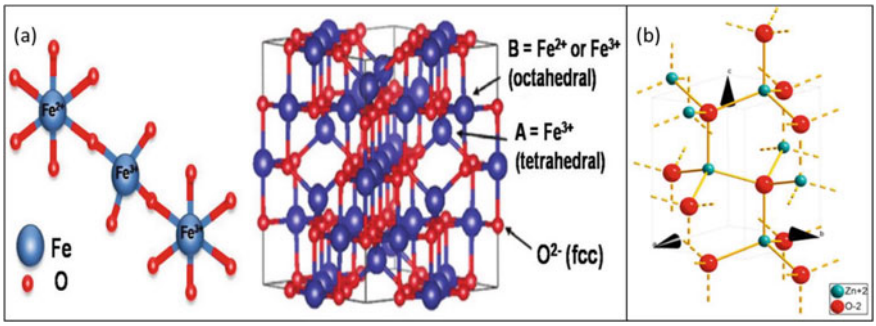

Fig. 7.3 Structures of Fe_3O_4 and ZnO [67]. Reproduced with permission from [98]. Copyright 2017, Walter de Gruyter GmbH

by [102] reported that an increase in the TiO_2 content from 0.05 g to 0.2 g in SA-cl-poly(AA)-TiO_2 O/I hydrogel nanocomposite increased anionic centres and the intrinsic charge repulsion within the hydrogel matrix, consequently enhancing the removal capacity for MB.

7.3 Conclusions

In conclusion, this chapter discusses recent studies applied for removing different types of dyes from an aqueous solution using biopolymer-based HNCs. Owing to various advantages such as low cost and easy design, the adsorption method is recognized as the most promising treatment technique for the removal of dyes. This work briefly discussed hydrogels, their classification, methods of synthesis and modifications with inorganic components to improve on their drawbacks. This contribution emphasized the importance of incorporating carbon compounds, clay content, and metal oxide nanoparticles in hydrogels for the removal of dyes. Additionally, various modified hydrogel nanocomposites are summarised in table form for easy study and comparisons depending on which content was used to modify them.

Acknowledgements This research was supported by the National Research Foundation (NRF) under the Thuthuka programme (UID. 117727), and the University of Limpopo (R202, R232, R355), South Africa.

Conflicts of Interest There are no conflicts of interest to declare.

References

1. A.S. Abreu, M. Oliveira, A.V. Machado, Effect of clay mineral addition on properties of bio-based polymer blends. Appl. Clay Sci. **104**, 277–285 (2015)
2. K.A. Adegoke, O.S. Bello, Dye sequestration using agricultural wastes as adsorbents. Water Resour. Ind. **12**, 8–24 (2015)
3. M. Ahmad, Y. Shi, A. Nisar, H. Sun, W. Shen, M. Wei, J. Zhu, Synthesis of hierarchical flower-ZnO nanostructures and their functionalization by Au nanoparticles for improved photocatalytic and high-performance Li-ion battery anodes. J. Meter. Chem. **21**, 7723–7729 (2011)
4. A. Aqel, K.M. Abou El-Nour, R.A. Ammar, A. Al-Warthan, Carbon nanotubes, science and technology part (I) structure, synthesis and characterisation. Arab. J. Chem. **5**(1), 1–23 (2012)
5. M. Arami, N.Y. Limaee, N.M. Mahmoodi, N.S. Tabrizi, Equilibrium and kinetics studies for the adsorption of direct and acid dyes from aqueous solution by soy meal hull. J. Hazard. Mater. **135**(1–3), 171–179 (2006)
6. S. Asadi, S. Eris, S. Azizian, alginate-based hydrogel beads as a biocompatible and efficient adsorbent for dye removal from aqueous solutions. ACS Omega **3**(11), 15140–15148 (2018)
7. A. Atta, M.A. Akl, A.M. Youssef, M.A. Ibraheim, Superparamagnetic core-shell polymeric nanocomposites for efficient removal of methylene blue from aqueous solutions. Adsorp. Sci. Technol. **31**(5), 397–419 (2013)
8. H. Bai, C. Li, G. Shi, A pH-sensitive graphene oxide composite hydrogel. Commun. Chem. **46**, 2376–2378 (2010)
9. P.S. Basavarajappa, S.B. Patil, N. Ganganagappa, K.R. Reddy, A.V. Raghu, C.V. Reddy, Recent progress in metal-doped TiO_2, non-metal doped/codoped TiO_2 and TiO_2 nanostructured hybrids for enhanced photocatalysis. Int. J. Hydrog. Energy. **45**(13), 7764–7778 (2020)
10. A. Bée, L. Obeid, R. Mbolantenaina, M. Welschbillig, D. Talbot, Magnetic chitosan/clay beads: a magsorbent for the removal of cationic dye from water. J. Magn. Magn. **421**, 59–64 (2017)
11. S. Biswas, T.K. Sen, A.M. Yeneneh, B.C. Meikap, Synthesis and characterization of a novel Ca-alginate-biochar composite as efficient zinc (Zn^{2+}) adsorbent: Thermodynamics, process design, mass transfer and isotherm modelling. Sep. Sci. Technol. **54**(7), 1106–1124 (2019)
12. M. Bodzek, Membrane technologies for the removal of micropollutants in water treatment, in *Advances in Membrane Technologies for Water Treatment. Woodhead Publishing* (2015), pp. 465–517
13. Braun D (2009) Origins and development of initiation of free radical polymerization processes. Int J Polym Sci. 2009: 893234.
14. S.K. Burley, G.A. Petsko, Weakly polar interactions in proteins. Adv. Protein Chem. **39**, 125–189 (1988)
15. F. Cadena, R. Rizvi, R.W. Peters, Feasibility studies for the removal of heavy metal from solution using tailored bentonite (Hazard. Ind. Waste), in *Proceedings of the 22nd Mid-Atlantic Industrial Waste Conference* (1990), pp. 77–94
16. N. Çankaya, Synthesis of graft copolymers onto starch and its semiconducting properties. Results Phys. **6**, 538–542 (2016)
17. S. Chatterjee, M.W. Lee, S.H. Woo, Adsorption of Congo red by chitosan hydrogel beads impregnated with carbon nanotubes. Bioresour. Technol. **101**(6), 1800–1806 (2010)
18. M. Chen, M. Zhong, J.A. Johnson, Light-controlled radical polymerization: mechanisms, methods, and applications. Chem. Rev. **116**, 10167–11021 (2016)
19. Q. Chen, L. Zhu, L. Huang, H. Chen, K. Xu, Y. Tan, P. Wang, J. Zheng, Fracture of the physically crosslinked first network in hybrid double network hydrogels. Macromolecules **47**(6), 2140–2148 (2014)
20. J.P. Cook, G.W. Goodall, O.V. Khutoryanskaya, V.V. Khutoryanskiy, Microwave-assisted hydrogel synthesis: a new method for crosslinking polymers in aqueous solutions. Macromol. Rapid Commun. **33**(4), 332–336 (2012)

21. T. Coradin, K. Wang, T. Law, L. Trichet, Type I collagen-fibrin mixed hydrogels: preparation, properties and biomedical applications. Gels **6**, 36 (2020)
22. C. Dannert, B.T. Stokke, R.S. Dias, Nanoparticle-hydrogel composites: from molecular interactions to macroscopic behavior. Polymers **11**(2), 275 (2019)
23. S. Dawood, T.K. Sen, Review on dye removal from its aqueous solution into alternative cost effective and non-conventional adsorbents. J. Chem. Process. Eng. **1**(1), 1–11 (2014)
24. B.G. Demczyk, Y.M. Wang, J. Cumings, M. Hetman, W. Han, A. Zettl, R.O. Ritchie, Direct mechanical measurement of the tensile strength and elastic modulus of multiwalled carbon nanotubes. Mater. Sci. Eng. **334**, 173–178 (2002)
25. M.I. Din, R. Khalid, Z. Hussain, Recent research on development and modification of nontoxic semiconductor for environmental application. Sep. Purif. Rev. 1–18 (2020)
26. O. Duman, T.G. Polat, C.Ö. Diker, S. Tunç, Agar/κ-carrageenan composite hydrogel adsorbent for the removal of methylene blue from water. Int. J. Biol. Macromol. **160**, 823–835 (2020)
27. B. Eftekhari-sis, V. Rahimkhoei, A. Akbari, H.Y. Araghi, Cubic polyhedral oligomeric silsesquioxane nano-cross-linked hybrid hydrogels: Synthesis, characterization, swelling and dye adsorption properties. React. Funct. Polym. **128**, 47–57 (2018)
28. E.A. Kamoun, X. Chen, M.S.M. Eldin, E.R.S. Kenawy, Crosslinked poly(vinyl alcohol) hydrogels for wound dressing applications: a review of remarkably blended polymers. Arab. J. Chem. **8**(1), 1–14 (2015)
29. A.M.A. Elhissi, W. Ahmed, I.U. Hassan, V.R. Dhanak, A.D. Emanuele, Carbon nanotubes in cancer therapy and drug delivery carbon nanotubes in cancer therapy and drug delivery. J. Drug Deliv. (2012)
30. M. Farrokhi, S.C. Hosseini, J.K. Yang, M. Shirzad-Siboni, Application of ZnO–Fe_3O_4 nanocomposite on the removal of azo dye from aqueous solutions: kinetics and equilibrium studies. Water Air Soil Pollut. **225**, 1–12 (2014)
31. S. Fazil, M. Bangesh, W. Rehman, K. Liaqat, S. Saeed, M. Sajid, I. Bibi, Mechanical, thermal, and dielectric properties of functionalized graphene oxide/polyimide nanocomposite films anomater. Nanotechnology **9**, 1–8 (2019)
32. R.A. Frimpong, J.Z. Hilt, Poly (n-isopropylacrylamide)-based hydrogel coatings on magnetite nanoparticles via atom transfer radical polymerization. Nanotechnology. **19**(17), 175101 (2008)
33. S. Garg, A. Garg, Hydrogel: Classification, properties, preparation and technical features. Asian J. Biomater. Res. **2**(6), 163–170 (2016)
34. S. Glass, B. Trinklein, B. Abel, A. Schulze, TiO_2 as photosensitizer and photoinitiator for synthesis of photoactive TiO_2-PEGDA hydrogel without organic photoinitiator. Front. Chem. **6**, 340 (2018)
35. V. Gómez, M.S. Larrechi, M.P. Callao, Kinetic and adsorption study of acid dye removal using activated carbon. Chemosphere **69**, 1151–1158 (2007)
36. K. Gopal, S. Sen, Adsorption of a few heavy metals on natural and modified kaolinite and montmorillonite: A review. Adv. Colloid Interface Sci. **140**, 114–131 (2008)
37. I.S. Grover, S. Singh, B. Pal, The preparation, surface structure, zeta potential, surface charge density and photocatalytic activity of TiO2 nanostructures of different shapes. Appl. Surf. Sci. **280**, 366–372 (2013)
38. J. Guanghui, L. Wang, H. Yu, W.A. Amer, L. Zhang, Recent progress on study of hybrid hydrogels for water treatment. Colloids Surf. A: Physicochem. Eng. Asp. **416**, 86–94 (2013)
39. M.R. Guilherme, F.A. Aouada, A.R. Fajardo, A.F. Martins, A.T. Paulino, M.F.T. Davi, A.F. Rubira, E.C. Muniz, Superabsorbent hydrogels based on polysaccharides for application in agriculture as soil conditioner and nutrient carrier: a review. Eur. Polym. J. **72**, 365–385 (2015)
40. V.K. Gupta, I. Ali, T.A. Saleh, A. Nayak, S. Agarwal, Chemical treatment technologies for wastewater recycling—an overview. Rsc Adv. **2**(16), 6380–6388 (2012)
41. H. Hosseini, M. Mashaykhi, New chitosan/silica/zinc oxide nanocomposite as adsorbent for dye removal. Int. J. Biol. Macromol. **131**, 520–526 (2019)
42. H. Hosseinzadeh, N. Khoshnood, Removal of cationic dyes by poly (AA-co-AMPS)/montmorillonite nanocomposite hydrogel. Desalin. Water Treat. **57**(14), 6372–6383 (2016)

43. H. Hosseinzadeh, Synthesis of carrageenan/multiwalled carbon nanotube hybrid hydrogel nanocomposite for adsorption of crystal violet from aqueous solution. Pol. J. Chem. Technol. **17**(2), 70–76 (2015)
44. H. Ismail, M. Irani, Z. Ahmad, Starch-based hydrogels: present status and applications. Int J Polym Mater. **62**(7), 411–420 (2013)
45. A.H. Jawad, A. Abdulhameed, M.S. Mastuli, Mesoporous crosslinked chitosan-activated charcoal composite for the removal of thionine cationic dye: Comprehensive adsorption and mechanism study. J. Polym. Environ. **28**, 1095–1105 (2020)
46. E.A. Kamoun, A.M. Omer, S.N. Khattab, H.M. Ahmed, A.A. Elbardan, In-situ UV-photopolymerized PVA-g-GMA hydrogels for biomedical applications: I. Synthesis, characterizations and grafting optimization. J. Appl. Pharm. Sci. **8**(1), 034–042 (2018)
47. W. Kangwansupamonkon, N. Klaikaew, S. Kiatkamjornwong, Green synthesis of titanium dioxide/acrylamide-based hydrogel composite, self -degradation and environmental applications. Eur. Polym. J. **107**, 118–131 (2018)
48. V. Katheresan, J. Kansedo, S.Y. Lau, Efficiency of various recent wastewater dye removal methods: a review. J. Environ. Chem. Eng. **6**(4), 4676–4697 (2018)
49. T.A. Khan, M. Nazir, I. Ali, A. Kumar, Removal of Chromium (VI) from aqueous solution using guar gum–nano zinc oxide biocomposite adsorbent. Arab. J. Chem. **10**(2), S2388–S2398 (2017)
50. M.C. Koetting, J.T. Peters, S.D. Steichen, N.A. Peppas, Stimulus-responsive hydrogels: Theory, modern advances, and applications. Mater. Sci. Eng. R Rep. **93**, 1–49 (2016)
51. T. Kumar, A. Thakur, A. Alexander, H. Badwaik, D.K. Tripathi, Modified chitosan hydrogels as drug delivery and tissue engineering systems: present status and applications. Acta Pharm. Sin. B. **2**(5), 439–449 (2012)
52. L. Largitte, R. Pasquier, A review of the kinetics adsorption models and their application to the adsorption of lead by an activated carbon. Chem. Eng. Res. Des. **109**, 495–504 (2016)
53. D.L. Leslie-pelecky, R.D. Rieke, Magnetic properties of nanostructured materials. Chem. Mater. **8**(8), 1770–1783 (1996)
54. J. Li, L. Fang, W.R. Tait, L. Sun, Preparation of conductive composite hydrogels from carboxymethyl cellulose and polyaniline with a nontoxic crosslinking agent. RSC Adv. **7**(86), 54823–54828 (2017)
55. Y. Liang, X. Zhao, P.X. Ma, B. Guo, Y. Du, X. Han, pH-responsive injectable hydrogels with mucosal adhesiveness based on chitosan-grafted-dihydrocaffeic acid and oxidized pullulan for localized drug delivery. J. Colloid Interface Sci. **536**, 224–234 (2019)
56. C. Liu, A.M. Omer, X. Ouyang, Adsorptive removal of cationic methylene blue dye using carboxymethyl cellulose/k-carrageenan/activated montmorillonite composite beads: Isotherm and kinetic studies. Int. J. Biol. Macromol. **106**, 823–833 (2018)
57. L. Liu, Q. Gao, X. Lu, H. Zhou, In situ forming hydrogels based on chitosan for drug delivery and tissue regeneration. Asian J. Pharm. Sci. **11**(6), 673–683 (2016)
58. G. Lytras, C. Lytras, D. Argyropoulou, N. Dimopoulos, G. Malavetas, A novel two-phase bioreactor for microbial hexavalent chromium removal from wastewater. J. Hazard. Mater. **336**, 41–51 (2017)
59. P. Majewski, B. Thierry, Functionalized magnetite nanoparticles—Synthesis, properties, and bio-applications. Crit. Rev. Solid State Mater. Sci. **32**(3–4), 203–215 (2007)
60. E. Makhado, M.J. Hato, Preparation and characterization of sodium alginate-based oxidized multi-walled carbon nanotubes hydrogel nanocomposite and its adsorption behaviour for methylene blue dye. Front Chem, **9**, 576913 (2021)
61. E. Makhado, S. Pandey, J. Ramontja, Microwave-assisted synthesis of xanthan gum-cl-poly (acrylic acid) based-reduced graphene oxide hydrogel composite for adsorption of methylene blue and methyl violet from aqueous solution. Int. J. Biol. Macromol. **119**, 255–269 (2018)
62. E. Makhado, S. Pandey, P.N. Nomngongo, J. Ramontja, Preparation and characterization of xanthan gum-cl-poly (acrylic acid)/ o-MWCNTs hydrogel nanocomposite as highly effective re-usable adsorbent for removal of methylene blue from aqueous solutions. J. Colloid Interface Sci. **513**, 700–714 (2018)

63. E. Makhado, S. Pandey, K.D. Modibane, M. Kang, M.J. Hato, Sequestration of methylene blue dye using sodium alginate poly (acrylic acid)@ ZnO hydrogel nanocomposite: kinetic, isotherm, and thermodynamic investigations. Int. J. Biol. Macromol. **162**, 60–73 (2020)
64. E. Makhado, S. Pandey, P.N. Nomngongo, J. Ramontja, 'Xanthan gum-cl-poly (acrylic acid)/reduced graphene oxide hydrogel nanocomposite as adsorbent for dye removal', in *International Conference on Advances in Science, Engineering and Waste Management (Asetwm-171)* (2017), pp.59–164
65. N. Malatji, E. Makhado, K.E. Ramohlola, K.D. Modibane, T.C. Maponya, G.R. Monama, M.J. Hato, Synthesis and characterisation of magnetic clay-based carboxymethyl cellulose-acrylic acid hydrogel nanocomposite for methylene blue dye removal from aqueous solution. Environ. Sci. Pollut. Res. **27**(35), 44089–44105 (2020)
66. N.M. Malatji, E, Modibane KD, Ramohlola KE, Maponya TC, Monama GR, Hato MJ, Removal of methylene blue from wastewater using hydrogel nanocomposites: a review. Nanomater. Nanotechnol. **11**, 18479804211039424 (2021)
67. H. Markides, M. Rotherham, A.J. El Haj, Biocompatibility and toxicity of magnetic nanoparticles in regenerative medicine. J. Nanomater. **13**, 13 (2012)
68. S. Mishra, G.U. Rani, G. Sen, Microwave initiated synthesis and application of polyacrylic acid grafted carboxymethyl cellulose. Carbohydr. Polym. **87**, 2255–2262 (2012)
69. H. Mittal, R. Jindal, B. Kaith, A. Maity, S.S. Ray, Flocculation and adsorption properties of biodegradable gum-ghatti-grafted poly (acrylamide-co-methacrylic acid) hydrogels. Carbohydr. Polym. **115**, 617–628 (2015)
70. H. Mittal, S.S. Ray, A study on the adsorption of methylene blue onto gum ghatti/TiO2 nanoparticles-based hydrogel nanocomposite. Int. J. Biol. Macromol. **88**, 66–80 (2016)
71. A.Y. Moreno-lópez, M.E. González-lópez, R. Manríquez-gonzález, J.R. Robledo-ortíz, Evaluation of the Cr (VI) adsorption performance of xanthate polysaccharides supported onto agave fiber-LDPE foamed composites. Water Air Soil Pollut. **230**(6), 1–21 (2019)
72. M. Muller, Understanding the origins of Cape Town's water crisis, (June 2017) (2018)
73. M.Y. Nassar, A.A. Ali, A.S. Amin, A facile Pechini sol–el synthesis of TiO_2/Zn2TiO_2/ZnO/C nanocomposite: an efficient catalyst for the photocatalytic degradation of orange G textile dye. RSC Adv. **7**(48), 30411–30421 (2017)
74. R. Nekooie, T. Shamspur, A. Mostafavi, Novel CuO/TiO_2/PANI nanocomposite: preparation and photocatalytic investigation for chlorpyrifos degradation in water under visible light irradiation. J. Photochem. Photobiol. **407**, 113038 (2020)
75. M.N. Ngoepe, M.J. Hato, K.D. Modibane, N.C. Hintsho-Mbita, *Biogenic Synthesis of Metal Oxide Nanoparticle Semiconductors for Wastewater Treatment* (Scrivener Publishing LLC, 2020), pp. 1–31
76. P. Nyamukamba, O. Okoh, L. Tichagwa, C. Greyling, Preparation of titanium dioxide nanoparticles immobilized on polyacrylonitrile nanofibres for the photodegradation of methyl orange. Int. J. Photoenergy. **2**, 1–9 (2016)
77. G. Ohemeng-Boahen, D.D. Sewu, S.H. Woo, Preparation and characterization of alginate-kelp biochar composite hydrogel bead for dye removal. Environ. Sci. Pollut. Res. **26**(32), 33030–33042 (2019)
78. P.M. Pakdel, S.J. Peighambardoust, A review on acrylic based hydrogels and their applications in wastewater treatment. J. Environ. Manag. **217**, 123–143 (2018)
79. Y. Park, G.A. Ayoko, R.L. Frost, Application of organoclays for the adsorption of recalcitrant organic molecules from aqueous media. J. Colloid Interface Sci. **354**(1), 292–305 (2011)
80. D. Pasqui, A. Atrei, G. Giani, M. De Cagna, R. Barbucci, Metal oxide nanoparticles as cross-linkers in polymeric hybrid hydrogels. Mater. Lett. **65**(2), 392–395 (2011)
81. N. Peng, D. Hu, J. Zeng, Y. Li, L. Liang, C. Chang, Superabsorbent Cellulose−clay nanocomposite hydrogels for highly efficient removal of dye in water. ACS Sustain. Chem. Eng. **4**, 7217–7224 (2016)
82. M. Pooresmaeil, Y. Mansoori, M. Mirzaeinejad, A.L.I. Khodayari, Efficient removal of methylene blue by novel magnetic hydrogel nanocomposites of poly (acrylic acid). Adv. Polym. Technol. **37**(1), 262–274 (2015)

83. Z. Rahmani, R. Sahraei, M. Ghaemy, Preparation of spherical porous hydrogel beads based on ion-crosslinked gum tragacanth and graphene oxide: study of drug delivery behavior. Adv. Polym. Technol. **194**, 34–42 (2018)
84. N. Ranganathan, J.R. Bensingh, A.M. Kader, S.K. Nayak, *Synthesis and Properties of Hydrogels Prepared by Various Polymerization Reaction Systems* (Springer International Publishing, Cham, Switzerland, 2018), pp. 1–25
85. K.G. Rao, C.H. Ashok, K.V. Rao, C.H.S. Chakra, Structural properties of MgO nanoparticles: synthesized by coprecipitation technique. Int. J. Sci. Res. 8–9 (2014)
86. D.A. Rivani, I. Retnosari, T.E. Saraswati, Influence of TiO_2 addition on the magnetic properties of carbon-based iron oxide nanocomposites synthesized using submerged arc-discharge. IOP Conf. Ser.: Mater. Sci. Eng. **509**, 012034 (2019)
87. C. Saikia, A. Hussain, A. Ramteke, H.K. Sharma, T.K. Maji, Crosslinked thiolated starch coated Fe_3O_4 magnetic nanoparticles: effect of montmorillonite and crosslinking density on drug delivery properties. Starke **66**(7–8), 760–771 (2014)
88. M.A.M. Salleh, D.K. Mahmoud, W.A. Karim, A. Idris, Cationic and anionic dye adsorption by agricultural solid wastes: a comprehensive review. Desalination **280**(1–3), 1–13 (2011)
89. A. Science, Adsorption of cationic dyes on activated carbon obtained from waste Elaeagnus stone. Adsorp. Sci. Technol. **34**(9–10), 512–525 (2016)
90. F. Shakib, A.D. Koohi, A.K. Pirzaman, Adsorption of methylene blue by using novel chitosan-g-itaconic acid/bentonite nanocomposite – equilibrium and kinetic study. Water Sci. Technol. **75**(8), 1932–1943 (2017)
91. C. Shen, Y. Shen, Y. Wen, H. Wang, W. Liu, Fast and highly efficient removal of dyes under alkaline conditions using magnetic chitosan-Fe(III) hydrogel. Water Res. **45**(16), 5200–5210 (2011)
92. S.R. Shirsath, A.P. Patil, R. Patil, J.B. Naik, P.R. Gogate, S.H. Sonawane, Removal of brilliant green from wastewater using conventional and ultrasonically prepared poly (acrylic acid hydrogel loaded with kaolin clay: a comparative study. Ultrason Sonochem. **20**(3), 914–923 (2014)
93. R.A. Shmeis, water chemistry and microbiology. Compr. Anal. Chem. **81**, 1–56 (2018)
94. V. Singh, P. Kumar, R. Sanghi, Progress in polymer science use of microwave irradiation in the grafting modification of the polysaccharides – A review. Prog. Polym. Sci. **37**(2), 340–364 (2012)
95. S.C. Smith, D.F. Rodrigues, Carbon-based nanomaterials for removal of chemical and biological contaminants from water: a review of mechanisms and applications. Carbon **91**, 122–143 (2015)
96. L. Song, M. Zhu, Y. Chen, K. Haraguchi, Temperature-and pH-sensitive nanocomposite gels with semi-interpenetrating organic/inorganic networks. Macromol Chem Phys. **209**(15), 1564–1575 (2008)
97. S. Stankic, S. Suman, F. Haque, J. Vidic, Pure and multi-metal oxide nanoparticles: synthesis, antibacterial and cytotoxic properties. J. Nanobiotechnology. **14**(1), 1–20 (2016)
98. I. Stefaniuk, B. Cieniek, I. Rogalska, I.S. Virt, A. Kosciak, Magnetic properties of ZnO: Co layers obtained by pulsed laser deposition method. Mater. Sci.-Pol. **36**(3), 439–444 (2017)
99. A.A. Subhi, V.M. Kiamahalleh, M. Firouzi, F. Yousefi, H.H. Kyaw, A.M. Abri, A. Firouzi, V.M. Kiamahalleh, Self-assembled graphene hydrogel composites for selective dye removal. Adv. Sustain. Syst. **4**(9), 2000055 (2020)
100. M. Tally, Y. Atassi, Optimized synthesis and swelling properties of a pH-sensitive semi-IPN superabsorbent polymer-based on sodium alginate-g-poly (acrylic acid-co-acrylamide) and polyvinylpyrrolidone and obtained via microwave irradiation. J. Polym. Res. **22**(9), 181 (2015)
101. S. Thakur, O. Arotiba, Synthesis, characterization and adsorption studies of an acrylic acid-grafted sodium alginate-based TiO2 hydrogel nanocomposite. Adsorp. Sci. Technol. **36**(1–2), 458–477 (2018)
102. S. Thakur, S. Pandey, O.A. Arotiba, Development of a sodium alginate-based organic/inorganic superabsorbent composite hydrogel for adsorption of methylene blue. Carbohydr. Polym. **153**, 34–46 (2016)

103. S. Vahidhabanu, D. Karuppasamy, I. Adeogun, Impregnation of zinc oxide modified clay over alginate beads: a novel material for the effective removal of Congo red from wastewater. RSC Adv. **7**(10), 5669–5678 (2017)
104. K. Varaprasad, T. Jayaramudu, E. Rotimi, Removal of dye by carboxymethyl cellulose, acrylamide and graphene oxide via a free radical polymerization process. Carbohydr. Polym. **164**, 186–194 (2017)
105. C. Vasile, D. Pamfil, E. Stoleru, M. Baican, New developments in medical applications of hybrid hydrogels containing natural polymers. Molecules **25**(7), 1539 (2020)
106. S. Wang, Y. Boyjoo, A. Choueib, A comparative study of dye removal using fly ash treated by different methods. Chemosphere **60**(10), 1401–1407 (2005)
107. X. Wang, X. Liu, H. Yuan, H. Liu, C. Liu, T. Li, Z. Guo, Non-covalently functionalized graphene strengthened poly (vinyl alcohol). Mater. Des. **139**, 372–379 (2018)
108. H. Xu, F.K. Shi, X.Y. Liu, M. Zhong, X.M. Xie, How can multi-bond network hydrogels dissipate energy more effectively: an investigation on the relationship between network structure and properties. Soft Matter **16**(18), 4407–4413 (2020)
109. J. Xu, X. Liu, X. Ren, G. Gao, The role of chemical and physical crosslinking in different deformation stages of hybrid hydrogels. Eur. Polym. J. **100**, 86–95 (2018)
110. M.T. Yagub, T.K. Sen, S. Afroze, H.M. Ang, Dye and its removal from aqueous solution by adsorption: A review. Adv. Colloid Interface Sci. **209**, 172–184 (2014)
111. J.Z. Yi, L.M. Zhang, Removal of methylene blue dye from aqueous solution by adsorption onto sodium humate/polyacrylamide/clay hybrid hydrogels. Bioresour. Technol. **99**(7), 2182–2186 (2008)
112. S.J. Young, W.L. Tang, Wireless zinc oxide based pH sensor system. J. Electrochem. Soc. **166**(9), B3047 (2019)
113. G. Yuan, B.K.G. Theng, P. North, N. Zealand, J. Churchman, W.P. Gates, Clays and clay minerals for pollution control. Dev. Clay Sci. **5**, 587–644 (2013)
114. M. Zhang, L. Chang, Y. Zhao, Z. Yu, Fabrication of zinc oxide / polypyrrole nanocomposites for brilliant green removal from aqueous phase. Arab. J. Sci. Eng. **44**(1), 111–121 (2019)
115. Q. Zhang, T. Zhang, T. He, L. Chen, Removal of crystal violet by clay/PNIPAm nanocomposite hydrogels with various clay contents. Appl. Clay Sci. **90**, 1–5 (2014)
116. Y. Zheng, J. Monty, R.J. Linhardt, Polysaccharide-based nanocomposites and their applications. Carbohydr. Res. **405**, 23–32 (2015)
117. Y. Zhou, L. Tang, G. Zeng, J. Chen, Y. Cai, Y. Zhang, G. Yang, Y. Liu, C. Zhang, W. Tang, Mesoporous carbon nitride-based biosensor for highly sensitive and selective analysis of phenol and catechol in compost bioremediation. Biosens. Bioelectron. **61**, 519–525 (2014)
118. M. Zhu, L. Xiong, T. Wang, X. Liu, C. Wang, Z. Tong, High tensibility and pH-responsive swelling of nanocomposite hydrogels containing the positively chargeable 2-(dimethylamino) ethyl methacrylate monomer. React. Funct. Polym. **70**(5), 267–271 (2010)
119. M. Zia, A.R. Phull, J.S. Ali, Challenges of iron oxide nanoparticles. Nanotechnol. Sci. Appl. **9**, 49–67 (2016)
120. M. Zirak, A. Abdollahiyan, B. Eftekhari-sis, M. Saraei, Carboxymethyl cellulose coated $Fe_3O_4@SiO_2$ core-shell magnetic nanoparticles for methylene blue removal: equilibrium, kinetic, and thermodynamic studies. Cellulose **25**(1), 503–515 (2017)

Chapter 8
The Effect of Zeolitic Imidazole Framework-8@Graphene Oxide on the Performance of Polymeric Membranes Used for Wasterwater Treatment

T. A. Makhetha and R. M. Moutloali

Abstract The practice of using zeolitic imidazole framework-8@graphene oxide (ZIF-8@GO) is increasing tremendously in membrane technology for wastewater treatment. This is not only due to the limitations posed by ZIF-8 or GO when used separately, but because of the interesting properties a composite of these materials (ZIF-8@GO) possesses, such as hydrothermal stability, porosity, crystallinity, hydrophilicity, and selectivity. Therefore, it is necessary to expand knowledge on the overall properties of the resultant ZIF-8@GO as well as the ZIF-8@GO incorporated into polymeric membranes. This chapter covers the literature on recent developments on ZIF-8@GO incorporated into polymeric membranes for wastewater treatment. The focus is on the morphological features, thermal and chemical stability, membrane performances i.e., rejection of pollutants from wastewater, water flux, selectivity as well as antifouling and or antibiofouling properties of these ZIF-8@GO embedded in polymeric membranes.

8.1 Introduction

Each person has the right to adequate, perpetual, accessible, safe, and cheap water for personal and domestic use. However, not everyone in the world has access to safe and readily available water [81, 86, 94]. It is worth noting that having clean and safe water can greatly boost every country's economy and significantly reduce

T. A. Makhetha
Department of Chemical Sciences, University of Johannesburg, Doornfontein, Johannesburg 2028, South Africa

R. M. Moutloali (✉)
Institute for Nanotechnology and Water Sustainability, College of Science, Engineering and Technology, University of South Africa, Florida Science Campus Florida, Johannesburg 1709, South Africa
e-mail: moutlrm@unisa.ac.za

M. J. Hato and S. Sinha Ray (eds.), *Functional Polymer Nanocomposites for Wastewater Treatment*, Springer Series in Materials Science 323,
https://doi.org/10.1007/978-3-030-94995-2_8

poverty, especially in African countries [86, 94]. Nonetheless, different factors such as increasing water scarcity, climate change, urbanization, population growth, and demographic changes have been identified to pose challenges to water supply systems [44, 46, 49]. As a result of these challenges, World Health Organisation (WHO) stated that, by 2025, half of the world's population would be living in water-stressed areas [99]. Consequently, there is a need to review and scrutinize the already existing membrane processes that are used for wastewater treatment for reuse to ensure the WHO projections are inappropriate.

Membrane processes such as reverse osmosis (R.O.), nanofiltration (N.F.), ultrafiltration (U.F.), and microfiltration have been extensively utilised for wastewater treatment due to their ease of preparation and operation, are cost-effective and possess high efficacy [20, 32, 44, 46, 49, 99]. However, these membrane technologies are hamstrung by their perceived high energy demands or chemical intensiveness during preparation and high fouling tendency, thus requiring frequent backwashing or cleaning [20, 32,44,99]. Furthermore, membrane fouling is considered as the number one drawback hindering the widespread adoption and use of membrane processes in wastewater treatment [44, 46, 49]. In definition, membrane fouling results from the deposition on the membrane surface or adsorption of organic filth such as proteins, natural organic matters, and humic substances as well as microorganisms [22]. It is worth noting that membrane fouling, caused by either bio or organic deposition, is highly affected by the membrane properties and characteristics that greatly dictate its application and performance [22]. In addition, there are other factors that play a crucial role in membrane fouling, i.e., the pH of the feed solution, the concentration of the solute in the feed, and the structure of the membrane [76]. Mitigation strategies to minimize fouling have resulted in the development of modified polymeric membranes leading to improved membrane performances and application.

The incorporation of porous and/or hydrophilic materials into polymeric membranes is currently considered one of the most effective ways to achieve functional membranes for wastewater treatment [32, 44, 46, 49, 58]. Consequently, intensive studies and reports dedicated to the utilisation of metal organic frameworks (MOFs) in membrane formulation due to their controllable pore aperture, pore size, diverse structures, morphologies, and their tunable functionalities [13, 14, 20]. These studies revealed that understanding key features of MOFs and how these interact with polymeric membrane matrices could ensure the production of defect-free MOF-integrated membranes for the filtration process [3]. It is worth noting that not all MOFs are water stable and compatible with the polymers utilized in membrane technology for wastewater treatment [3, 14, 44, 46, 49]. This has led to carbon-based material such as graphene oxide (GO) being used as a dispersant for MOFs as well as to enhance the water stability of the MOFs [11, 43, 47, 55, 57, 69, 89]. GO is a 2D carbon material with oxygenated functional groups,such as carboxyl, hydroxyl, and epoxy, contained on its edge and on the basal plane [53]. These functional groups bestow GO with good hydrophilicity. Furthermore, the oxygenated functional groups make GO reactive, making its surface modification easier and hence used to anchor MOFs increasing their compatibility with the polymer matrix [53, 103].

Wang et al. [11] fabricated an electrospun membrane from polylactic acid (PLA) polymer modified with ZIF-8@GO filler for methylene blue (MB) adsorption and its photodegradation from wastewater. An increase in hydrophilicity and enhanced mechanical strength of the polymer matrix was observed with the incorporation of the ZIF-8@GO filler. The resultant PLA/ZIF@GO composite membranes exhibited enhanced adsorption capacity and photocatalytic efficacy for MB compared to Zhang et al., which rejected only 50% of methyl blue using ZIF-8/HPEI hybrid filler modified PAN [97].

On the other hand, Wang and co-workers [89] investigated the effect of ZIF-8@GO on the antibacterial performances of thin-film composite membranes. The authors found that the increasing ZIF-8@GO content enhanced the antimicrobial properties of the thin film composite membranes. Furthermore, it was also reported that a synergistic effect of the hydrophilic GO and porous ZIF-8 improved the permeability of the thin film composite membranes without compromising on their solute rejection properties. A similar positive contribution resulting from the incorporation of ZIF-8@GO composite fillers on hydrophilicity, water flux, dye rejection as well as fouling resistance in ultrafiltration membrane was reported by [97]. Furthermore, we also reported on how the antibiofouling membrane properties were enhanced by the incorporation of ZIF-8@GO encapsulating the well-known antimicrobial agents, viz. silver and copper nanoparticles [57].

The chapter summarises recent progress on MOFs@GO composite and its use to modify polymeric membranes for wastewater treatment. The focus is on the impact of ZIF-8@GO on structural and morphological features of the resultant membranes; i.e., membrane pore size or shape, surface roughness, and hydrophilicity and their influence on the membrane performance parameters such as water flux/permeability, solute rejection mechanisms, and the effect of the composites on membrane fouling.

8.2 General Description of Metal–Organic Framework (MOFs)

Metal–organic frameworks (MOFs) are classified as both organic and inorganic materials due to their constituents, i.e., transition metal cations (such as Co, Zn, Zr, and Cu) and multidentate organic linker (such as terephthalic acid and 2-methylimidazole) [36]. The formation of MOFs is through the coordination of the metal clusters with the functional groups from the ligand/linker; hence they are also called porous coordination frameworks [35]. MOFs have interesting features such as a high surface area with their porosity and pore sizes much greater than those of molecular sieve materials that can be controlled or tuned from micro to mesoporous by simple methods [12, 32, 44, 46, 49, 99].

MOFs are divided into different categories based on their metal clusters and the linker used. More insight on the differences in MOFs is presented in the sections below. Thus far, there is isoreticular metal–organic frameworks (IRMOFs) [6, 30,

54, 70, 84, 96], zeolitic imidazolate frameworks (ZIFs) [4, 5, 7, 59, 65], materials of institute lavoisier frameworks (MILs) [10, 15,16, 18, 30, 60, 61, 67], University of Oslo (UiO) [8, 34, 51, 93], etc. New types of MOFs are being developed, looking at using lanthanides and actinides metals with different linkers [28, 78]. The f-orbital lanthanides and actinides are less available for bonding which results in big particle size in comparison to the d-orbital transition metals [78]. Furthermore, due to less available bonding sites, the lanthanides metal center forms the first coordination sphere that constitutes the primary building units (PBU) of the lanthanide MOFs. The PBU then combines into larger, unique polymeric subunits that are repeated throughout the entire framework that is known as the secondary building unit (SBU) [28]. Subsequently, these lanthanides and actinides MOFs provide enhanced catalytic binding sites compared to the transition metal MOFs [28].

8.2.1 Isoreticular Metal–Organic Frameworks (IRMOFs)

Isoreticular MOFs are the ones from organic ligands of different sizes, but with a common symmetry/geometry resulting to MOFs of related topologies, but with expanded pore sizes and volumes [73]. IRMOFs series have similar primitive cubic packing (pcu) topology and can be fabricated from MO–C clusters where M is a metal and different ligands as demonstrated in Fig. 8.1 [6, 30, 54, 70, 84, 96]. The varied ligand result to change in surface area, physical and chemical properties; hence these are used for various applications such as gas adsorption, catalysis, and sensors

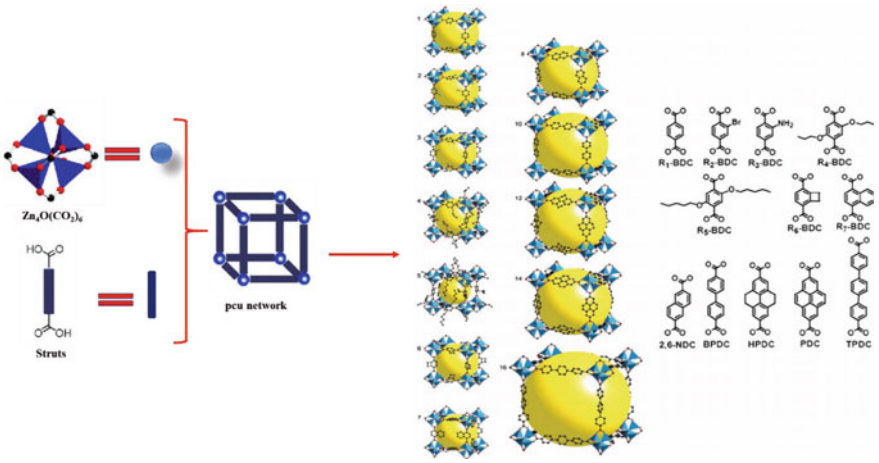

Fig. 8.1 Description of the formation of IRMOFs and structural represantation of IRMOFs and the structure of the ligand derivatives of IRMOFs family. Yellow central sphere represents open pore spaces. Reproduced with permission from [96] and [70]. Copyright 2012, Royal Society of Chemistry and 2014, Springer-Verlag Berlin Heidelberg

[6, 30, 54, 70, 84, 96]. However, IRMOFs are not applicable in water research since they easily degrade in a humid environment even at room temperature due to the rupture of the bond between a metal atom and the central oxygen from the metal cluster [6]. The molecular length and breadth of the organic ligand control the size of the cavities (yellow spheres) of the resultant MOFs.

8.2.2 Zeolitic Imidazolate Frameworks (ZIFs)

Extensive research has been done on MOFs in the past decades, which led to the development of the subfamily zeolitic imidazolate frameworks (ZIFs) [4, 5, 7, 59, 65]. The main constituents of ZIFs are the two transition metals, i.e., zinc and cobalt, and a range of imidazolate linkers coordinated in a tetrahedral shape that is similar to that in crystalline aluminosilicate zeolite and hence their generic name (Fig. 8.2) [59]. The coordination of ZIFs is built from M–I.M–M (M = tetrahedrally coordinated metal ion, I.M. = imidazolate, and its derivative) bonding with a M–I.M.–M angle of 145°, which is similar to the Si–O–Si angle in zeolites (Fig. 8.3) [4, 7, 59]. Interestingly with ZIFs, their structure depends primarily on the type of solvent used and the linker imidazolate (Fig. 8.4) [4, 5, 7, 59, 65]. It has been observed that when the functionalized linkers are used, greater structural diversity in ZIFs is possible. Similarly, ZIFs are thermally and chemically stable; moreover, ZIFs have been shown to be water stable in comparison to other MOFs [4, 5, 7, 59, 65]. This is due to the strong metal to nitrogen bond that shows intensive resistance to alkali water and organic solvents [3]. Furthermore, ZIFs are hydrophobic; therefore, water molecules

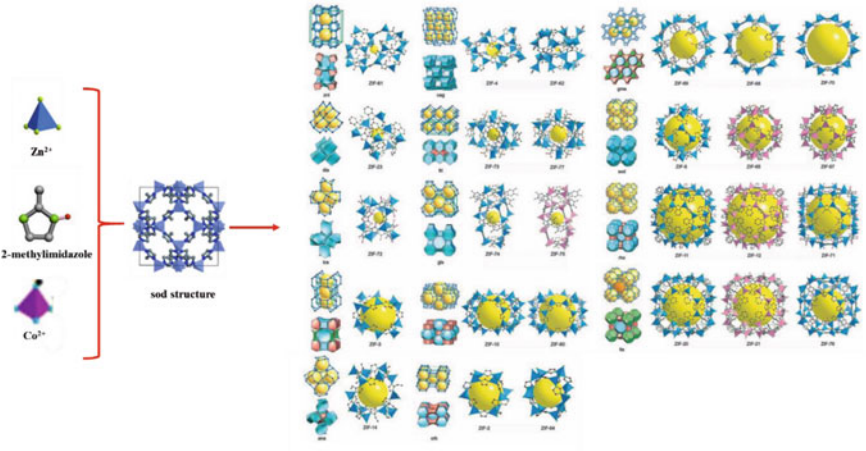

Fig. 8.2 Representation of assembly of different types of ZIFs and their respective topologies. Yellow central sphere represents open pore spaces. Reproduced with permission from [5]. Copyright 2008, American Association for the Advancement of Science

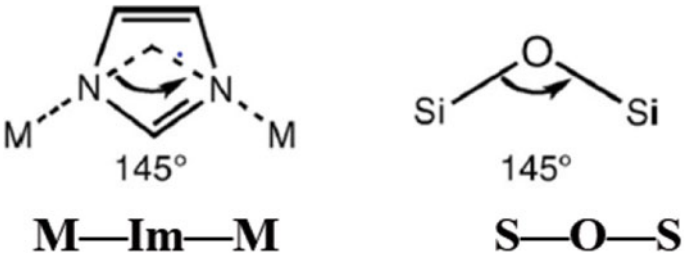

Fig. 8.3 General structural model of ZIFs showing angle similarities with the aluminosilicate zeolites. Reproduced with permission from [59]. Copyright 2020, Taylor & Francis Online

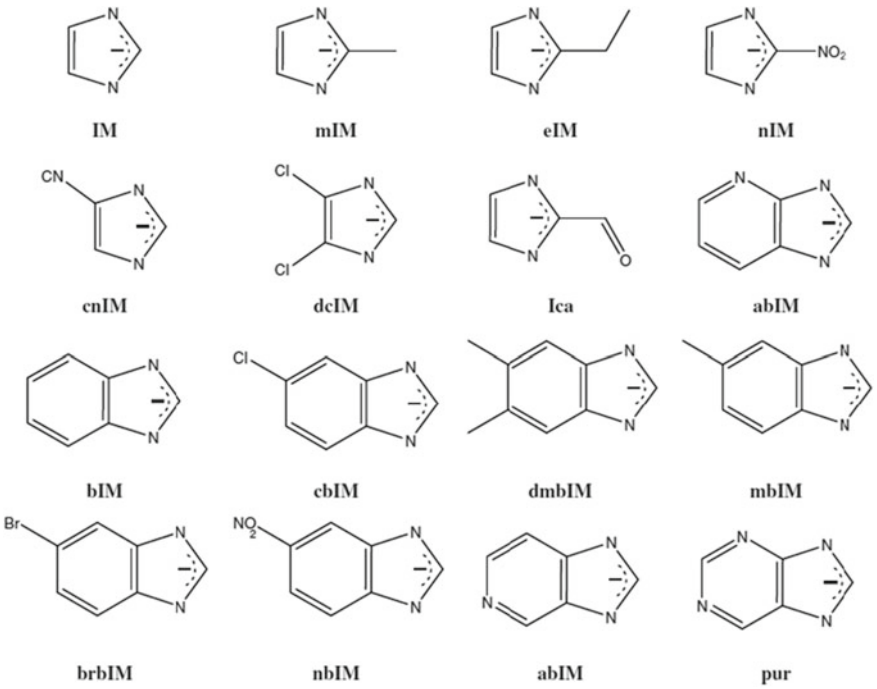

Fig. 8.4 Different types of imidazole ligands used for the synthesis of ZIFs. Reproduced with permission from [7]. Copyright 2014, Springer Nature Switzerland AG

cannot penetrate through the framework pores to destroy their structure [59]. ZIFs have been widely applied in gas storage/separation, catalysis and recently in water purification and wastewater treatment [4, 5, 7, 59, 65].

8.2.3 *Materials of Institute Lavoisier Frameworks (MILs)*

MILs were firstly discovered in 2000 by Millange and Serre et al. [18]. These types of MOFs are formed from the chemically inert metals such as Cr, Fe, Sc, V, Al, Ti, Ni, and Mn. and the benzene-1,4-dicarboxylate linkers (Fig. 8.5) [10, 15,16,18, 30, 60, 61, 67]. The structure of MILs is made by coordinating benzene-1,4-dicarboxylate ligands metal centres that are octahedrally connected and share trans-corners to give infinite, linear inorganic chains [10, 15,16,18, 30, 60, 61, 67]. This yields an open structure with diamond-shaped channels running parallel to the inorganic chains, as presented in Fig. 8.6. MILs are known for their flexibility which allows them to expand and contract when exposed to stimuli such as pH change, temperature, the introduction of guest molecules, and pressure without any change in their crystalline structure [10, 15,16,18, 60, 61, 67]. Such MOFs have been used in various applications such as catalysis, sensing, drug delivery and degradation or capture of pollutants [10, 15,16,18, 60, 61, 67].

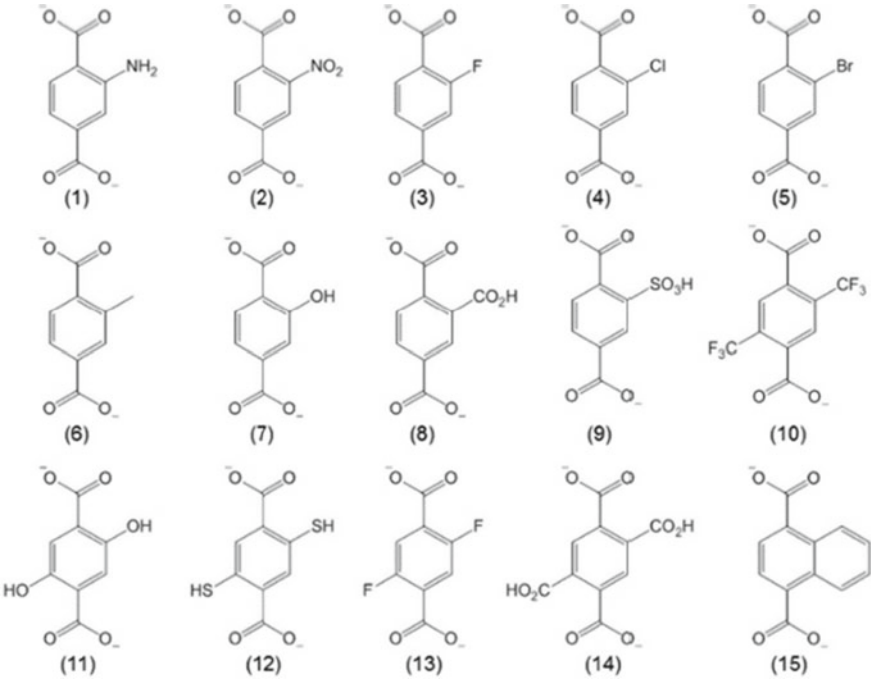

Fig. 8.5 Different types of ligands used to synthesize MILs. Reproduced with permision from [82]. Copyright 2020, John Wiley and Sons

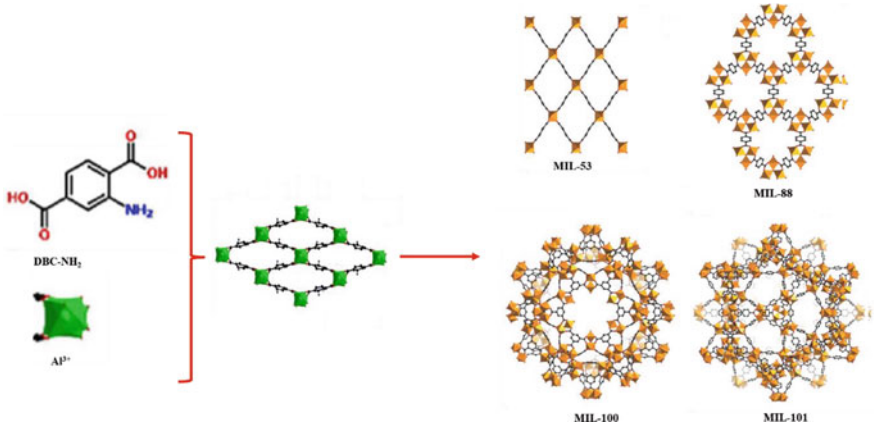

Fig. 8.6 Representation of assembly of different MILs. Reproduced with permission from [91]. Copyright 2020, Royal Society of Chemistry

8.2.4 University of Oslo (UiO)

UiO-66 MOF was first synthesized at the University of Oslo and hence its name. Similar to other MOFs such as MILs, UiO-66 is formed when the 1,4-benzenedicarboxylate organic linkers coordinate to Zr metal ions in clusters contained as $Zr_6O_4(OH)_4$ nodes (Fig. 8.7) that are different to that of MILs [8, 34, 51, 93]. UiO-66 MOFs present an octahedron shape and are known to be stable in acids andwater vapor, and are thermally stable [93]. As such, they have been widely used in aqueous applications such as dye adsorption and pervaporation [20].

8.2.5 Summary of MOFs

From the general description of MOFs, it is evident that not all MOFs are suitable for water application without modification. Therefore, some factors need to be considered when choosing MOFs to be used in water-related applications. It is also worth noting that the structure and the morphology of the MOFs are not only dependent on the building blocks and the linker used, as shown in Figs. 8.1, 8.3, 8.5 and 8.7. In essence, some factors such as temperature, compositional parameters (i.e., pH, type of salt and molar ratio), and solvent influence the structure and the morphology of MOFs [3]. For example: during the synthesis of MOFs, usually, the solvents are not incorporated within the framework; however, they might direct the crystal growth of the MOFs by acting as directing agents [29, 42, 74]. Furthermore, the nucleation growth of MOFs can be increased, which then results in a smaller particle size of MOFs by using more reactive metal precursors, i.e., using $Zn(NO_3)_2$ instead of using $ZnSO_4$ [102].

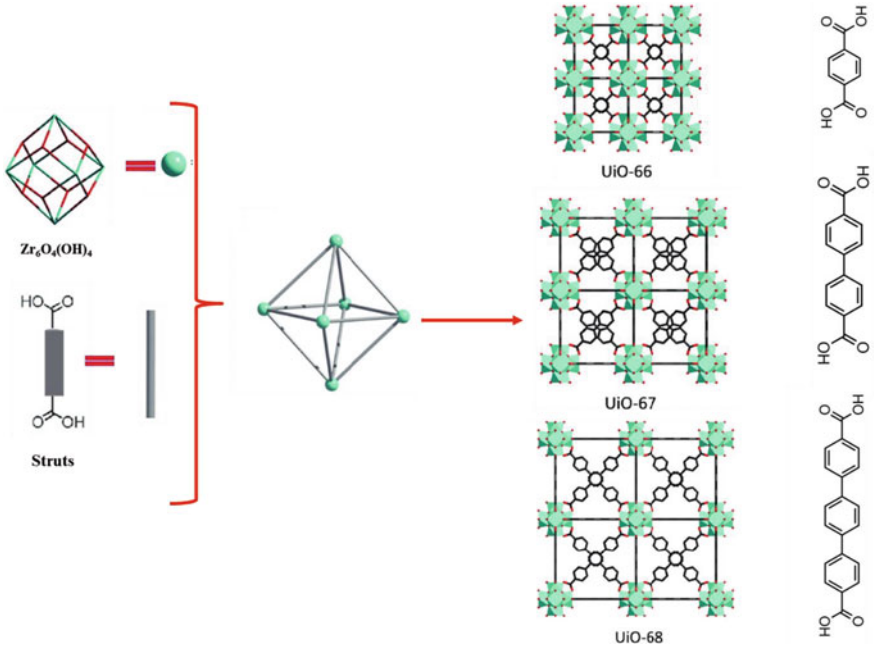

Fig. 8.7 Representation of assembly of different UIO-66 MOFs. Reproduced with permission from [105]. Copyright 2018 John Wiley and Sons

Additionally, the molar ratio between the linkers and the metals does play a huge role; the excess of the linker might slow down the growth rate as it will function as a stabilizing agent [52, 74]. Another important factor to consider is high temperatures used for the synthesis of MOFs since excessively high synthesis temperature may oxidize metal ions [74]. Thus, MOFs are recently used as precursors for metal oxides [71]. Finally, the addition of additives such as trimethylamine (TEA) and cetyltrimethylmmonium bromide (CTAB) might affect the growth rate resulting in smaller particle sizes [25, 66].

8.3 Factors to Consider When Choosing MOFs in Water Application

8.3.1 MOFs Should Have High Water Stability

MOFs need to be water stable for them to be applied in water research, such as in membrane technology for water treatment and purification. Most MOFs, such as isoreticular MOF-5 and HKUST (Hong Kong University of Science and

Technology), a metal–organic framework made up of copper nodes with 1,3,5-benzenetricarboxylic acid struts between them, are susceptible to moisture and hydrolyze, resulting in decomposition and displacement of the building block leading to a loss of crystallinity and porosity of MOFs [6]. As a result, only a handful of MOFs are stable in water without any modification. These include MOFs with high valence metal ions such as Zr^{4+}, Ti^{4+}, Cr^{3+}, and Fe^{3+} coordinated to ligands shown in Figs. 8.6 and 8.7, these include MOFs such as MILs and UiO [34, 60, 67, 93]. Their stability is due to the charge density of these high valence metals that is related to their corresponding ionic radius. In this case, the stability of MOFs is enhanced since the smaller the effective ionic radius is linked to the high charge density of the metal ion [3].

Other water-stable MOFs are those synthesized using azolate based organic ligands such as imidazolates, pyrazlates, triazolates, and tetrazolates (Fig. 8.4) [5, 59, 65]. The stability of the azolate ligands is ascribed to their higher pKa values [45]. This results in the stability of the ligands being maintained even though low valence metal ions are used, e.g., Zn in ZIF-8 is one of the perfect examples [59]. Furthermore, the strong bond formed between metal-nitrogen is maintained, resulting in higher water stability of the ZIFs [5].

Modification of MOFs with specific functional groups can prevent water molecules from entering into their framework structure. For instance, the introduction of the hydrophobic functional groups such as methyl groups and non-polar alkyl groups enhances water stability of the resultant MOFs [45]. Consequently, hydrophobic pore surfaces and encapsulated metal ions provide steric hindrance as a mechanism that blocks water from seeping into the frameworks. Ultimately the exclusion of water molecules in the framework structure imparts and enhances the water stability of MOFs.

Finally, the formulation of the core–shell MOFs does play a crucial role in enhancing the water stability of the MOFs. In this case, the water-stable MOFs act as a shell that protects the water-sensitive core [3, 45]. Most interestingly, MOFs@MOFs materials offer a synergistic effect, and new properties are often realized in these types of materials [44, 46, 49, 68, 95]. In adsorption and separation application, MOFs@MOFs materials are fabricated from MOFs with different apertures in order to serve as molecular sieves [95]. As such, the MOF with a larger opening will act as a cargo transport highway, while the MOF with a smaller opening will act as a filter [95].

Furthermore, these MOFs@MOFs materials are synthesized using different synthesis routes, i.e., epitaxial growth, post-modification, and one-pot synthesis for MOFs@MOFs materials [44, 46, 49, 68, 95]. These synthesis routes offer different structural features as well as different properties that can be utilized for different applications [95]. In definition, epitaxial growth is the seeding/growing of one MOFs on the surface of the other MOF through see-mediated synthesis, e.g., growth of ZIF-8@ZIF-67 or vice versa [44, 46, 49 68, 95]. On the other hand, a post modification route is the most flexible method for the synthesis of MOFs@MOFs materials, wherein, different strategies are employed such as Ostwald ripening-mediated

method, selective trans-metalation method, internal extended growth method, post-synthetic ligand exchange, retrosynthetic design, and surfactant-mediated over-growth method [95]. Finally, in the one-pot synthesis method, the metal ions and ligands of the inner and outer MOFs are added into the reaction system simultaneously [95]. Nonetheless, the porosity of MOFs@MOFs materials is of paramount, especially in separation application.

8.3.2 *Suitable Pore Size for MOFs Appropriate for Use in Membrane Technology*

MOFs have a high controllable level of porosity that makes them suitable to be used in all membrane types, i.e., reverse osmosis, nanofiltration, ultrafiltration, and microfiltration membranes [20]. In these cases, the aperture of their cages and the pore sizes play a crucial role in the membrane process resulting in enhanced water flux by providing alternative water pathways, decreasing water resistance, and reducing tortuosity (Fig. 8.8) [39]. The pore size of the MOFs does affect the rejection of pollutants; small pore size and aperture cage are mostly preferred to allow water transport while preventing transport of dissolved ions across the membrane [14]. As such, the appropriate pore or cavity size of the MOFs in membrane technology is the small pore size that can only allow water molecules while preventing other small dissolved salts; this is referred to as molecular sieving. In a case where the pore size of the MOF is big enough to allow pollutants within the pores, there is an interaction of the pollutants with the adjacent surfaces of the MOF; hence adsorptions will take place within the MOF cavities [44, 46, 49]. The selection of the pore size does also

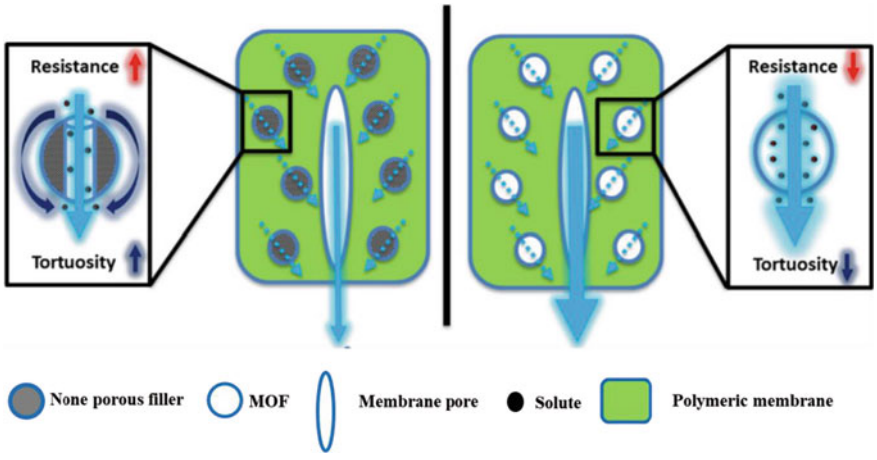

Fig. 8.8 Representation of the water transport through the macropores inside the MOF incorporated into polymeric membrane. Reproduced with permission from [39]. Copyright 2015 Elsevier

depend on the targeted pollutant, similarly in gas separation since gas molecules are different in size [44, 46, 49].

8.3.3 *Importance of Uniform Dispersibility of Fillers in Composite Membranes*

Free-standing layers of MOFs with uniform pore size and high level of porosity can be used to ensure consistent properties throughout MOF membranes [44, 46, 49]. However, these membranes can barely be approved for practical application due to their poor mechanical strength. Therefore, MOFs incorporated into membranes are widely used and approved [3, 43, 47, 99]. As such, MOFs are generally used as nanofillers, and the dispersion of MOFs crystallites plays an important role in the performance of the composite membranes [3, 43, 47, 99]. The concentration or loading of MOF nanofillers below 5 wt.% is the most appropriate quantities to use for resulting in uniform dispersion in the membrane matrices (Kadhom and Deng, 2018b). However, MOFs are not entirely compatible with most polymer matrices. Hence, in other instances, a compatibilizer or a dispersant such as carbonaceous materials (graphene oxide, carbon nanotubes) play a crucial role in properly dispersing MOFs in a matrix [41, 106]. As the concentration of the MOF nanofillers increases, the surface energy of the MOF particles is reduced as a result of high surface energy that is caused by Van der Waals forces (Manuscript et al., no date), leading to agglomeration. Poor dispersion compromises the mechanical properties of the membranes resulting in poor membrane performances [41, 106]. Furthermore, a high concentration of MOF filler may result in changes in the rheology of the membrane matrix affecting the physical and chemical properties of the resultant membrane, as a result, decreasing membrane performances such as water flux, rejection as well as fouling resistance. (Manuscript et al., no date). Consequently, there is a need to investigate different strategies to employ to improve the MOF/polymer interface.

So far, a great number of approaches have been used to improve MOF/polymer interface, such as using different methods for preparing the dope solution, surface modification of the MOFs or the polymer, adding interface agents, i.e., ionic liquids, and using MOF composites, i.e., MOF@GO [48]. Most of these approaches have shown interesting results; however, there is still more to be done to improve the interfacial voids found between the MOF and the polymer [48]. However, few interfacial voids and better MOF/polymer interactions have been reported for MOF composites due to better compatibility between the GO and most polymers [55,57, 43, 47, 87, 106].

8.4 ZIF-8@GO Fillers Used in Membrane Technology for Wastewater Treatment

MOFs have been used as fillers in membrane technology for wastewater treatment [27]. However, MOFs as inorganic fillers are incompatible with organic polymer matrix, which has led to the use of hybrid fillers that emanated from the concern of poor dispersion of the inorganic filler in the organic polymeric membrane. Consequently, the use of carbonaceous materials as compatibilizers or dispersants has proven to be very crucial [11, 89]. It is worth noting that, in most cases, the composite membrane will exhibit both the properties of the individual materials used to form the hybrid filler [11, 56, 57, 89]. Interestingly, in membrane technology, the filler material improves the properties of the resultant composite membrane; these include the physico-chemical, i.e., improved surface morphology, enhanced thermal stability, improved mechanical properties, improved membrane performance, i.e., water flux, rejection, and fouling resistance. Therefore, understanding the individual properties of the materials such as MOFs and GO as well as the resultant composite is crucial as it provides insight into how the morphology and/ or structure of the resultant composite membranes can be influenced, leading to better membrane performance.

8.4.1 Morphology

There are three different groups of membranes, i.e., biological membranes, artificial membranes, and theoretical membranes [72]. This chapter focuses on artificial membranes such as R.O., NF, U.F., and M.F. with asymmetric structure mostly used in industries [72]. A typical asymmetric membrane structure is shown in Fig. 8.9 and consists of two layers that can be viewed from its cross-section. This type of membrane consists of a top dense thin layer usually referred to as the top skin layer, and a bottom porous sublayer [62, 72]. These two layers play a crucial role. The dense top layer controls the performance, such as the permeation properties and water flux of the membrane. The porous sublayer only provides mechanical strength to the membrane. On the other hand, the membranes with symmetric structures do not possess top dense or porous bottom layers and are uniform throughout (Fig. 8.9). There are two types of asymmetric membranes, (1) an *integrally skinned* asymmetric membrane where the material of the top layer and porous sublayer is the same [19]. (2) The composite membrane where the polymer of the top skin layer is different from the polymer of the porous sublayer [19]. Interestingly, the porous sublayer can be modified separately to optimize the overall performances of the membrane in comparison to the integrally skinned asymmetric membrane [19, 72]. For example, the porous layer can be optimized by choosing the amount of the polymer used that affects the viscosity of the casting solution, as a result affecting the exchange rate of water and solvent. The addition of the pore former, e.g., poly(vinyl pyrrolidone) is

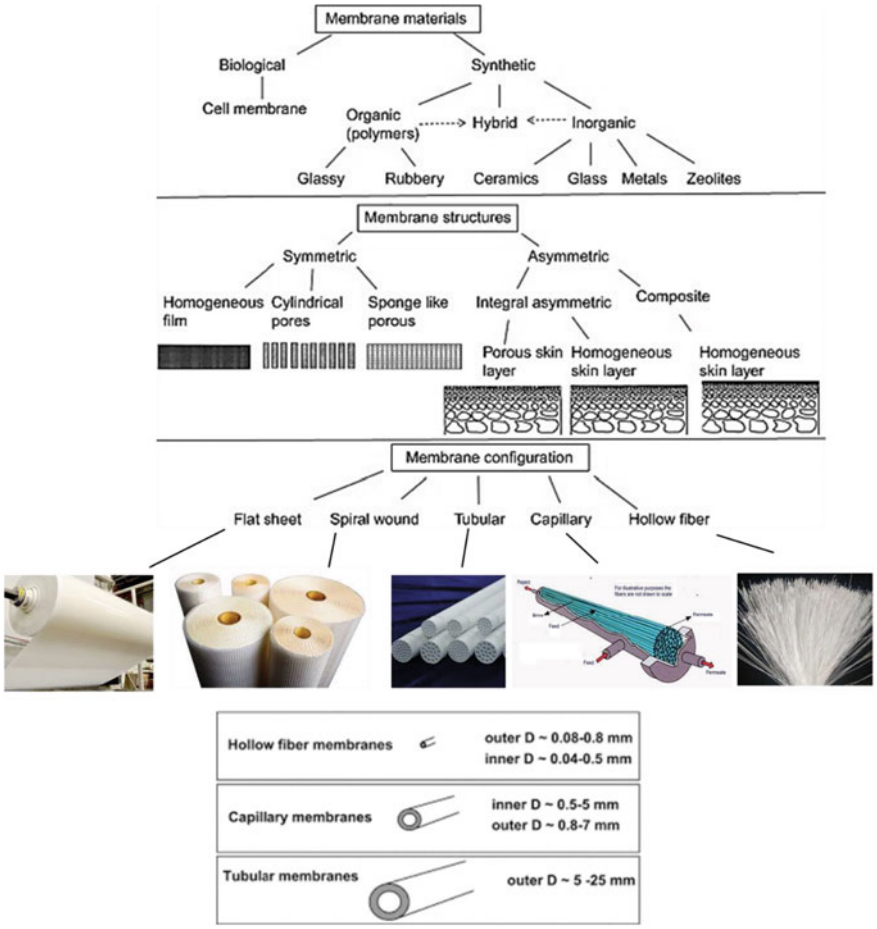

Fig. 8.9 Classification of membranes based on materials of construction, structural attributes, configuration and diameter of the configuration. Reproduced with permission from [19]. Copyright 2019 Elsevier

also used to optimize the porous layer [41]. The top layer can be modified by understanding the effects and the amount of the monomers that are used to fabricate the top layer (W J [37, 38]. For example, m-phenylenediamine (MPD) aromatic diamine and trimesoyl chloride (TMC) acid chloride have proven to be the most successful monomers for the fabrication of the top layer of the composite membrane (W J [37, 38].

The properties of membrane pore structures, such as pore size, pore size distribution, pore density, surface roughness, etc., are the backbone of the membrane processes since such properties control the filtration characteristics of membranes [19, 62, 72]. Membrane preparation protocols that are geared towards controlling the physical properties like pore size and pore size distributions of the membranes

are continuously being developed. These include the phase inversion method that is divided into four different main types (i.e., non-solvent-induced phase separation (NIPS), vapor induced phase separation (VIPS), thermally induced phase separation (TIPS), and solvent evaporation-induced phase separation (SEIPS)). NIPS, TIPS, and VIPS are extensively used for producing polymer membranes, whereas SEIPS involves the use of liquid monomers for the production of membranes [21, 83]. The difference between these methods is the mechanism in which the phase inversion process occurs [83]. Wherein TIPS method uses high temperatures to prepare a dope polymer solution thereafter cooled to induce phase separation followed by polymer solidification [50, 83]. On the other hand, in NIPS, a homogeneous solution of the polymer and the solvent is cast on a glass plate and subsequently submerged into a coagulation bath containing a non-solvent, e.g., deionized water; hence, precipitation occurs due to the exchange of solvent into non-solvent [21, 55]. In contrast to NIPS and TIPS, the phase inversion processes in the VIPS method occur in the open air under-regulated humidity [64].

There are fundamental factors that affect the phase inversion process in membrane formation when using NIPS, TIPS, and VIPS methods, these include the choice of solvent-nonsolvent system, the composition of the coagulation bath, the composition of the polymer solution, and film casting conditions [21, 83]. As such, the desired membrane is achieved by optimizing the above-mentioned factors. Furthermore, additives, such as organic, i.e., poly(vinyl pyrrolidone) and poly(ethylene glycol), as well as inorganic additives, i.e., nanoparticles, are often used as a third component during membrane formation [21, 83]. These additives are often utilized to regulate membrane pore formation, pore structure, pore distribution, and chemical properties, which then influence the membrane performance as well as the membrane application [21, 64, 83]. There are numerous techniques that are utilized to assess the effectiveness of these various factors in membranes formation. For example, Younas and co-workers investigated the effect of coagulation residents on the morphology, mechanical properties as well as gas transport behavior of the resultant membranes [50]. The findings revealed that the pores increased with increased exposure of the membranes in the coagulation bath, which allowed enough time for de-mixing to occur. Furthermore, it was realized that an increase in pore density resulted in a thin dense layer that positively influenced the resistance of the membranes towards gas transport [50].

The usage of several techniques to determine pore size and distribution characteristics of the membranes include the mercury porosimetry, permporometry, bubble point method, thermoporometry, and the adsorption method, as well as methods based on liquid or gas transport, microscopic methods such as scanning electron microscopy (SEM), transmission electron microscopy (TEM), and atomic force microscopy (AFM) are commonplace [62, 72]. Herein, the focus will be limited to the microscopic methods, i.e., SEM and AFM. These two techniques are of interest in this chapter since they provide a clear and visual morphological insight with respect to pore size, pore density, pore distribution, as well as surface roughness. Moreover, each technique can provide more than a single information about the characteristics

of the membrane pore, and the results obtained are independent of the other parameters unlike the other mentioned techniques. Whereas, in other techniques such as the bubble point technique and porosimetry, only the radius of the largest pore is determined, and the results depend mostly on the contact angle as well as the surface tension of the membrane [85].

8.4.1.1 Sem

SEM is an electron microscope that uses a focused beam of electrons that react with the sample to produce a topological image. In membranes, a top surface and a cross-section are usually investigated where the top surface reveals the surface pores of the membranes. SEM usually underestimates pore diameters due to the metal coating that is necessary to increase conductivity [31]. The measured pore diameter value varies with the coating rate, coating period, and pore shape [31, 62]. It is worth noting that the pore shape is usually not cylindrical but funnel-shaped, so the coating can reduce the pore size leading to underestimation of the actual size [72]. The structural changes/defects may also occur due to the damage by the electron beam or by the requirement to operate in a high vacuum [72]. Nonetheless, SEM is widely used in membrane technology to assess the topography of the membrane.

The effect of ZIF-8@GO fillers on membrane topography is dependent on the membrane fabrication protocol used. For instance, its effects on membranes formed using phase inversion for U.F. membranes are different from that obtained using interfacial polymerization process for N.F. and R.O. membranes. For instance, in the phase inversion process, ZIF-8@GO filler affects the rate at which the de-mixing process occurs therefore impacting/influencing the membrane pore size, pore distribution, and the shape of the pores that are formed [19, 72]. For example, we observed a decrease in membrane pore size but an increase in pore density and pore distribution as the amount of ZIF-8@GO composite in the PES composite membranes was increased in comparison to pristine PES membrane [56]. Furthermore, the cross-section of the composite membranes demonstrated a formation of a sponge-like membrane compared to the pristine membrane at higher ZIF-8@GO loading [56]. This variation is dependent on the influence the hydrophilic GO has on the rate of solvent de-mixing and final deposition of the filler within the membrane polymer matrix. In this case, the combination of porous filler and hydrophilic GO support consequently increased water flux by affording the membrane more water transport pathways and increased hydrophilicity that plays a crucial role in membrane performances [3, 11, 57, 89, 97, 106].

In interfacial polymerization (I.P.), the fillers, i.e., ZIF-8@GO, affect the rate of crosslinking between aliphatic/diamine monomer in the aqueous phase and the acid chloride monomer in the organic phase (Fig. 8.10) [37, 38, 89]. Subsequently, the thickness of the thin film is affected, which plays a huge role in membrane performance [37, 38]. It is worth mentioning that the filler effect is usually observed when the filler is dispersed in the organic phase because the diffusion rate of the I.P. process is generally controlled in the organic layer [3, 37, 38]. The SEM images of

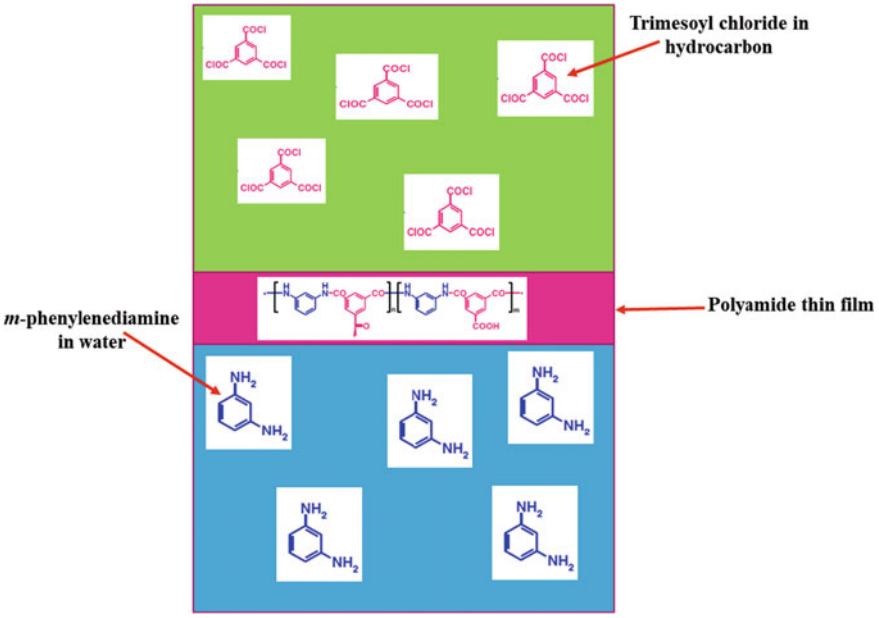

Fig. 8.10 Representation of the formation of polyamide thin film. Reproduced with permission from (Lau, Ismail, Misdan and Kassim 2012). Copyright 2012 ELSEVIER

thin film composite membranes usually show a thin layer onto the porous substrate, and in some cases, irregular structure is observed, which is assumed to be a result of the growth of initial polyamide clumps caused by the defect in the interface at the beginning of crosslinking.

8.4.1.2 Afm

Recently, the AFM technique has found widespread usage for the study of membrane surfaces. AFM provides atomic-level images and has become a crucial technique for obtaining images of the membrane surface materials. This technique does not require any special sample preparation, as is the case for SEM above. Interestingly, AFM can show three-dimensional images of the surfaces. The quantitative information obtained from AFM provides the microscopic details of the surface structure that is used to obtain a variety of surface roughness parameters as well as in some cases the width of surface pores and surface porosity. Visualizing the effects of fouling and chemical modification on surface morphology is another potential benefit of using this technique. Researchers revealed that the surface roughness of the membrane influence the surface area that is available for contact with foulants [31, 72, 104]. Therefore, surface roughness plays a critical part in establishing the magnitude and

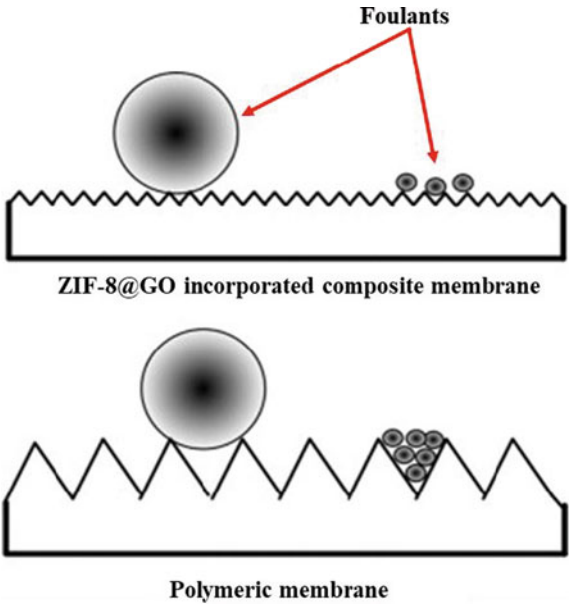

Fig. 8.11 Representation of the affinity of foulants towards the rougher polymeric membrane and poor affinity towards the smoother ZIF-8@GO modified membrane

nature of membrane surface fouling [31, 72, 104]. Due to the observed correlation between higher surface roughness the increased propensity for surface fouling (Fig. 8.11), great effort into creating membranes with smoother surfaces to minimize fouling has been made. The incorporation of hydrophilic ZIF-8@GO fillers has led to a reduced surface roughness which subsequently enhances fouling resistance of the composite U.F. membrane (Fig. 8.11) [11, 26, 92, 106]. The reduced surface roughness emanates from the affected rate of de-mixing in the phase inversion method and the rate of crosslinking in interfacial polymerization.

8.4.2 Membrane Wettability

Membrane wettability studies usually involve the measurement of contact angles as the primary data, which indicates the degree of wetting when a membrane surface and liquid interact [24, 100]. Small contact angles ($\theta = 90°$) correspond to high wettability, while large contact angles ($\theta = 90°$) correspond to low wettability [24, 100]. The contact angle values are presented in Fig. 8.12. A lower contact angle value signifies the hydrophilic nature of the material, i.e., the high affinity of water molecules toward the membrane substrate [24, 100]. Hydrophilic literally means "water loving" and such materials easily adsorb water molecules due to the presence of active polar functional groups [100]. The higher contact angle indicates the hydrophobic nature of the surface. Hydrophobic materials possessing this characteristic have the opposite

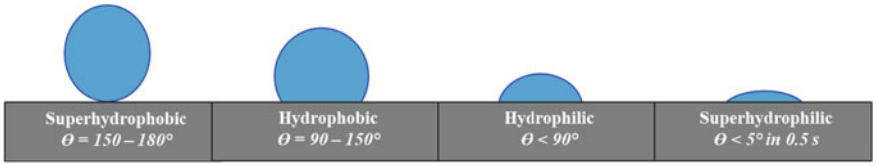

Fig. 8.12 Demonstration of contact angle formed by a sessile liquid drop on a smooth surface

response to water interaction compared to hydrophilic materials. Hydrophobic materials "water hating" have little or no tendency to interact with water, and water tends to "bead" on their surfaces [24, 100]. The contact angle measurement is in addition also influenced by the physical properties of the membranes such as heterogeneity, surface roughness, pore size, and pore distribution [24]. Suppose a membrane is highly porous due to the incorporation of ZIF-8@GO composite. In that case, the contact angle value may become very low due to the combination of functional groups on GO and porosity afforded by the ZIF-8. In the case where the membrane incorporated only ZIF-8, the overall surface character is less hydrophilic at high filler content. Hence, the observed contact angles are higher compared to its GO analog.

Similarly, the contact angle value of a membrane of higher surface roughness is higher compared to the other membrane of lower surface roughness [11, 56, 57, 89]. Generally, as the contact angle values decreased (membrane become hydrophilic), the flux rate has increased, a behavior observed for composite membranes containing ZIF-8@GO [11, 56, 57, 89]. Hydraulic permeability of the membrane significantly influenced the surface hydrophilicity. These involve the secondary forces of interactions such as dipole–dipole, induced dipole–dipole, Van der Waals forces, electrostatic interaction, hydrogen bonding, etc., between the solution and membrane [24]. This also results in relatively higher fluxes.

8.4.3 Water Flux

Water flux is greatly affected by various factors such as membrane hydrophilicity, membrane roughness, membrane pore size, pore density as well as pore distribution. As such, ZIF-8@GO composites have a strong influence on the above-mentioned factors, hence resulting in improved water flux of the composite membrane [11, 56, 57, 89]. Van der Bruggen et al. [89] reported an increase in water flux and permeability owing to the hydrophilic and porous characters of GO and ZIF-8, respectively. This is similar results to our results [56] which was attributed to a decrease in tortuosity owing to the hydrophilic properties of GO and the porous nature of ZIF-8 that allowed for an alternative flow path for water molecules infiltrate through the composite filler (Fig. 8.8). Similarly, Ye et al. and Sun et al. reported a significant increase in water flux and permeation due to the incorporation of UiO-66-NH_2/GO and UiO-66@GO, respectively [43, 47, 69] in comparison to UiO and GO when used separately. An

increase in flux for the hybrid material is due to the synergistic effect from the MOF and GO; hence more research is focused on using MOF@GO fillers. Furthermore, ZIF-8@GO is extensively used as a filler in membrane technology due to ZIF-8 water stability, the compatibility of the filler with different polymer matrixes as well as selective properties in rejection of various pollutants [11, 56, 89].

8.4.4 Fouling Resistance

One of the utmost unfavorable problems in the pressure-driven membrane process such as reverse osmosis (R.O), nanofiltration (N.F), ultrafiltration (U.F) and microfiltration (M.F) is fouling, which hinders the long-term usage and efficiency of the membranes [22, 76]. Fouling is due to the adsorption or deposition of particles, colloids, proteins, macromolecules, salts, etc., at the membrane surface or inside the pores [22, 76]. Generally, fouling is reduced by enhancing the surface hydrophilicity and reducing the surface roughness of the membrane surfaces [22, 76].

Membrane surface hydrophilicity is the affinity of the membrane to attract water molecules towards itself while repelling hydrophobic pollutants [24, 100]. As such, water molecules form a water layer on the hydrophilic membrane surface, reducing the contact between the hydrophobic pollutants and the membrane surface [24, 100]. This phenomenon plays an important role in fouling resistance. For example, Kang et al. and Lee et al. revealed that GO as a filler material increases the hydrophilicity of the composite membranes, subsequently enhancing fouling properties of the composite membranes [40, 98]. Similarly, incorporation of ZIF-8@GO onto polymeric membranes was shown to improve membrane hydrophilicity and therefore increase fouling resistance [11, 56, 89].

The surface roughness of the membrane also plays a crucial role in fouling propensity, as demonstrated by various researchers. As such, Zhang et al. investigated the mechanism and implications of surface roughness and fouling relationship in RO membrane [75]. It was shown that the rougher surface with valleys contributes to an increase in membrane fouling where foulants are trapped within the valleys [75]. Furthermore, it was revealed that the low surface roughness normally has evenly distributed water flux with minimized effects of drag force while making better use of shear force resulting in an increase in fouling resistance [75]. We also reported similar findings, wherein an increase in fouling resistance was observed for membranes with smoother surface roughness in comparison to rougher membrane surfaces [56, 57].

8.4.5 Wastewater Treatment

Wastewater emanates from municipal discharge, agricultural activities and industrial discharge contaminated by dyes, heavy metals, radioactive nuclides, pesticides as well as miscellaneous and emerging contaminants which ultimately reduce the

quality of drinking water [79]. Consequently, different strategies have been employed for wastewater treatment, such as membrane technology [17], ion exchange [33], and adsorption [79]. These techniques can be utilized to extract valuable constituents for reuse, separate solutes, and ultimately remove all solutes [1, 2]. However, the process depends on the type of technique used, type of contaminant, and material [2, 79]. Herein, the interest is on membrane technology for the removal of solutes from wastewater.

So far, rejection of various contaminants using polymeric membranes is due to size exclusion, depending on the size of the membrane pore and that of the pollutants, electrostatic interaction, hydrogen bonding, etc. [77, 101]. For example, Chang and co-workers investigated the effect of size exclusion in nanofiltration membrane [9]. The results revealed that the pore size of the membranes has much influence on size exclusion compared to cross-flow velocity and the transmembrane pressure [9]. Van Dijk et al. studied the role of electrostatic repulsion between the solute and the membrane at different pH using nanofiltration membranes [88]. On the other hand, Shen et al. explained electrostatic interaction formed between the ion from the pollutants with water molecules forming a shell around the ion, making it difficult for the ions to pass through the membrane [77]. However, rejection percentages using polymeric membranes have been demonstrated to be low.

To enhance rejection % as well as selectivity, ZIF-8, GO, and ZIF-8@GO composite have been used for selective removal of various hazardous pollutants from wastewater [56, 63, 80]. Selective rejection of the pollutants via ZIF-8@GO containing composite membranes were also found to proceed through a number of different mechanisms such as electrostatic interactions, acid–base interactions, hydrogen bonding, stacking/interactions, and hydrophobic interactions (Fig. 8.13) [11, 23, 56, 90]. It has also been observed that sometimes, for a particular selectivity process, multiple interactions might take place to afford 100% of rejection [23].

Jhung et al. reviewed the effect of MOFs selectivity on the adsorptive removal of conventional organic contaminants from wastewater [23]. The authors investigated the possible interactions between the pollutants and the MOFs. Their findings revealed that there is a number of interactions that play a crucial role in different types of adsorption depending on the type of the targeted pollutant and the MOF used. Additionally, Chen and co-workers explored the adsorption of organic and inorganic pollutants using ZIF-8@GO [90]. It was realized that the adsorption mechanisms of ZIF-8@GO towards Pb(II) were complexation and electrostatic attraction, whereas the π–π bond was the dominating adsorption mechanism for 1-naphthylamine.

8.5 Conclusion

The chapter first described the different types of MOFs as well as their different properties. These are subsequently illustrated with respect to the types of application each MOF is suitable for. It is further indicated that only water-stable MOFs are suitable for application in membrane technology unless the further modification

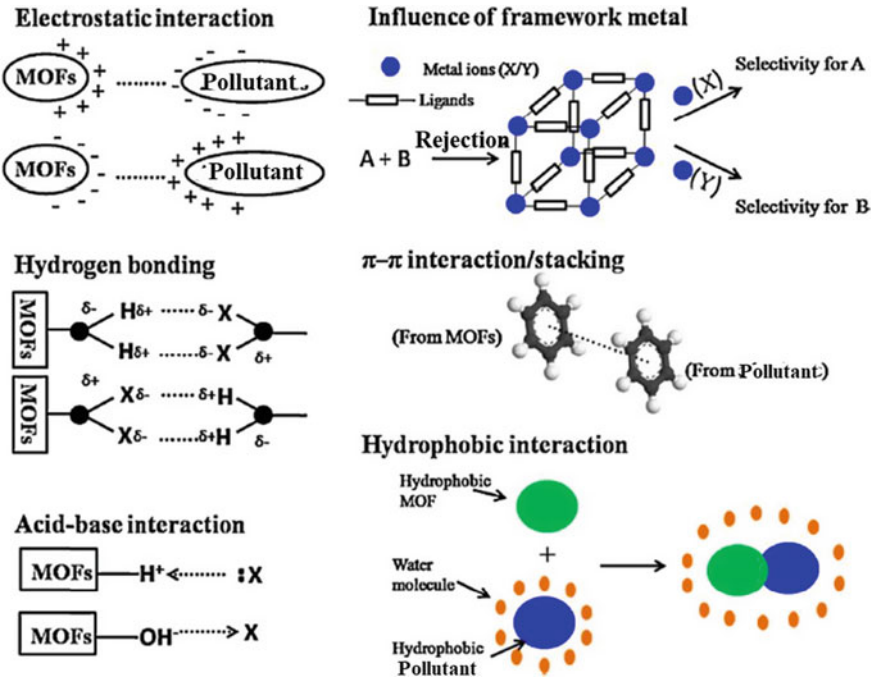

Fig. 8.13 Possible mechanisms for selective removal of pollutants from wastewater. Reproduced with permission from [23]. Copyright 2015 ELSEVIER

is done to enhance the water stability of the MOF. In addition to water stability, MOFs deemed suitable for membrane technology must possess appropriate pore sizes as well as be compatible with the polymer matrix are other critical considerations. The chapter also showed that proper dispersion of the MOFs in the polymer matrix is enhanced through the use of the carbonaceous dispersant, namely GO. The MOF@GO composite has proven to improve the surface morphology of the membranes by modulating pore density, reducing surface roughness, and enhancing surface hydrophilicity. These improved surface characteristics result in enhanced membrane performance, i.e., high water flux due to synergistic effect from porous MOF and hydrophilic GO, rejection efficiency of the membranes is also influenced by the use of hybrid material; as such, multi rejection mechanisms is realized, resulting in the selectivity of the pollutants. Ultimately, the chapter has demonstrated that the use of a zeolitic organic framework coupled with graphene oxide is currently providing enhanced characteristics in the membrane for water treatment and thus offers a promising future role in the field.

References

1. M.A. Abdel-fatah, Nanofiltration systems and applications in wastewater treatment: review article. Ain Shams Eng. J. **9**(4), 3077–3092 (2018). https://doi.org/10.1016/j.asej.2018.08.001
2. N. Abdullah et al., Recent trends of heavy metal removal from water/wastewater by membrane technologies. J. Ind. Eng. Chem. (2019). https://doi.org/10.1016/j.jiec.2019.03.029
3. N. Abdullah et al., Insights into metal-organic frameworks-integrated membranes for desalination process: a review. Desalination **500**, 114867 (2021). https://doi.org/10.1016/j.desal.2020.114867
4. H. Amrouche et al., Prediction of thermodynamic properties of adsorbed gases in zeolitic imidazolate frameworks. RSC Adv. **2**(14), 6028–6035 (2012). https://doi.org/10.1039/c2ra00025c
5. R. Banerjee, High-throughput synthesis of zeolitic imidazolate frameworks and application to CO_2 capture. Science **319**, 939–944 (2008). https://doi.org/10.1126/science.1152516
6. L. Bellarosa et al., On the mechanism behind the instability of isoreticular metal-organic frameworks (IRMOFs) in humid environments. Chem. Eur. J. **18**(39), 12260–12266 (2012). https://doi.org/10.1002/chem.201201212
7. S. Bhattacharjee et al., Zeolitic imidazolate frameworks: synthesis, functionalization, and catalytic/adsorption applications. Catal. Surv. Asia **18**(4), 101–127 (2014). https://doi.org/10.1007/s10563-014-9169-8
8. J.H. Cavka et al., A new zirconium inorganic building brick forming metal organic frameworks with exceptional stability. J. Am. Chem. Soc. **130**(42), 13850–13851 (2008). https://doi.org/10.1021/ja8057953
9. E. Chang et al., A simplified method for elucidating the effect of size exclusion on nanofiltration membranes. Sep. Purif. Technol. **85**, 1–7 (2012). https://doi.org/10.1016/j.seppur.2011.05.002
10. J. Chen et al., A facile synthesis for uniform tablet-like TiO2/C derived from materials of institut lavoisier-125(Ti) (MIL-125(Ti)) and their enhanced visible light-driven photodegradation of tetracycline. J. Colloid Interface Sci. **571**, 275–284 (2020). https://doi.org/10.1016/j.jcis.2020.03.055
11. X. Dai et al., Zeolitic Imidazole Framework/graphene oxide hybrid functionalized poly(lactic acid) electrospun membranes: a promising environmentally friendly water treatment material. ACS Omega **3**(6), 6860–6866 (2018). https://doi.org/10.1021/acsomega.8b00792
12. C. Duan et al., Water-based routes for synthesis of metal-organic frameworks: a review. Sci. China Mater. **63**(5), 667–685 (2020). https://doi.org/10.1007/s40843-019-1264-x
13. W.A. El-Mehalmey et al., Strong interplay between polymer surface charge and MOF cage chemistry in mixed-matrix membrane for water treatment applications. ACS Appl. Mater. Interfaces. **12**(24), 27625–27631 (2020). https://doi.org/10.1021/acsami.0c06399
14. A. Elrasheedy et al., Metal organic framework based polymer mixed matrix membranes: review on applications in water purification. Membranes **9**(7) (2019). https://doi.org/10.3390/membranes9070088
15. S.K. Elsaidi et al., Flexibility in metal-organic frameworks: a fundamental understanding. Coord. Chem. Rev. **358**, 125–152 (2018). https://doi.org/10.1016/j.ccr.2017.11.022
16. J.F. Eubank et al., Porous, rigid metal(III)-carboxylate metal-organic frameworks for the delivery of nitric oxide. APL Mater. **2**(12) (2014). https://doi.org/10.1063/1.4904069
17. E.O. Ezugbe, S. Rathilal, Membrane technologies in wastewater treatment: a review. Membranes (2020). https://doi.org/10.3390/membranes10050089
18. F. Millange, G.F. Christian Serre, Synthesis, structure determination and properties of MIL-53as and MIL-53ht: the first CrIII hybrid inorganic–organic microporous solids: CrIII(OH)·{O2C–C6H4–CO2}·{HO2C–C6H4–CO2H}x. R. Soc. Chem. **601**(2), 51–56 (2000)
19. J.M. Gohil, R.R. Choudhury, Introduction to nanostructured and nano-enhanced polymeric membranes: preparation, function, and application for water purification. Nanoscale Mater. Water Purif.. Elsevier Inc (2019). https://doi.org/10.1016/B978-0-12-813926-4.00038-0

20. Q. Gu et al., 'Metal-organic frameworks (MOFs)-boosted filtration membrane technology for water sustainability. APL Mater. **8**(4) (2020). https://doi.org/10.1063/5.0002905
21. G.R. Guillen et al., Preparation and characterization of membranes formed by nonsolvent induced phase separation: a review. Ind. Eng. Chem. Res. **50**(7), 3798–3817 (2011). https://doi.org/10.1021/ie101928r
22. W. Guo, H.H. Ngo, J. Li, A mini-review on membrane fouling. Biores. Technol. **122**, 27–34 (2012). https://doi.org/10.1016/j.biortech.2012.04.089
23. Z. Hasan, S.H. Jhung, Removal of hazardous organics from water using metal-organic frameworks (MOFs): plausible mechanisms for selective adsorptions. J. Hazard. Mater. **283**, 329–339 (2015). https://doi.org/10.1016/j.jhazmat.2014.09.046
24. R.S. Hebbar, A.M. Isloor, A.F. Ismail, *Contact Angle Measurements*, *Membrane Characterization*. Elsevier B.V (2017). https://doi.org/10.1016/B978-0-444-63776-5.00012-7
25. S. Hu et al., Effects of monocarboxylic acid additives on synthesizing metal-organic framework NH2-MIL-125 with controllable size and morphology. Cryst. Growth Des. **17**(12), 6586–6595 (2017). https://doi.org/10.1021/acs.cgd.7b01250
26. A. Huang, B. Feng, Facile synthesis of PEI-GO@ZIF-8 hybrid material for CO2 capture. Int. J. Hydrogen Energy **43**(4), 2224–2231 (2018). https://doi.org/10.1016/j.ijhydene.2017.12.070
27. N.A. Ibrahim et al., 'Development of polyvinylidene fluoride (PVDF)-ZIF-8 membrane for wastewater treatment, in *IOP Conference Series: Earth and Environmental Science* (2018). https://doi.org/10.1088/1755-1315/140/1/012021
28. T. Islamoglu et al., From transition metals to lanthanides to actinides: metal-mediated tuning of electronic properties of isostructural metal-organic frameworks. Inorg. Chem. **57**(21), 13246–13251 (2018). https://doi.org/10.1021/acs.inorgchem.8b01748
29. F. Israr et al., Scope of various solvents and their effects on solvothermal synthesis of Ni-BTC. Quim. Nova **39**(6), 669–675 (2016). https://doi.org/10.5935/0100-4042.20160068
30. C. Janiak, J.K. Vieth, MOFs, MILs and more: Concepts, properties and applications for porous coordination networks (PCNs). New J. Chem. **34**(11), 2366–2388 (2010). https://doi.org/10.1039/c0nj00275e
31. D. Johnson, N. Hilal, *Atomic Force Microscopy (AFM)*, *Membrane Characterization*. Elsevier B.V (2017). https://doi.org/10.1016/B978-0-444-63776-5.00007-3
32. M. Kadhom, B. Deng, Metal-organic frameworks (MOFs) in water filtration membranes for desalination and other applications. Appl. Mater. Today **11**, 219–230 (2018). https://doi.org/10.1016/j.apmt.2018.02.008
33. N. Kansara et al., Wastewater treatment by ion exchange method: a review of past and recent researches. Environ. Sci.-Indian J.**12**(4), 143–150 (2016). http://www.tsijournals.com/articles/wastewater-treatment-by-ion-exchange-method-a-review-of-past-and-recent-researches.pdf
34. M.J. Katz et al., A facile synthesis of UiO-66, UiO-67 and their derivatives. Chem. Commun. **49**(82), 9449–9451 (2013). https://doi.org/10.1039/c3cc46105j
35. N.A. Khan, Z. Hasan, S.H. Jhung, Beyond pristine metal-organic frameworks: preparation and application of nanostructured, nanosized, and analogous MOFs. Coord. Chem. Rev. **376**, 20–45 (2018). https://doi.org/10.1016/j.ccr.2018.07.016
36. K. Kumar et al., Inorganica chimica acta a review on contemporary metal – organic framework materials. Inorg. Chim. Acta **446**, 61–74 (2016). https://doi.org/10.1016/j.ica.2016.02.062
37. W.J. Lau et al., 'A recent progress in thin fi lm composite membrane : a review' **287**, 190–199 (2012). https://doi.org/10.1016/j.desal.2011.04.004
38. W.J. Lau et al., A recent progress in thin film composite membrane: a review. Desalination **287**, 190–199 (2012). https://doi.org/10.1016/j.desal.2011.04.004
39. J. Lee et al., Metal – organic framework-based porous matrix membranes for improving mass transfer in forward osmosis membranes. J. Membr. Sci. **492**, 392–399 (2015). https://doi.org/10.1016/j.memsci.2015.06.003
40. J. Lee et al., Graphene oxide nanoplatelets composite membrane with hydrophilic and antifouling properties for wastewater treatment. J. Membr. Sci. **448**, 223–230 (2013). https://doi.org/10.1016/j.memsci.2013.08.017

41. T.H. Lee et al., High-performance polyamide thin-film nanocomposite membranes containing ZIF-8/CNT hybrid nanofillers for reverse osmosis desalination. Ind. Eng. Chem. Res. **59**(12), 5324–5332 (2020). https://doi.org/10.1021/acs.iecr.9b04810
42. S. Leubner et al., Solvent impact on the properties of benchmark metal-organic frameworks: acetonitrile-based synthesis of CAU-10, Ce-UiO-66, and Al-MIL-53. Chem. Eur. J. **26**(17), 3877–3883 (2020). https://doi.org/10.1002/chem.201905376
43. J. Li et al., The performance of UiO-66-NH2/graphene oxide (GO) composite membrane for removal of differently charged mixed dyes' Chemosphere**237**, 124517 (2019). https://doi.org/10.1016/j.chemosphere.2019.124517
44. J. Li et al., Metal-organic framework membranes for wastewater treatment and water regeneration. Coord. Chem. Rev. **404**, 213116 (2020). https://doi.org/10.1016/j.ccr.2019.213116
45. N. Li et al., Governing metal – organic frameworks towards high stability 8501–8513 (2016). https://doi.org/10.1039/c6cc02931k
46. T. Li et al., Double layer MOFs M-ZIF-8@ZIF-67: The adsorption capacity and removal mechanism of fipronil and its metabolites from environmental water and cucumber samples. J. Adv. Res. **24**, 159–166 (2020). https://doi.org/10.1016/j.jare.2020.03.013
47. W. Li, Metal–organic framework membranes: production, modification, and applications. Prog. Mater Sci. **100**, 21–63 (2019). https://doi.org/10.1016/j.pmatsci.2018.09.003
48. R. Lin et al., Metal organic framework based mixed matrix membranes: an overview on filler/polymer interfaces. J. Mater. Chem. A **6**(2), 293–312 (2018). https://doi.org/10.1039/c7ta07294e
49. R.B. Lin et al., Microporous metal-organic framework materials for gas separation. Chem **6**(2), 337–363 (2020). https://doi.org/10.1016/j.chempr.2019.10.012
50. M. Liu et al., Formation of microporous polymeric membranes via thermally induced phase separation: a review. Front. Chem. Sci. Eng. **10**(1), 57–75 (2016). https://doi.org/10.1007/s11705-016-1561-7
51. Liu, X. (2020) 'Metal-organic framework UiO-66 membranes', 14(2), 216–232.
52. Y. Liu et al., Effect of metal-ligand ratio on the CO2 adsorption properties of Cu-BTC metal-organic frameworks. RSC Adv. **8**(62), 35551–35556 (2018). https://doi.org/10.1039/c8ra07774f
53. J. Ma, D. Ping, X. Dong, 'Recent developments of graphene oxide-based membranes: A review'. Membranes **7**(3) (2017). https://doi.org/10.3390/membranes7030052
54. Z. Mai, D. Liu, Synthesis and applications of isoreticular metal-organic frameworks IRMOFs-n (n = 1, 3, 6, 8). Cryst. Growth Des. **19**(12), 7439–7462 (2019). https://doi.org/10.1021/acs.cgd.9b00879
55. T.A. Makhetha, R.M. Moutloali, Antifouling properties of Cu(tpa)@GO/PES composite membranes and selective dye rejection. J. Membr. Sci. **554**(January), 195–210 (2018). https://doi.org/10.1016/j.memsci.2018.03.003
56. T.A. Makhetha, R.M. Moutloali, Stable zeolitic imidazolate framework-8 supported onto graphene oxide hybrid ultrafiltration membranes with improved fouling resistance and water flux. Chem. Eng. J. Adv.**1**, 100005 (2020). https://doi.org/10.1016/j.ceja.2020.100005
57. T.A. Makhetha, R.M. Moutloali, Incorporation of a novel Ag–Cu@ZIF-8@GO nanocomposite into polyethersulfone membrane for fouling and bacterial resistance. J. Membr. Sci. **618**, 118733 (2021). https://doi.org/10.1016/j.memsci.2020.118733
58. M. Miculescu et al., Graphene-based polymer nanocomposite membranes: a review. Polym. Adv. Technol. **27**(7), 844–859 (2016). https://doi.org/10.1002/pat.3751
59. E.D. Miensah et al., Zeolitic imidazolate frameworks and their derived materials for sequestration of radionuclides in the environment: a review. Crit. Rev. Environ. Sci. Technol. **50**(18), 1874–1934 (2020). https://doi.org/10.1080/10643389.2019.1686946
60. F. Millange, R.I. Walton, MIL-53 and its isoreticular analogues: a review of the chemistry and structure of a prototypical flexible metal-organic framework. Isr. J. Chem. **58**(9), 1019–1035 (2018). https://doi.org/10.1002/ijch.201800084

61. A.S. Munn et al., M(ii) (M = Mn Co, Ni) variants of the MIL-53-type structure with pyridine-N-oxide as a co-ligand. CrystEngComm **15**(45), 9679–9687 (2013). https://doi.org/10.1039/c3ce41268g
62. M.A. Mutalib et al., Chapter 9 - Scanning Electron Microscopy (SEM); and Energy-Dispersive X-Ray (EDX); Spectroscopy, Membrane Characterization, Elsevier B.V (2017). https://doi.org/10.1016/B978-0-444-63776-5.00009-7
63. J. Nambikkattu, J. Jose, N.J. Kaleekkal, Materials today: proceedings tailoring the performance of thin-film composite membrane using ZIF-8 for wastewater treatment. Mater. Today: Proc. **47**, 1394–1399 (2021). https://doi.org/10.1016/j.matpr.2021.02.619
64. N.I.M. Nawi et al., Development of hydrophilic PVDF membrane using vapour induced phase separation method for produced water treatment. Membranes **10**(6), 1–17 (2020). https://doi.org/10.3390/membranes10060121
65. K. Noh, J. Lee, J. Kim, Compositions and structures of zeolitic imidazolate frameworks. Isr. J. Chem. **58**(9), 1075–1088 (2018). https://doi.org/10.1002/ijch.201800107
66. N.A.H.M. Nordin et al., Aqueous room temperature synthesis of zeolitic imidazole framework 8 (ZIF-8) with various concentrations of triethylamine. RSC Adv. **4**(63), 33292–33300 (2014). https://doi.org/10.1039/c4ra03593c
67. M. Oveisi, M.A. Asli, N.M. Mahmoodi, MIL-Ti metal-organic frameworks (MOFs) nanomaterials as superior adsorbents: synthesis and ultrasound-aided dye adsorption from multicomponent wastewater systems. J. Hazard. Mater. **347**, 123–140 (2018). https://doi.org/10.1016/j.jhazmat.2017.12.057
68. Y. Pan et al., Core-Shell ZIF-8@ZIF-67-derived CoP nanoparticle-embedded N-doped carbon nanotube hollow polyhedron for efficient overall water splitting. J. Am. Chem. Soc. **140**(7), 2610–2618 (2018). https://doi.org/10.1021/jacs.7b12420
69. J. Pang et al., Exploring the sandwich antibacterial membranes based on UiO-66/graphene oxide for forward osmosis performance. Carbon **144**, 321–332 (2019). https://doi.org/10.1016/j.carbon.2018.12.050
70. R. Sabouni, H. Kazemian, S. Rohani, Carbon dioxide capturing technologies: a review focusing on metal organic framework materials (MOFs). Environ. Sci. Pollut. Res. **21**(8), 5427–5449 (2014). https://doi.org/10.1007/s11356-013-2406-2
71. R.R. Salunkhe, Y.V. Kaneti, Y. Yamauchi, Metal-organic framework-derived nanoporous metal oxides toward supercapacitor applications: progress and prospects. ACS Nano **11**(6), 5293–5308 (2017). https://doi.org/10.1021/acsnano.7b02796
72. Sataloff, R. T., Johns, M. M. and Kost, K. M. (1990) *Synthetic Membranes for Membrane Processes*.
73. G.E.M. Schukraft et al., Isoreticular expansion of polyMOFs achieves high surface area materials. Chem. Commun. **53**(77), 10684–10687 (2017). https://doi.org/10.1039/c7cc04222a
74. R. Seetharaj et al., Dependence of solvents, pH, molar ratio and temperature in tuning metal organic framework architecture. Arab. J. Chem. **12**(3), 295–315 (2019). https://doi.org/10.1016/j.arabjc.2016.01.003
75. C. Shang, D. Pranantyo, S. Zhang, Understanding the roughness-fouling relationship in reverse osmosis: mechanism and implications. Environ. Sci. Technol. **54**(8), 5288–5296 (2020). https://doi.org/10.1021/acs.est.0c00535
76. Q. She et al., Membrane fouling in osmotically driven membrane processes: a review. J. Membr. Sci. **499**, 201–233 (2016). https://doi.org/10.1016/j.memsci.2015.10.040
77. M. Shen, S. Keten, R.M. Lueptow, Rejection mechanisms for contaminants in polymeric reverse osmosis membranes (2016), pp. 36–47
78. G. Skorupskii et al., Efficient and tunable one-dimensional charge transport in layered lanthanide metal-organic frameworks. ChemRxiv (2018), pp. 1–23. https://doi.org/10.26434/chemrxiv.7253192
79. N.H. Solangi et al., 'n Pr pr oo f'. J. Hazard. Mater. 125848 (2021). https://doi.org/10.1016/j.jhazmat.2021.125848

80. Y. Song et al., Journal of Water Process Engineering E ffi cient removal and fouling-resistant of anionic dyes by nano fi ltration membrane with phosphorylated chitosan modi fi ed graphene oxide nanosheets incorporated selective layer'. J. Water Process. Eng. **34**(November 2019), 101086 (2020). https://doi.org/10.1016/j.jwpe.2019.101086
81. J. Spencer, The sustainable development goals. Des. Glob. Chall. Goals **12**, 25 (2021). https://doi.org/10.4324/9781003099680-3
82. D. Sun et al., Pore-environment engineering in multifunctional metal-organic frameworks. Chin. J. Chem. **38**, 509–524 (2020). https://doi.org/10.1002/cjoc.201900493
83. X.M. Tan, D. Rodrigue,'a review on porous polymeric membrane preparation. Part I: production techniques with polysulfone and poly (Vinylidene Fluoride). Polymers **11**(8) (2019)
84. D.J. Tranchemontagne, J.R. Hunt, O.M. Yaghi, Room temperature synthesis of metal-organic frameworks: MOF-5, MOF-74, MOF-177, MOF-199, and IRMOF-0. Tetrahedron **64**(36), 8553–8557 (2008). https://doi.org/10.1016/j.tet.2008.06.036
85. B. Tylkowski, I. Tsibranska, Overview of main techniques used for membrane characterization. J. Chem. Technol. Metall. **50**(1), 3–12 (2015)
86. United Nations (2020) 'The Sustainable Development Goal 6 Global Acceleration Framework', 17. Available at: www.unwater.org/publications/the-sdg-6-global-acceleration-framework/.
87. K. Ventura et al., Superparamagnetic MOF@GO Ni and Co based hybrid nanocomposites as efficient water pollutant adsorbents. Sci. Total Environ. **738**, 139213 (2020). https://doi.org/10.1016/j.scitotenv.2020.139213
88. A R.D. Verliefde et al., The role of electrostatic interactions on the rejection of organic solutes in aqueous solutions with nanofiltration **322**, 52–66 (2008). https://doi.org/10.1016/j.memsci.2008.05.022
89. J. Wang et al., Zeolitic Imidazolate framework/graphene oxide hybrid nanosheets functionalized thin film nanocomposite membrane for enhanced antimicrobial performance. ACS Appl. Mater. Interfaces **8**(38), 25508–25519 (2016). https://doi.org/10.1021/acsami.6b06992
90. J. Wang et al., Journal of Colloid and Interface Science Exploration of the adsorption performance and mechanism of zeolitic imidazolate framework-8 @ graphene oxide for Pb (II) and 1-naphthylamine from aqueous solution. J. Colloid Interface Sci. **542**, 410–420 (2019). https://doi.org/10.1016/j.jcis.2019.02.039
91. Q. Wang et al., Recent advances in MOF-based photocatalysis: environmental remediation under visible light. Inorg. Chem. Front. **7**, 300–339 (2020). https://doi.org/10.1039/c9qi01120j
92. N. Wei et al., Fabrication of an amine-modified ZIF-8@GO membrane for high-efficiency adsorption of copper ions. New J. Chem. **43**(14), 5603–5610 (2019). https://doi.org/10.1039/C8NJ06521G
93. J. Winarta et al., A decade of uio-66 research: a historic review of dynamic structure, synthesis mechanisms, and characterization techniques of an archetypal metal-organic framework. Cryst. Growth Des. **20**(2), 1347–1362 (2020). https://doi.org/10.1021/acs.cgd.9b00955
94. World Health Organization and UN-Habitat, *Progress on wastewater treatment - Piloting the monitoring mehtodology and intial findings for SDG indicator 6.3.1*, *Guidelines on Sanitation and Health* (2018)
95. M.X. Wu et al., Core-Shell MOFs@MOFs: diverse designability and enhanced selectivity. ACS Appl. Mater. Interfaces **12**(49), 54285–54305 (2020). https://doi.org/10.1021/acsami.0c16428
96. W. Xuan et al., Mesoporous metal–organic framework materials. Chem. Soc. Rev. **41**(5), 1677–1695 (2012). https://doi.org/10.1039/c1cs15196g
97. L. Yang, Z. Wang, J. Zhang, ('Zeolite imidazolate framework hybrid nanofiltration (NF) membranes with enhanced permselectivity for dye removal.' J. Membr. Sci. **532**, 76–86 (December 2016) (2017). https://doi.org/10.1016/j.memsci.2017.03.014
98. Y. Yoon et al., Comparing graphene oxide and reduced graphene oxide as blending materials for polysulfone and polyvinylidene difluoride membranes. Appl. Sci. (Switzerland) **10**(6) (2020). https://doi.org/10.3390/app10062015

99. Q. Yuan, G. Zhu, A review on metal organic frameworks (MOFs) modified membrane for remediation of water pollution. Environ. Eng. Res. **26**, 3–2 (2020). https://doi.org/10.4491/eer.2019.435
100. Y. Yuan, T.R. Lee, *Contact Angle and Wetting Properties* (2013). https://doi.org/10.1007/978-3-642-34243-1
101. M. Zahid et al., *Role of Polymeric Nanocomposite Membranes for the Removal of Textile Dyes from Wastewater* (Elsevier Inc., Aquananotechnology, 2021). https://doi.org/10.1016/B978-0-12-821141-0.00006-9
102. G. Zhan, H.C. Zeng, Alternative synthetic approaches for metal-organic frameworks: transformation from solid matters. Chem. Commun. **53**(1), 72–81 (2017). https://doi.org/10.1039/c6cc07094a
103. W.H. Zhang et al., Graphene oxide membranes with stable porous structure for ultrafast water transport. Nat. Nanotechnol. (2021). https://doi.org/10.1038/s41565-020-00833-9
104. Z. Zhong et al., Membrane surface roughness characterization and its influence on ultrafine particle adhesion. Sep. Purif. Technol. **90**, 140–146 (2012). https://doi.org/10.1016/j.seppur.2011.09.016
105. H. Zhou et al., Stable Metal-Organic Frameworks: Design, Synthesis, and Applications. Adv. Mater. **30**, 1704303 (2018). https://doi.org/10.1002/adma.201704303
106. T. Zhu et al., ZIF-8@GO composites incorporated polydimethylsiloxane membrane with prominent separation performance for ethanol recovery. J. Membr. Sci. **598**, 117681 (2020). https://doi.org/10.1016/j.memsci.2019.117681

Index

M. J. Hato and S. Sinha Ray (eds.), *Functional Polymer Nanocomposites for Wastewater Treatment*, Springer Series in Materials Science 323,
https://doi.org/10.1007/978-3-030-94995-2